

---

Theses and Dissertations

---

Fall 2014

## Bank erosion processes in streams in the U.S. Midwest

Tommy Ekamitra Sutarto  
*University of Iowa*

Follow this and additional works at: <https://ir.uiowa.edu/etd>



Part of the [Civil and Environmental Engineering Commons](#)

Copyright © 2014 Tommy Ekamitra Sutarto

This dissertation is available at Iowa Research Online: <https://ir.uiowa.edu/etd/6648>

---

### Recommended Citation

Sutarto, Tommy Ekamitra. "Bank erosion processes in streams in the U.S. Midwest." PhD (Doctor of Philosophy) thesis, University of Iowa, 2014.

<https://doi.org/10.17077/etd.33aa-qae0>

---

Follow this and additional works at: <https://ir.uiowa.edu/etd>



Part of the [Civil and Environmental Engineering Commons](#)

**BANK EROSION PROCESSES IN STREAMS IN THE U.S.  
MIDWEST**

by  
Tommy Ekamitra Sutarto

A thesis submitted in partial fulfillment  
of the requirements for the Doctor of  
Philosophy degree in Civil and Environmental Engineering  
in the Graduate College of  
The University of Iowa

May 2014

Thesis Supervisor: Professor Athanasios N. Papanicolaou

Copyright by  
TOMMY EKAMITRA SUTARTO  
2014  
All Rights Reserved

Graduate College  
The University of Iowa  
Iowa City, Iowa

CERTIFICATE OF APPROVAL

---

PH.D. THESIS

---

This is to certify that the Ph.D. thesis of

Tommy Ekamitra Sutarto

has been approved by the Examining Committee for the thesis requirement for the Doctor of Philosophy degree in Civil and Environmental Engineering at the May 2014 graduation.

Thesis Committee: \_\_\_\_\_  
Athanasios N. Papanicolaou, Thesis Supervisor

\_\_\_\_\_  
A. Jacob Odgaard

\_\_\_\_\_  
Allen Bradley

\_\_\_\_\_  
Frank Weirich

\_\_\_\_\_  
Christopher Wilson



To my parents and my wonderful wife, Yenny who has patiently accompanied me through difficult times

## ACKNOWLEDGEMENTS

I would like to extend my deepest gratitude to my advisor, Professor Athanasios N. Papanicolaou, for his guidance, encouragement, and patience during my education at The University of Iowa. He has helped me to develop the ability to think critically, as well as introduced me to various approaches for solving any research problem.

I would also like to acknowledge and thank to my committee members, Professors Jacob Odgaard, Allen Bradley, and Frank Weirich, as well as Dr. Christopher Wilson, for their willingness to serve on my Thesis committee and their constructive advice for improving this Thesis.

Additional thanks are extended to the following: Dr. Eddy J. Langendoen for his assistance with the Conservational Channel Evolution and Pollutant Transport System (CONCEPTS) model, which was used in this bank erosion study; Dr. Christopher Wilson for his assistance with the hydrological and sediment data used in this study, as well as for his constructive discussion regarding the PEEPs; Dr. Filippo Bressan for his assistance with the field work at the Camp Cardinal and South Amana sites; and my fellow research team Achilleas Tsakiris, Ben Abban, Ken Wacha, Iordanis Moustakidis, Will Ettema, Bradley Reuter, and Fabienne Bertrand for all their help, constructive discussions, and the good times that we have shared together.

The funding for this research was provided by my Fulbright Scholarship and Professor Papanicolaou's research funding.

## ABSTRACT

Rivers in the U.S. Midwest are dynamic systems that can be natural laboratories for understanding the different modes of bank erosion, namely fluvial erosion, mass erosion, and mass failure. Fluvial and mass erosion are hydraulically driven and semi-continuous, whereas mass failure is episodic and often catastrophic. Being catastrophic, mass failure and its driving mechanisms have received considerable attention comparatively to mass and fluvial erosion. However, the linkage between hydraulically driven erosion and mass failure has not been examined fully. We hypothesize that fluvial and mass erosion affect the memory and response of the system by creating favorable hydrogeomorphic conditions for mass failure.

This dissertation addresses three major shortcomings in the bank erosion literature, including the confusion surrounding critical erosional strength values for mass and fluvial erosion ( $\tau_{c,m}$  and  $\tau_{c,f}$ , respectively). The herein results clearly show that these two parameters are different, with  $\tau_{c,m}$  being three to five times greater than  $\tau_{c,f}$ . Therefore, excluding mass erosion estimates from sediment budgets or stability analyses can lead to significant errors in quantifying or predicting bank retreat and channel geometry. In addition, this study offered a methodological improvement for measuring the  $\tau_{c,m}$  in-situ using Photo-Electric Erosion Pins, which semi-automatically measure mass erosion to generate erosional strength and erodibility values that are currently missing in the literature. This study also addressed the preconceived notion in morphodynamic modeling that bank soil profiles are homogeneous and universal strength/ cohesion parameters adequately represent the bank soil profile. This study shows that bank soil heterogeneity is present and significantly affects bank stability.

Therefore, heterogeneity along a bank face must be assessed in at least three locations to provide adequate input data for bank erosion models. Finally, this study suggests that Factors of Safety for mass failure must be complemented with those for fluvial and mass erosion to avoid underestimating mass failure by as much as 30%. Hence, this study provides agencies like the U.S. Department of Agriculture key data regarding the total contributions from the different modes of bank erosion and channel, itself, to the stream sediment load for strategic targeting of Best Management Practices and in-streams stabilization structures.

## TABLE OF CONTENTS

LIST OF TABLES.....	viii
LIST OF FIGURES.....	ix
LIST OF SYMBOLS.....	xiv
<b>CHAPTERS</b>	
1 PROBLEM STATEMENT.....	1
2 DEFINITION OF EROSIONAL PROCESSES.....	4
2.1 Fluvial Erosion.....	4
2.2 Mass Erosion.....	6
2.3 Mass Failure.....	9
2.4 Interaction among Fluvial Erosion, Mass Erosion and Mass Failure....	10
3 CRITICAL NEEDS.....	14
3.1 Integrated Bank Stability Analysis.....	14
3.2 Differentiations for the Terms $\tau_{c,f}$ , $\tau_{c,m}$ , and $c'$ .....	16
3.3 Distribution of $\tau_{c,f}$ , $\tau_{c,m}$ , and $c'$ along a Bank Profile.....	17
3.4 Current Techniques: Limitations and Opportunities.....	18
3.4.1 Fluvial Erosion.....	18
3.4.2 Mass Erosion.....	20
4 OBJECTIVES AND HYPOTHESES.....	23
5 SITE DESCRIPTION.....	25
6 PROCEDURE AND METHODOLOGY.....	30
6.1 Field Component: Mass Erosional Strength Determination.....	31
6.1.1 PEEP Component Description.....	34
6.1.2 PEEP Calibration.....	38
6.1.3 PEEP and Pressure Transducer Installation.....	39
6.1.4 Preliminary Data Visualization and Interpretation.....	42
6.1.5 PEEP Data Processing.....	44
6.1.6 Near-bank Shear Stress Determination.....	50
6.2 Filed Component: Soil Sample Extraction.....	51
6.3 Laboratory Component.....	54
6.3.1 Soil Index Properties.....	55
6.3.2 Bulk Density Heterogeneity.....	55

6.3.3 Mechanical Strength Measurements.....	57
6.3.4 Fluvial Erosional Rate Measurements.....	58
6.4 Modeling Component.....	64
7 RESULTS.....	68
7.1 Soil Index Properties.....	68
7.2 Bulk Density Heterogeneity.....	68
7.3 Fluvial Erosional Strength.....	74
7.4 Frequency and Magnitude of Mass Erosion .....	80
7.5 Mass Erosional Strength.....	86
7.6 Mechanical Strength.....	88
7.7 Comparison among Mechanical, Mass Erosional, and Fluvial Erosional Strengths.....	90
7.8 Factor of Safety and Bank Retreat.....	90
7.9 Effect of Soil Heterogeneity on Bank Retreat and Stability.....	98
7.10 Sediment Contribution from Different Modes of Bank Erosion.....	100
8 DISCUSSION OF RESULTS AND CONCLUSIONS.....	103
APPENDIX A SOIL TEXTURE AND CLASSIFICATION.....	111
APPENDIX B DIRECT SHEAR EQUIPMENT AND TEST RESULTS.....	114
APPENDIX C PRELIMINARY CONDUIT FLUME TEST.....	121
APPENDIX D CONDUIT FLUME TEST CONDITION .....	125
APPENDIX E CONDUIT FLUME TEST RESULTS.....	131
APPENDIX F PHOTO ELECTRONIC EROSION PIN (PEEP).....	140
APPENDIX G INPUTS AND RESULTS OF CONCEPTS SIMULATION.....	148
APPENDIX H RESULTS OF OTHER STUDIES.....	156
REFERENCES.....	158

## LIST OF TABLES

### Table

6.1	The specification of PEEP used in the present study.....	37
7.1	Soil index properties for Clear Creek bank soils.....	69
7.2	Summary of fluvial erosional strength values obtained from conduit flume tests.....	77
7.3	Summary of erodibility values for fluvial erosion obtained from conduit flume tests.....	78
7.4	Summary of erosion lengths quantified for site 2.....	87
7.5	Mechanical strength parameters for Clear Creek bank soils.....	89
7.6	Bank layers, ground water elevation, and Manning's boundary roughness for CONCEPTS model for site 2.....	92
7.7	Bank soil parameters for CONCEPTS model for site 2.....	93
7.8	Mass of sediment generated from the bank at site 2 during the period between October 1, 2007 and March 28, 2013.....	101
7.9	Percentage of sediment derived from the bank at site 2 during the period between October 1, 2007 and March 28, 2013.....	102
D1	Conduit flume test condition.....	126
F1	Calibration coefficients for PEEPs installed at site 1.....	140
F2	Calibration coefficients for PEEPs installed at site 2.....	141
H1	Results of other studies using undisturbed soils.....	157

## LIST OF FIGURES

Figure		
2.1	Fluvial erosion.....	5
2.2	A conceptual figure showing different modes of bank erosion.....	7
2.3	An idealistic illustration of fluvial and mass erosion .....	8
2.4	Mass erosion.....	8
2.5	Conceptual model of erosional process dominance at the watershed scale	11
3.1	Mass failure in the upper Minnesota River.....	15
3.2	Illustration of the modes of bank erosion: from fluvial to mass failure.....	16
3.3	Devices for fluvial erosion study. (a) Jet device. (b) Straight mini-flume. (c) Rotating cylinder. (d) Race-way shaped flume.....	20
5.1	Study site: (a) The Clear Creek, IA watershed. (b) The headwaters site (site 1). (c) The mouth site (site 2). (d) Cross-sections at site 1. (e) Cross-sections at site 2.....	26
5.2	Historical planform changes in Clear Creek from 1937 to present.....	27
6.1	Photo Electronic Erosion Pin (PEEP).....	33
6.2	PEEP exposure length after a flood event.....	35
6.3	Data loggers and solar panels attached to a pole on the nearby floodplain...	36
6.4	A reference PEEP was secured on the nearby floodplain.....	37
6.5	Calibration of Photo Electronic Erosion Pin (PEEP).....	39
6.6	PEEP installation. (a) Site 1. (b) Site 2.....	41
6.7	Time series of water stage and PEEP outputs deployed at site 2. (a) Water stage. (b) Outputs from PEEP B2, $V_{cs}$ , and the reference PEEP, $V_{rp}$ , .....	45
6.8	Methodological procedure for estimating PEEP exposure length.....	46



6.9	Comparison between non-moving-averaged and moving-averaged exposure length. (a) Time series of exposure length without performing moving-average analysis. (b) Time series of moving-averaged exposure length.....	49
6.10	Sample extraction. (a) A sketch of the sample extraction scheme applied for the left and right banks at site 1 and 2. (b) Extraction of soil blocks from the right bank, cross section CC 1 at site 2. Inset: Soil was wrapped in cheese cloth before being transported from the field to the laboratory.....	53
6.11	Gamma attenuation test. (a) Selective soil samples, from the crest, midbank, and toe of the right bank, cross section CC 1 at site 2. (b) The radioactive source emitted collimated gamma radiation through the sample.....	56
6.12	A photograph showing the conduit flume used in the present study.....	59
6.13	Dimensions of the conduit flume and its components.....	60
6.14	Bed load fraction as a function of particle diameter, $d$ , and dimensionless shear stress, $\tau^*$ . ....	65
6.15	Representative cross-sections (facing downstream) with average bank soil properties: (a) Cross section SA 2, site 1. (b) Cross section CC 1, site 2....	66
7.1	Twelve (12) oven-dried bank soil samples from site 1 and 2.....	70
7.2	Clear Creek bank soils. Fresh sand was deposited on the flood plain at site 2 after a flood event.....	71
7.3	Bulk density profile obtained from gamma attenuation analyses.....	73
7.4	Six examples of the conduit flume test results for site 1. The tested soil samples were extracted from cross section SA 2 at site 1: (a) Left bank-crest. (b) Left bank-midbank. (c) Left bank-toe. (d) Right bank-crest. (e) Right bank-midbank. (f) Right bank-toe.....	75
7.5	Six examples of the conduit flume test results for site 2. The tested soil samples were extracted from cross section CC 1 at site 2: (a) Left bank-crest. (b) Left bank-midbank. (c) Left bank-toe. (d) Right bank-crest. (e) Right bank- midbank.(f) Right bank-toe.....	76
7.6	Time series of water stage and exposure length for PEEPs at site 1. (a) Water stage. (b) Moving-averaged and estimated exposure length for PEEP A1, (b) PEEP A2, and (c) PEEP A3.....	82

7.7	Time series of water stage and exposure length for PEEPs at site 2. (a) Water stage. (b) Moving-averaged and estimated exposure length for PEEP B1, (c) PEEP B2, (d) PEEP B3, and (e) PEEP B4.....	83
7.8	Time series of estimated exposure length along with synchronous near bank shear stress at site 2. (a) Result for the crest (PEEP B1), (b) upper midbank (PEEP B2), (c) lower midbank (PEEP B3), and (d) toe of the bank (PEEP B4).....	85
7.9	Determination of mass erosional strength, $\tau_{c,m}$ .....	87
7.10	Factors of safety for mass failure, $FS_{mf}$ , predicted by CONCEPTS. (a) Left bank. (b) Right bank.....	94
7.11	Factors of safety for fluvial erosion, $FS_f$ , predicted by CONCEPTS. (a) Left bank-crest. (b) Left bank-midbank. (c) Left bank-toe.....	96
7.12	Factors of safety for fluvial erosion, $FS_f$ , predicted by CONCEPTS. The simulation was performed for six (6) cross-sections at site 2. The time window herein was focused for the period prior to, during and right after the June 20, 2009 flood event: (a) Right bank-crest. (b) Right bank-midbank. (c) Right bank-toe.....	97
7.13	The bank retreat at cross section CC 6, site 2, simulated by CONCEPTS...	98
7.14	The bank retreat at cross section CC 6, site 2, simulated by CONCEPTS: (a) Homogeneous banks with the entire bank soils are identical to crest soils. Planar failure occurred at the right bank. (b) Homogeneous banks with the entire bank soils are identical to toe soils.....	99
A1	Size distribution for the bank soils extracted from site 1 and site 2.....	112
A2	USDA textural classification for twelve (12) bank soil samples extracted from site 1 and 2.....	113
B1	A direct shear test instrument (ELE D-300A series). (1) shear box; (2) container; (3) proving ring; (4) manual control; (5) vertical LVDT transducer (0.4232 v/mm); (6) horizontal LVDT transducer (0.4173 v/mm); (7) LVDT transducer (0.7378 v/mm) for measuring the deflection of proving ring; (8) load hanger. Inset: A soil specimen was carefully placed into the shear box before testing.....	114
B2	Result of direct shear test for soil sample originated from the crest of the left bank, cross section SA2 at site 1.....	115

B3	Result of direct shear test for soil sample originated from the midbank of the left bank, cross section SA2 at site 1.....	115
B4	Result of direct shear test for soil sample originated from the toe of the left bank, cross section SA2 at site 1.....	116
B5	Result of direct shear test for soil sample originated from the crest of the right bank, cross section SA2 at site 1.....	116
B6	Result of direct shear test for soil sample originated from the midbank of the right bank, cross section SA2 at site 1.....	117
B7	Result of direct shear test for soil sample originated from the toe of the right bank, cross section SA2 at site 1.....	117
B8	Result of direct shear test for soil sample originated from the crest of the left bank, cross section CC1 at site 2.....	118
B9	Result of direct shear test for soil sample originated from the midbank of the left bank, cross section CC1 at site 2.....	118
B10	Result of direct shear test for soil sample originated from the toe of the left bank, cross section CC1 at site 2.....	119
B11	Result of direct shear test for soil sample originated from the crest of the right bank, cross section CC1 at site 2.....	119
B12	Result of direct shear test for soil sample originated from the midbank of the right bank, cross section CC1 at site 2.....	120
C1	Water-concentration response to the increase of discharge in the conduit flume.....	122
C2	Preliminary conduit flume run to determine the adjustment time for flow meter due to flow increment.....	123
C3	An example of conduit flume run.....	124
E1	Fluvial erosional strength and erodibility coefficient .....	131
F1	Relation between normalized cell series output, $R_r$ , and PEEP exposure length, $L$ , for PEEPs installed at site 1.....	140
F2	Relation between normalized cell series output, $R_r$ , and PEEP exposure length, $L$ , for PEEPs installed at site 2.....	141

F3	Voltage signal recorded from PEEP A1, A3, and reference PEEP at site 1 during deployment period.....	142
F4	Unprocessed exposure length recorded from PEEPA1 and A3 at site 1 during deployment period.....	143
F5	Processed exposure length without moving average analysis for PEEP A1 and A3 at site 1 during deployment period.....	144
F6	Voltage signal recorded from PEEP B1, B2, B3, and B4 along with their reference cells at site 2 during deployment period.....	145
F7	Unprocessed exposure length recorded from PEEP B1, B2, B3, and B4 at site 2 during deployment period.....	146
F8	Processed exposure length without moving average analysis for PEEP B1, B2, B3, and B4 at site 2 during deployment period.....	147
G1	CONCEPTS inputs. (a) Hydrograph. (b) Water level.....	149
G2	Initial groundwater profile based on Liang and Zang (2012) near the bank at site 2.....	150
G3	Near bank shear stress, $\tau_w$ , predicted by CONCEPTS for the left bank of six (6) cross-sections at site 2.....	151
G4	Near bank shear stress, $\tau_w$ , predicted by CONCEPTS for the right bank of six (6) cross-sections at site 2.....	152
G5	Measured and model-predicted bank cross sections for site 2. (a) Cross section CC1. (b) Cross section CC2. (c) Cross section CC3. (d) Cross section CC4. (e) Cross section CC5. (f) Cross section CC6.....	153

## LIST OF SYMBOLS

### Symbol

$A$	=	flow area ( $m^2$ )
$A_c$	=	clay activity
$A_s$	=	surface area of soil sample ( $m^2$ )
$f$	=	friction factor
$C$	=	water sediment concentration ( $kg/m^3$ ) or ( $mg/L$ )
$c_1, c_2, \dots, c_6$	=	calibration coefficients
$C_{avg}$	=	average water sediment concentration ( $kg/m^3$ )
$clay$	=	percent clay (%)
$c'$	=	effective cohesion or mechanical strength (Pa)
$D_{50}$	=	mean particle diameter (m)
$d_{eff}$	=	effective diameter (m)
$d_h$	=	hydraulic diameter (m)
$E_f$	=	fluvial erosion rate ( $kg/m^2/s$ )
$E_m$	=	mass erosion rate ( $kg/m^2/s$ )
$F_w$	=	hydrostatic confining force exerted into the bank profile (N)
$FS_f$	=	factor of safety for fluvial erosion
$FS_m$	=	factor of safety for mass erosion
$FS_{mf}$	=	factor of safety for mass failure
$g$	=	gravitational acceleration ( $m/s^2$ )
$h$	=	elevation of water table above the bottom of the aquifer (m); water stage (m)
$h_o$	=	constant river stage (m)

- $K_s$  = saturated hydraulic conductivity (m/s)  
 $L$  = Length of the slice plane base (m); tube exposure length (m)  
 $LL$  = liquid limit (%)  
 $l$  = dewatering length (m)  
 $M_f$  = erodibility coefficient in term of fluvial erosion (kg/m<sup>2</sup>/s)  
 $M_m$  = erodibility coefficient in term of mass erosion (kg/m<sup>2</sup>/s)  
 $m, m'$  = experimental exponent assumed to equal 1  
 $n$  = porosity  
 $P$  = wet perimeter (m)  
 $PI$  = plasticity index (%)  
 $PL$  = plastic limit (%)  
 $P_c$  = fractions of clay  
 $P_{vfs}$  = fraction of very fine sand  
 $Q$  = flow rate (m<sup>3</sup>/s)  
 $q_o$  = recharge rate under steady state condition (m/s)  
 $R$  = hydraulic radius (m)  
 $R_r$  = normalized output of photo-resistant PEEP  
 $R_o$  = Rouse number  
 $Re_{d_{eff}}$  = Reynolds number in term of effective diameter  
 $S$  = bed slope  
 $S_f$  = Friction slope  
 $S_r$  = soil shear strength (Pa)  
*silt-clay* = percent of particles having diameter less than 0.063 mm (%)

- $U$  = bulk velocity (m/s)  
 $u$  = soil pore water pressure (Pa)  
 $u_*$  = friction velocity (m/s)  
 $V_{CS}$  = cell series output (millivolt)  
 $V_{rP}$  = reference PEEP output (millivolt)  
 $W$  = weight (N)  
 $w_s$  = average settling velocity (mm/s)  
 $X$  = horizontal extent of the aquifer (m)  
 $x$  = horizontal coordinate (m)  
 $\alpha$  = angle of planar failure surface (degree)  
 $\beta$  = permeability coefficient ( $s^{-1}$ )  
 $\Delta L$  = erosion depth (cm)  
 $\Delta C_{avg}$  = difference in average concentration ( $kg/m^3$ )  
 $\varepsilon$  = wall roughness (m)  
 $\kappa$  = von Karman constant  
 $\nu$  = kinematic viscosity of water ( $1.01E-06 m^2/s$ )  
 $\rho_w$  = mass density of water ( $kg/m^3$ )  
 $\rho_{bulk}$  = soil bulk density ( $kg/m^3$ )  
 $\rho_s$  = soil particle density ( $kg/m^3$ )  
 $\sigma$  = normal stress (Pa)  
 $\tau_{c,f}$  = fluvial erosional strength (Pa)  
 $\tau_{c,m}$  = Mass erosional strength (Pa)  
 $\tau_{c, estimated}$  = erosional strength estimated from an empirical equation (Pa)

$\tau_{c \text{ flume}}$  = erosional strength obtained from a flume test (Pa)

$\tau_w$  = near bank or side-wall shear stress (Pa)

$\phi^b$  = angle expressing the rate of increase in shear strength relative to the matric suction (degree)

$\phi'$  = effective internal friction angle (degree)



## CHAPTER 1 PROBLEM STATEMENT

Bank erosion in Midwestern streams has caused severe and extensive damage (on the scale of \$1.1 billion in Western Iowa alone; Hadish, 1994) to highway and county road infrastructure including bridge abutments, pipelines, and fiber-optic lines, as well as loss of farmland adjacent to the stream channel. Government agencies, such as the Iowa Department of Transportation (IDOT) and the Hungry Canyons Alliance (HCA), have constructed more than 700 weirs, flumes, and other types of grade control structures in Iowan streams to stabilize the channel reaches and prevent further damage to downstream infrastructure. However bank erosion is expected to continue in Iowa due to several factors including the lack of alluvial sand delivery and significant anthropogenic activities (Simon and Rinaldi, 2000).

This ongoing bank erosion phenomenon prompts the following questions:

1. Can we mitigate bank erosion?
2. What are the dominant modes of bank erosion?
3. Which monitoring and laboratory methods can be used to further improve our understanding of the different bank erosion modes and improve the parameterization?
4. Can researchers and engineers develop a reliable model based on field-laboratory observations to predict bank erosion under different hydrologic and geomorphologic conditions?

Current efforts by county and city agencies include some monitoring of bank erosion at highway and bridge crossings using established procedures, such as surveys, and checklists for a “healthy bank” based on slope and other criteria, which have been

reasonably effective. However, a method to evaluate holistically the eminent problem of bank erosion is lacking. One of the primary reasons for this deficiency stems from the lack of field- and laboratory-oriented research related to the processes triggering and producing bank erosion.

Moreover, previous studies have shown that bank erosion not only has detrimental effects on infrastructure but it is a significant contributing source to the total sediment load in streams with disadvantageous effects on water quality and aquatic life (e.g., Walling et al., 1999; Simon and Klimetz, 2008; Wilson et al., 2008). Sedimentation of bank-derived material has been shown to change streambed topography and hydrology and decrease dissolve oxygen in stream water. This may adversely affect critical fish spawning habitat and threat species richness (e.g., Boulton and Suter, 1986; Gauge et al., 2004). As a result, different streambank stabilization practices have been adopted in many riverine systems to mitigate bank erosion (e.g., Biedenharn et al., 1997; Flosi et al., 2010). However, an established methodology for implementing and assessing bank stabilization practices is still under-developed (e.g., Simon and Pollen, 2006).

In a nutshell, to address the aforementioned problems of bank erosion, a deeper understanding of the main modes of bank erosion, their interrelation, and the methods for quantifying these different modes of bank erosion are still needed.

The main purpose of this study was twofold. First, to develop a combined field-laboratory method for measuring bank soil resistance (i.e., shear strengths) to various types of bank erosion (e.g., fluvial erosion, mass erosion, and mass erosion). Second, to implement the strength values obtained from the above method into a hydrodynamic/

bank erosion model for predicting the stability and the retreat of stream banks due to the interaction of the different types of bank erosion.

## CHAPTER 2 DEFINITION OF EROSIONAL PROCESSES

Bank retreat is the integrated product of three erosional processes, namely fluvial erosion, mass erosion, and mass failure (American Society of Civil Engineers, ASCE, Task Committee, 1998; Huang et al., 2006; Rinaldi and Darby, 2008). In this chapter, these three modes of bank erosion are discussed briefly in terms of their definitions, triggering mechanisms, key parameters of resistance, and the interconnection among those modes of bank erosion. This discussion will provide a theoretical foundation for the later analysis, in particular for developing an integrated bank stability analysis and predicting bank retreat rates, which are the concerns in this study.

### 2.1 Fluvial Erosion

Fluvial or surface grain erosion, which is the lower limit of bank erosion, represents the entrainment of individual soil grains or flocs (Fig. 2.1) from the bank face due to the hydrodynamic shear of the streamflow (e.g., Lawler, 1993; Gaskin et al., 2003; Papanicolaou et al., 2006; Rinaldi and Darby, 2008). Fluvial erosion is considered a “low amplitude” erosion process that is quasi-continuous and commences when the fluid shear forces acting over the bank face supersede the resistance offered by the soil grains or flocs (e.g., Millar and Quick, 1998). A surrogate measure of this resistance is the *fluvial erosional strength*,  $\tau_{c,f}$  (e.g., Partheniades, 1965; Kandiah, 1974), which is a microscale quantity. For cohesive bank soils, this resistance is the product of the inter-particle forces of attraction or repulsion, including electrostatic, van der Waals, hydration, and biological forces (e.g., Arulanandan, 1975; Commission of the European Community, 1993; Van Klaveren and McCool, 1998; Ravisangar et al., 2005; Papanicolaou et al., 2007; Grabowski et al., 2011 ).

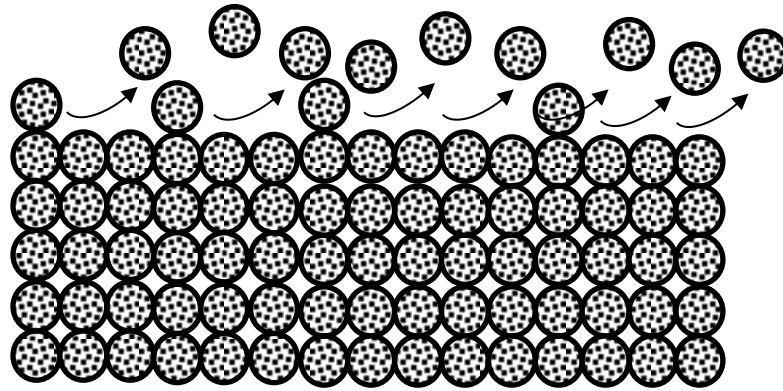


Figure 2.1 Fluvial erosion.

The rate of fluvial erosion,  $E_f$ , in  $\text{kg/m}^2/\text{s}$ , can be determined by an excess shear stress formula similar to the one introduced by Kandiah (1974):

$$E_f = M_f \left( \frac{\tau_w}{\tau_{c,f}} - 1 \right)^m \quad (2.1)$$

where  $M_f$  ( $\text{kg/m}^2/\text{s}$ ) is the erodibility coefficient;  $\tau_w$  (Pa) is the near bank or side-wall shear stress exerted by the flow on the bank face; and  $m$  is assumed to be equal to 1 for most cohesive soils that are consolidated and “aged” for more than 24 days, such as those found in most banks (e.g., Vermeyen, 1995).

The stability of a streambank against fluvial erosion can be expressed with a factor of safety,  $FS_f$ , that defines the relationship between the resisting force,  $\tau_{c,f}$ , and the driving hydrodynamic force,  $\tau_w$  (e.g., Millar and Quick, 1998).  $FS_f$  can be expressed as follows:

$$FS_f = \frac{\tau_{c,f}}{\tau_w} \quad (2.2)$$

The bank face will likely experience fluvial erosion when  $FS_f < 1$ . In contrast, the bank soils will be resistant to fluvial action if  $FS_f > 1$ .

## 2.2 Mass Erosion

The second mode of bank erosion is mass erosion, which is also a quasi-continuous process (Vermeyen, 1995), however, it requires higher-magnitude hydrodynamic shear stresses to occur than fluvial erosion (Huang et al., 2006). Due to the higher shear forces, mass erosion proceeds at a higher rate of erosion and results in larger retreats of the bank soil comparatively to fluvial erosion but smaller retreats with respect to mass failure. It is classified as an “intermediate amplitude” erosional process (e.g., Gaskin et al., 2003). The retreat length scale for fluvial erosion is usually in millimeters, whereas, for mass erosion is in centimeters and for mass failure in meters (Fig. 2.2).

A conceptual schematic, found in Figure 2.3, illustrates the sequence of occurrence of fluvial (red circle-marked line) and mass erosion (blue square-marked line) processes for a homogeneous soil as function of the shear stress magnitude. Clearly, there is a regime change in the mode of bank erosion from fluvial to mass erosion once the shear stress increases and surpasses a threshold value for the onset of mass erosion, which is called *mass erosional strength*,  $\tau_{c,m}$ . This change is depicted by the slope variation of the erosion line in Figure 2.3. The slope of the segment corresponding to mass erosion is higher than the one for fluvial erosion, indicating higher erosion rates or retreat rates. During mass erosion due to the higher rate of erosion, the retreat manifests as the detachment of soil chunks or clods (Fig. 2.4) from the bank profile or with the removal of soil layers in the form of “thin sheets” (e.g., Mazurek et al., 1999; Gaskin et al., 2003; Winterwerp and van Kesteren, 2004; Huang et al., 2006; Kothiyari and Jain, 2008; Winterwerp et al., 2012).

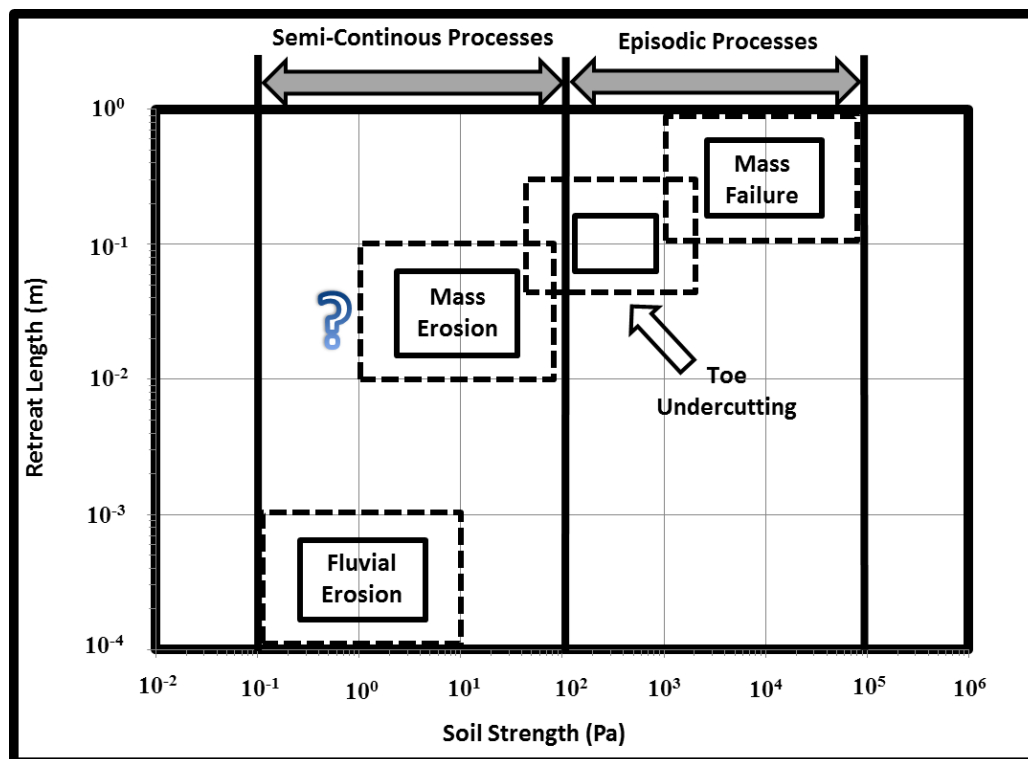


Figure 2.2 A conceptual figure showing different modes of bank erosion.

Similar to fluvial erosion, the mass erosion rate,  $E_m$ , can be determined by an excess shear stress formula:

$$E_m = M_m \left( \frac{\tau_w}{\tau_{c,m}} - 1 \right)^{m'} \quad (2.3)$$

and the stability of a streambank against mass erosion can also be expressed with a factor of safety,  $FS_m$ , that is the ratio between the resisting force,  $\tau_{c,m}$ , and the driving hydrodynamic force,  $\tau_w$ .  $FS_m$  can be written as follows:

$$FS_m = \frac{\tau_{c,m}}{\tau_w} \quad (2.4)$$

Clods or chunks of soils will detach from the bank face (Fig. 2.4) when  $FS_m < 1$ . In contrast, the bank soil will be resistant to mass erosion (but it is likely to experience

fluvial erosion) when  $FS_m > 1$  and  $FS_f < 1$ .

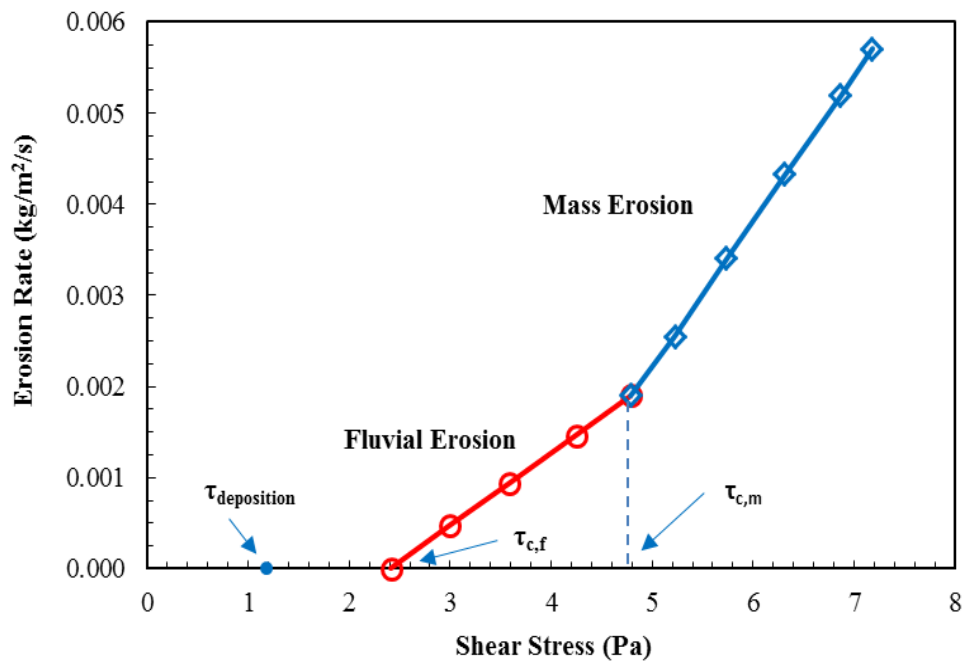


Figure 2.3 An idealistic illustration of fluvial and mass erosion (redrawn from Vermeyen, 1995). Fluvial erosion (red circle-marked line) occurs at the lower range of shear stress while mass erosion (blue square-marked line) ensues at the upper range of shear stress.

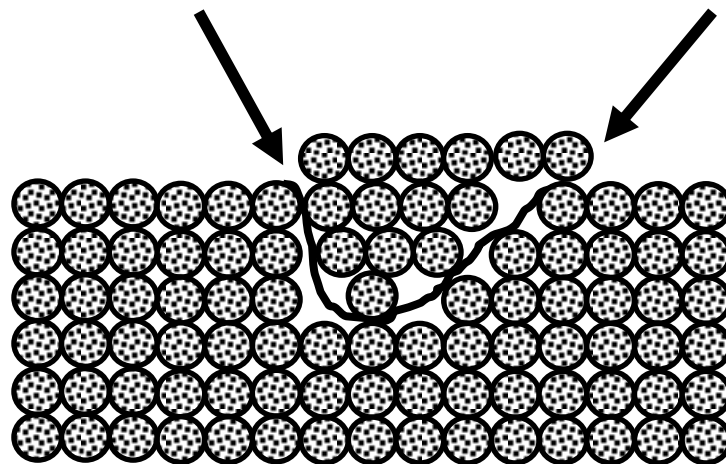


Figure 2.4 Mass erosion (redrawn from Winterwerp and Van Kesteren, 2004).



### 2.3 Mass Failure

The third mode of bank erosion is mass failure, which denotes the upper limit of bank retreat, and it is considered a “high amplitude” erosion process in terms of its contributions to the instream sediment budget (e.g., Darby et al., 2007). Mass failure usually occurs with the collapse or slumping of soil blocks “en masse” along an embedded plane (planar failure) due to different but often interrelated mechanisms, such as, the development of positive pore water pressure within the bank profile (e.g., Thorne, 1982; Pizzuto, 1984; Millar and Quick, 1998; Simon and Rinaldi, 2000; Simon and Collison, 2002); the rapid drawdown of water stage (e.g., Langendoen, 2000, 2010); and the occurrence of high seepage gradient forces (e.g., Chu-Agor et al., 2009; Midgley et al., 2012; Fox and Felice, 2013). In addition to slumping, there are other forms of mass failure, such as rotational, piping or sapping (e.g. Thorne, 1982; Langendoen, 2000), all of which occur at discrete times and more often during the later stages of a runoff event (e.g., Lawler et al., 1997; Rinaldi and Darby, 2008).

The en masse collapse of a soil block is determined by the relationship between its bulk weight and different resisting forces, such as those derived from root vegetation and the temporary confining pressure of the stream water that is present during high stages (e.g., Pollen and Simon, 2005; Pizzuto, 2009), but more predominantly its soil shear strength,  $S_r$ , integrated over the slip plane area. According to the Mohr-Coulomb theory, the shearing strength of a soil block,  $S_r$ , is dependent on the internal friction angle,  $\phi'$ , and a macroscale parameter,  $c'$ , in Pa, that is also known in the literature as the *soil mechanical strength* (e.g., Millar and Quick, 1998; Pollen and Simon, 2005; Pizzuto,

2009). The soil shear strength,  $S_r$ , in Pa, is defined as follows (Fredlund and Rahardjo, 1993):

$$S_r = c' + \sigma \tan \phi' - u \tan \phi^b \quad (2.5)$$

where  $\sigma$  (Pa) is the normal stress produced by the weight of the soil block;  $\phi'$  (degrees) refers to the internal friction angle;  $u$  (Pa) is the soil pore water pressure; and  $\phi^b$  (degrees) is the angle expressing the rate of increase in shear strength relative to the matric suction. When the bank is saturated, matric suction diminishes and  $\tan \phi' = \tan \phi^b$ .

When quantifying the factor of safety,  $FS_{mf}$ , for a soil block in a bank profile, the block is first subdivided into multiple vertical slices to ensure adequate representation of all soil layering found in the block. The driving and resisting forces are then calculated for each slice and integrated over the whole block. The factor of safety can then be estimated as follows (Langendoen et al., 2009):

$$FS_{mf} = \frac{\sec \alpha \sum_{j=1}^K L_j S_{rj}}{\tan \alpha \sum_{j=1}^K W_j - F_w} \quad (2.6)$$

where  $\alpha$  (degrees) is the angle of the planar failure surface;  $K$  is the total number of block slices;  $j$  denotes the slice number;  $L$  (m) is the length of the slice plane base;  $W$  (N) is the slice weight; and  $F_w$  (N) is the hydrostatic confining force exerted on the bank profile. The bank is considered stable if  $FS_{mf} > 1$ , whereas the bank is unstable if  $FS_{mf} < 1$ .

#### **2.4 Interaction among Fluvial Erosion, Mass Erosion and Mass Failure**

The three erosion modes described in the previous sections (fluvial erosion, mass erosion and mass failure) are likely to act in conjunction. Particularly in the middle and lower reaches of drainage basins, bank retreat is likely to be driven by a combination of

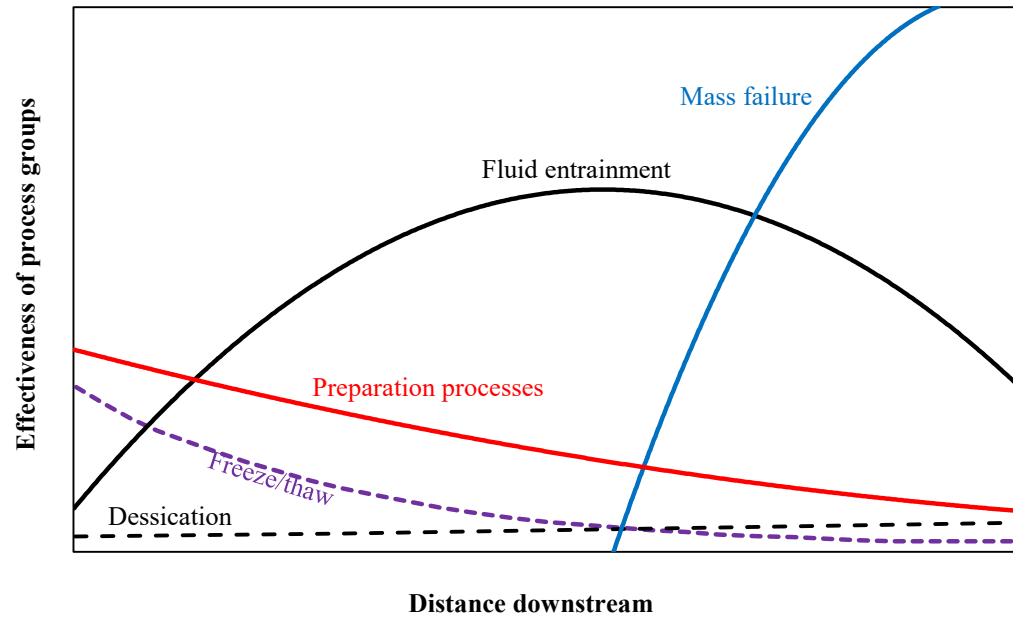


Figure 2.5 Conceptual model of erosional process dominance at the watershed scale (Rinaldi and Darby, 2008; After Lawler, 1992).

the hydraulic forces of the flow, and mass failures driven by gravity (Fig. 2.5). Generally, mass failure will most likely dominate bank retreat in the lower reaches of a watershed where the critical bank height is more often exceeded (ASCE Task Committee, 1998). On the other hand, fluvial and mass erosion will dominate in the middle reaches of a watershed where the stream power, and therefore, the shearing action of flow is highest (Fig. 2.5, Lawler, 1992). This conceptual figure provides some general insight into the dominant bank erosion process and the potential interaction among those different modes at different location in a watershed. Although this conception is not always valid as many other factors such as bank soil composition, seepage, groundwater dynamics, and the presence of roots may dictate the dominant mode of erosion at certain locations within a watershed, the figure provides a good representation of the relationship between different processes along a river continuum.

In the middle and lower reaches of a drainage basin, fluvial and mass erosion can play an important role as a triggering mechanism for mass failure (Langendoen, 2000; Simon and Pollen, 2006). The two processes, which most often occur at the basal layer of the bank, may cause bank steepening and toe undercutting, leading to mass failure (e.g., Hilldale, 2001). From a modeling perspective, the integration of the three bank erosion modes in a single framework is very important in order to estimate correctly the timing and frequency of mass failure, as well as the bank retreat (Rinaldi and Darby, 2008).

To capture fully the complex interactions between the three modes of bank erosion, it is necessary to investigate bank changes at the intra-event scale. Logistical and safety concerns usually limit the frequency of monitoring to relatively coarse timescales, at best perhaps before and after individual flow events. This is problematic because the “flow event window” is not the same thing as the “bank erosion event window”, making it difficult to resolve erosion thresholds, timing and rates (Lawler, 2005). Numerical modeling approaches can provide alternative ways to solve the problem.

Few attempts have been made to investigate bank erosion dynamics combining fluvial erosion, pore water pressure changes, and bank stability into a single, integrated, modeling framework. Simon et al. (2003) used three models (*Seep/w* in combination with the *ARS Toe-Erosion* and *Bank-Stability* models) to simulate bank response to flow events, employing a series of constructed, rectangular-shaped, hydrographs of a specified height and duration.

Alternative examples of numerical simulations for bank retreat in which fluvial erosion, seepage, and mass failure models were fully integrated are the recent studies on the Sieve and Cecina Rivers in Italy (Dapporto et al., 2003; Rinaldi and Darby, 2008). Most noteworthy is that these simulation results were qualitatively distinct from conceptual models of bank sediment delivery processes founded on event-scale analyses. Previous studies have mostly emphasised mass failure as a quasi-catastrophic event, which typically occurs on the falling limb of event hydrographs. In contrast, some of these simulations suggested that mass failure can occur as a series of erosion episodes, at frequent intervals as progressive fluvial erosion undermines the bank and triggers failures throughout the flow event. These simulations demonstrated how modeling the interactions between hydraulic and geotechnical processes can predict qualitatively different outcomes (in terms of the nature of the onset and timing of bank sediment delivery to the alluvial sedimentary system) compared to the results derived from existing models that treat these processes in isolation.

## CHAPTER 3 CRITICAL NEEDS

### 3.1 Integrated Bank Stability Analysis

Different streambank stabilization practices have been adopted in many riverine systems worldwide to mitigate bank erosion (e.g., Biedenharn et al., 1997; Flosi et al., 2010). An established methodology for implementing and assessing bank stabilization practices is still, however, under-developed (e.g., Simon and Pollen, 2006). This, in part, stems from the fact that a deep understanding of the main modes of bank erosion, as well as their interrelation and the methods for quantifying them, are still lacking.

Currently, few established approaches to assess bank stability consider all three modes of bank erosion, namely fluvial erosion, mass erosion, and mass failure (e.g., Millar and Quick, 1998; Wynn and Mostaghimi, 2006; Langendoen et al., 2009; Pizzuto, 2009) and in most cases, the stability analysis of a bank is only based on mass failure estimations.

Most attention has been given to mass failure, the upper limit of bank erosion, while only few studies have considered fluvial and mass erosion (Papanicolaou et al., 2006; Rinaldi and Darby, 2008). It is relatively easier to identify and quantify catastrophic mass failure, which typically occurs as falling slumps or sliding layers of bank soil (Fig. 3.1) during infrequent time periods. Yet, it is difficult to monitor fluvial and mass erosion, which occur at the grain or clod scale and on a rather continuous basis (Fig. 3.2).

It is not surprising, therefore, that less attention has been given to mass erosion and fluvial erosion even though, in many instances, they have been shown to affect bank stability by being a precursor to mass failure. Several field observations (e.g.,

Lawler,1995; Pizzuto, 2009) and modeling studies (e.g., Duan, 2005; Darby et al., 2007; Rinaldi and Darby, 2008) have revealed that fluvial erosion leads to toe undercutting, resulting in the removal of basal bank support, the formation of cantilevers, and eventually mass failure (e.g., Hilldale, 2001). These studies have highlighted the importance of including fluvial erosion and mass erosion to bank stability analysis due to their quasi-continuous nature and interconnection with mass failure.

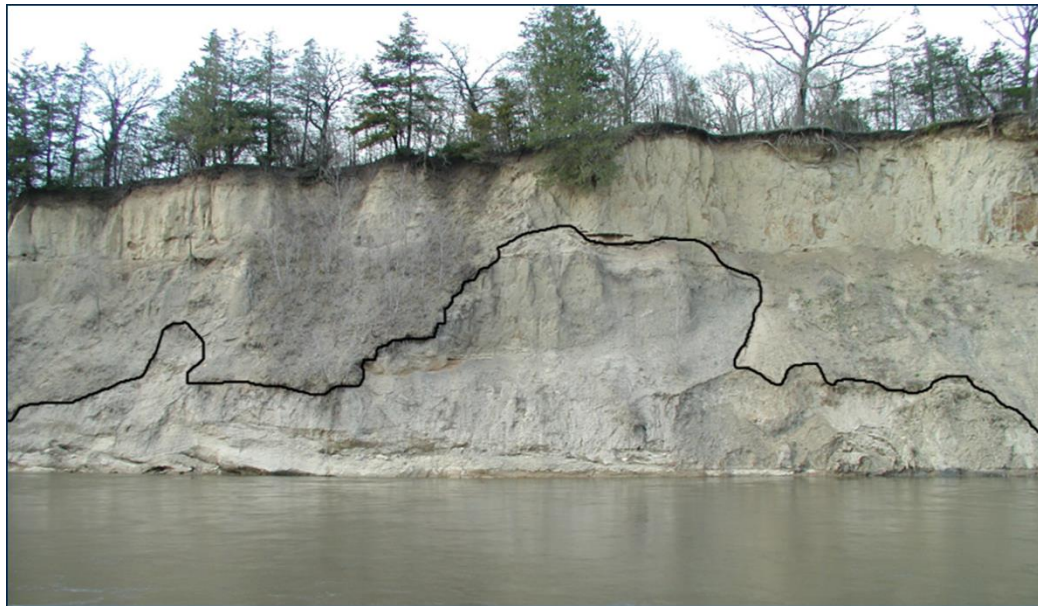


Figure 3.1 Mass failure in the upper Minnesota River (source: Dave Thomas).

In several numerical modeling studies (e.g., Darby et al., 2007; Rinaldi et al., 2008; Luppi et al., 2009; Midgley et al., 2012) the role of mass erosion has either not been considered or has been used interchangeably with fluvial erosion (e.g., Rinaldi et al., 2008). In some cases due to the absence of data for quantifying mass erosion, the erodibility coefficient,  $M_m$ , values were “adjusted” to estimate retreat lengths that were

comparable to measured ones (e.g., Van De Wiel and Darby, 2004; Darby et al., 2007; Rinaldi et al., 2008). As a result, bank retreat and, thus, the sediment load can be under- or over-estimated depending on the problem conditions under investigation (e.g., Luppi et al., 2009; Midgley et al., 2012).

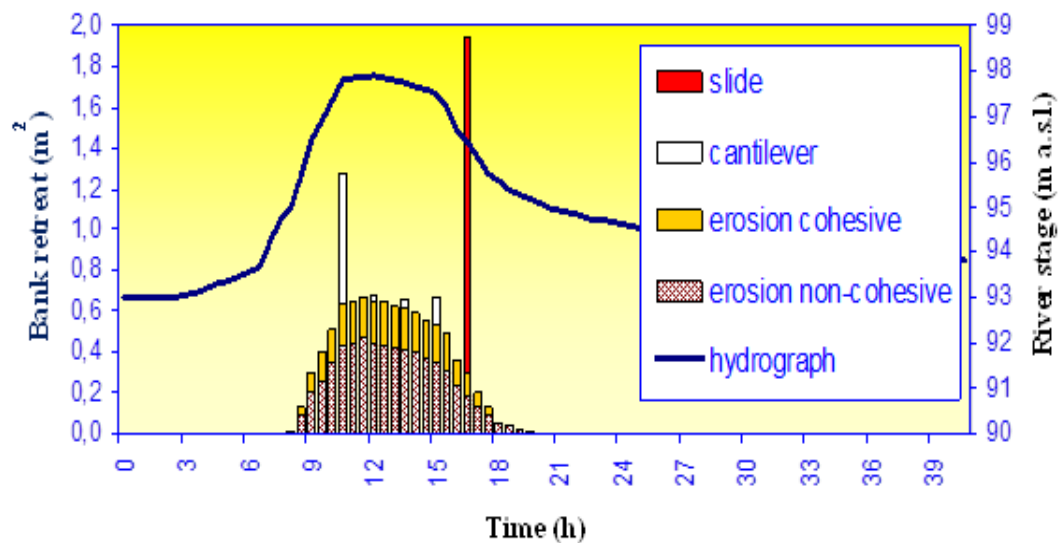


Figure 3.2 Illustration of the modes of bank erosion: from fluvial to mass failure (source: Thanos Papanicolaou and Massimo Rinaldi).

### 3.2 Differentiations for the Terms $\tau_{c,f}$ , $\tau_{c,m}$ , and $c'$

Further complicating matters in bank stability studies is the confusion surrounding the erosional processes and their corresponding strength terms, namely  $\tau_{c,f}$ ,  $\tau_{c,m}$ , and  $c'$ , across different disciplines (e.g., geomorphology, agricultural and civil engineering, physical geography). These terms have been used arbitrarily to determine bank erosion or failure without a full phenomenological grasp of their meanings and ranges of applicability. This mix-up has been triggered, in parts, by the lack of reliable datasets



recording the differences between fluvial erosional, mass erosional, and mechanical strengths for soils extracted from the same sites (Schofield, 1998). Preliminary evidence from past research (e.g., Kamphuis and Hall, 1983; Zreik et al., 1998; Huang et al., 2006), however, shows that  $c'$  can range anywhere from 1 to 3 orders of magnitude greater than  $\tau_{c,f}$ , but a systematic evaluation is still lacking. In addition, there have been several occasions reported in the literature, where the differences in the  $\tau_{c,m}$  and  $\tau_{c,f}$  either have not been fully understood or have been presumed to be insignificant, even though in some recent studies (Gaskin et al., 2003; Huang et al., 2006; Kothiyari and Jain, 2008)  $\tau_{c,m}$  has been found to be 3 to 6 times larger than  $\tau_{c,f}$ . In this study, a number of systematic in-situ and laboratory tests and analyses were performed on bank soil samples from the same site to examine their fluvial erosional, mass erosional, and mechanical strengths. These data have allowed us to quantify the magnitude differences among the different measures of soil strength and to improve our understanding of the different modes of bank erosion and the importance of integrating them in bank stability analysis.

### 3.3 Distribution of $\tau_{c,f}$ , $\tau_{c,m}$ , and $c'$ along a Bank Profile

Few studies provide the distribution of  $\tau_{c,f}$ ,  $\tau_{c,m}$ , and  $c'$  along a bank profile and its characteristic locations, or layers (i.e., crest, midbank, and toe). Instead most studies typically assume homogeneous, well compacted soils along the bank profile but this may not always be the case especially in streams subjected to frequent flash floods or streams found in estuarine environments (Papanicolaou and Maxwell, 2006). In both cases, crest soils may contain heterogeneous soft soil deposits (e.g., Wilson et al., 2012) and exhibit different  $\tau_{c,f}$ ,  $\tau_{c,m}$ , and  $c'$  values compared to those, for example, found at the toe or

midbank of the bank profile. To address this issue, this study provided a systematic analysis, where 60 soil samples were extracted from different locations along the downslope of a bank profile (e.g., crest, midbank, and toe) (see section 6.2) and were analyzed in the laboratory for their  $c'$  and  $\tau_{c,f}$  values (see section 6.3.3 and 6.3.4). This study also provides a novel methodology for quantifying  $\tau_{c,m}$  value, with in-situ data, which is not found in the literature.

### 3.4 Current Techniques: Limitations and Opportunities

The protocol for determining the mechanical strength,  $c'$ , of a bank soil required the use of a direct shear device, which is a widely accepted instrument and for this purpose it will not be discussed in this section. However, the methods for estimating fluvial erosional strength,  $\tau_{c,f}$ , and mass erosional strength,  $\tau_{c,m}$ , remain poorly defined and open for further improvement. This study seeks to develop novel methodologies to overcome the limitations of current techniques for measuring fluvial and mass erosion.

#### 3.4.1 Fluvial Erosion

Various methods have been described in the literature to identify the onset of fluvial erosion and to quantify the corresponding fluvial erosional parameters, namely  $\tau_{c,f}$  and  $M_f$ . These methods can be divided into in-situ and laboratory techniques. The in-situ techniques predominantly use a submerged jet device (Fig. 3.3a) or a mini-flume (Fig. 3.3b) (e.g., Paterson, 1989; Aberle et al., 2003; Hanson and Cook, 2004; Clark and Wynn, 2007). Both devices have advantages associated to their portability and practicality in use, but they also have significant limitations. Jet devices, for instance, apply an impinging flow to the soil surface (e.g., Paterson, 1989; Hanson and Cook,

2004) and the resulting force inter-changes between normal and shear as the scour hole evolves, which deviates from the true shear action presumed to be the key instigator of bank fluvial erosion. On the other hand, mini-flumes exert a shear force over the sample, but they usually have short lengths restricting their ability to low flow and shear stress values. Due to this limitation, the mini-flume is applicable only for estuarine bed sediments, which are mostly comprised of soft flocculent deposits that are eroded at low shear stresses (e.g., McNeil et al., 1996; Zreik et al., 1998; Roberts and Jepsen, 2001; Aberle et al., 2003).

Several laboratory techniques have also been described in the literature for estimating  $\tau_{c,f}$  and  $M_f$  (e.g., Arulanandan et al., 1980). Based on their operation, there are several types of laboratory flumes, namely straight open channel (e.g., Ghebreiyessus et al., 1994; Dennett, et al., 1998; Hildale, 2001; Papanicolaou et al., 2007), annular, rotating annular (Fig. 3.3c) (e.g., Parcure and Mehta, 1985; Kuijper et al., 1989; Krishnappan, 1993; Gharabaghi et al., 2007), race-way shaped (Fig. 3.3d) and closed conduit flumes (e.g., McNeil, 1996). Each of the devices mentioned above has its own advantages and limitations. The rotating cylinder, for instance, uses less water and soil and can directly measure the rate of erosion (Chapuis and Gatien, 1986), but it requires complex sample preparation and testing procedures (Lim and Khalili, 2009). The rotating annular flume has an infinite flow length for establishing fully developed flow. However, it generates significant secondary currents, which produce non-uniform shear stress distributions in the lateral direction.

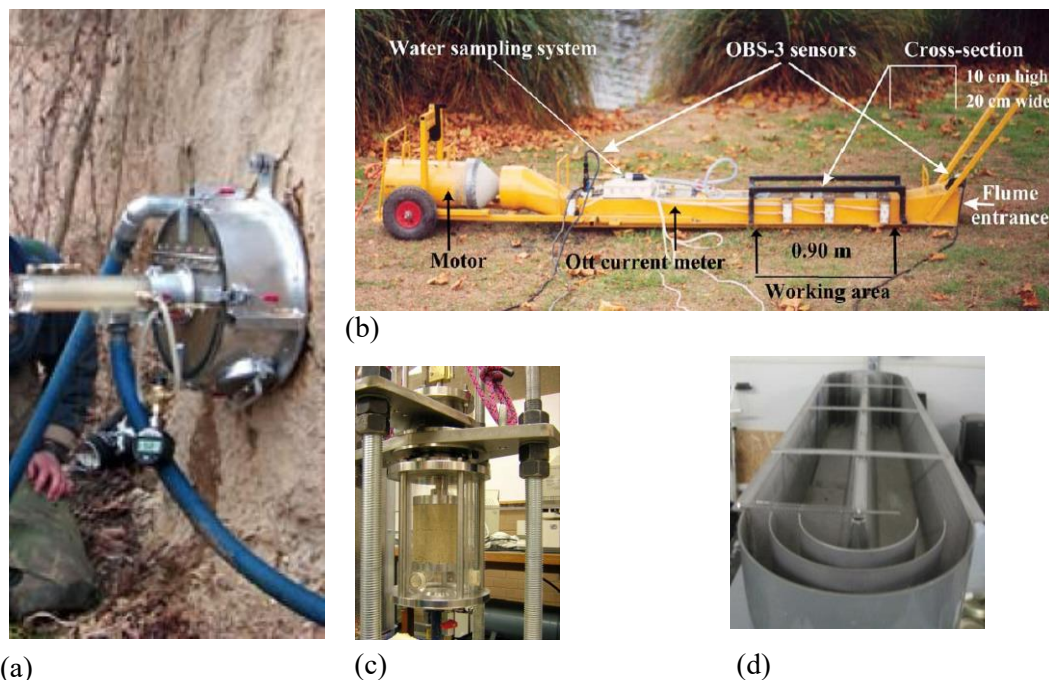


Figure 3.3 Devices for fluvial erosion study. (a) Jet device (Hanson and Cook, 2004). (b) Straight mini-flume (Aberle et al., 2003). (c) Rotating cylinder (Lim and Khalili, 2009). (d) Race-way shaped flume (source: Thanos Papanicolaou).

In summary, current devices for estimating  $\tau_{c,f}$  and  $M_f$  have significant limitations, which can be summarized as the following: 1) They do not deliver an applied shear to the surface of the sample, which mimics the driving mechanism of fluvial erosion; and 2) They generate only low flows which are not suited for analyzing well compacted bank cohesive soils (e.g., Papanicolaou et al., 2007). To address these key limitations, this study developed a unique method using conduit flume device to quantify fluvial erosion, which will be described further in section 6.3.4.

### 3.4.2 Mass Erosion

A critical review of the literature reveals that while mass failure and fluvial erosion to some extent have received considerable attention over the last quarter of the

century, the quantification of mass erosion remains open due to the following reasons: 1) Traditional methods, such as surveys of channel cross-sectional areas, terrestrial photogrammetry and measurements of erosion pin exposure lengths which, are manual and discrete in time, can neither capture the quasi-continuous nature of mass erosion nor relate bank retreat lengths to different hydrologic events in terms of timing, duration and magnitude (e.g., Chapuis, 1986; Kampuis, 1990; Gaskin et al., 2003; Julian and Torres, 2006; Lawler, 2005 and 2008); 2) The confusion surrounding the fluvial and mass erosional processes and their corresponding parameterization due to the absence of a comprehensive dataset for quantifying mass erosion (e.g., Chapuis and Gatién, 1986; Chapuis 1986a; Yong-Hui et al., 2008; Partheniades, 2009) as described earlier in section 3.2.

Clearly, mass erosion estimations would be greatly benefited from measuring devices that could enable: 1) The detection of the full episodicity of bank change, including event timings; 2) Automated observations of the retreat length magnitude/timing information for specific erosion events for developing relations between retreat lengths and shear forces triggering mass erosion (Lawler, 1992); and, 3) Quantitative measures for key parameters such as  $\tau_{c,m}$  and  $M_m$ . Laboratory devices, such as flumes, jet devices, and other devices, cannot reliably provide repeated measures of mass erosion in the laboratory due to the potential for sediment exhaustion during the experiments resulting in errors in the estimation of  $\tau_{c,m}$  (Chapuis, 1986; Kampuis, 1990; Gaskin et al., 2003). On the other hand, popular remote sensing techniques, such as the Bathymetric Light Detection and Ranging (LiDAR) technology, are not suited for capturing the localized response of a bank to a hydrologic event due to their limited

accuracy for quantifying event-based, bank retreats at length scales corresponding to mass erosion, which as noted, occur at the centimeter scale (e.g., Thoma et al., 2005; Notebaert et al., 2009; Pizzuto et al., 2010).

In this study, a methodology for quantifying mass erosion is developed using in-situ, novel approaches found in the geophysical research literature (e.g., Hildale and Raff, 2008; Muste et al., 2012). A device, namely the Photo Electronic Erosion Pin (PEEP) (see section 6.1 for description), which utilizes sunlight intensity (“photo”=light) to quantify the degree of exposure, was adopted to provide automated, localized, quasi-continuous measurements of mass erosion retreat lengths in response to different magnitude hydrologic events.

## CHAPTER 4 OBJECTIVES AND HYPOTHESES

This study seeks to improve our fundamental understanding of the interlinkage between hydraulically driven erosion and mass failure, as well as refine the current approaches for bank stability analyses. Unique and systematic field, laboratory, and modeling analyses were performed to achieve the following specific objectives:

- 1) Develop field and laboratory protocols for facilitating measurements of fluvial erosional strength,  $\tau_{c,f}$ , mass erosional strength,  $\tau_{c,m}$ , and mechanical strength,  $c'$ , of bank soils collected from the same sites.
- 2) Assess the role of soil bulk density heterogeneity on fluvial erosional strength,  $\tau_{c,f}$ , and mechanical strength,  $c'$ , at the crest, midbank, and toe of a bank profile.
- 3) Improve our understanding of the types of bank erosion processes and the differences in magnitude of fluvial erosional strength,  $\tau_{c,f}$ , mass erosional strength,  $\tau_{c,m}$ , and mechanical strength,  $c'$ , that dictate the onset of fluvial erosion, mass erosion, and mass failure, respectively.
- 4) Conduct a comprehensive bank stability analysis that is phenomenologically sound by considering both fluvial erosion and mass failure.

In this study, it is hypothesized that hydraulically driven erosion creates favorable conditions for mass failure and that heterogeneity in bulk soil properties plays an important role in the response of stream banks to different hydrologic regimes. Therefore fluvial erosional, mass erosional, and mechanical strengths at different locations along the bank profile are required when performing a bank stability analysis.

It is also hypothesized that the onset and rate of fluvial erosion can be described by an excess shear law with two key parameters, namely, an erodibility coefficient,  $M_f$ , and fluvial erosional strength,  $\tau_{c,f}$ . The erodibility coefficient reflects the effects of bulk density heterogeneity and consolidation history (or age) of the bank soil, whereas the fluvial erosional strength is a surrogate measure of cohesion. A laboratory conduit flume technique could be employed to estimate these two parameters due to two main reasons: 1) It applies a shear force to the surface of the sample, which is similar to the driving mechanism of fluvial erosion (i.e., shearing action); and 2) The flow in the conduit flume is pressurized and exerts high shear stress, allowing for the analysis of well compacted bank cohesive soils in general (e.g., Papanicolaou et al., 2007).

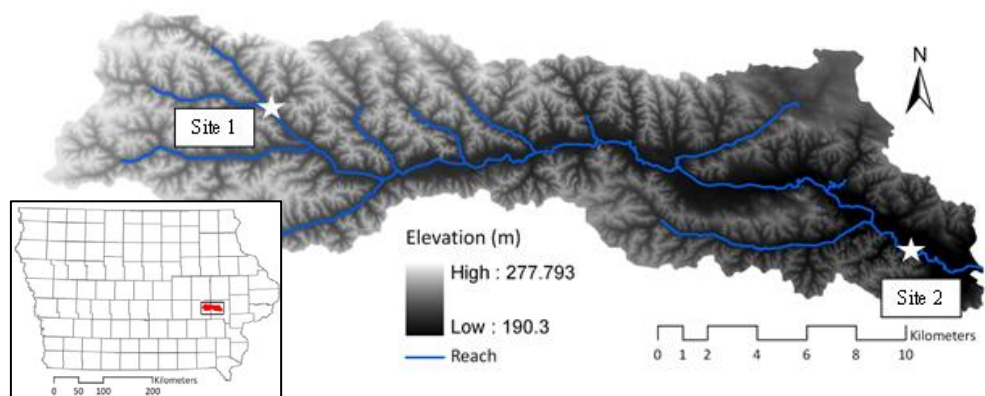
Additionally, it is hypothesized that the onset and rate of mass erosion can also be represented by an excess shear law with the two dominant parameters, namely, erodibility coefficient,  $M_m$ , and mass erosional strength,  $\tau_{c,m}$ . Those parameters can be estimated using Photo Electronic Erosion Pins (PEEPs), which are capable of performing in-situ, quasi-continuous monitoring of bank retreat (in the scale of centimeter) for specific mass erosion events.



## CHAPTER 5 SITE DESCRIPTION

This study was conducted in the Clear Creek, IA watershed, which is a tributary of the Iowa River and located in south-eastern Iowa (Fig. 5.1). Clear Creek is an ideal stream for quantifying bank erosion due to favorable geomorphic and hydrologic conditions (e.g., frequent flash flooding and highly erodible bank material) causing the stream to have an active, laterally-migratory channel. In addition, bank erosion in Clear Creek has been further exacerbated from anthropogenic activities, including the onset of intense farming in early 1930s, channel straightening in the 1950s, and the ongoing clearing of the vegetation along the channel floodplain (e.g. Langel, 1996; Landwehr and Rhoads, 2003; Rayburn and Schulte, 2009). The current planform of Clear Creek is characterized with a sinuosity between 1.27 and 1.49 and has very few similarities with its planform in the early 1900s, which had gently sloping bank profiles and was lined with large trees. Figure 5.2 provides a perspective of the changing channel planform from 1937 (prior to channelization), to 1951 (after channel straightening) and the present.

The other motivating factor for performing this study in Clear Creek was the availability of several key hydrological and bank soil data, especially at the two study reaches, namely, site 1 in the headwaters (Fig. 5.1b, d), and site 2 near the mouth (Fig 5.1 c, e) of Clear Creek, where the network of PEEPs was installed. For instance, flow discharge and water stage data for site 2 have been provided by the existing USGS stream gage #05454300 while for site 1 through a water level sensor (Global Water WL 16) and an available stage-discharge relation (Abaci and Papanicolaou, 2009). These data are of paramount importance for relating fluid action to bank retreat for different erosion events.



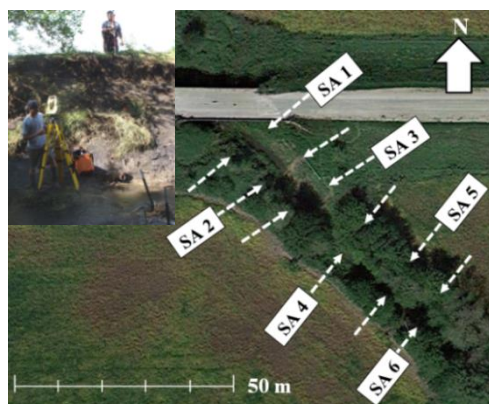
(a)



(b)



(c)



(d)



(e)

Figure 5.1 Study site: (a) The Clear Creek, IA watershed. (b) The headwaters site (site 1). (c) The mouth site (site 2). (d) Cross-sections at site 1. (e) Cross-sections at site 2.

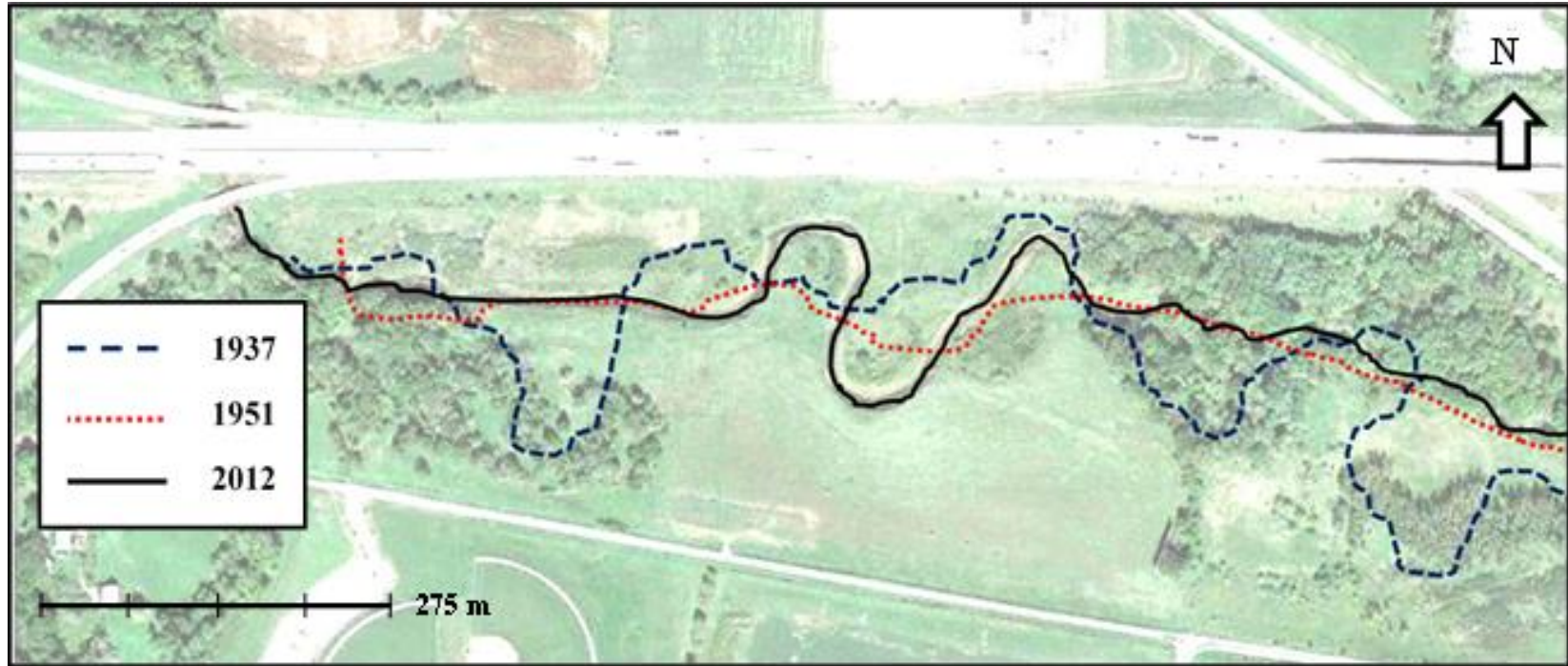


Figure 5.2 Historical planform changes in Clear Creek from 1937 to present, modified from Langel (1996).

The two study sites, have been strategically selected because they represent dissimilar bank soil properties and correspond to different hydrologic regimes with implications on the frequency in which bank erosion occur and the magnitude of bank retreats at the two sites (e.g., Oneal, 2009; Wilson et al., 2012; Sutarto et al., in press). Clear Creek, at site 1, is a 2<sup>nd</sup> order stream, whereas, at site 2 is a 4<sup>th</sup> order (Abaci and Papanicolaou, 2009). The average flow rate at site 1 is 0.25 m<sup>3</sup>/s (or 5.9 x 10<sup>6</sup> m<sup>3</sup>/yr) and at site 2 is 2.05 m<sup>3</sup>/s (or 64.6 x 10<sup>6</sup> m<sup>3</sup>/yr).

Last but not least, Clear Creek has recently been named by the U.S. National of Science Foundation as a Critical Zone Observatory (CZO). It is located in the vicinity of the University of Iowa, allowing for frequent field visits during PEEP deployment and operation.

The bank soils in Clear Creek watershed area consist of a deep layer of glacial till overlain by a thin layer of silty colluvium or silty alluvium (e.g., Oneal, 2009). The bank soils tend to be dark gray to brown, noncalcareous, silt clay loam or loam that are associated with the Holocene channel belt of the Iowa River valley (Bettis, 1995). The bank soil at site 1, where Clear Creek predominately behaves as an erosive, incised channel, contains higher portion of silt ( $61.55 \pm 6.23\%$ ) and almost equal portions of clay and sand. On the other hand, at site 2 sand ( $52.79 \pm 11.43\%$ ) and silt ( $39.44 \pm 10.43\%$ ) are both prominent with a lower portion of clay ( $7.77 \pm 2.30\%$ ). At site 2, Clear Creek is erosive but at the same time works as a depository environment due to the backwater effects from its confluence with the Iowa River and the material influx from upstream (Sutarto et al., in press). The sand fraction at site 2 is more abundant at the bank crest where sand has been deposited during flooding (e.g., Wilson et al., 2012). The bank soils



at site 1 have slightly larger bulk density than those at site 2, although both sites, as expected, present an increasing trend in bulk density magnitude along the bank profile (Sutarto et al., in press). On average, the bank height at both sites is approximately 3.2 m and the bank angle of the bank face with respect to the horizontal is about 34° based on geodetic surveys of 6 cross sections at site 1 and 2 (Fig. 5.1d and 5.1e). Clear Creek has an approximate length of 40 river-km with an average slope of 0.001 (Loperfido et al., 2009) and drains approximately 270 km<sup>2</sup> of mixed agricultural urban lands to the Iowa River. The estimated transported sediment load is 0.15 kg/s (or 5.0 x 10<sup>3</sup> tons/yr) and 0.76 kg/s (or 23.9 x 10<sup>3</sup> tons/yr) for sites 1 and 2, respectively (Abaci and Papanicolaou, 2009; Wilson et al., 2012).

The climate in Clear Creek is characterized by cold winters, hot summers, and wet springs. The estimated mean annual precipitation is 889 mm with high intensity thunderstorms common from April to September and a snowfall water equivalent of 76.2 mm/yr (Papanicolaou and Abaci, 2008).

## **CHAPTER 6 PROCEDURE AND METHODOLOGY**

The nature of this study is threefold, consisting of field, laboratory, and analytical-modeling sub-studies to improve current methods for bank stability analysis by addressing the critical needs in conception and methodology surrounding bank stability analysis. First, field excursions were conducted to obtain measurements of channel cross-sectional topography and mass erosional strength of bank soils at two sites along a midsized Midwestern stream in south eastern Iowa, as a necessary precursor for performing a bank stability analysis. The initial channel cross-sections were obtained from a geodetic survey performed on October 1, 2007, and the mass erosional strength of bank soils were determined from a field study conducted between May and December, 2009. Photo-Electric Erosion Pins (PEEPs) were installed at these two sites to monitor mass erosion, in order to quantify the mass erosional strength and erodibility. The use of the PEEP is described in greater detail later in this chapter. Additionally, soil samples were extracted from the banks at both sites between July and October, 2011 and 2012 for further analysis in the laboratory.

Second, the bank soil samples collected during the field excursions were then brought into the laboratory for further analyses to generate data for soil index properties (namely, soil composition, bulk density, and Atterberg limits), bulk density profiles, as well as mechanical and fluvial erosional strengths. Standardized methodologies (ASTM D422-63, ASTM 4254-91, and ASTM 3080-90) were used to determine soil composition, bulk density, and mechanical strength. The Atterberg limits were quantified using fall cone technique. Attenuation of an Americium-241 radioactive source was used to determine the bulk density profiles of the collected soil samples, while a conduit flume

was used to determine the fluvial erosional strength. These attenuation and erosion flume methods are described in more detail within this chapter.

Finally, the channel surveys, as well as the soil index properties and erosional strength measures obtained from the field and laboratory components of this study were used as input parameters for an established one-dimensional, channel evolution model, namely the Conservational Channel Evolution and Pollutant Transport System (CONCEPTS version 2.0; Langendoen and Alonso, 2008) to estimate the factors of safety for mass failure ( $FS_{mf}$ ) and fluvial erosion ( $FS_f$ ), and simulate the bank retreat as a result of either fluvial erosion or mass failure or the interaction between the two modes of erosion. In the present study, special attention was paid to those times when the  $FS_f$  near the bank toe was less than unity as this condition could result in bank toe undercutting and the formation of cantilevers, leading to mass failure. The predicted bank profile obtained from the model was then compared against cross-sectional measurements obtained for a period of two hydrological cycles (i.e., from October 1, 2007 to March 8, 2013).

### **6.1 Field Component: Mass Erosional Strength Determination**

One of the overarching goals of this study is the development of a methodology for quantifying mass erosion using in-situ, novel approaches that could adequately capture retreat length magnitude and timing in response to changes in stage (e.g., Hilldale and Raff, 2008; Muste et al., 2012). Recent research in geomorphology and estuarine dynamics (e.g., Lawler, 1991; 1992; Lawler, 2005; Lawler, 2008; Bertrand, 2010) has shown that the Photo Electronic Erosion Pin (PEEP) sensor, its operational principle is

based on sunlight exposure and intensity (“photo”=light), could be employed to provide localized, quasi-continuous recordings of mass erosion retreat lengths in response to different magnitude hydrologic events. The PEEP technology has been successfully used to monitor tidal effects on sediment dynamics, wind effects on high magnitude erosion rates (e.g., Couperthwaite et al., 1998), and bed elevation change in the swash zone (Horn and Lane, 2006). PEEPs have been recently utilized to monitor erosion rates in several bank erosion studies in the U.K. and to a lesser extent in the U.S.A. (e.g., Lawler, 2008; Bertrand, 2010).

The PEEP sensor is a simple optoelectronic device containing a series of photo-resistant (Fig. 6.1) or photo-voltaic cells, which are enclosed within a waterproof, transparent, acrylic tube (e.g., Lawler, 1991 and 1992; Rickly-Klausmeyer pers. comm.). See section 6.1.1 for a further description of the sensor. The photo-resistant cells require an external electric energy source (e.g. solar panel) for their energy supply, while photo-voltaic cells generate their own electric power by converting solar radiation into direct current electricity. In spite of these differences, both types, photo-resistant and photo-voltaic PEEPs, operate under the same principle by generating an analogue voltage proportional to the total length of the acrylic tube exposed to sunlight (Lawler, 1991; 1992). Subsequent retreat of the bank face exposes more cells, or interchangeably diodes, to the sunlight, thereby increasing the sensor voltage output. This information is then correlated to bank retreat for developing relations between retreat lengths and shear forces triggering mass erosion.

Herein, photo-resistant PEEPs (Fig. 6.1) were utilized in a representative



stream of the U.S. Midwest with mostly cohesive, loess-derived banks (i.e., Clear Creek, IA, USA) in order to improve our fundamental understanding of mass erosion and capture, semi-continuously, retreat length magnitude and timing information in response to changes in stage during a hydrograph, as well as provide unique data to be used towards the estimation of  $\tau_{c,m}$ . Such data are lacking in the literature for mass erosion. For this reason, PEEPs were placed at the crest, upper-midbank, lower-midbank and toe of the studied banks to provide simultaneous measures of the mass erosional strength along the bank profile, and aid to the assessment of the role of bank soil heterogeneity on mass erosion.

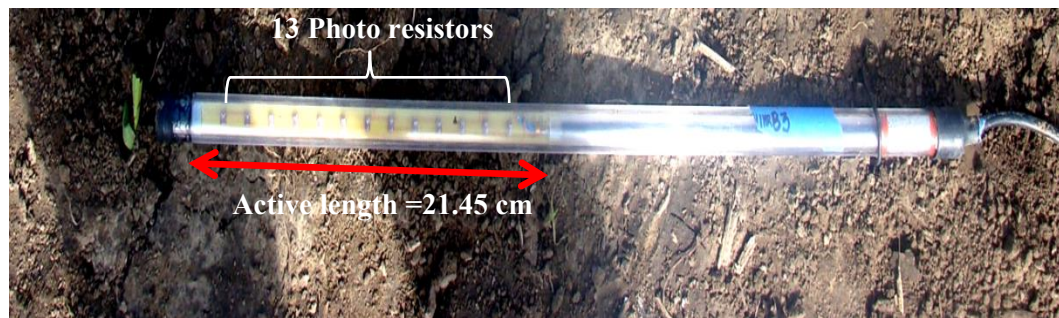


Figure 6.1 Photo Electronic Erosion Pin (PEEP)

This effort was complemented with a statistical treatment of the retreat length time series data through the performance of a moving average to identify key events in terms of their magnitude and frequency of occurrence for mass erosion. In concert to this effort, a unique and systematic PEEP data processing routine (e.g., filtering, correcting and smoothing) was also developed to remove the effects of ambient light changes due to

solar orientation, or equivalently low light intensity and other factors (e.g., turbidity) on the bank retreat length estimation (Lawler, 1991; 1992).

### 6.1.1 PEEP Component Description

This study utilized the photo-resistance PEEPs (Fig. 6.1) to identify the onset of mass erosion and quantify retreat rates for different corresponding stresses (Rickly-Klausmeyer pers. comm.). The lower purchase cost and off-the-shelf availability of the photo-resistance sensors, along with the availability of solar panels for providing the necessary energy were some of the criteria used for proceeding with the acquisition of the photo-resistance PEEPs (note: the photo-voltaic may present other advantages when compared to the photo-resistant PEEPs but a complete evaluation of the pros and cons of the two systems was not the focus of the dissertation).

A PEEP system consists of the photodiode sensors; a data logger, solar panel, and a “reference” photodiode. The photodiode or PEEP sensor, as it is called hereafter, consists of a series of thirteen (13) photo-resistance diodes/cells spaced 1.65 cm apart and placed on a motherboard inside a transparent, water-proof acrylic tube (Fig. 6.1). The active length of this sensor is 21.45 cm and coincides with the length of the photo-resistant cell array (i.e., the yellow color motherboard in Figure 6.1). It is at the front part of the PEEP tube.

As the observed bank erodes, the length of the PEEP sensor and, therefore, the cell series inside the PEEP are gradually exposed to the sunlight (Fig. 6.2). Larger exposure lengths correspond to a higher number of cells exposed to the sunlight, as well as the cell series output,  $V_{CS}$ , that is generated and sent via a cable to a data logger. The data logger in this study is placed on the back side of the sensor and is attached to a pole

along with the solar panels located on the nearby floodplain and at a close proximity to the PEEPs (Fig. 6.3).

The PEEPs were deployed between May 18 and June 22, 2009 for site 1 and between June 4 and December 1, 2009 for site 2. Based on the ambient light conditions prevailing during the period of May 2009 through December 2009 three panels were used to ensure adequate energy supply for the four PEEPs per site. The PEEPs were unable to produce meaningful data at night because the diodes were light dependent.



Figure 6.2 PEEP exposure length after a flood event.

An integral component of the photo-resistant PEEP system is the reference PEEP sensor (Bertrand, 2010). The reference PEEP was mounted on a cement block surface and secured on the nearby floodplain for sites 1 and 2 (Fig. 6.4) in order to provide unobstructed reference PEEP voltage outputs,  $V_{rP}$ , that represented the maximum (fully exposed) outputs for any ambient light condition (McDermott and Sherman, 2009). This type of data,  $V_{rP}$ , was needed for two reasons. First, for detecting when the PEEP is fully exposed ( $V_{CS} \approx V_{rP}$ ) and need to be reset (Hydro Scientific Ltd., 2004). The PEEP

resetting time was an important piece of information for processing the data (discussed later in section 6.1.5).



Figure 6.3 Data loggers and solar panels attached to a pole on the nearby floodplain.

Second, the reference value,  $V_{rp}$ , was employed as a baseline value for the cell voltage output,  $V_{cs}$ , to account for minor fluctuations in sunlight intensity or temporary shadows. This ratio  $\frac{V_{cs}}{V_{rp}}$  was related to the exposure length of the PEEP through a calibration procedure, to be described in section 6.1.2.

Finally, the data outputs from all PEEP sensors, including the reference PEEP, were stored in a data logger (Fig. 6.3). The data logger was preset in this study to record the  $V_{cs}$  from each PEEP every 15 seconds and to store 15-minute averages following the

methodology provided by other studies focused on bank erosion (e.g., Lawler et al., 1997; Lawler, 2008; Mitchell et al., 2003; Horn and Lane, 2006; McDermott and Sherman, 2009). A detailed technical specification of this device is shown in Table 6.1.



Figure 6.4 A reference PEEP was secured on the nearby floodplain.

Table 6.1 The specification of PEEP used in the present study.

<b>Description</b>	<b>Photo-resistant PEEP</b>
Manufacturer	Rickly Hydrological Co.
Tube length (cm)	55
Total sensor length (cm)	59
Active length (cm)	21.45
Tube external diameter (cm)	1.8
Number of cells in series	13
Number of reference cells	0
Number of thermistors	0
Spacing between neighboring cells (cm)	1.65
Reference cell output(mV)	0 - 1
Cell series output (mV)	0 - 1



### 6.1.2 PEEP Calibration

The calibration process of the PEEP sensors was conducted outdoors on a bright sunny day (no clouds, on May 20<sup>th</sup> 2009). The PEEPs, including the reference PEEPs, were placed horizontally on a fixed leveled datum (a flat table with a 3D leveling bubble) so all had the same exposure and orientation with respect to the emitted sunlight (Fig. 6.5). During this process the voltage ratio of the exposed diodes relative to the reference value,  $\frac{V_{CS}}{V_{RP}}$ , and the measured exposure length of the PEEP were recorded. Initially, a black sleeve covered all diodes per PEEP except the two reference PEEPs that remained fully exposed to the sunlight at all times (Fig. 6.5). The sleeves were gradually pulled back during the calibration process at known distances mimicking bank retreat. The time interval between exposures of two neighboring diodes was preset to four (4) minutes to allow sufficient period for sunlight exposure. The measurement window for each diode was every fifteen (15) seconds, which is identical to the data logger recordings discussed earlier (Rickly-Klausmeyer pers. comm.). The exposed length was manually measured with a tape and caliper and correlated with the normalized voltage readings  $\frac{V_{CS}}{V_{RP}}$ .

To determine the calibration relationship, the tube exposure length,  $L$ , was plotted against the measured voltage-reference value ratio,  $R_r = \frac{V_{CS}}{V_{RP}}$ , and fit with a regression line (Fig. F1 and F2). The following polynomial relationship (namely, the 2D NIST Hahn Model) was used for estimating the PEEPs exposure length:

$$L = \frac{(c_1 + c_2 R_r + c_3 R_r^2 + c_4 R_r^3)}{(1 + c_5 R_r + c_6 R_r^2 + c_7 R_r^3)} \quad (6.1)$$

where  $V_{CS}$  and  $V_{RP}$  are expressed in millivolts. The coefficients  $c_1$ ,  $c_2$ ,  $c_3$ ,  $c_4$ ,  $c_5$ ,  $c_6$ , and  $c_7$  were determined for each PEEP using open-source software at the following website:

<http://zunzun.com/Equation/2/NIST/NIST%20Hahn/>. Tables F1 and F2 summarize those coefficients for each PEEP used in this study.

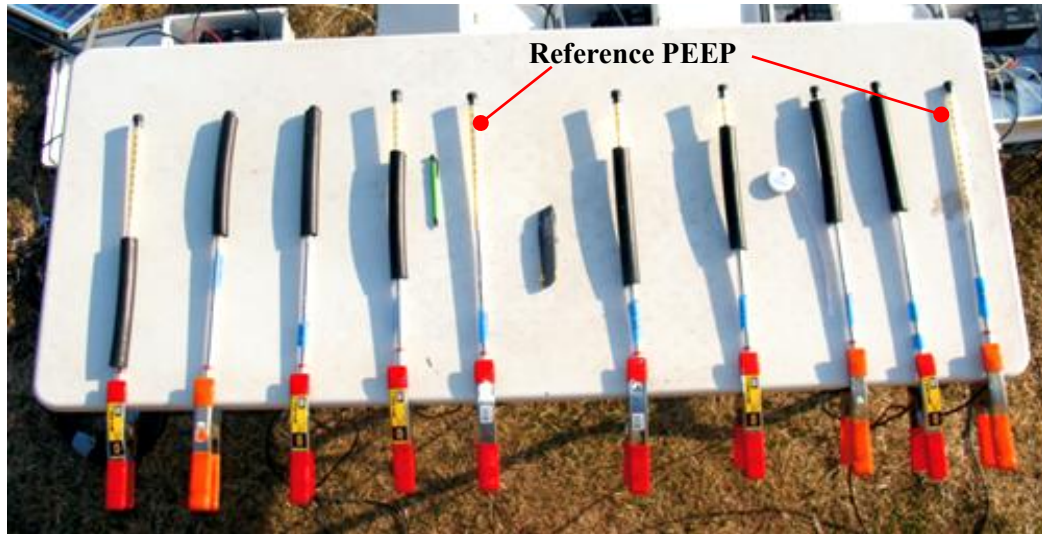


Figure 6.5 Calibration of Photo Electronic Erosion Pins (PEEPs). Photo-resistant PEEP were placed on the table on a nearby flood plain. Tubular light-tight sleeves were used to cover the entire cells within the PEEP tubes. The sleeves were then gradually pulled back with known distances to mimic bank erosion.

### 6.1.3 PEEP and Pressure Transducer Installation

Following calibration, the PEEP were initially inserted horizontally into the bank face through pre-augured holes (70 cm x 1.6 cm) such that they were completely buried in the bank soil. The hole was carefully drilled to avoid significant disturbance to the surrounding bank soils. Before inserting the PEEP into the hole, the cable at the end of the sensor was attached to the side of acrylic tube with sufficient slack to avoid snapping the cable. The PEEP and attached cable were then inserted fully in the bank face. The cable was then run back up the bank face to the data logger through a garden hose for additional protection and fixed to the bank surface.

At the headwater site or site 1, Clear Creek near South Amana, three PEEPs were installed between May 18 and June 22, 2009 along a vertical transect of the right bank. Specifically, PEEPs A1, A2, and A3 were inserted into the crest, midbank, and toe of the right bank (looking downstream), respectively (Fig. 6.6a) for monitoring bank retreat at site 1. In addition, a reference PEEP was secured on the adjacent floodplain in order to provide unobstructed reference PEEP voltage outputs that represented the maximum (fully exposed) outputs for any ambient light condition. These PEEPs were removed on June 22, 2009 following a flash flood at the site due to the significant erosion that had occurred.

At the mouth site or site 2, Clear Creek at Camp Cardinal, four PEEPs were inserted into the bank face between June 4 and December 1, 2009 with a reference PEEP secured on the adjacent floodplain (Fig. 6.6b). Similarly, PEEPs B1, B2, B3, and B4 were deployed at the crest, upper midbank, lower midbank, and toe of the right bank, respectively (Fig. 6.6b). At site 2 more PEEPs were employed because the mass erosion process is far more active when compared to site 1.

The PEEP measurements were complemented with stage measurements in order to relate observed erosion depth or retreat length,  $\Delta L$ , to water stage and ultimately to the near-bank shear stress,  $\tau_w$ . At site 1, the volumetric flow rate was determined using a stage-discharge relationship (Abaci and Papanicolaou, 2009) based on established methods from the U.S. Geological Survey (Kennedy, 1984). The stage was measured at 15-minute intervals, similar to the PEEP logging rate, using a vented pressure transducer (i.e., Global Water WL16 Water Level Logger), with an accuracy of  $\pm 0.2\%$  at temperatures between  $1.7^\circ\text{C}$  and  $22.2^\circ\text{C}$  (Global Water Instrumentation, 2009),



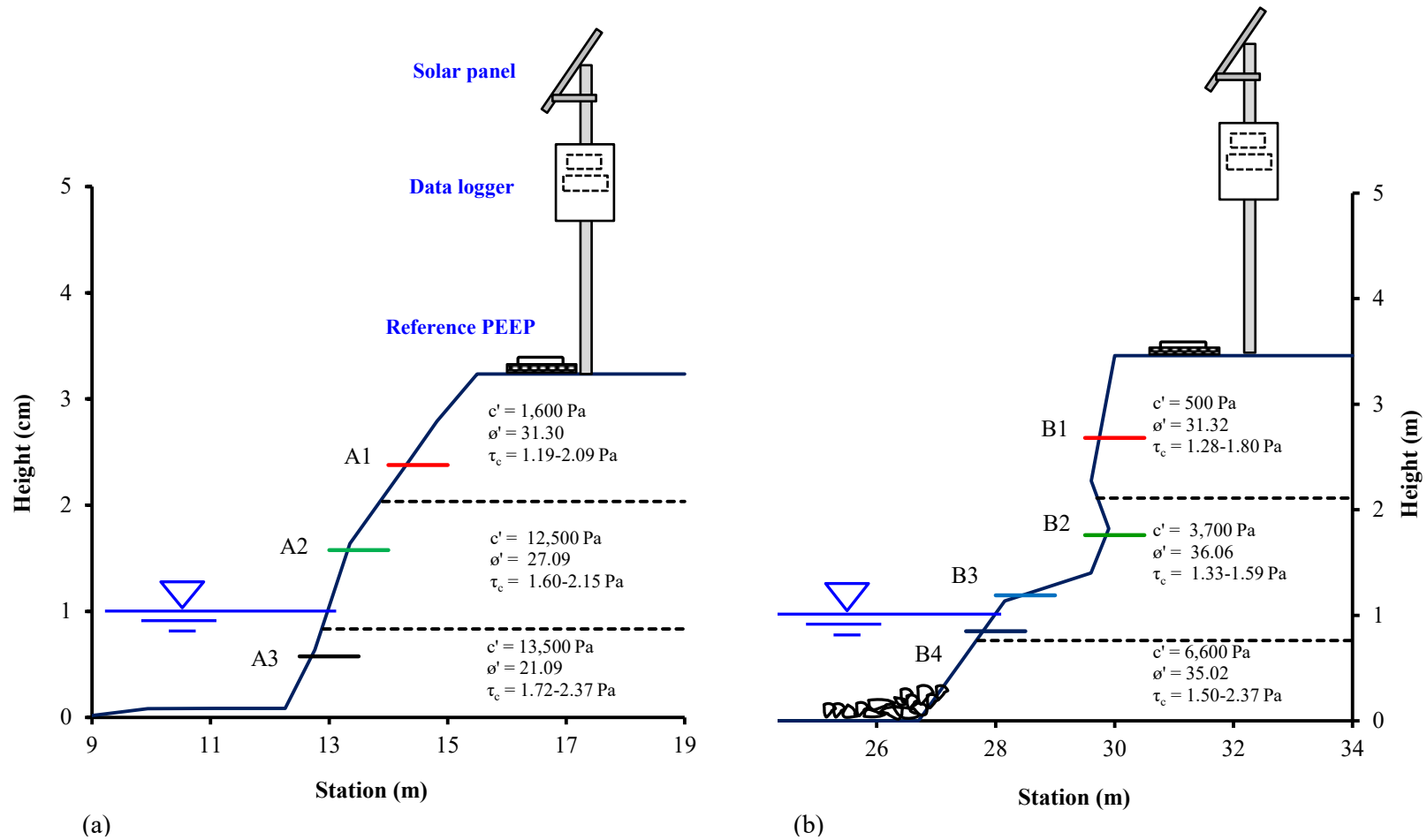


Figure 6.6 PEEP installation. (a) Site 1. (b) Site 2

and an enclosed data logger. The pressure transducer was installed 10 cm above the streambed within a stilling well to minimize the effects of waves and water current on the measurements (Abaci and Papanicolaou, 2009). At site 2, the water stage data were obtained from the existing USGS stream gauge (#05454300; Clear Creek near Coralville, IA) and the discharge was determined using the established USGS rating curve.

#### 6.1.4 Preliminary Data Visualization and Interpretation

As a first step in the analysis, the time series of water stage were plotted to gain an insight on the dynamicity (i.e., timing and magnitude) of various flow events at sites 1 and 2 and assess if the collected flow data were sufficient for establishing the correspondence between the observed retreat lengths from the PEEPs and near wall shear stress via the stage obtained from the pressure gages. As an example, Figure 6.7a shows a time series of water stage at a 15-minute interval recorded at site 2. There were at least six (6) major flood events (e.g., June 19, July 8, July 10, August 27, October 22, and October 29, 2009) which could trigger quantifiable amounts of mass erosion and help us establish the  $\tau_w - \Delta L$  correspondence at this site.

At site 1, the headwaters, the flow barely exceeded baseflow conditions for most of the year and the creek experienced its highest flow rates during the wettest months of April –June, although the flow events in these months are predominately flashy (Denn, 2010; Wilson et al., 2012). As a result, the study period at site 1 was short (between May 18 and June 22, 2009) and only 1 major flood event (June 19, 2009) was recorded, thereby limiting our ability to establish a  $\tau_w - \Delta L$  correspondence at this site. Nonetheless, the June 19<sup>th</sup> major flood event results still offer unique insight into the measured mass erosion rates at the crest, midbank and toe of site 1 (see for example

Figure 7.6) and allow for making comparisons with the corresponding locations of the bank profile at site 2.

The second step in the analysis involved plotting the cell series outputs,  $V_{CS}$ , from each PEEP along with the synchronous outputs from the reference PEEP,  $V_{RP}$ , defined in section 6.1.1. Figures F.3 and F.6 shows the plots of cell series outputs,  $V_{CS}$ , along with the synchronous outputs from the reference PEEP,  $V_{RP}$ , for the PEEPs installed at site 1 and site 2, respectively. This type of plot allowed for comparing graphically the cell series outputs,  $V_{CS}$ , with the maximum (fully exposed) outputs,  $V_{RP}$ , and for detecting when the PEEP was fully exposed ( $V_{CS} \approx V_{RP}$ ) needing to be reset (Hydro Scientific Ltd., 2004). The PEEP resetting time was important information for processing the data (discussed later in section 6.1.5). Figure 6.7b shows a plot of cell series outputs,  $V_{CS}$ , (black dashed line) from PEEP B2 along with the synchronous outputs from the reference PEEP,  $V_{RP}$ , (red dashed line). The black and red dashed lines nearly overlapped fully after the June 19, 2009 and October 29, 2009 flood events, indicating that PEEP B2 was nearly fully exposed after those two events. To continue the monitoring activity, this PEEP was reset on July 7, 2009.

As is also shown in Figure 6.7b, the cell series outputs,  $V_{CS}$ , from PEEP B2 dropped several times due to the collective effects of PEEP submergence and elevated turbidity associated with the occurrence of majors flood events (e.g., June 19, July 8, July 10, August 27, October 22, and October 29, 2009). The missing data between July 13 and August 16 were attributed to flowing debris and leaves that temporarily covered the PEEP diodes. No biofouling was observed. It is important to note that the reference PEEP outputs,  $V_{RP}$ , (red dashed line, Fig. 6.7b) tended to be constant at 1 millivolt since

these readings represent the “flood plain” ambient light intensity, which is not attenuated by water depth and turbidity.

In short this preliminary data visualization revealed that submergence of the PEEPs in water and turbidity could potentially have a significant effect on the PEEP outputs due to attenuation of the ambient light intensity (e.g., McDermott and Sherman, 2009). Based on the IOWATER transparency data, transparency within the water column can vary between 10 and 60 cm, corresponding to Total Suspended Solids (TSS) concentrations of 90 mg/l to 1000 mg/l (Loperfido, 2009). Therefore, the exposure length,  $L$ , information obtained from the calibration formulas, Eq. 6.1, will need to be “corrected” by accounting for the effects of turbidity and submergence. Moreover, the PEEPs were calibrated for the “flood plain” ambient light intensity which is not the “true” ambient light intensity received by the PEEPs in the stream, especially, during high submergence and high levels of turbidity. To address these shortcomings, this study provided a unique procedure, depicted in Figure 6.8 and detailed in the next section 6.1.5, for processing (e.g., “*filtering*”, “*correcting*”, and “*smoothing*”) the exposure length,  $L$ , information obtained from the calibration formula, Eq. 6.1.

#### 6.1.5 PEEP Data Processing

The goal of the data processing was to obtain an estimate of PEEP exposure length,  $L$ , from the raw data ( e.g.,  $V_{CS}$ ,  $V_{RP}$ ) in order to identify mass erosion events and quantify bank retreats. The first step in this data processing was to quantify the PEEP exposure length,  $L$ , by applying the calibration formula (Eq. 6.1) and using the  $V_{CS}$ , and  $V_{RP}$  data obtained from the PEEP measurements. This procedure did not necessarily yield

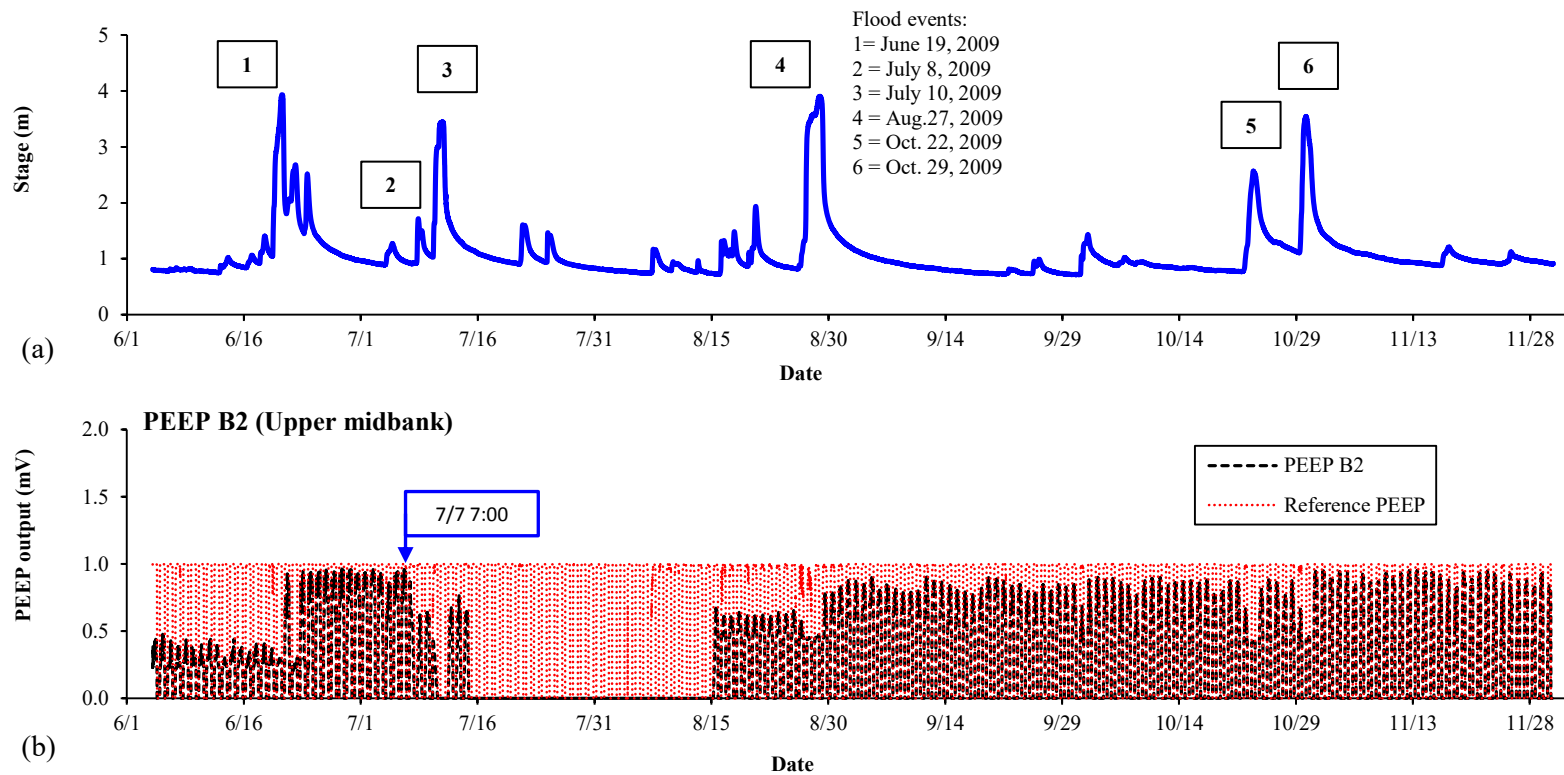


Figure 6.7 Time series of water stage and PEEP outputs deployed at site 2. (a) Water stage. (b) Outputs from PEEP B2,  $V_{CS}$ , (black dashed line) and the reference PEEP,  $V_{RP}$ , (red dashed line).

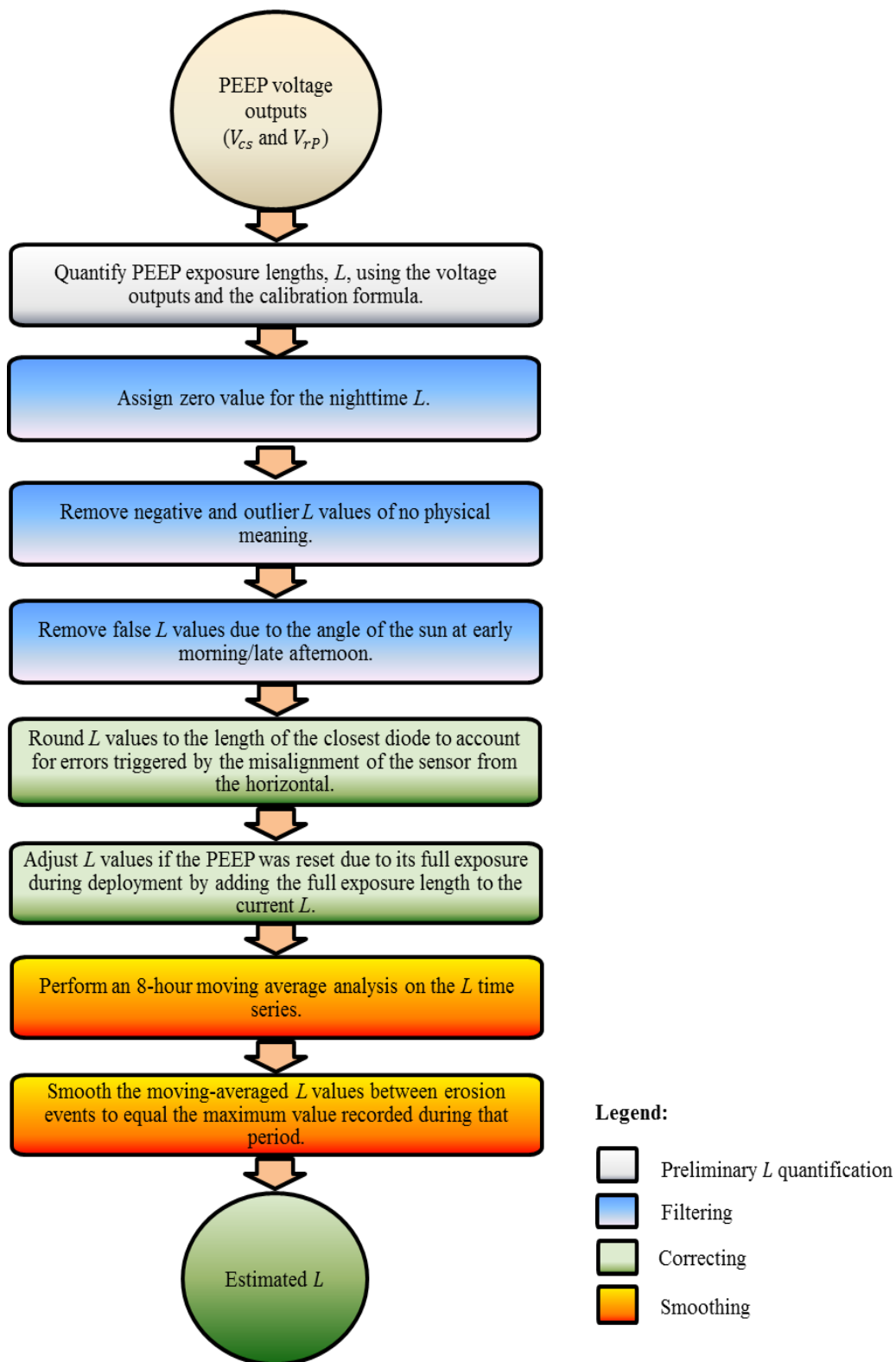


Figure 6.8 Methodological procedure for estimating PEEP exposure length.

a zero magnitude  $L$  for nighttime data, despite the fact that  $R_r = 0$ , instead it yielded a value of  $L = c_1$ . This issue was resolved by assigning  $L = 0$  for the nighttime. Moreover, Eq. 6.1 might result in meaningless (below zero or unreasonably large)  $L$  values if the normalized outputs,  $R_r$ , were outside the calibration range (Fig. F4 and F7). This was typically related to data recorded by the PEEP in early morning or evening when the ambient light intensities were low. On the contrary, in some cases, bright dawn and dusk sunshine with low-angled orientation had activated the cell series deep within the bank, causing “wrong” peak voltage outputs, and thus large  $L$  values, unrelated to erosion (Hydro Scientific Ltd., 2004). These meaningless  $L$  values, from the physical point of view, were removed from the data series. The steps described above define the “*filtering*” process.

The next procedure in the data processing was the “*correction*”. Herein, the filtered  $L$  values from the first step were corrected for several factors. The first correction was related to the cell spacing within the PEEP (1.65 cm for photo-resistant PEEP). It was considered that any measured  $L$  values less than 1.65 cm, or the size of the cell spacing, were meaningless and were rounded to the closest multiple of the cell spacing as the voltage outputs are supposed to be constant between two neighboring cells. Such an error was attributed due to the misalignment of the PEEPs from the horizontal position or due to poor water transparency and presence of scattered clouds. Vibration caused by the potential induced spiral motion of the impinging flow must also be considered as a potential source of error (Couperthwaite et al., 1998; Mitchell et al., 1999; Prosser et al., 2000; Lawler et al., 2001; Lawler, 2005; Lawler, 2008). Moreover, the  $L$  values were corrected to be no more than the PEEP active length of 21.45 cm an error that could be

caused during the full exposure of the PEEPs and their misalignment from their initial horizontal place with respect to the water surface elevation. In this study, PEEPs B1, B2 and B3 were reset on July 7, 2009 and the second reset was performed on September 11, 2009 for PEEP B1. For these PEEPs, their  $L$  values were corrected by adding to their new outputs their maximum pre-reset value. Figures F5 and F8 show the result at this stage of data processing for all PEEPs installed at site 1 and 2, respectively.

As an example, Figure 6.9a shows the time series of exposure length,  $L$ , (black dashed line) for PEEP B1 after assigning zero value for the nighttime  $L$ , removing meaningless  $L$  values, and applying corrections to the remainder  $L$  values as it was described earlier. The plot shows that the daily peaks of exposure length,  $L$ , are still highly varied.. This variability in daily peak values confirm that the effect of ambient light changes is still embodied within the time series data requiring further processing of the data.

To minimize the variability in daily peak values of the time series of exposure lengths (black dashed line in Figure 6.9a), a “*smoothing*” procedure was performed using the concept of moving average (Whittaker and Robinson, 1967). The time series was first smoothed with an 8-hour interval moving average. The 8-hour moving interval was used herein since larger time intervals would provide similar results, based on our analysis with 11-hour and 24-hour moving intervals (Bertrand, 2010). This moving-average approach was effective as it resulted to more stable daily peaks and more visible erosion-related increases (black dashed line in Figure 6.9b) comparatively to the non-moving-averaged  $L$  (black dashed line in Figure 6.9a). However, further smoothing was



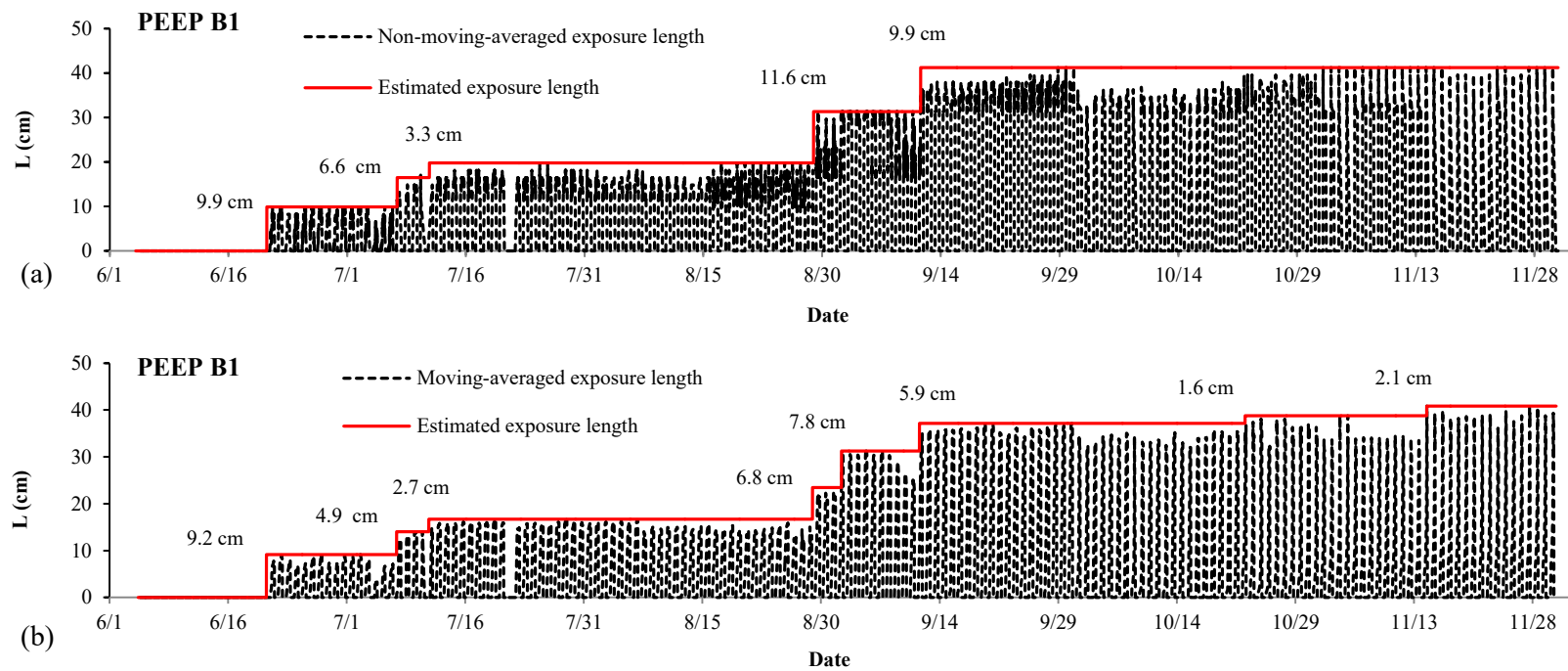


Figure 6.9 Comparison between non-moving-averaged and moving-averaged exposure length. (a) Time series of exposure length without performing moving-average analysis. (b) Time series of moving-averaged exposure length.

still required to completely eliminate the effect of ambient light changes including the typical diurnal cycle. This step was the last step in data processing and was performed by leveling the moving-averaged  $L$  values with the maximum value (red solid line, Fig. 6.9b) starting from the previous erosion event. This was performed under the presumption that the maximum PEEP voltage output provides the closest estimate of the “true” exposure length of the PEEP (e.g., McDermott and Sherman, 2009; Lawler et al., 2001). This assumption is shown to be reasonable at this stage of data processing as the “false” peak values had been removed and the effect of ambient light changes had been minimized from the time series. The red solid line in Figure 6.9b is an example of the final result from data processing and represents the best estimate of exposure length,  $L$ , and is referred to hereafter as the “estimated  $L$ ”. An increase  $\Delta L$  in the estimated  $L$  represents the occurrence of a new mass erosion event.

For the purposes of examining the effectiveness of the 8-hour moving average smoothing, the estimated  $L$  (red solid line in Figure 6.9b) was compared with its counterpart (red solid line in Fig. 6.9a) of non-moving averaged  $L$ . Unlike the estimated- $L$  line (red solid line) in Figure 6.9b, the estimated- $L$  line (red solid line) in Figure 6.9a shows only five (5) erosion events and failed to detect erosion events on September 1, October 22, and November 14, 2009. This confirms the significance of the 8-hour moving average smoothing for obtaining more meaningful results.

#### 6.1.6 Near-bank Shear Stress Determination

In this study, the measurements of water stage,  $h$ , were used as input for a 1D channel evolution model, namely the Conservational Channel Evolution and Pollutant Transport System (CONCEPTS version 2.0, Langendoen and Alonso, 2008) to generate a

time series of the corresponding near-bank shear stress, by assuming a steady, uniform flow within the study reach where in this instance the near bank shear stress,  $\tau_w$ , exerted on each layer  $i$  along the bank profile was quantified as (Langendoen and Simon, 2008):

$$\tau_{w_i} = \rho g R_i S_f \quad (6.2)$$

where  $\rho$  ( $\text{kg/m}^3$ ) is the mass density of water;  $g$  ( $\text{m/s}^2$ ) is the gravitational acceleration;  $R_i = A_i/P_i$  is the hydraulic radius corresponding to each layer  $i$ , and  $S_f$  denotes the friction slope.

This assumption holds true within the vicinity of the PEEPs as the flow depth could be approximated as steady within the cross sectional area where the PEEPs were placed during an event. The runs from CONCEPTS were performed within reaches at sites 1 and 2 (a 67-m and a 129-m stream reach, respectively), which included the cross sectional areas where the PEEPs were deployed (Sutarto et al., in press). More information on CONCEPTS and the application of the model at Clear Creek can be found in Langendoen and Alonso (2008) and section 6.4 in Sutarto et al. (in press), respectively. In addition, the water stage,  $h$ , data were used to identify the time of PEEP submergence. This information was important to distinguish if the retreat detected by the PEEP was due to flow shearing action or other mechanisms (e.g. mass failure).

## 6.2 Field Component: Soil Sample Extraction

The field work was focused at two sites near the headwaters and mouth of Clear Creek. Herein the headwaters site is referred to as site 1 (Fig. 5.1a, 5.1b and 5.1d), while the site near the mouth of Clear Creek is referred to as site 2 (Fig. 5.1a, 5.1c and 5.1e). These two sites are contrasting as they are mostly comprised of semi-cohesive bank soils

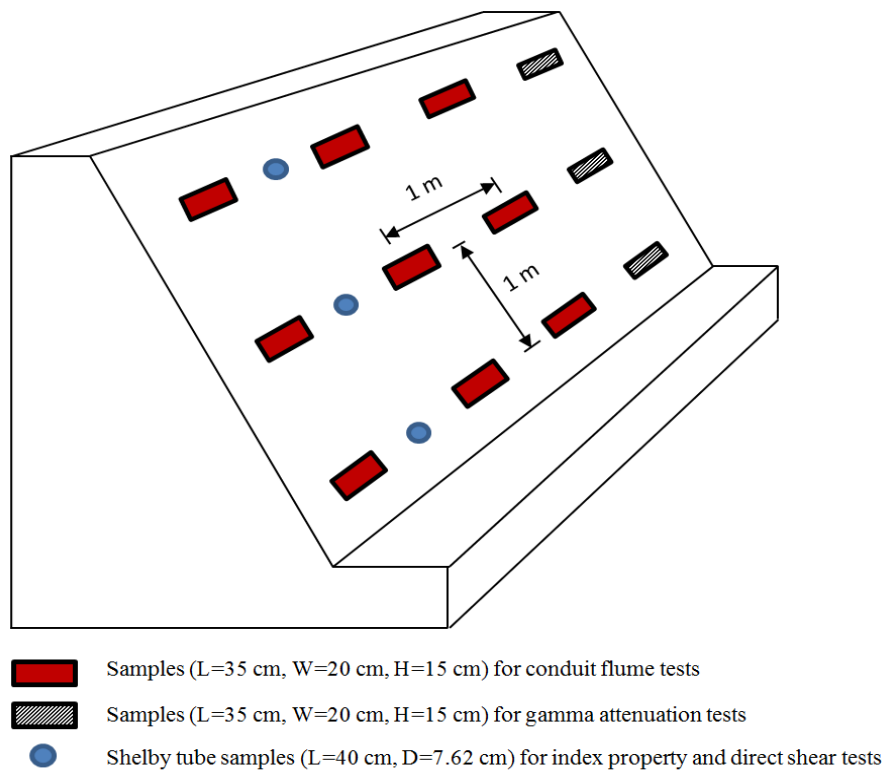
with distinctly different soil index properties and experience different hydrodynamic forces.

Sixty (60) bank soil samples were extracted and brought to the laboratory for performing mass and fluvial erosional strength analyses. Soil extractions were performed at cross sections SA 2, site 1 (Fig. 5.1d) and CC 1, site 2 (Fig. 5.1e). The extraction scheme for each bank profile is described in Figure 6.10a.

The soil samples were extracted from the crest, midbank, and toe of the left and right banks at both sites 1 and 2 for measuring key soil index properties and more importantly for characterizing the effects of potential soil heterogeneity on mechanical & erosional strengths along a bank profile. Twelve (12) “undisturbed” soil samples were extracted using 40-cm long Shelby tubes (ID = 7.62 cm) (Fig. 6.10a) for determining the soil index properties and mechanical strength parameters ( $c'$  and  $\phi'$ ).

The remaining forty-eight (48) soil samples were extracted from the same locations (Fig. 6.10a) for determining the degree of heterogeneity in the bank soils and conducting the fluvial erosion tests. In particular, twelve (12) out of these forty-eight (48) samples were selected for assessing the degree of heterogeneity of the bank soils and its implications to  $\tau_{c,f}$  using attenuation measurements of a gamma radiation source. The remaining thirty-six (36) soil samples were employed in the fluvial erosion tests to determine  $\tau_{c,f}$ . The fact that more samples were extracted for performing the fluvial erosion experiments than the mechanical strength and gamma detector tests was justifiable by the emphasis placed in this study on the  $\tau_{c,f}$  estimation (see Papanicolaou et al., 2007).

The samples were extracted between July and October of 2011 for site 2 and



(a)



(b)

Figure 6.10 Sample extractions. (a) A sketch of the sample extraction scheme applied for the left and right banks at site 1 and 2. Figure not to scale. (b) Extraction of soil blocks from the right bank, cross section CC 1 at site 2. Inset: Soil was wrapped in cheese cloth before being transported from the field to the laboratory.

between September and October of 2012 for site 1 thereby isolating the effects of the freeze-thaw cycle and soil desiccation on  $\tau_{c,f}$  estimation (Bullock et al., 1988). This allowed for comparisons of  $\tau_{c,f}$  values with other sites that exhibit similar soil index properties and geometric attributes but do not experience freeze-thaw effects. Each sample was extracted with a consistent procedure. Initially, the grass on the bank face was cut to the soil surface, thereby keeping the roots intact and avoiding any damage to the soil structure. Soil blocks (length = 35 cm; width = 20 cm; height = 15 cm) were then excavated from the bank face with two long soil blades and a wire saw (Fig. 6.10b). The removed soil blocks were carefully wrapped in cheese cloth, covered in wax, and placed within plastic boxes to minimize soil water loss and prevent cracking due to dehydration. The samples were stored in the laboratory at a constant room temperature of 20° C.

### 6.3 Laboratory Component

The laboratory component included the use of state-of-the-art equipment, such as a gamma attenuation detector, a direct shear device, and an erosional conduit flume, for measuring soil heterogeneity, mechanical strength parameters (i.e.,  $c'$  and  $\phi'$ ), and fluvial erosional strength parameters (i.e.  $\tau_{c,f}$  and  $M_f$ ) respectively, of the soils along the bank profile (see sections 6.3.2 to 6.3.4). These measurements allowed for a comparison between  $c'$  and  $\tau_{c,f}$ , as well as an assessment of the role that soil heterogeneity plays on  $c'$  and  $\tau_{c,f}$  variability along a bank profile. In addition, the measurements for  $c'$  and  $\tau_{c,f}$  were compared with corresponding measurements reported in the literature to facilitate discussion of the methods and associated results deduced in the present study and their extrapolation to sites exhibiting similar soil properties. The various steps in the laboratory analysis are described below.

### 6.3.1 Soil Index Properties

Soil index properties were determined for the twelve (12) Shelby-tube soil samples. The particle size distribution and soil texture were obtained through sieving and by using a hydrometer for the finer fraction (ASTM D422-63). The bulk density was quantified using the weight and volume of the soil samples extracted from the Shelby tube (ASTM 4254-91). The Atterberg limits (i.e., liquid limit, *LL*, and plastic limit, *PL*) were determined using a fall cone test (Budhu, 2011). Other estimated indices included the plasticity index, *PI*, and clay activity,  $A_c$ .

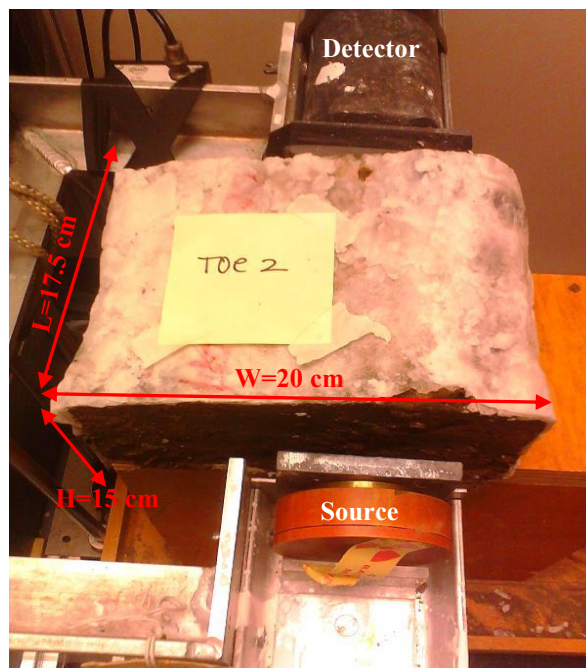
### 6.3.2 Bulk Density Heterogeneity

To assess the degree of soil heterogeneity, twelve (12) soil samples from the crest, midbank and toe of the banks at site 1 and 2 were cut in half length wise (i.e., length = 17.5 cm; width = 20 cm; height = 15 cm) (Fig. 6.11a) so they could fit into the gamma attenuation detector set-up (Fig. 6.11b) and enable bulk density profile measurements throughout the entire samples. The bulk density measurements were conducted using an automated gamma radiation scanning system that consisted of a 550-mCi Americium (Am-241) gamma radiation source (measured at 60keV) and a Harshaw 6S2/2-X NaI(Tl) detector (Fig. 6.11b) with an integrated photomultiplier for detecting of the attenuated radiation. The signal from the detector was amplified and then passed through a single-channel analyzer (Harshaw NC-22) operated in windowed mode to filter out noise. Collimation was provided by a lead plate that was 9.5-mm thick with a 6.35-mm circular hole for the source beam and a 0.889 x 36.8-mm slit for the detector, machined in a 31.8-mm deep block of lead. The same system was also used in Papanicolaou and Maxwell (2006). A QuickBASIC program controlled the stepper motor and gamma counter; the





(a)



(b)

Figure 6.11 Gamma attenuation test. (a) Selective soil samples, from the crest, midbank, and toe of the right bank, cross section CC 1 at site 2. (b) The radioactive source emitted collimated gamma radiation through the sample. The radioactivity was attenuated as it passed through the soil sample. The detector received this attenuated signal, which was a function of the sample bulk density.



photon count was recorded at specified heights, over a two-second interval. The interval was determined via a  $\chi^2$  test according to Knoll (1979) beginning at a specified time. The system was calibrated in advance by using reworked soil from Clear Creek of known water content; the recorded gamma count rates were then regressed to develop an equation that relates bulk density and the attenuation by the soil mixture (Papanicolaou and Maxwell, 2006). Attenuation measurements were collected along a grid with 1-cm spacings both vertically and laterally until the whole surface area was scanned. The attenuated radiation signal at each grid point was averaged over the entire length. Error of 3–5% for the volume fraction of solids is typical, and is highest at very low volume fractions, due to the statistical nature of radiation interactions. The duration for each scan per sample was nearly 3 hrs on an average.

### 6.3.3 Mechanical Strength Measurements

A direct shear device (Fig. B.1) was used to measure  $c'$  and  $\phi'$  for the twelve (12) Shelby-tube samples. Based on ASTM D 3080-98, sub-samples from the Shelby tubes were carefully cut to fit in the dimensions of the shear box (diameter = 6.34 cm; height = 2.5 cm). Once in the shear box, each sample was consolidated by gradually increasing the normal stress using ASTM D 2435-96 for the following loads: 7, 12, 25, 50, 100, and 200 kPa. Each load was applied to the sample until 90% consolidation was attained. This process lasted up to 9 hours per stress increment. After consolidation, the horizontal and vertical deformations, as well as the corresponding applied shear stresses were recorded simultaneously. This procedure was repeated for a range of at least three normal stresses per sample (see Fig. B.2 to B.12). The slope of the best fit line through

these data points provided the internal friction angle,  $\phi'$ , and the y-intercept provided the mechanical strength,  $c'$ .

#### 6.3.4 Fluvial Erosional Rate Measurements

A water-and-sediment recirculating, straight conduit flume with a rectangular 10-cm x 5-cm cross-section and a 305-cm useful length was utilized (Fig. 6.12 and 6.13) to estimate  $\tau_{c,f}$ . It is important to note that the purpose of the flume was not to replicate the exact hydrodynamic conditions of the study site but to allow for the estimation of  $\tau_{c,f}$  under controlled flow conditions by generically replicating the governing mechanisms of fluvial erosion, i.e., the shearing action of the flow. This type of flume was preferred over other available devices including jet tests, annular flumes, and open channel flumes for the following reasons: 1) The conduit flume delivers an applied shear to the surface of the sample, which is similar in nature to the driving mechanism of fluvial erosion, i.e., shearing action; and 2) The flow in the conduit flume is pressurized, allowing for a wider range of applied bed shear stresses than open-channel flumes thus making the conduit flume suited for the analysis of well compacted bank cohesive soils in general (e.g., Papanicolaou et al., 2007).

Each experimental run began by removing the soil sample from the wax coating and cutting it with a razor and wire saw to fit in the sample box, or tray, with the dimensions length = 30 cm; width = 10 cm; height = 5 cm (Fig. 6.12). Every effort was made to minimize the disturbance of the sample surface micro-roughness. The tray location was 215 cm downstream of the upstream diffuser (Fig. 6.13). This distance is over 40 times the conduit height to ensure a fully developed boundary layer over the sediment sample (e.g., McNeil et al., 1996). Jack screws underneath the tray allowed for

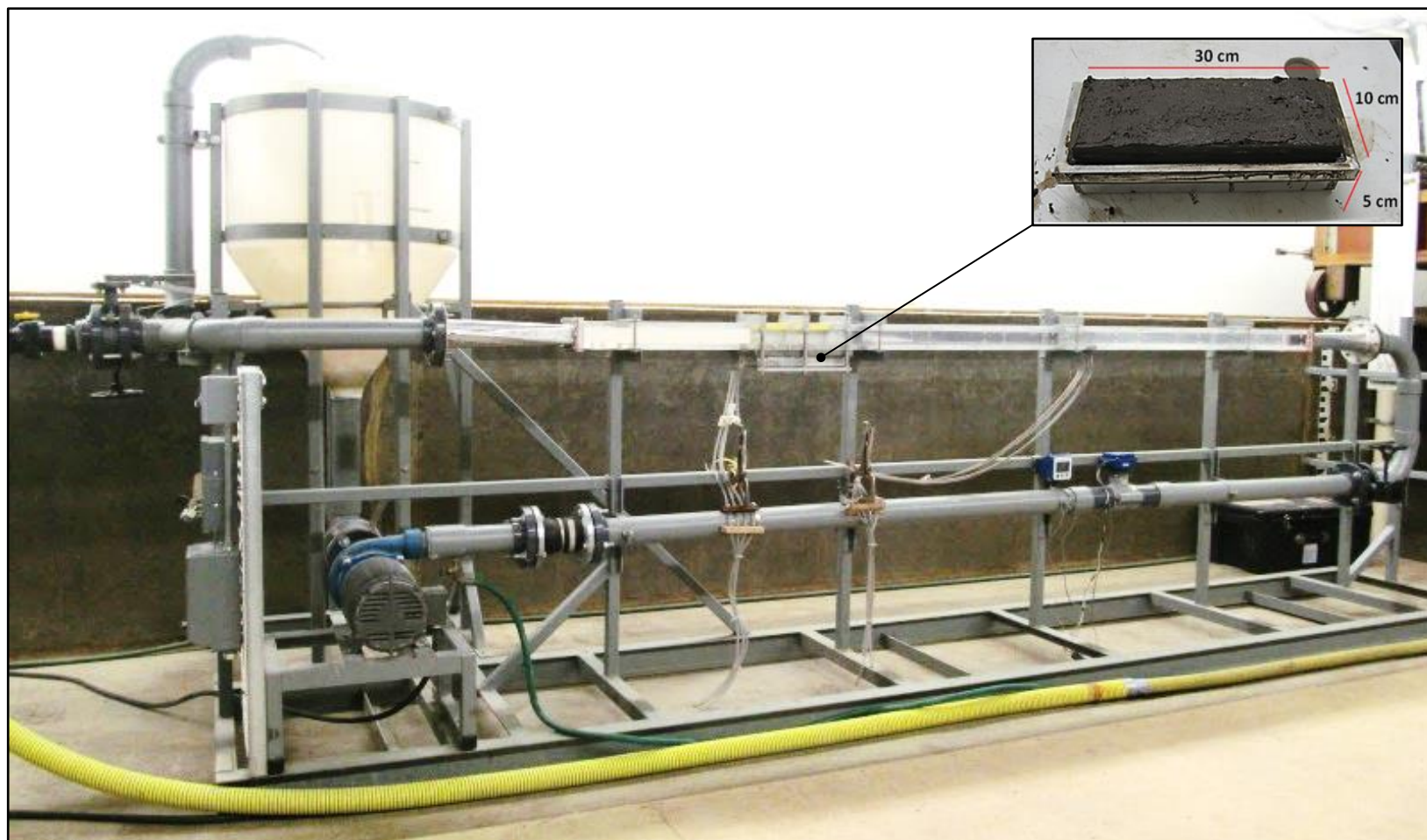


Figure 6.12 A photograph showing the conduit flume used in the present study.

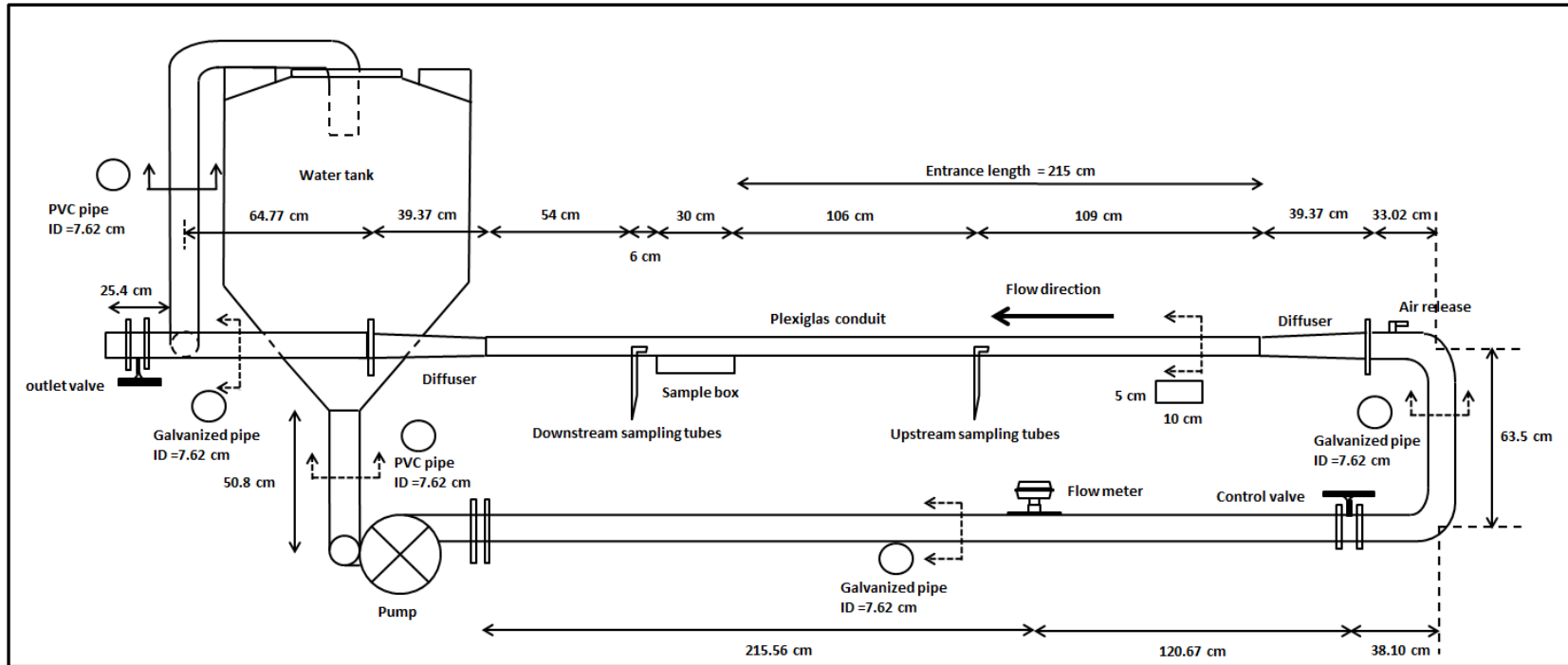


Figure 6.13 Dimensions of the conduit flume and its components.

minor adjustments so that the soil sample surface becomes even with the flume bed. The remainder of the flume bed and the top of the conduit duct were covered with fine sandpaper (roughness height,  $\varepsilon = 0.0002$  m) to closely replicate the surface micro roughness of the soil (Papanicolaou et al., 2007) and lessen the effects of a roughness change on the flow.

To operate the conduit flume, water was pumped with a variable-speed pump (7.5 hp, 3450 rpm) from a conical storage tank (Fig. 6.12 and 6.13) through a 7.62-cm ID galvanized pipe into the 50-cm<sup>2</sup> rectangular Plexiglas conduit (Fig. 6.13). A flow meter was attached to the galvanized supply pipe to measure the flow rate,  $Q$ , in the flume (Fig. 6.12 and 6.13). The operational flow rate of the flume ranged from 0.0025 to 0.0117 m<sup>3</sup>/s based on the lower and upper limits needed to maintain fully developed turbulent flow conditions. These flow rates corresponded to bulk velocities of 0.5 to 2.3 m/s and applied shear stresses of 1 to 19 Pa.

During a run, the flow rate and corresponding applied shear stress were increased every 10 min by adjusting the variable speed control (Papanicolaou et al., 2007). The results of preliminary flume tests (Fig C.1 and C.2) showed that the 10-minute interval was sufficient to allow the water concentration and flow rate in the flume to stabilize. Suspended sediment samples were collected at the end of the 10-min time step in two (2), 1-L bottles from sampling ports placed just downstream of the sample box. The sampling ports consisted of four Tygon tubes (ID = ~5 mm) (Fig. 6.12 and 6.13) that extended from the bottom of the conduit flume into the bottle. For each soil sample, up to 5 stress levels were tested (Fig. C.3) in order to provide sufficient number of ( $E_f, \tau_w$ )

data points to determine  $\tau_{c,f}$ . Following the completion of an experimental run, the flume was thoroughly flushed.

After all stress levels were completed for a given sample, the sediment concentration per bottle was measured through filtration using pre-weighed glass microfiber filters (nominally 1.0  $\mu\text{m}$  pore sizes). The filters and collected sediment were then oven-dried at 60° C until a constant weight was reached (~48 hr). The concentrations of the two, 1-L bottles collected for each stress level were then averaged ( $C_{avg}$ ). The above steps were repeated for thirty-six (36) samples.

The above steps were repeated for thirty-six (36) samples. The values of  $\tau_w$  were determined using the Darcy-Weisbach expression:

$$\tau_w = \frac{\rho U^2}{8} f \quad (6.3)$$

where  $\rho_w$  ( $\text{kg/m}^3$ ) is density of water,  $U$  (m/s) is bulk velocity, and  $f$  is Darcy-Weisbach friction factor which is provided in Haaland (1983):

$$\frac{1}{\sqrt{f}} = -1.8 \log \left[ \frac{6.9}{Re_{d_{eff}}} + \left( \frac{\varepsilon}{3.7d_{eff}} \right)^{1.11} \right] \quad (6.4)$$

herein  $\varepsilon$  (m) is the wall roughness provided by the fine sand paper (0.0002 m in this case);  $Re_{d_{eff}}$  is the Reynolds number determined by  $Re_{d_{eff}} = Ud_{eff}/\nu$ , with  $\nu$  being kinematic viscosity of water ( $1.01 \times 10^{-6} \text{ m}^2/\text{s}$ ); and  $d_{eff}$  (m) is the effective diameter of the rectangular conduit and is equal to  $(1.029)*d_h$  (White, 2008) with  $d_h$  (m) being the hydraulic diameter of the rectangular conduit (0.0667 m in this case).

The erosion rate,  $E_f$  ( $\text{kg/m}^2/\text{s}$ ), for each sample was determined as follows:

$$E_f = \frac{\Delta C_{avg} * Q}{A_s} \quad (6.5)$$

where  $\Delta C_{avg}$  ( $\text{kg/m}^3$ ) denotes the difference in average concentration between two consecutive flow increases;  $Q$  ( $\text{m}^3/\text{s}$ ) is the flow rate; and  $A_s$  ( $\text{m}^2$ ) is the surface area of the soil sample ( $0.03 \text{ m}^2$ ). The  $\tau_{c,f}$  was determined for each sample by plotting the pairs of  $E_f$  and  $\tau_w$  and extrapolating a best fit line to  $E_f = 0$  (Papanicolaou et al., 2007). The erosion rate,  $E_f$ , and excess shear stress  $\left(\frac{\tau_w}{\tau_{c,f}} - 1\right)$  were also plotted, and the slope of the fitted line represented the erodibility coefficient,  $M_f$ .

Overall, 180 conduit flume runs (36 samples x 5 stress increments/sample) were completed. In order for the reader to assess the level of detail and labor that is needed per experimental run the detailed experimental conditions for each of the samples tested are included in Table D.1. During the runs the error in measuring the concentration column (or erosion) was less than 5%. Bedload motion of large individual flocs was not observed in these tests as most of the particles were predominately transported in suspension. This is seen here for the flume runs with the low values of the Rouse number ( $R_o < 1$ ; Table D.1, column 8) suggesting that the concentration of the suspended material follows a uniform distribution (Raudkivi, 1998). To predict the dominant transport mode (i.e., bedload or suspended load) in the conduit flume test, the flume test conditions of three representative soil samples (CC-L-M2, CC-R-C4, and CC-R-T5) were analyzed for their dimensionless shear stresses or Shields parameters which depend on shear stress,  $\tau_w$ , in Pascal, and sediment diameter,  $D_{50}$ , in meter. The shields parameter is

$$\tau^* = \frac{\tau_w}{(\rho_s - \rho_w)gD_{50}} \quad (6.6)$$

where  $\rho_s$  ( $\text{kg/m}^3$ ) is density of sediment and  $g$  ( $\text{m/s}^2$ ) is gravitational acceleration. The dimensionless shear stress,  $\tau^*$ , values of those tests were all above the Brownlie and

McCave curves (Fig. 6.14), which represent the initiation of suspension. More importantly, the  $\tau^*$  values of those representative conduit flume tests were all above the 5% bed load threshold curve of Roberts et al. (2003) (Fig. 6.14), indicating that bed load fraction was less than 5%.

#### 6.4 Modeling Component

The  $c'$  and  $\tau_{c,f}$  values, as well as the soil index properties obtained from the analyses described in section 6.3 and the available hydrological data for Clear Creek (Fig. G.1), were used to generate input parameters for the CONCEPTS model. CONCEPTS is a 1D model that can simulate two types of mass failure (namely, planar slip and cantilever) and fluvial erosion. For more detailed information about CONCEPTS, the reader is directed to Langendoen and Alonso (2008) and Langendoen and Simon (2008).

In CONCEPTS, a bank profile can be divided into several layers allowing the user to account for variability in soil properties (e.g., bulk density, mechanical strength, and erosional strength) along the profile by assigning specific values for each layer. In the present study, the left and right banks at each cross-section were divided into 3 layers (Fig. 6.15a and 6.15b) as the samples from the crest, midbank, and toe were found to have different mechanical and fluvial erosional strengths (See Results Chapter 7). In addition, CONCEPTS quantifies the near bank shear stress,  $\tau_w$ , at the different layers and predicts the onset and magnitude of fluvial erosion for each layer. These features make the model an ideal tool for simulating both mass failure and fluvial erosion of banks characterized with heterogeneous soils, such as the ones in the present study.

To quantify  $FS_{mf}$ , Eq. 2.5 and Eq. 2.6 were employed in CONCEPTS and inputs for the water table dynamics, positive and negative pore water pressure, water confining



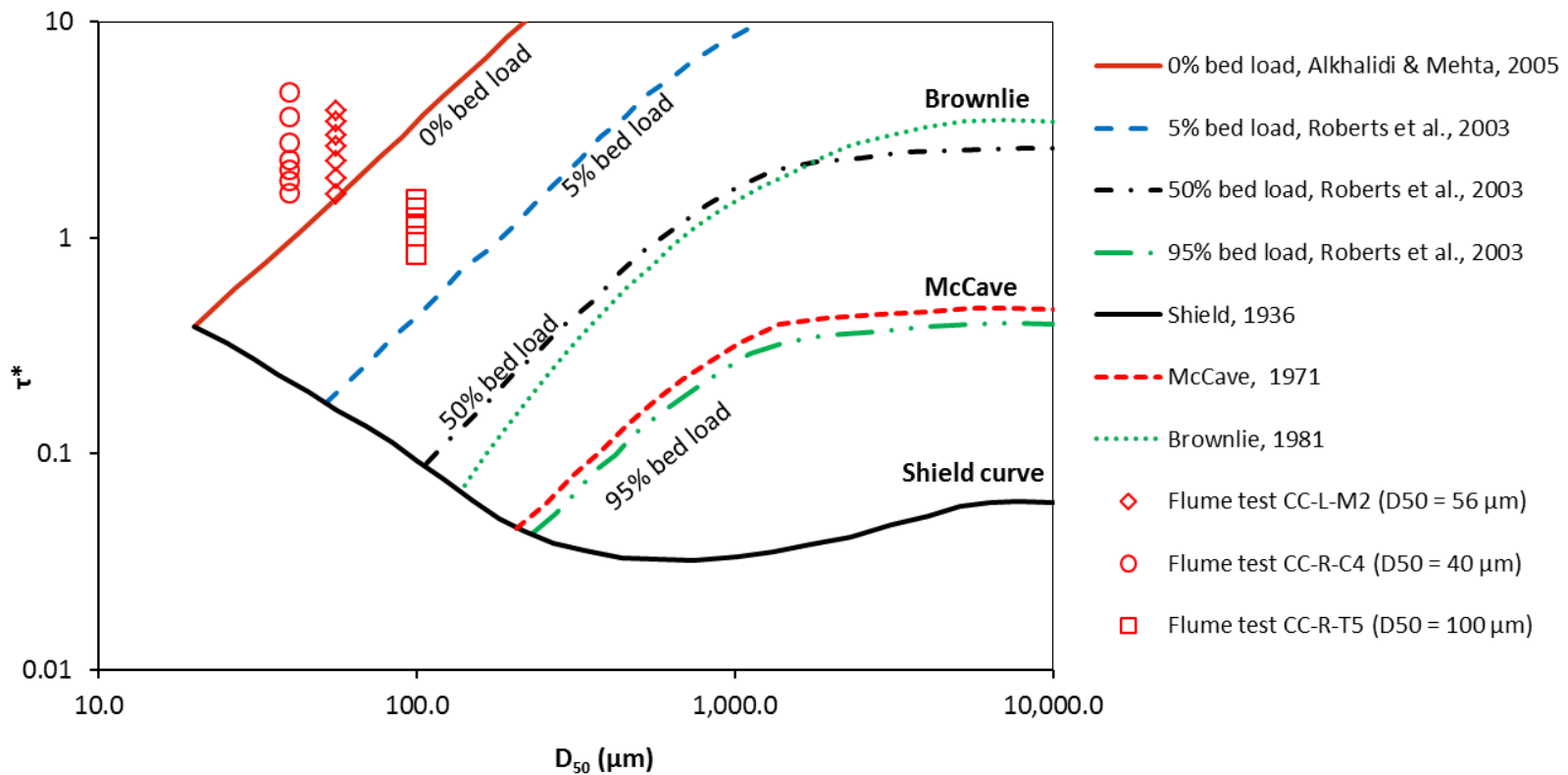


Figure 6.14 Bed load fraction as a function of particle diameter,  $D_{50}$ , and dimensionless shear stress,  $\tau^*$ . Shield curve defines the initiation of motion. McCave and Brownlie represent the initiation of suspension. The 95%, 50%, and 5% bedload threshold curves were based on Roberts et al. (2003). The 0% bed load threshold curve was originated from Alkhalidi & Mehta (2005).

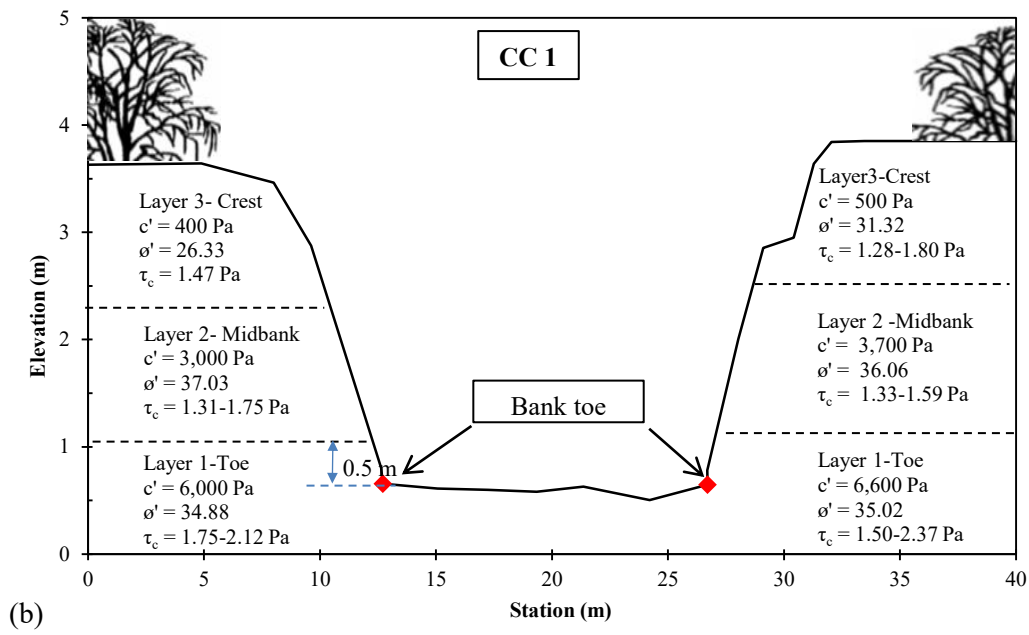
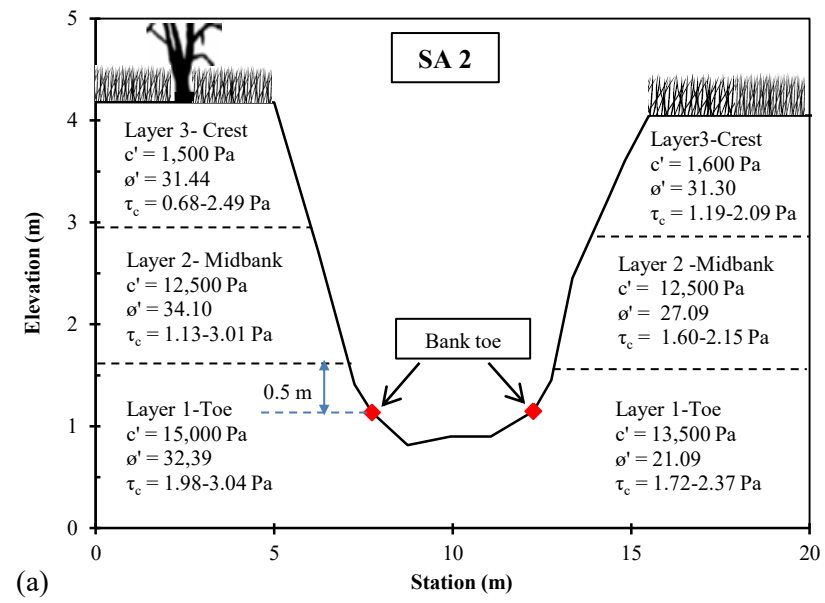


Figure 6.15 Representative cross-sections (facing downstream) with average bank soil properties: (a) Cross section SA 2, site 1. (b) Cross section CC 1, site 2.

pressure, and the effects of soil layering within a block were incorporated (Langendoen and Simon, 2008). The stability analysis was performed for different potential failure planes to determine the plane that corresponds to the minimum  $FS_{mf}$  value by using a modified quadratic fitting process (Langendoen and Simon, 2008).

The initial condition for the ground water table elevation (Fig G.2) was estimated using a steady state groundwater profile function provided by Liang and Zang (2012) for the hydrological data on October 1, 2007:

$$h^2(x, 0) = h_o^2 + \frac{q_o}{K_s}(X^2 - x^2) \quad (6.7)$$

where  $h$  (m) is the elevation of the water table above the bottom of the aquifer;  $h_o$  (m) is the constant river stage corresponding to the initial condition (October 1, 2007);  $q_o$  (m/s) is the recharge rate under steady state condition;  $K_s$  (m/s) is saturated hydraulic conductivity;  $X$  (m) is the horizontal extent of the aquifer; and  $x$  (m) is the horizontal coordinate. To incorporate the role of bank and bed surface irregularities, variations in shape and size of the channel cross section, obstruction in the channel, vegetation, and meandering of the channel on the estimation of roughness in CONCEPTS, different values of the Manning roughness coefficient were determined for the floodplains, bank profiles and streambed based on the guidelines provided by Arcement and Schneider (1989) for channels exhibiting similar properties like Clear Creek.

## CHAPTER 7 RESULTS

### 7.1 Soil Index Properties

In general, the bank soils at the headwaters site (site 1) were predominantly silt ( $61.55 \pm 6.23\%$ ) with lesser amounts of clay ( $17.62 \pm 5.46\%$ ) and sand ( $20.84 \pm 7.37\%$ ) (see Table 7.1, column 1-3, and Fig. A.1). Thus, they were classified as silt loams based on the USDA classification system (Fig. 7.1 and A.2). Unlike the samples at site 1 in which silt was dominant, the bank soils at the mouth site (site 2) had more equal portions of sand ( $52.79 \pm 11.43\%$ ) and silt ( $39.44 \pm 10.43\%$ ) with a low portion of clay ( $7.77 \pm 2.30\%$ ) (see Table 7.1, column 1-3, and Fig. A.1). The crest and toe soils were classified as sandy loams while the midbank soils were silt loams based on the USDA classification system (Fig. 7.1 and A.2). The sand fraction was slightly dominant at the toe and more specifically at the crest where sand was deposited during a June 20, 2009 flood event (Fig. 7.2). The plasticity index  $PI$  for both sites (Table 7.1, column 8) ranged from 12 to 19; the prevalent clay type based on XRD analysis is illite (Clay Mica) - smectite, with the average surface activity,  $A_c$ , values (Table 7.1, column 9), being 0.75 and 1.37, respectively, for sites 1 and 2 (Theregowda et al., 2006).

### 7.2 Bulk Density Heterogeneity

The bulk density measurements (Table 7.1, column 5) had an increasing trend from the crest to the toe of the bank at both sites 1 and 2, thereby suggesting a higher degree of consolidation in the toe soils comparatively to the midbank and crest soils and implying the presence of a rather heterogeneous soil profile (see further elaboration with the discussion of Figure 7.3 below). At site 1, the average bulk density values were

Table 7.1 Soil index properties for Clear Creek bank soils.

Sampling Location		Sand %	Silt %	Clay %	D <sub>50</sub> (mm)	ρ <sub>bulk</sub> (kg/m <sup>3</sup> )	LL %	PL %	PI %	A <sub>c</sub>
		(1)	(2)	(3)	(4)	(5)	(6)	(7)	(8)	(9)
Site 1, SA 2, left bank	Crest	15.00	70.16	14.84	0.027	1,404	31.88	13.60	18.27	0.91
	Midbank	15.00	61.22	23.78	0.020	1,989	39.28	21.39	17.89	0.60
	Toe	30.00	53.73	16.27	0.049	1,974	28.98	15.69	13.30	0.68
Site 1, SA 2, right bank	Crest	20.00	67.41	12.59	0.028	1,654	32.24	16.23	16.01	0.96
	Midbank	15.00	59.90	25.10	0.022	1,826	38.65	21.29	17.36	0.58
	Toe	30.04	56.89	13.11	0.045	1,936	23.09	10.36	12.73	0.76
Site 2, CC 1, left bank	Crest	65.00	30.54	4.46	0.130	1,553	NA	NA	NA	NA
	Midbank	40.00	49.59	10.41	0.056	1,794	27.50	13.31	14.19	1.18
	Toe	65.00	28.46	6.54	0.100	2,014	NA	NA	NA	NA
Site 2, CC 1, right bank	Crest	43.00	49.91	7.09	0.040	1,299	31.49	19.12	12.36	1.22
	Midbank	45.00	47.17	7.83	0.058	1,618	30.21	15.24	14.97	1.71
	Toe	58.74	30.95	10.31	0.100	1,880	NA	NA	NA	NA

Note: percent of sand, silt and clay were determined from sieving and hydrometer tests; liquid limit LL, and plastic limit PL, were measured by fall cone technique; plasticity index PI = LL- PL; clay activity Ac = PI/clay percentage. The numbers in the parentheses are the column numbers.

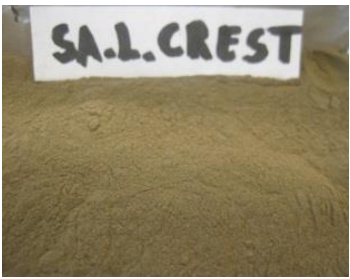








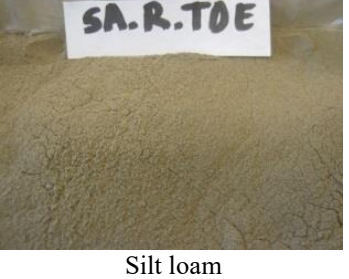


	Site 1		Site 2	
	Left bank	Right bank	Left bank	Right bank
<b>Crest</b>	 <p>SA.L.CREST</p> <p>Silt loam</p>	 <p>SA.R.CREST</p> <p>Silt loam</p>	 <p>CC.L.CREST</p> <p>Sandy loam</p>	 <p>CC.R.CREST</p> <p>Silt loam</p>
<b>Mid bank</b>	 <p>SA.L.MID</p> <p>Silt loam</p>	 <p>SA.R.MID</p> <p>Silt loam</p>	 <p>CC.L.MID</p> <p>Silt loam</p>	 <p>CC.R.MID</p> <p>Silt loam</p>
<b>Toe</b>	 <p>SA.L.TOE</p> <p>Silt loam</p>	 <p>SA.R.TOE</p> <p>Silt loam</p>	 <p>CC.L.TOE</p> <p>Sandy loam</p>	 <p>CC.R.TOE</p> <p>Sandy loam</p>

Figure 7.1 Twelve (12) oven-dried bank soil samples from site 1 and 2.





Figure 7.2 Clear Creek bank soils. Fresh sand was deposited on the flood plain at site 2 after a flood event.

1,529 kg/m<sup>3</sup>, 1,908 kg/m<sup>3</sup> and 1,955 kg/m<sup>3</sup>, respectively, for the crest, midbank, and toe, while at site 2 they were 1,426 kg/m<sup>3</sup>, 1,706 kg/m<sup>3</sup> and 1,908 kg/m<sup>3</sup>, respectively. In addition, the bank soils at site 1 had overall higher bulk densities comparatively to the bank soils at site 2 suggesting that soils at site 1 were more “aged” (or less reworked) than the soils at site 2. This finding was not surprising considering that the bank profile at site 2 contained newly deposited finer sand material, which mostly originated from the river sediment bed during overbank flows, and was reconfirmed with penetrometer measurements (Wilson et al., 2012). The bulk density measurements (Table 7.1, column 5) also showed that the heterogeneity among the three layers for site 2 was higher comparatively to site 1.

Figure 7.3 shows examples of the bulk density profiles measured with gamma attenuation for three representative samples from the crest, midbank, and toe of the right bank at cross section CC 1. The bulk density values measured with the gamma attenuation scanning system, when integrated over the sample height of about 15 cm, compared overall well with the bulk density values determined using standard methods (Table 7.1, column 5). Nonetheless, the density profiles over the height of 15 cm in Figure 7.1 revealed that soils from the crest and midbank exhibited higher heterogeneity as seen by the scatter in the attenuation data. The soil from the bank toe, however, had a fairly constant density profile thereby implying a rather homogeneous soil. A similar trend was found for samples at cross section SA 2 although the degree of heterogeneity among the three layers at the headwaters site was less comparatively to that at the mouth (i.e., CC 1). CC1 had a higher heterogeneity especially at the crest due to the finer fraction sand deposition during frequent flooding at this site (Fig. 7.2).



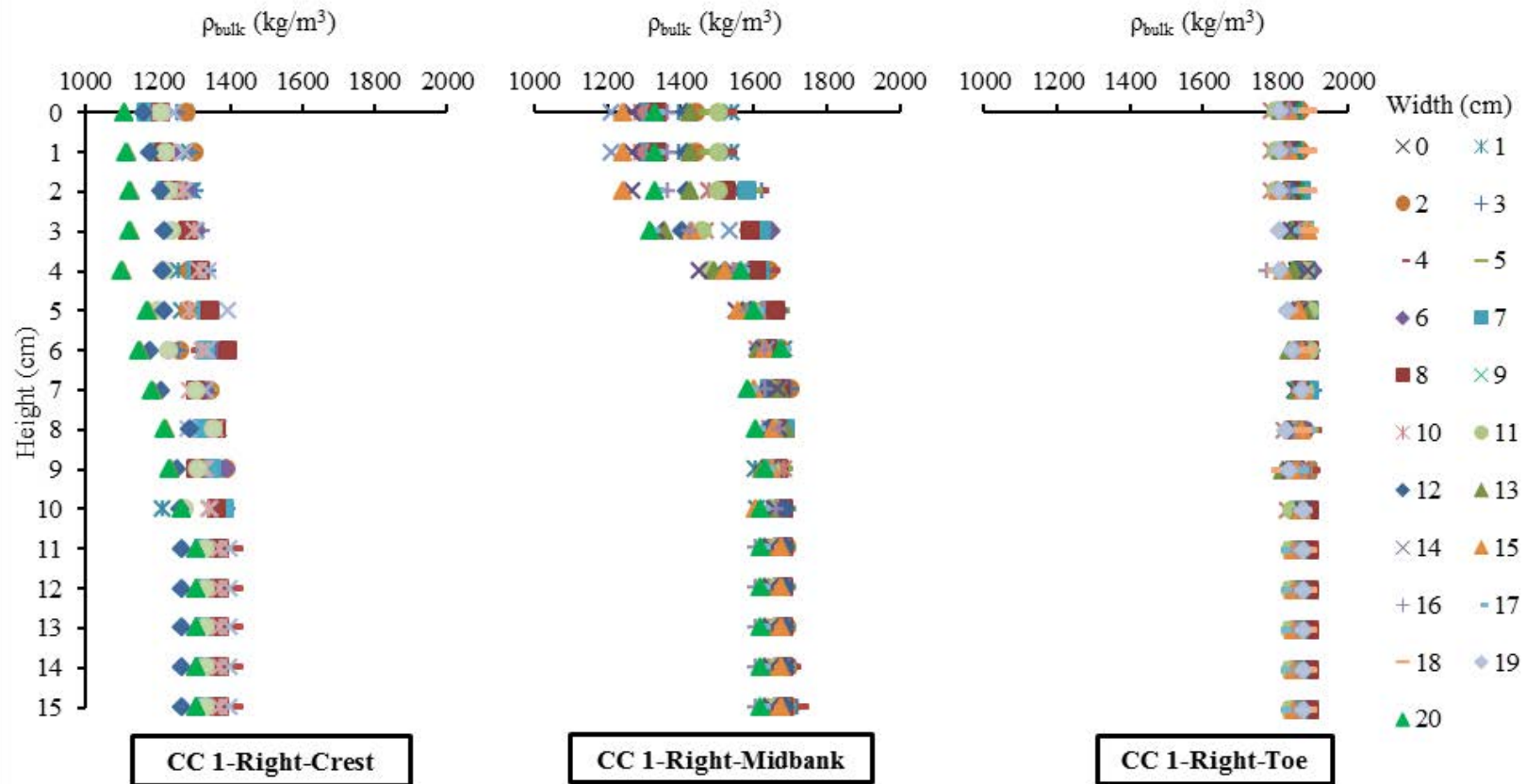


Figure 7.3 Bulk density profile obtained from gamma attenuation analyses. Representative samples from the right bank, cross section CC1 at site 2, were analyzed using gamma attenuation to measure bulk density. The height and width are the distance from the top and side of soil sample, respectively, to the measurement point. The scatter in the data points for the crest and midbank samples demonstrates heterogeneity in bulk density. In contrast, the toe soil exhibited a collapse of data points signifying the homogeneity in bulk density.

### 7.3 Fluvial Erosional Strength

For each of the thirty six (36) samples run in the conduit flume, a plot of  $E$  versus  $\tau_w$  was developed to estimate the fluvial erosional strength,  $\tau_{c,f}$ . Figures 7.4 and 7.5 provide the  $E$  versus  $\tau_w$  plots for 12 representative samples from the crest, midbank, and toe at cross sections SA 2 and CC 1, respectively. The plots of  $E$  versus  $\tau_w$  for all soil samples can be found in Figure E.1. A summary of the  $\tau_{c,f}$  values for all thirty six (36) samples can be found in Table 7.2a and 7.2b (columns 2 and 9). The results from the fluvial erosional tests show a consistent trend of  $E$  varying nearly linearly with  $\tau_w$ , which has also been reported in the literature for homogeneous samples (e.g., Papanicolaou et al., 2007; Veeraraghavan, 2007; Partheniades, 2009). Of the thirty six (36) samples analyzed with the conduit flume, only nine (9) samples exhibited low correlations with  $R^2$  values lower than 0.55 due to large scatter in the  $(E, \tau_w)$  data. These samples mostly originated from the crest (n=5) and midbank (n=3) layers and exhibited heterogeneity in bulk density, a finding that was supported by the gamma source attenuation results (an example is the CC1-Right-Midbank in Figure 7.3). Worm burrows observed in some of the samples originated from the midbanks also contributed to the observed scatter of the  $(E, \tau_w)$  data points for the nine (9) samples (e.g., Vermeyen, 1995; Widdows et al., 1998; Grabowski et al., 2011).

The results of the conduit flume runs (Table 7.2a, 7.2b columns 2 and 9) revealed an increasing trend in magnitude of  $\tau_{c,f}$  moving downslope along the bank profiles for all cross sections. A similar trend was reported earlier for the bulk density (Table 7.1, column 5). This correspondence suggests a positive correlation between  $\tau_{c,f}$  and bulk

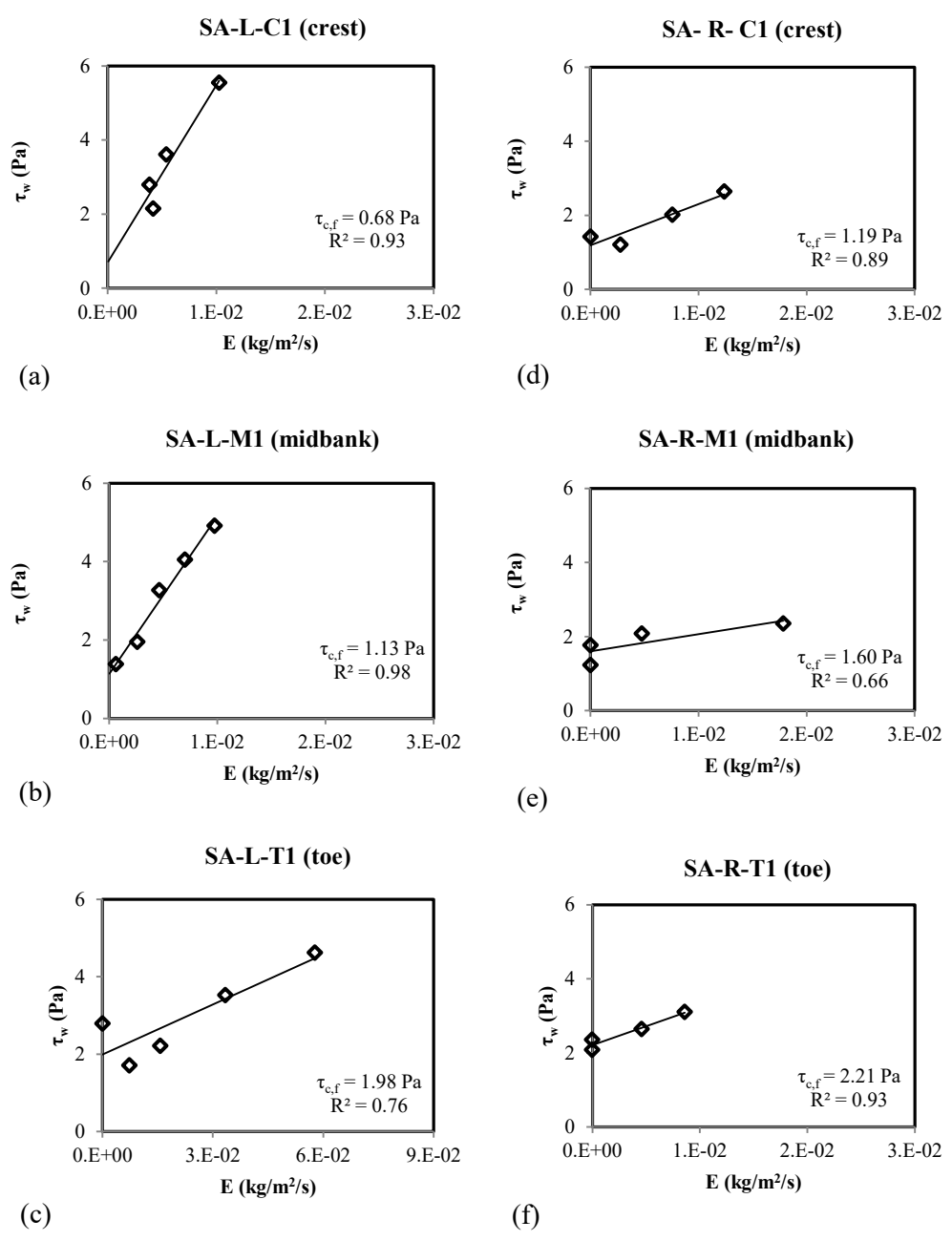


Figure 7.4 Six examples of the conduit flume test results for site 1. The tested soil samples were extracted from cross section SA 2 at site 1: (a) Left bank-crest. (b) Left bank-midbank. (c) Left bank-toe. (d) Right bank-crest. (e) Right bank-midbank. (f) Right bank-toe. The  $\tau_{c,f}$  is determined as the y-intercept or stress where  $E=0$ .

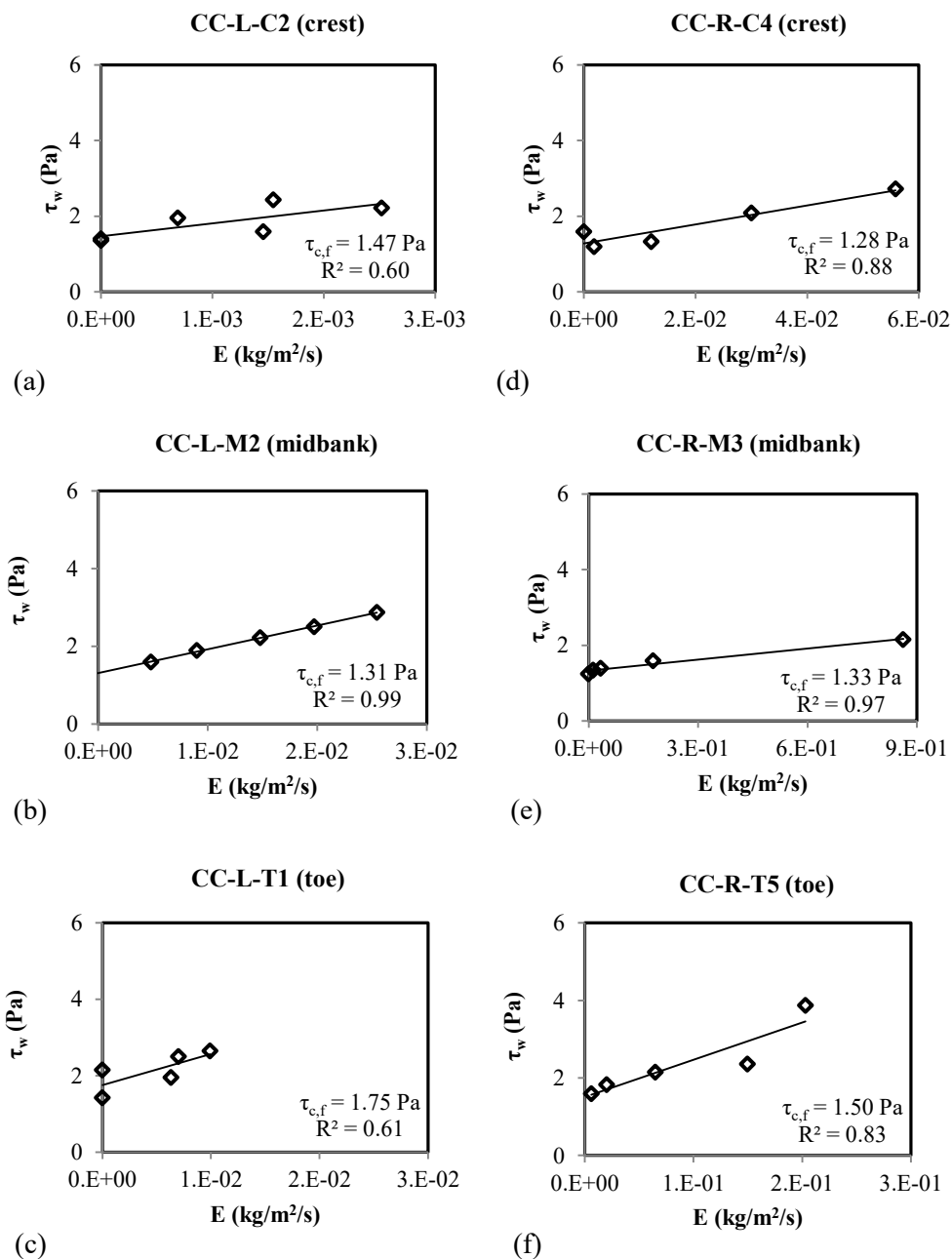


Figure 7.5 Six examples of the conduit flume test results for site 2. The tested soil samples were extracted from cross section CC 1 at site 2: (a) Left bank-crest. (b) Left bank-midbank. (c) Left bank-toe. (d) Right bank-crest. (e) Right bank- midbank.(f) Right bank-toe. The  $\tau_{c,f}$  is determined as the y-intercept or stress where  $E=0$ .

Table 7.2 Summary of fluvial erosional strength values obtained from conduit flume tests.

Sampling location	Left Bank						Right Bank					
	Sample ID	$\tau_{c,f}$ (Pa)	$\tau_{c,f \text{ avg.}}$ (Pa)	Std. Dev. (Pa)	Dev. (%)	Avg Dev. (%)	Sample ID	$\tau_{c,f}$ (Pa)	$\tau_{c,f \text{ avg.}}$ (Pa)	Std. Dev. (Pa)	Dev. (%)	Avg Dev. (%)
	(1)	(2)	(3)	(4)	(5)	(6)	(7)	(8)	(9)	(10)	(11)	(12)
<b>Site 1, SA2</b>												
Crest	SA-L-C1	0.68				60.38	SA-R-C1	1.19				17.01
	SA-L-C2	2.49	1.71	0.93	45.70	40.25	SA-R-C2	1.59	1.44	0.21	10.43	11.34
	SA-L-C3	1.96				14.68	SA-R-C3	1.53				6.59
Midbank	SA-L-M1	1.13				46.75	SA-R-M1	1.60				8.17
	SA-L-M2	3.01	2.12	0.94	41.97	31.17	SA-R-M2	1.19	1.48	0.25	19.81	13.21
	SA-L-M3	2.22				4.78	SA-R-M3	1.65				11.64
Toe	SA-L-T1	1.98				21.02	SA-R-T1	2.21				5.31
	SA-L-T2	3.04	2.51	0.53	21.37	14.25	SA-R-T2	2.37	2.10	0.34	12.98	12.19
	SA-L-T3	2.50				0.35	SA-R-T3	1.72				18.29
<b>Site 2, CC1</b>												
Crest	CC-L-C1	1.67				6.29	CC-R-C3	1.30				11.19
	CC-L-C2	1.47	1.57	0.14	6.29	6.29	CC-R-C4	1.28	1.46	0.30	12.26	15.64
	CC-L-C3	NA <sup>a</sup>				NA <sup>a</sup>	CC-R-C5	1.80				23.45
Midbank	CC-L-M1	1.75				14.17	CC-R-M1	1.49				1.40
	CC-L-M2	1.31	1.53	0.31	14.17	14.17	CC-R-M2	1.59	1.47	0.13	8.13	6.35
	CC-L-M3	NA <sup>a</sup>				NA <sup>a</sup>	CC-R-M3	1.33				9.53
Toe	CC-L-T1	1.75				8.86	CC-R-T1	1.60				12.25
	CC-L-T2	1.90	1.92	0.18	1.24	6.73	CC-R-T2	2.37	1.83	0.48	29.88	19.92
	CC-L-T4	2.12				10.10	CC-R-T5	1.50				17.62

Note: the numbers in parentheses are the column number; <sup>a</sup>Sample was disrupted when it was cut for fitted in the tray.

Table 7.3 Summary of erodibility values for fluvial erosion obtained from conduit flume tests.

Sampling location	Left Bank						Right Bank					
	Sample ID	M <sub>f</sub> (kg/m <sup>2</sup> s)	M <sub>f avg.</sub> (kg/m <sup>2</sup> s)	Std.Dev. (kg/m <sup>2</sup> s)	Dev. (%)	Avg. Dev. (%)	Sample ID	M <sub>f</sub> (kg/m <sup>2</sup> s)	M <sub>f avg.</sub> (kg/m <sup>2</sup> s)	Std. Dev. (kg/m <sup>2</sup> s)	Dev. (%)	Avg. Dev. (%)
	(1)	(2)	(3)	(4)	(5)	(6)	(7)	(8)	(9)	(10)	(11)	(12)
<b>Site 1, SA2</b>												
Crest	SA-L-C1	1.40E-03				97.57	SA-R-C1	1.02E-02				27.32
	SA-L-C2	1.89E-02	5.76E-02	8.27E-02	67.21	109.85	SA-R-C2	6.00E-03	1.40E-02	1.05E-02	57.24	84.56
	SA-L-C3	1.53E-01				164.78	SA-R-C3	2.59E-02				84.56
Midbank	SA-L-M1	2.80E-03				89.30	SA-R-M1	3.13E-02				12.20
	SA-L-M2	1.22E-02	2.62E-02	3.27E-02	53.38	95.12	SA-R-M2	4.00E-02	3.57E-02	6.15E-03	12.20	12.20
	SA-L-M3	6.35E-02				142.68	SA-R-M3	NA				NA
Toe	SA-L-T1	4.08E-02				13.98	SA-R-T1	1.91E-02				14.48
	SA-L-T2	7.87E-02	4.74E-02	2.85E-02	65.92	43.94	SA-R-T2	4.04E-02	2.23E-02	1.67E-02	80.90	80.90
	SA-L-T3	2.28E-02				51.93	SA-R-T3	7.50E-03				66.42
<b>Site 2, CC1</b>												
Crest	CC-L-C1	NA					CC-R-C3	6.99E-02				62.31
	CC-L-C2	3.30E-03	3.30E-03	NA	NA	NA	CC-R-C4	4.79E-02	4.31E-02	2.95E-02	11.22	62.31
	CC-L-C3	NA <sup>a</sup>					CC-R-C5	1.14E-02				73.53
Midbank	CC-L-M1	2.82E-01				85.76	CC-R-M1	5.08E-01				19.02
	CC-L-M2	2.16E-02	1.52E-01	1.84E-01	85.76	85.76	CC-R-M2	1.68E-02	6.27E-01	6.78E-01	97.32	116.34
	CC-L-M3	NA <sup>a</sup>				NA	CC-R-M3	1.36E+00				116.34
Toe	CC-L-T1	1.74E-02				16.55	CC-R-T1	6.43E-02				22.50
	CC-L-T2	NA	2.09E-02	4.88E-03	NA	16.55	CC-R-T2	4.04E-02	8.30E-02	5.44E-02	51.31	73.80
	CC-L-T4	2.43E-02				16.55	CC-R-T5	1.44E-01				73.80

Note: the numbers in parentheses are the column number.

<sup>a</sup>Sample was disrupted when it was cut for fitted in the tray.

density, a finding which was also observed in other studies (e.g., Parker et al., 1995; Zreik et al., 1998; Krone, 1999; Wynn and Mostaghimi, 2006). The observed trends for  $\tau_{c,f}$  and bulk density along the downslope of the bank profiles at sites 1 and 2 were also in correspondence with the trend for  $c'$  to be described in section 7.5.

Further, the  $\tau_{c,f}$  values at site 1 were consistently higher in magnitude than the values at site 2 (Table 7.2; columns 2 and 9) as the bank soils at site 1 had a higher silt and clay content than site 2. A similar finding has been presented by Veeraraghavan (2007) where silt loam had an average  $\tau_{c,f} = 3.10$  Pa and sandy loam had an average  $\tau_{c,f} = 1$  Pa. Several other studies (e.g., Kamphuis and Hall, 1983; Panagiotopoulos et al., 1997; Julian and Torres, 2006; Kothiyari and Jain, 2008; Layzell et al., 2014) have also reported a positive correlation of the finer fraction of sediment content with  $\tau_{c,f}$ .

A summary of erodibility coefficient,  $M_f$ , values for all thirty six (36) samples can be found in Table 7.3 (columns 2 and 9). The  $M_f$  values for site 1 were between  $1.40 \times 10^{-3}$  and  $1.87 \times 10^{-2}$  kg/m<sup>2</sup>s while site 2 had a wider range of  $M_f$  values, which were between  $3.30 \times 10^{-3}$  to and  $5.08 \times 10^{-1}$  kg/m<sup>2</sup>s. These values were within the range reported in the literature for erodible bank soils (e.g., Layzell et al., 2014). There was no trend found in  $M_f$  value along the downslope of the bank profile like what was found for bulk density and  $\tau_{c,f}$ . Additionally, there was no relationship between  $M_f$  and other parameters in this study, namely, bulk density, bulk density heterogeneity, soil composition, and  $\tau_{c,f}$  as reported in other studies (e.g., Hanson and Simon, 2001; Layzell et al., 2014). This finding prompted a question whether there were other dominant factors that may have affected  $M_f$  in this study besides bulk density heterogeneity and soil composition. Further study is required to address this issue.

#### 7.4 Frequency and Magnitude of Mass Erosion

Figure 7.6 demonstrates the time series of water stage (Fig.7.6a) at site 1 along with the synchronous moving-averaged and estimated  $L$  for PEEP A1 (Fig. 7.6b), A2 (Fig. 7.6c), and A3 (Fig. 7.6d) deployed at the crest, midbank, and toe, respectively. The PEEPs were deployed on May 18 and removed from the site on June 22, 2009 after the June 19, 2009 flood event, which fully exposed them. The June 19, 2009 flood event was an extreme flash-flood event that caused bank overtopping by nearly 0.5 m within less than 5 hours. No significant events capable of triggering mass erosion occurred thereafter, thus limiting the monitoring period considerably when compared to site 2. Figure 7.6 shows the time series of the 8-hour moving-averaged  $L$  data (black dashed lines) at all locations in the profile at site 1 and provides the retreat length associated with the June 19, 2009 flood.

In Figure 7.6c, the data were lost between May 18 and June 4, 2009 due to a technical problem with the data logger that recorded the output from PEEP A2. Despite the short monitoring period, the PEEP deployment at site 1 had successfully provided important information on the erosion depths associated with the June 19, 2009 flood event at the crest, midbank and toe along the downslope of the bank. The crest soil eroded the most with an erosion depth of 13 cm (Fig. 7.6b) although, due to its location, experienced less shear stress,  $\tau_w$ , during the event comparatively to the other two locations. This finding suggests that the crest soil was weaker than the midbank and toe soils, which eroded by 5.1 cm and 9.7 cm (Fig. 7.6c and 7.6d), respectively. This trend agrees with the results of Sutarto et al. (in press) that reported an increasing soil bulk density, and, thus, soil age and strength along the downslope of bank profile at this



location. There could be an additional reason for the weaker crest soils other than it being a less dense soil. Lawler et al. (1999) and more recently Pizzuto (2009) postulated that subaerial processes and freeze-thaw cycles can have a significant contribution to the weakening of the soil usually starting from the midsection of the bank and extending to the bank crest.

Figure 7.7 shows the time series of water stage (Fig. 7.7a) at site 2 in relation to the 8-hour moving-averaged and estimated  $L$  for PEEP B1 (Fig. 7.7b), B2 (Fig. 7.7c), B3 (Fig. 7.7d), and B4 (Fig. 7.7e) installed at the crest, upper midbank, lower midbank, and toe, respectively. This monitoring activity successfully recorded the frequencies and retreat lengths at these locations, which occurred between June 4 and December 1, 2009 (red solid lines in Figure 7.7b, 7.7c, 7.7d, and 7.7e). The numbers of erosion events were 8, 4, 5, and 1 for the crest, upper midbank, lower midbank, and toe of the bank, respectively. The high frequency of occurrence of mass erosion at the crest is depicted by the “staircase shape” of the time series shown in Fig. 7.7b. The decreasing number of erosion events along the downslope of the bank profile suggests that the bank soils had an increasing strength moving from the crest to the toe of the bank despite the fact that in the downslope direction the stress increases. This trend had to do with the fact the crest soil at this site was predominantly less compacted, heterogeneous sand deposit (e.g., Wilson et al, 2012) and therefore it was more erodible comparatively to those for midbank and toe soils. The time series of estimated  $L$  was then plotted against the synchronous near-bank stress,  $\tau_w$ , generated by CONCEPTS for the different locations of the bank face at site 2 where the PEEPs were installed (Fig. 7.8a, 7.8b, 7.8c, and 7.8d).

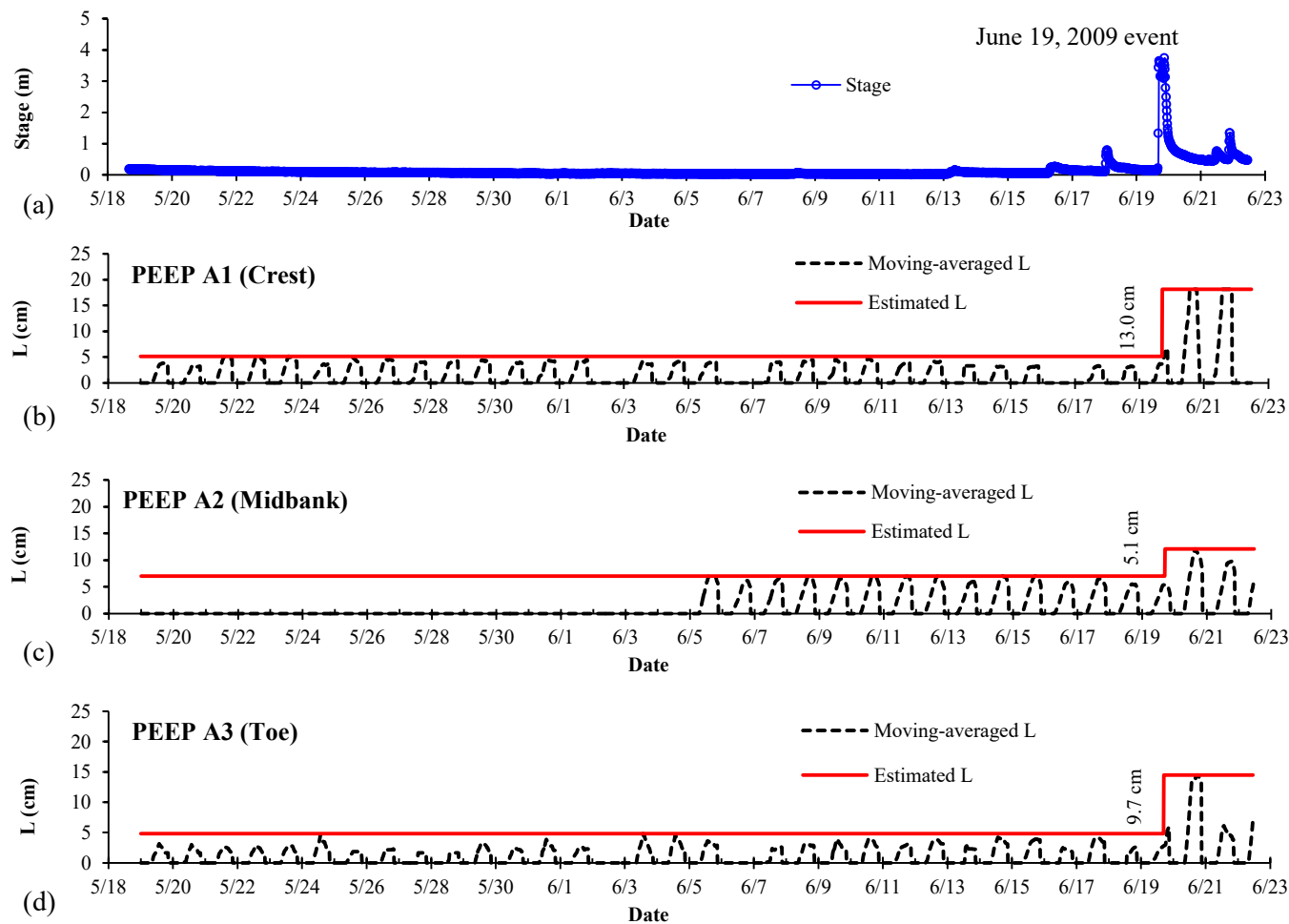


Figure 7.6 Time series of water stage and exposure length for PEEPs at site 1. (a) Water stage. (b) Moving-averaged and estimated exposure length for (b) PEEP A1, (c) PEEP A2, and (d) PEEP A3. The increases in estimated exposure length represent the erosion depths corresponding to erosion events.

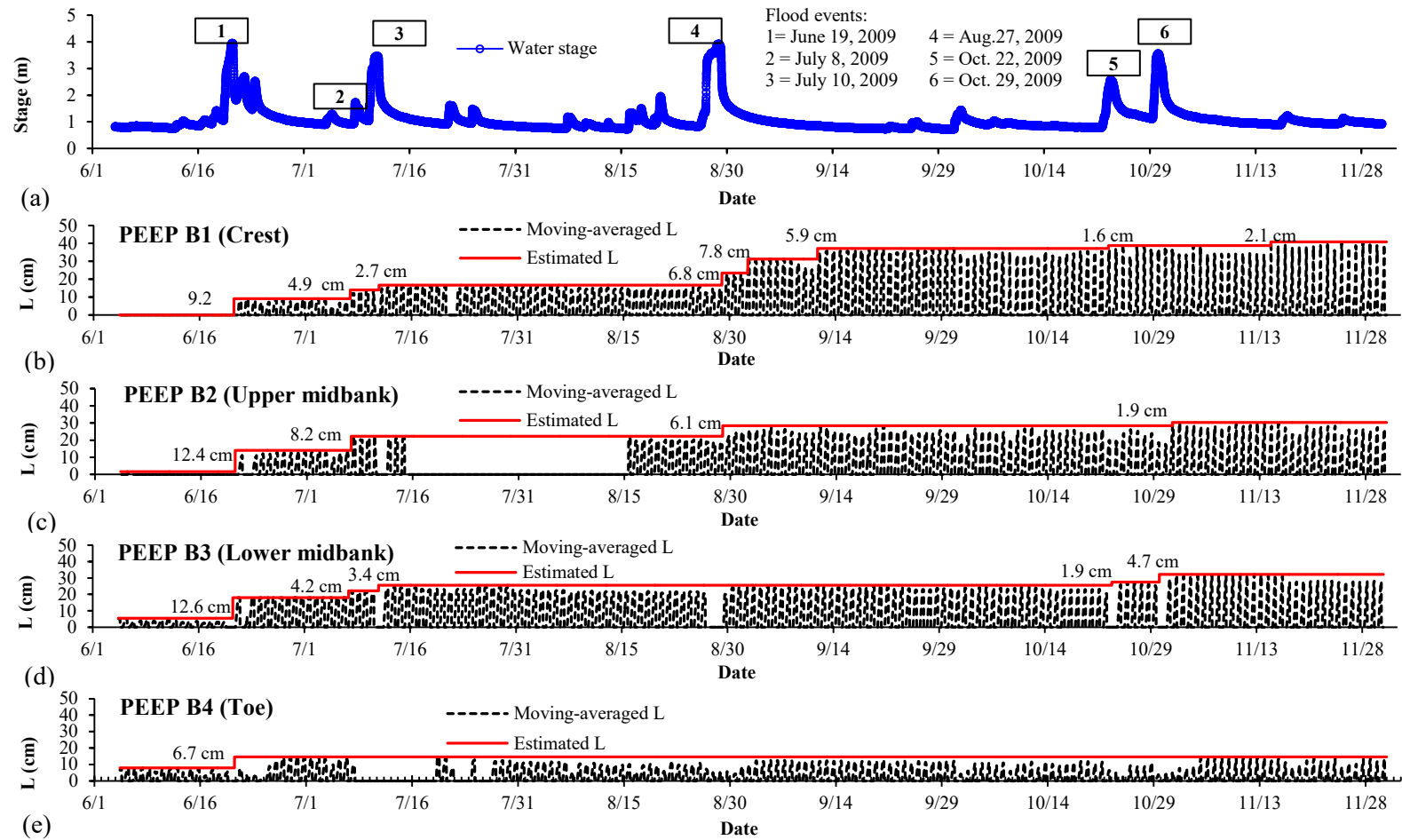


Figure 7.7 Time series of water stage and exposure length for PEEPs at site 2. (a) Water stage. (b) Moving-averaged and estimated exposure length for PEEP B1, (c) PEEP B2, (d) PEEP B3, and (e) PEEP B4.

The time series of estimated  $L$  was then plotted against the synchronous near-bank stress,  $\tau_w$ , generated by CONCEPTS for the different locations of the bank face at site 2 where the PEEPs were installed (Fig. 7.8a, 7.8b, 7.8c, and 7.8d). These plots provide unique information about not only the frequencies and magnitudes of mass erosion occurring at site 2, but more importantly the magnitudes of near bank shear stress,  $\tau_w$ , that corresponded to each erosion event. Mass erosion intensifies during the event or post-event, which typically corresponds to the falling limb of the hydrograph. The excess bank erosion is believed to be the cumulative impact of the rapid drawdown of the hydrograph and the impact of the hydraulic forces, a similar observation has been made by Mitchell et al. (1999) in U.K. Streams and Darby et al. (2007) in the Sieve River, Italy. This type of information regarding mass erosion is lacking in the bank erosion literature, and it is crucial to identify in a more definitive manner the erosional responses of bank soils to different hydraulic shear stresses under a wide range of shear stresses and flood events.

The plots of estimated  $L$  and near-bank stresses, such as the ones presented in Figures 7.8a, 7.8b, 7.8c, and 7.8d, can help decipher mass erosion events triggered by the fluid action from other bank erosion events that were not directly triggered by the shearing action of flow (e.g., pop-out failures). Examples of erosion events that were not directly triggered by the shearing action of flow are seen in Figure 7.8a where the second, fifth, sixth, seventh, and eighth erosion events occurred during periods when there was no increase in streamflow (and shear stress).

In addition, there were some instances when the PEEPs did not record a measurable bank retreat during a flow event with a sufficiently high enough shear stress to cause mass

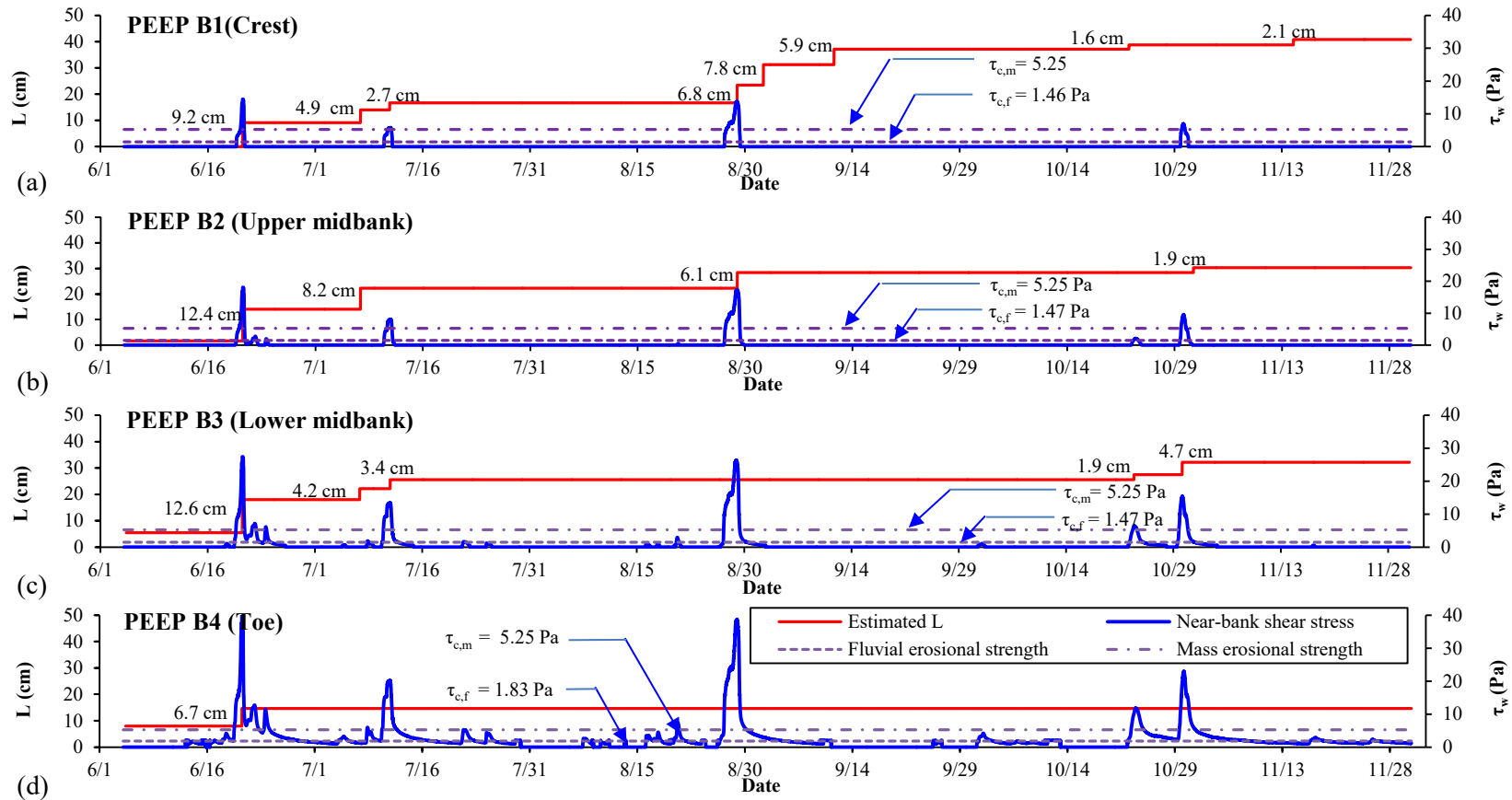


Figure 7.8 Time series of estimated exposure length along with synchronous near bank shear stress at site 2. (a) Result for the crest (PEEP B1), (b) upper midbank (PEEP B2), (c) lower midbank (PEEP B3), and (d) toe of the bank (PEEP B4). Fluvial and mass erosional strengths were also presented for comparing the two strengths and with near bank shear stresses.

erosion. For example, during the August 24, 2009 flood event, the PEEPs at the lower midbank and toe (PEEPs B3 and B4, respectively) measured no retreat despite experiencing shear stresses in excess of 25 Pa (Fig. 7.8c and 7.8d). The majority of these instances (8 out of 12) occurred at the lower midbank and the toe. Thus, it is suspected that woody debris or previously slumped bank material temporarily protected the bank face surrounding these lower PEEPs from further erosion.

Table 7.4 summarizes the retreat lengths at site 2 during runoff events resulting from mass erosion and during non-event periods due to non-hydraulic driven erosion (e.g., pop-out failure). Based on Table 7.4, the retreat caused by mass erosion was larger than the retreat due to non-hydraulic driven erosion for the lower locations of the bank face (i.e., all except for the bank crest) during the study period. This outcome challenges the common notion that hydraulically-driven erosion, namely fluvial and mass erosion, was not a significant contributor to the annual bank retreat and bank derived sediment load.

### 7.5 Mass Erosional Strength

To determine the mass erosional strength,  $\tau_{c,m}$ , of the bank soil, pairs of near bank shear stresses and erosion depths  $[\tau_w, E]$  were collected for each erosion event detected by the PEEPs and plotted along with the results of conduit flume test, which represent fluvial erosion (see Figure 7.9). The data points can be grouped into three locations, namely along the y-axis, along the x-axis, and along a best-fit line in the middle of the graph. The values that plotted along the y-axis correspond to those non-hydraulic erosion events mentioned in the previous section (e.g., pop-out failure, mass failure). Additionally, the values that plot along the x-axis correspond to the values near the lower parts of the bank that were periodically protected by woody debris or slumped bank material. These data points were not included when fitting a linear regression line to the remainder of the data in this

graph (Fig. 7.9). The mass erosional strength corresponds to the intersection of fluvial and mass erosion lines, which was equal to 5.51 Pa for the bank soil at site 2. It is the break point between fluvial erosion and the accelerated mass erosion and represented with a change in slope. The corresponding  $\tau_w$  versus  $E$  values for the conduit flume experiments give us the fluvial erosional strength for the bank soils at site 2. This value was 1.26 Pa (Fig. 7.9).

Table 7.4 Summary of erosion lengths quantified at site 2.

Location	Erosion lengths (cm)		
	Mass erosion	Non-hydraulic erosion	Total
Crest	18.7	22.3	41.0
Upper midbank	18.5	10.1	28.6
Lower midbank	22.6	4.2	26.8
Toe	6.7	0.0	6.7

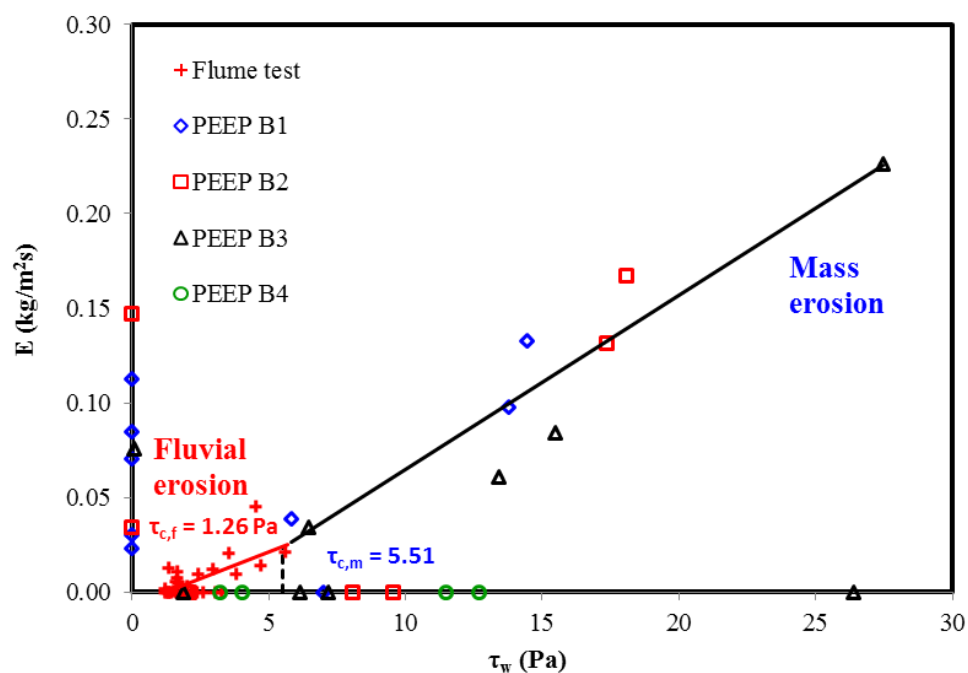


Figure 7.9 Determination of mass erosional strength,  $\tau_{c,m}$ . The  $\tau_{c,m}$  value was determined by drawing a fitting line on the plot of shear stress and erosion depth  $[\tau_w, \Delta L]$  data points obtained at the crest, upper midbank, lower midbank, and toe of the bank. The  $\tau_{c,m}$  value corresponds to the x-intercept of the fitting line.

Thus, the value for the mass erosional strength (5.51 Pa) is larger than the corresponding fluvial erosional strength at site 2 (Sutarto et al., in press). In addition, the best-fit line for the data obtained from PEEPs has a different slope comparatively to the one obtained from the conduit flume tests. This finding provides convincing evidence that the PEEPs were able to detect mass erosion, which occurs at a greater rate than what was determined for fluvial erosion.

Unfortunately, it is difficult to compare the  $\tau_{c,m}$  value obtained in this study with those reported in the literature, which used a variety of laboratory devices. Nevertheless, good agreement was found with the studies using similar, predominantly silt, undisturbed soil samples like those by Chapuis (1986a) and Kamphuis et al. (1990) that reported  $\tau_{c,m}$  values of 4.2 Pa and 0-6 Pa, respectively. On the other hand, Gaskin et al. (2003) reported quite large  $\tau_{c,m}$  values, which were in between 6 and 20 Pa for homogeneous, estuarine clay bank soils that contained 75% clay and 15% silt. This high  $\tau_{c,m}$  value was assumed to be affected by large clay content within the soils (e.g., Panagiotopoulos et al., 1997). However, further study is still required to understand whether the clay content affects  $\tau_{c,m}$ , as it does with  $\tau_{c,f}$ .

## 7.6 Mechanical Strength

The  $c'$  values for the samples collected at both sites (Table 7.5, column 1) showed a consistent behavior in terms of strength with an increasing trend in magnitude along the downslope profile per bank. In addition, when  $c'$  was compared between the two sites, the  $c'$  for site 1 was overall higher in magnitude than the  $c'$  for site 2. These trends are also seen with the bulk density as discussed earlier in section 7.2. A positive correlation



between  $c'$  and bulk density has been reported in the literature as higher bulk density in most cases indicates higher effective stress (e.g., Ayers, 1987; Bardet et al., 2011).

Table 7.5 Mechanical strength parameters for Clear Creek bank soils.

Sampling Location		$c'$	$\theta'$
		(Pa)	(deg.)
		(1)	(2)
Site 1, SA 2, left bank	Crest	1,500	31.44
	Midbank	12,500	34.10
	Toe	15,000	32.39
Site 1, SA 2, right bank	Crest	1,600	31.30
	Midbank	12,500	27.09
	Toe	13,500	21.09
Site 2, CC 1, left bank	Crest	400	26.33
	Midbank	3,000	37.03
	Toe	6,000	34.88
Site 2, CC 1, right bank	Crest	500	31.32
	Midbank	3,700	36.06
	Toe	6,600	35.02

Note: the numbers in the parentheses are column numbers.

The  $c'$  values recorded herein are in a general agreement with the values reported by Lohnes and Handy (1968), Lohnes et al. (2001), Yang et al. (2005), and Veeraraghavan (2007) for sites exhibiting relatively similar properties. For example, Lohnes et al. (2001) reported  $c'$  values ranging between  $6.91 \pm 4.19$  kPa and  $7.65 \pm 5.59$  kPa, respectively, for loess with high plasticity and glacial till deposits found in Iowa (Prior, 1976; Lohnes et al., 2001; Yang et al., 2005; Oneal, 2009). Yang et al. (2005) reported  $c'$  values in the range of 2.7 to 12 kPa for glacial till soils with a texture of silt clay loam extracted across six (6) counties in southern Iowa.

### 7.7 Comparison among Mechanical, Mass Erosional, and Fluvial Erosional Strengths

The differences between mechanical and fluvial erosional strengths were 2 to 3 orders of magnitude for the crest soils and 3 to 4 orders of magnitude for the midbank and toe soils at sites 1 and 2 (Tables 7.2, and 7.5). A similar relationship (e.g., 3 to 5 orders of magnitude) was found for other undisturbed bank soils in the studies of Kamphuis and Hall (1983), Hilldale (2001), Darby et al. (2007), Veeraraghavan (2007), Papanicolaou et al. (2007), and Langendoen and Simon (2008) (see Table H.1).

The mass erosional strength,  $\tau_{c,m}$ , for the bank soils at the right bank of site 2 was 5.51 Pa (section 7.5) or 2 to 4 times higher than their corresponding  $\tau_{c,f}$ , which were between 1.28 and 2.37 Pa (Table 7.2). This finding was supported by recent studies from Gaskin et al. (2003) and Huang et al. (2006) that found the  $\tau_{c,m}$  to be 3 to 6 times larger than  $\tau_{c,f}$ .

### 7.8 Factor of Safety and Bank Retreat

The factors of safety for mass failure and fluvial erosion ( $FS_{mf}$  and  $FS_f$ ) for the six cross sections at site 2 were determined with CONCEPTS from October 1, 2007 to March 8, 2013 using the input data derived from the laboratory analysis and are summarized in Tables 7.6 and 7.7. This version of CONCEPTS was unable to determine the factor of safety for mass erosion. The initial bank profiles for the simulation were obtained from a geodetic survey performed on October 1, 2007. The initial ground water elevation and the Manning's roughness coefficient were calculated via the methods described earlier in section 6.4. Table 7.7 is an important companion to Table 7.6 and provides a summary of the different soil properties for each bank soil layer (defined

earlier) within the simulated stream reach which were obtained from the methods described in sections 6.3.

For illustrating the utility of estimating both  $FS_{mf}$  and  $FS_f$ , the flood event of June 20, 2009 is described here in a more detail. The whole bank profile was submerged during this event thereby allowing for comparisons of  $FS_f$  among the crest, midbank and toe. Regarding the  $FS_{mf}$ , Figures 7.10a and 7.10b depict the changes occurring prior to, during, and immediately following this event for the left and right banks, respectively. The dashed lines indicate the flow rate, while the other six lines represent the  $FS_{mf}$  variation for the six different cross sections at site 2. The values of  $FS_{mf}$  remain all above unity indicating that the banks were geotechnically stable prior to, during and right after the June 20, 2009 event. The spiked increase in  $FS_{mf}$  during the event was due to the increase in the water confining pressure associated with the rise in the flow stage (Langendoen, 2000). The stability of the banks predicted by the model prior to, during and right after the June 20, 2009 event were supported by the geodetic surveys and visual observations of the bank profiles, which suggested no mass failures.

In quantifying  $FS_{mf}$ , CONCEPTS accounts for positive and negative pore water pressure, water confining pressure, and the effects of soil layering within a block were incorporated (Langendoen and Simon, 2008). However, it is important to note that the effect of roots on the soil shear strength was not considered in this study, although they can increase the soil shear strength and therefore factor of safety,  $FS_{mf}$ , by a factor of 3 to 5 (Thorne and Tovey, 1981; Polen and Simon, 2005).

Table 7.6 Bank layers, ground water elevation, and Manning's boundary roughness for CONCEPTS model for site 2.

Descriptions	Cross section					
	CC 1 (1)	CC 2 (2)	CC 3 (3)	CC 4 (4)	CC 5 (5)	CC 6 (6)
<b>Layer depth below top bank surface (m)</b>						
Left bank: Toe	4.31-2.31	4.56-2.56	4.73-2.73	4.90-2.90	4.88-2.88	4.68-2.68
Midbank	1.15-2.31	1.28-2.56	1.36-2.73	1.45-2.90	1.44-2.88	1.34-2.68
Crest	0.00-1.15	0.00-1.28	0.00-1.36	0.00-1.45	0.00-1.44	0.00-1.34
Right bank: Toe	4.70-2.70	4.56-2.56	4.21-2.21	4.54-2.54	4.71-2.71	4.37-2.37
Midbank	1.35-2.70	1.28-2.56	1.10-2.21	1.27-2.54	1.35-2.71	1.18-2.37
Crest	0.00-1.35	0.00-1.28	0.00-1.10	0.00-1.27	0.00-1.35	0.00-1.18
<b>Initial ground water elevation (m) via eq. 6.7</b>						
Left bank	2.50	2.50	2.50	2.50	2.50	2.50
Right bank	2.50	2.50	2.50	2.50	2.50	2.50
<b>Manning's roughness (s/m<sup>1/3</sup>)</b>						
Left floodplain	0.110	0.110	0.110	0.110	0.110	0.110
Left bank	0.085	0.080	0.080	0.080	0.080	0.080
Streambed	0.050	0.050	0.050	0.050	0.050	0.050
Right bank	0.085	0.080	0.080	0.080	0.080	0.080
Right floodplain	0.110	0.110	0.110	0.110	0.110	0.110

Note: the numbers in the parentheses are column numbers.

Table 7.7 Bank soil parameters for CONCEPTS model for site 2.

Parameters	Left bank			Right bank		
	Toe	Midbank	Crest	Toe	Midbank	Crest
	(1)	(2)	(3)	(4)	(5)	(6)
Bulk density, $\rho_{\text{bulk}}$ (kg/m <sup>3</sup> )	2,014	1,794	1,553	1,880	1,618	1,299
Particle density, $\rho_s$ (kg/m <sup>3</sup> )	2,480	2,492	2,589	2,535	2,539	2,439
Porosity, n	0.35	0.45	0.49	0.42	0.46	0.47
Permeability, $\beta$ (s <sup>-1</sup> )	3.95E-8	3.95E-8	3.95E-8	4.35E-8	4.35E-8	4.35E-8
Fluvial erosional strength, $\tau_{c,f}$ (Pa)	1.94	1.53	1.47	1.83	1.47	1.46
Erodibility, M (m/s/Pa)	5.35E-6	5.54E-5	1.45E-6	2.41E-5	2.64E-4	2.27E-5
Cohesion, c' (Pa)	6,000	3,000	400	6,600	3,700	500
Friction angle, $\phi'$ (deg.)	34.88	37.03	26.33	35.02	36.06	31.32
Suction angle, $\phi^b$ (deg.)	17	17	17	17	17	17

Note: the numbers in the parentheses are column numbers.

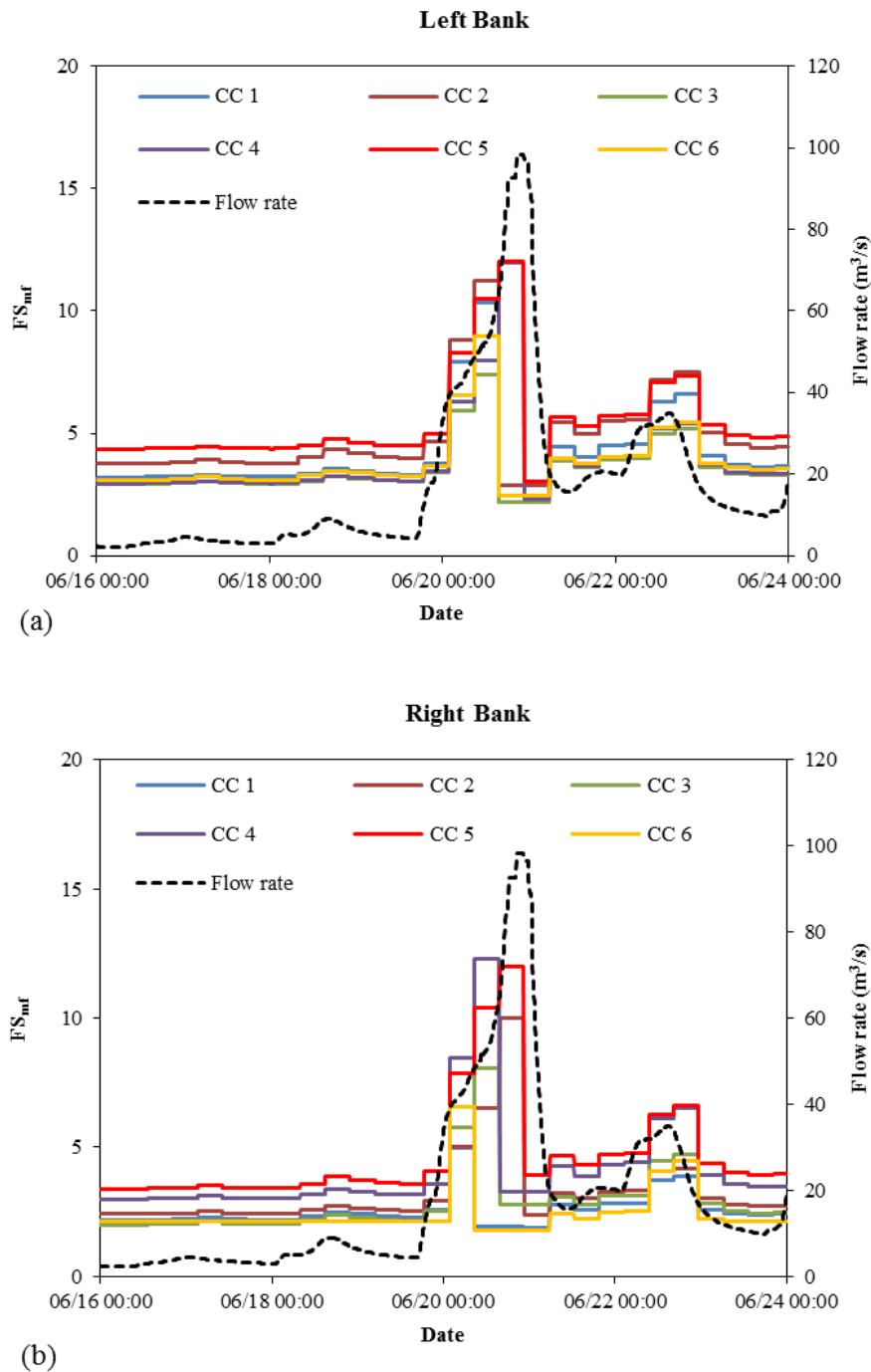


Figure 7.10 Factors of safety for mass failure,  $FS_{mf}$ , predicted by CONCEPTS. The simulation was performed for 6 cross sections at site 2. The time window herein was focused on the period prior to, during and right after the June 20, 2009 flood event: (a) Left bank. (b) Right bank.

Figures 7.11 and 7.12 illustrate the changes in  $FS_f$  prior to, during, and following after the June 20, 2009 flood event for the same cross sections at site 2. In Figures 7.11 and 7.12, the dashed lines show the flow rate while the other six lines represent the  $FS_f$  for the six different cross sections. The  $FS_f$  values were determined for the crest, midbank, and toe of the left and right banks. According to Fig. 7.11 and 7.12, all three layers experienced fluvial erosion during the June 20, 2009 event. The toe layer experienced the highest fluvial erosion as it experienced higher near bank shear stress,  $\tau_w$ , and thereby presented the lowest factor of safety with respect to fluvial erosion comparatively to the other two layers. This was despite the fact that  $\tau_{c,f}$  at the toe was slightly higher than that of the midbank and crest soils (see section 7.3). Moreover, the  $FS_f$  for cross section CC 6 remained lower than for the other cross sections (Fig. 7.11 and 7.12) as the former was subjected to higher near bank shear stress,  $\tau_w$ , comparatively to other cross sections (Fig. G.3 and G.4).

Another noteworthy bank stability result is that CONCEPTS successfully simulated fluvial erosion at all six cross sections of site 2 (Fig. G.5). Cross section CC 6 is presented in Figure 7.13, as it shows most visually the resulting bank toe undercutting. The surveys performed on October 1, 2007 and March 8, 2013 depicted the occurrence of bank toe erosion or undercutting at the left and right bank of cross section CC 6. In Figure 7.13, the measured initial and final bank profiles are represented by the dashed black and red lines, respectively. The predicted bank profile at the end of the simulation period (March 8, 2013) is shown with the cross-marked brown line. The predicted bank profile dated on March 8, 2013 (cross-marked brown line) agrees well with the measured one (unmarked red line), confirming the accuracy of this simulation result.

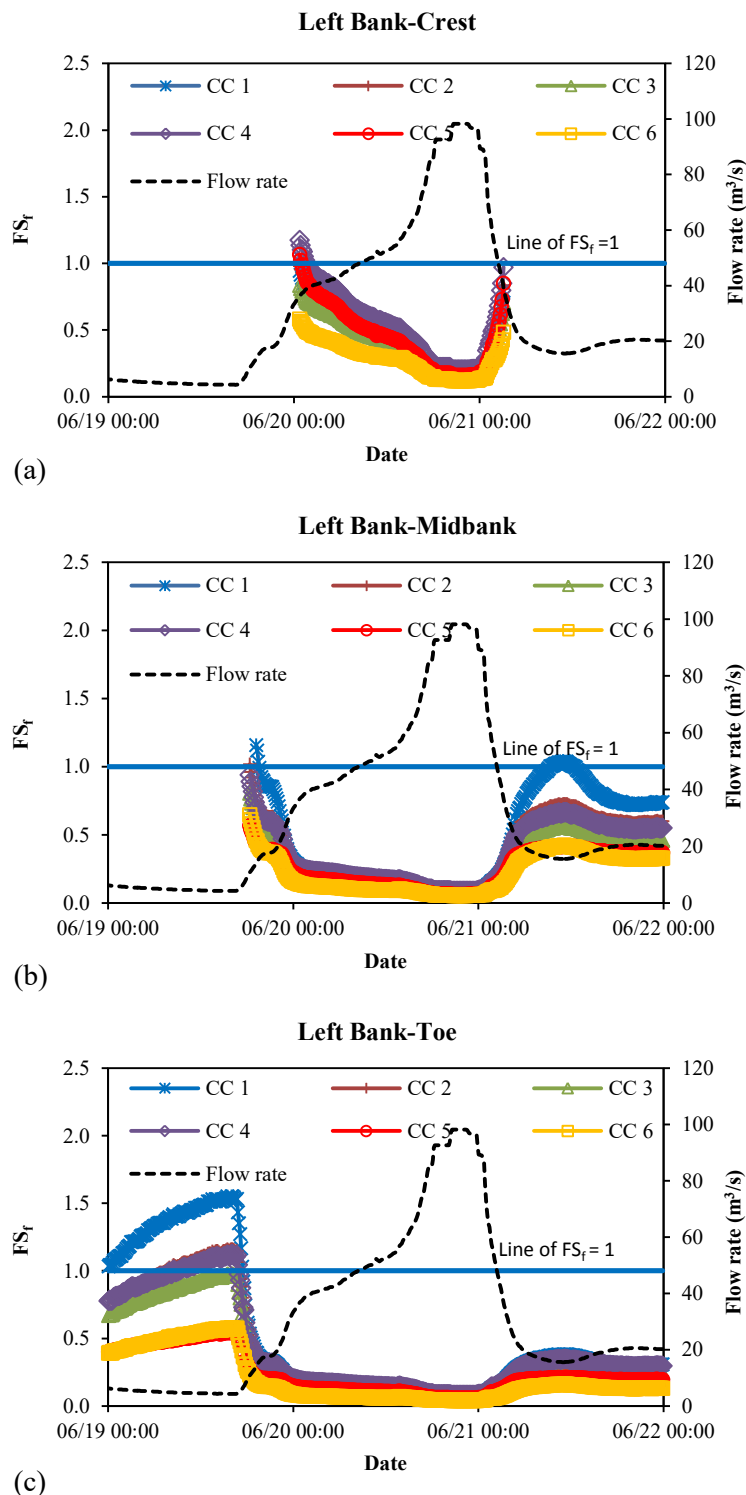
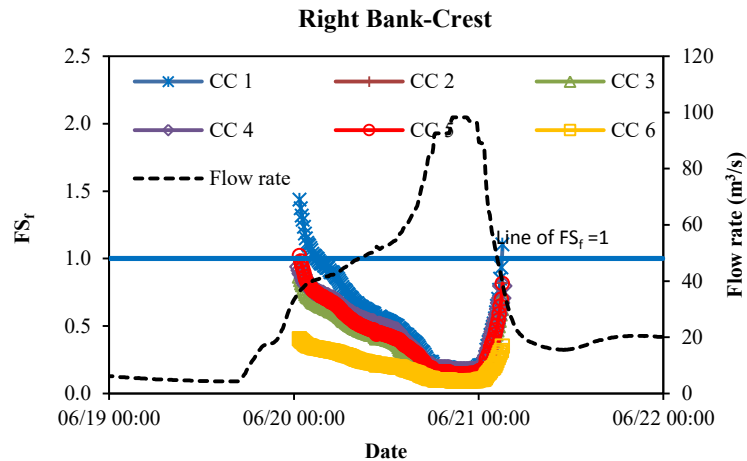
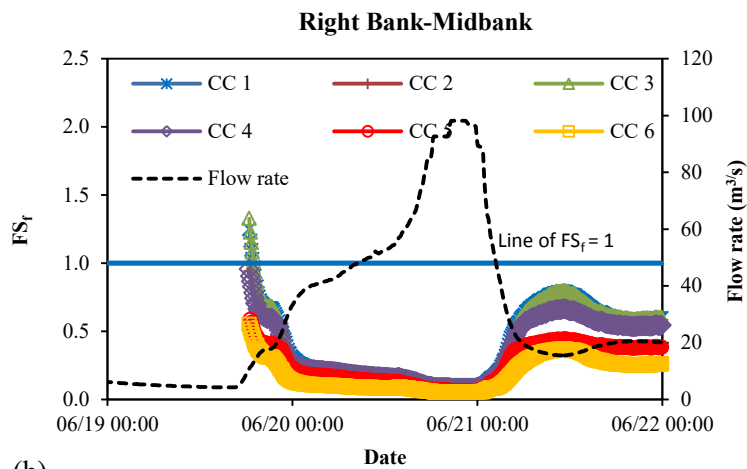


Figure 7.11 Factors of safety for fluvial erosion,  $FS_f$ , predicted by CONCEPTS. The simulation was performed for six (6) cross sections at site 2. The time window herein was focused for the period prior to, during and right after the June 20, 2009 flood event: (a) Left bank-crest. (b) Left bank-midbank. (c) Left bank-toe.

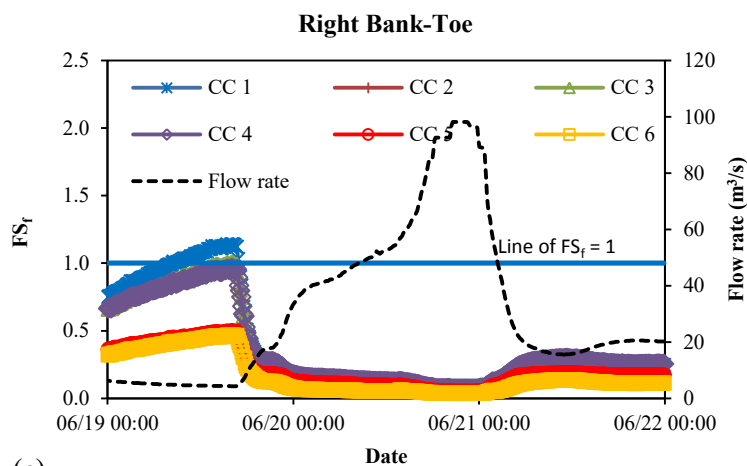




(a)



(b)



(c)

Figure 7.12 Factors of safety for fluvial erosion,  $FS_f$ , predicted by CONCEPTS. The simulation was performed for six (6) cross sections at site 2. The time window herein was focused for the period prior to, during and right after the June 20, 2009 flood event: (a) Right bank-crest. (b) Right bank-midbank. (c) Right bank-toe.

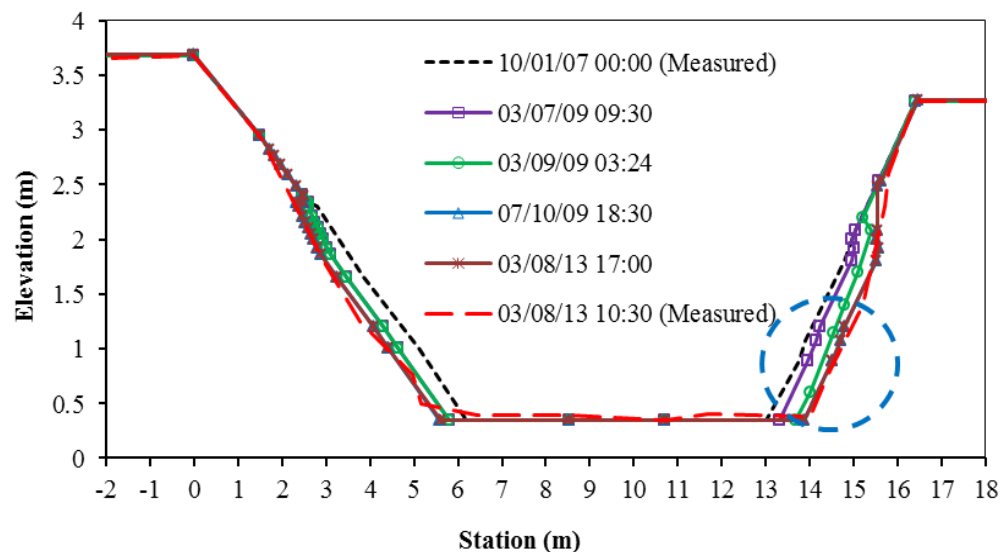


Figure 7.13 The bank retreat at cross section CC 6, site 2, simulated by CONCEPTS. The retreat of the bank line predominantly occurred at the lower part of the bank due to fluvial erosion that occurred during the period of October 2007 to March 2013.

### 7.9 Effect of Soil Heterogeneity on Bank Retreat and Stability

The importance of accounting for bank heterogeneity in the above stability analysis was illustrated here by assuming that the cross sectional geometry for CC6 was comprised of homogeneous soil properties. In that sense, the bank profile was treated as one homogenous layer by assigning constant values for bulk density, mechanical strength and erosional strength in all three layers. Figure 7.14 illustrates the effects of bank property homogeneity on the evolution of bank profile and was in contrast to Figure 7.13 where soil property heterogeneity is considered based on the measured properties. In constructing Figure 7.14 two conditions were considered: 1) The soil properties of all layers were identical to those of the crest (Tables 7.6 and 7.7); and 2) The soil properties of all layers were identical to those of the toe. The results show that in the homogeneous

case most of the erosion occurs in the upper part of the bank due to planar failure contrary to the measured in-situ observations and the heterogeneous simulations, shown in Figure 7.13, where bank toe undercutting was observed and predicted, respectively. In both cases, this exercise demonstrates the need of accounting for heterogeneity in soil properties (e.g., bulk density, mechanical strength and erosional strength) along the profile when a stability analysis is performed.

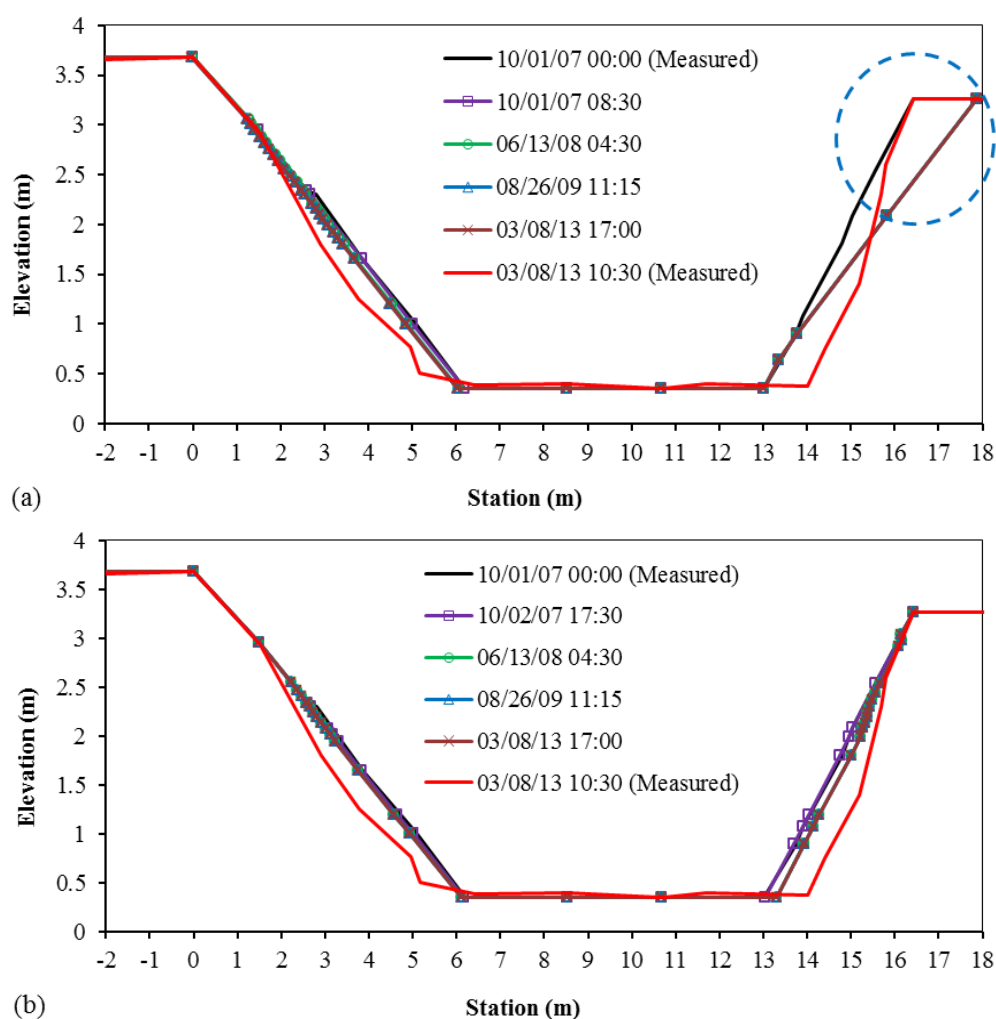


Figure 7.14 The bank retreat at cross section CC 6, site 2, simulated by CONCEPTS: (a) Homogeneous banks with the entire bank soils are identical to crest soils. Planar failure occurred at the right bank. (b) Homogeneous banks with the entire bank soils are identical to toe soils. No significant retreat was predicted.

### 7.10 Sediment Contribution from Different Modes of Bank Erosion

Three different CONCEPTS simulations were performed to quantify the relative amounts of sediment in tons generated from the different modes of bank erosion (i.e., fluvial erosion, mass erosion, and mass failure) for the stream reach at site 2 between October 1, 2007 and March 28, 2013.

The first simulation provided the total contribution from all three modes of bank erosion by using the following modules in CONCEPTS: 1) bank stability; 2) hydraulic erosion; and 3) sediment transport. The fluvial erosional strength,  $\tau_{c,f}$ , and erodibility,  $M_f$ , obtained from the laboratory conduit flume tests for each bank soil layer (i.e., crest, midbank, and toe) were used to initiate hydraulically driven erosion. The results of this simulation are presented in Table 7.8 (column 2). The total amount of sediment produced through all modes of bank erosion was 89.19 tons.

The second simulation was conducted to quantify the contributions derived from only fluvial and mass erosion. For this simulation, CONCEPTS was run using only the hydraulic erosion and sediment transport modules, with the bank stability analysis module being deactivated to avoid simulating mass failure. Similar to the first simulation, the fluvial erosional strength,  $\tau_{c,f}$ , and erodibility,  $M_f$ , values from the conduit flume tests were used. The results of this simulation are presented in Table 7.8 (column 3). The amount of sediment derived from fluvial and mass erosion was 74.39 tons.

The third simulation was to quantify the contribution of sediment derived from only mass erosion. Similar to the second simulation, CONCEPTS was run with the hydraulic erosion and sediment transport modules being activated and the bank stability

module being deactivated. The onset of hydraulically driven erosion was assigned the mass erosional strength,  $\tau_{c,m}$ , and erodibility,  $M_m$ , values instead of the corresponding values for fluvial erosion, thereby ensuring only mass erosion was simulated. The results of the third simulation used to isolate the relative proportions of mass erosion are in Table 7.8 (column 4). The amount of sediment derived from mass erosion was 18.44 tons.

Table 7.8 Mass of sediment generated from the bank at site 2 during the period between October 1, 2007 and March 28, 2013.

Sediment size	Mass of sediment (tons)		
	<sup>a</sup> Mass failure + fluvial erosion + mass erosion	<sup>b</sup> Fluvial erosion + mass erosion	<sup>c</sup> Mass erosion
(1)	(2)	(3)	(4)
Clay:	15.50	12.80	3.04
Fine Silt:	13.70	11.30	2.06
Medium Silt	13.00	10.80	2.31
Coarse Silt:	41.20	35.00	8.30
Very Fine Sand:	5.62	4.34	2.68
Fine Sand:	0.17	0.15	0.05
Medium Sand:	0.00	0.00	0.00
Coarse Sand:	0.00	0.00	0.00
Very Coarse Sand	0.00	0.00	0.00
Very Fine Gravel:	0.00	0.00	0.00
Fine Gravel	0.00	0.00	0.00
Medium Gravel:	0.00	0.00	0.00
Coarse Gravel:	0.00	0.00	0.00
Very Coarse Gravel:	0.00	0.00	0.00
	89.19	74.39	18.44

<sup>a</sup>Bank stability, hydraulic erosion, and sediment transport modules were run.

<sup>b</sup>Hydraulic erosion and sediment transport modules were run. Fluvial erosional strength was used to determine the onset of hydraulic erosion.

<sup>c</sup>Hydraulic erosion and sediment transport modules were run. Mass erosional strength was used to determine the onset of hydraulic erosion.

In summary, fluvial erosion provided more than half (57%) the total sediment mass from the channel banks at the site 2 stream reach, whereas mass erosion provided an additional 26.5% of the total sediment (Table 7.9). The majority of sediment that was eroded was coarse silt and very fine sand, which corresponds to the dominant sediment size found in the bank soils of site 2 (Table 7.1). Thus, these simulation data support the need to consider both fluvial and mass erosion processes in a bank stability analysis, as the two modes can produce the majority of channel sediment (>80% in this case) transported downstream.

Table 7.9 Percentage of sediment derived from the bank at site 2 during the period between October 1, 2007 and March 28, 2013.

<b>Mode of Erosion</b>	<b>Mass of sediment (tons)</b>	<b>Percentage (%)</b>
<b>(1)</b>	<b>(2)</b>	<b>(3)</b>
Fluvial erosion	50.77	56.9
Mass erosion	23.62	26.5
Mass failure	14.81	16.6

## **CHAPTER 8**

### **DISCUSSION OF RESULTS AND CONCLUSIONS**

The contributions of this research span across the spectrum of the different modes of bank erosion. A critical and scholastic view of the problem was undertaken. An extensive literature review on this topic revealed two major shortcomings. The first shortcoming deals with bank stability theory, which typically ignores the effects of fluvial and mass erosion. This shortcoming is addressed here by offering an improved understanding and modulation of fluvial and mass erosion that is complemented with a physically based bank erosion model developed to address different forms of mass failure. A key interrelated contribution for addressing this shortcoming is the effort provided to interconnect the effects of a continuous process, such as fluvial erosion with the episodic occurrence of mass failure. The impact of this research on that topic led to a finding that exclusion of fluvial erosion from the bank stability analysis can lead to up to 30% underestimation of the total eroded mass of sediment within a specified time interval.

The second shortcoming is the realization that only a small number of studies have considered the role of mass erosion. There is a confusion surrounding the term mass erosion usually with the term fluvial erosion. Both processes are semi-continuous although mass erosion has an accelerated rate of erosion and occurs more infrequently comparatively to fluvial erosion, as it is a result of a higher shear stress. This study offers unique data about the mass erosional strength and compares it with the corresponding fluvial erosional strength. This finding is complemented with a methodological advancement towards the estimation of the mass erosional strength. Current laboratory methods used to provide estimates of fluvial erosional strength cannot be effectively

employed to provide accurate repeatable measures of the critical erosional strength for mass erosion. Sediment exhaustion during the laboratory runs is a critical detriment. Based on that realization, the photo-electronic erosion pins, also known as PEEPS, were adopted from the discipline of coastal engineering and considered to provide, for the first time, unique in-situ measurements of the mass erosional strength and insight into the retreat lengths during a hydrological cycle. It was found that the mass erosional strength is at least 3 to 6 times higher in magnitude than the fluvial erosional strength, which agrees with the limited number of reported studies. Each of the findings as they relate to these two shortcomings are described below in great detail.

By combining systematic field and laboratory protocols and using devices, such as PEEPS, a gamma attenuation detector, direct shear device, and state-of-the-art conduit flume, this study offers some unique methodological advances for determining the mechanical, mass erosional and fluvial erosional strengths of streambanks with semi-cohesive soils, as well as the effects of soil heterogeneity on these parameters. To the best of our knowledge very few studies have systematically examined bank soil properties in such detail along a bank profile and in different riverine segments (e.g., headwaters and mouth) leading to unique datasets with the goal of supporting a comprehensive bank stability analysis that considers both mass failure and fluvial erosion. Such a dual, complementary analysis is pertinent especially in flashy systems where toe cantilever failure due to the ensuing of fluvial erosion is ubiquitous and can result into mass failure.

The CONCEPTS model was used herein to demonstrate the following: 1) The need to incorporate fluvial erosion and estimate  $FS_f$  in a bank stability analysis along



with mass failure; and 2) The importance of accounting for bank heterogeneity in the stability analysis. To do so, the soil and channel properties for the crest, midbank, and toe of bank profile derived from the field and laboratory analyses were fed into CONCEPTS to estimate  $FS_{mf}$  and  $FS_f$ . In CONCEPTS, the bank profile can be divided into several layers allowing the user to account for the variability in soil properties (e.g., bulk density, mechanical strength, and erosional strength) along the profile by assigning specific values for each layer. For quantifying  $FS_{mf}$ , CONCEPTS also accounts for water table dynamics, positive and negative pore water pressure, and water confining pressure (Langendoen and Simon, 2008). In addition, CONCEPTS can quantify the near bank shear stress,  $\tau_w$ , at the different layers and predict the onset and magnitude of fluvial erosion for each layer. These features make this model an ideal tool for simulating cross-sectional mass and fluvial erosion of banks characterized by heterogeneous soils such as the ones in the present study.

However, there were several constraints when using CONCEPTS for this study. CONCEPTS (v. 2.0) does not have a direct input for the effects of roots on bank stability, although, other studies have demonstrated that roots may improve soil shear strength (e.g., Pollen and Simon, 2005). Other studies (e.g., Simon and Collison, 2002) have adjusted the shear strength value to account for roots; however, this was not done in this study due to the lack of measurement data with roots. Additionally, CONCEPTS does not account for erosion of the crest soil due to receding floodwaters from the floodplain to the channel, as it is a 1D model.

Despite these limitations, it was shown in this study (Fig. 7.13) that estimates of

$FS_{mf}$  must be complemented with the estimates of  $FS_f$  to avoid underestimating mass failure. Otherwise, using mass failure alone in a stability analysis ignores the potential for interconnection between bank toe undercutting and planar failure and may lead to the underestimation of mass failure over an interval by as much as 30-40% of the eroded mass. This is illustrated with the simulations at site 2 where based on standalone  $FS_{mf}$  calculations it is suggested that the banks are stable (i.e.,  $FS_{mf} > 1$ ); however, this is not the case based on corroborated evidence provided from the geodetic surveys and reconfirmed by the performed modeling exercise.

Second, the importance of accounting for bank heterogeneity in the stability analysis was illustrated here by assuming that the cross sectional geometry for CC6 was comprised of homogeneous soil properties. In that sense, the bank profile was treated as one homogenous layer by assigning constant values for bulk density, mechanical strength and erosional strength in all three layers. The results show that in the homogeneous case, most of the erosion occurred in the upper part of the bank due to planar failure contrary to the measured cross sections and the heterogeneous simulations, shown in Figure 7.13, where bank toe undercutting was shown to take place. This exercise demonstrated the need of accounting for heterogeneity in soil properties (e.g., bulk density, mechanical strength and erosional strength) along the profile when a stability analysis is performed.

Third, the differences in the  $\tau_{c,m}$  and  $\tau_{c,f}$  can be significant where  $\tau_{c,m}$  in this study has been found to be 3 to 6 times larger than  $\tau_{c,f}$ . Hence, mass erosion should not be ignored nor be assumed to be having the same contributions as fluvial erosion. As a matter of fact this research summarizes the erosion retreat lengths for mass erosion and mass pop-up failure (non-hydraulic driven erosion) that occurred during the monitoring

period at different location along the bank profile at site 2. Based on the completed analysis, the retreats caused by mass erosion were larger in instances than certain types of mass failure, mainly due to subaerial processes, for most the lower half of the bank (except for the bank crest) during the study period. This outcome challenges the common notion that the hydraulic-driven erosion, here we focus to mass erosion, is not a significant contributor to the annual bank retreat and bank derived sediment load.

Finally, mass erosion estimations were greatly benefited from measuring devices like the PEEPs because they could enable the detection of the full episodicity of bank change, including event timings and provide automated observations of the retreat length magnitude/timing information. The deployment of PEEPs was complemented with a statistical treatment of the retreat length time series data through the performance of a moving average to identify ubiquitous key mass erosion events in terms of magnitude and their frequency of occurrence for mass erosion. In concert to this effort, a unique and systematic PEEP data processing routine (e.g., filtering, correcting and smoothing) was also developed to remove the effects of ambient light changes due to solar orientation, or equivalently low light intensity and other factors (e.g., turbidity) on the bank retreat length estimation (Lawler, 1991 and 1992).

The specific findings of this research are summarized as follows.

1. The differences between mechanical and erosional strengths are 2 to 4 orders of magnitude for the undisturbed semi-cohesive bank soils which are classified as silt loam and sandy loam (Fig. 6.15). This quantitative difference between the two soil strength

parameters, which is also supported by previous studies, reemphasizes that those two parameters represent soil resistance for different bank failure mechanisms.

2. For streams characterized by frequent flash floods, such as Clear Creek, their bank soils have heterogeneity in terms of bulk density with an increasing trend in bulk density along the downslope of the bank. This heterogeneity is more pronounced for bank soils at the mouth of the stream that contain newly fresh deposited material at the crest and midbank sections from recent floods (Fig. 7.2).

3. The mechanical and erosional strengths have a positive correlation with the bulk density. It is found that the fluvial erosional strength and mechanical strength increase along the downslope of banks similar to the trend exhibited by bulk density (Tables 7.2 and 7.5). This positive correlation between bulk density and mechanical and erosional strengths is prevalent for bank soils extracted from the headwaters (site 1) and near the mouth (site 2) of Clear Creek.

4. For banks that consist of heterogeneous soils such as those in Clear Creek, there is a variability of mechanical and erosional strengths along the downslope of the banks following the trend in bulk density. The variability of mechanical and erosional strengths along the downslope of the banks highlights the need to acquire both mechanical and fluvial erosional strengths for the three layers along a bank profile (namely crest, midbank, and toe) as is the case in the present study to improve the commonly adopted protocols that typically assume homogeneous, well compacted soils along a bank profile.

5. PEEPS provided not only semi-continuous recordings of retreat rates over a

long period of time but they did provide reliably with error less than 12% of the measured retreat length when compared with corresponding measurements obtained from geodetic surveys for identical locations at sites 1 and 2.

Along with these findings and contributions, there are some caveats. Future work must consider the effects of freeze-thaw cycles on fluvial erosional strength, mass erosional strength, and mass failure. This need remains in the US Midwest where freeze-thaw cycles are prevalent throughout parts of the year. In addition, new research on bank stability should utilize new technology such as photoelectronic erosion pins, known as PEEPS, to provide continuous records of bank retreat during a hydrological cycle. Such observations can elucidate the dynamic evolution of bank profiles in relation to stage, as well as provide unique data for model verification in future simulations. There is also a need to utilize two-dimensional or three-dimensional models (Darby et al., 2010) to provide a more accurate description of the side wall shear stress distribution along the bank profile. Such models could better account for the effects of planform geometry and localized roughness on secondary current contributions to the side wall shear stress (Papanicolaou et al., 2007). Last but not least, more light needs to be shed on the parameterization of the fluvial erosional strength and methods used for its estimation. A number of studies have recently highlighted the need to identify the pros and cons of the different techniques used to estimate the erosional strengths and such a need still persists. In addition, more research needs to focus on the systematic preprocessing and post-processing of the PEEP data considering the fact that PEEPS could reproduce reliably a bank profile prior and after the on-set of a mass erosion event. Future research efforts should be invested to examine the role of vibrations and spinning of the PEEP probes due

to the flow action, the effects total suspended sediment, poor water transparency and presence of scattered clouds as it relates to the ambient light conditions.

**APPENDIX A**  
**SOIL TEXTURE AND CLASSIFICATION**

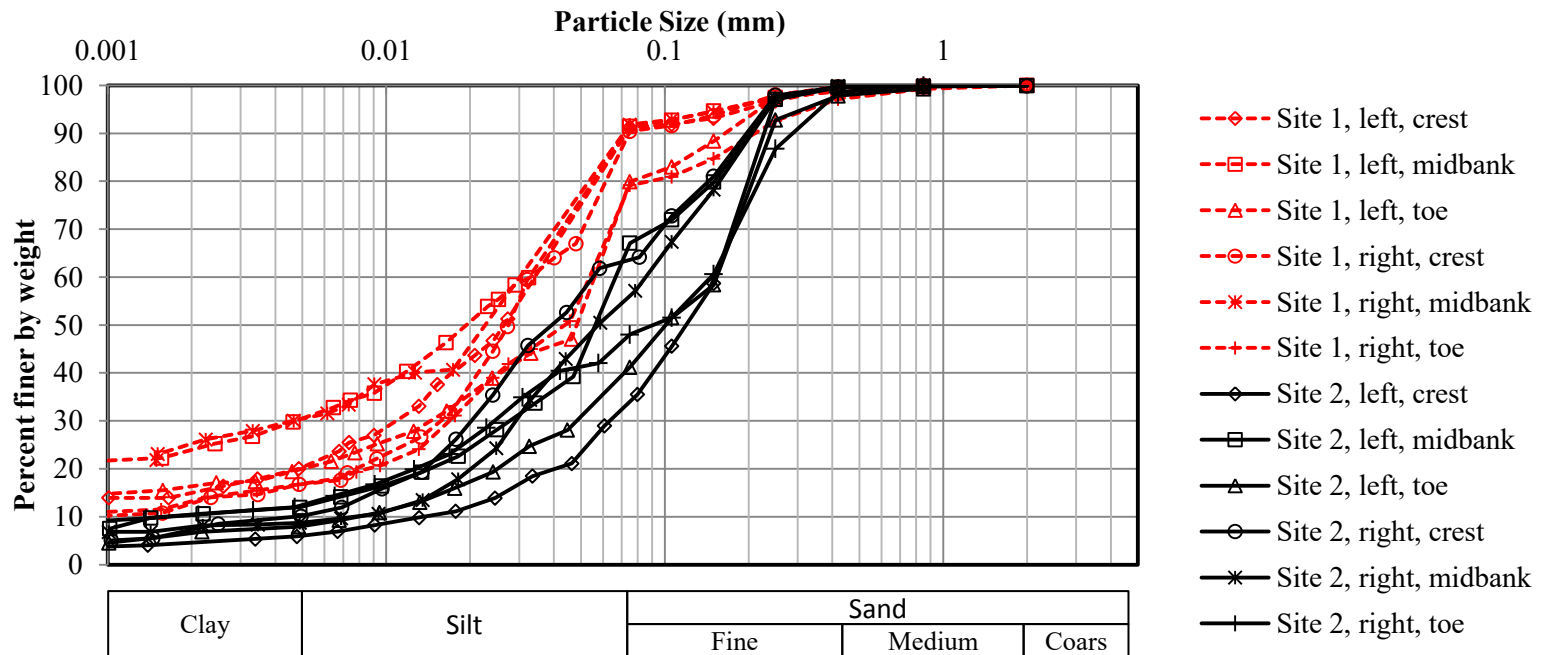


Figure A1. Size distribution for the bank soils extracted from site 1 and site 2.



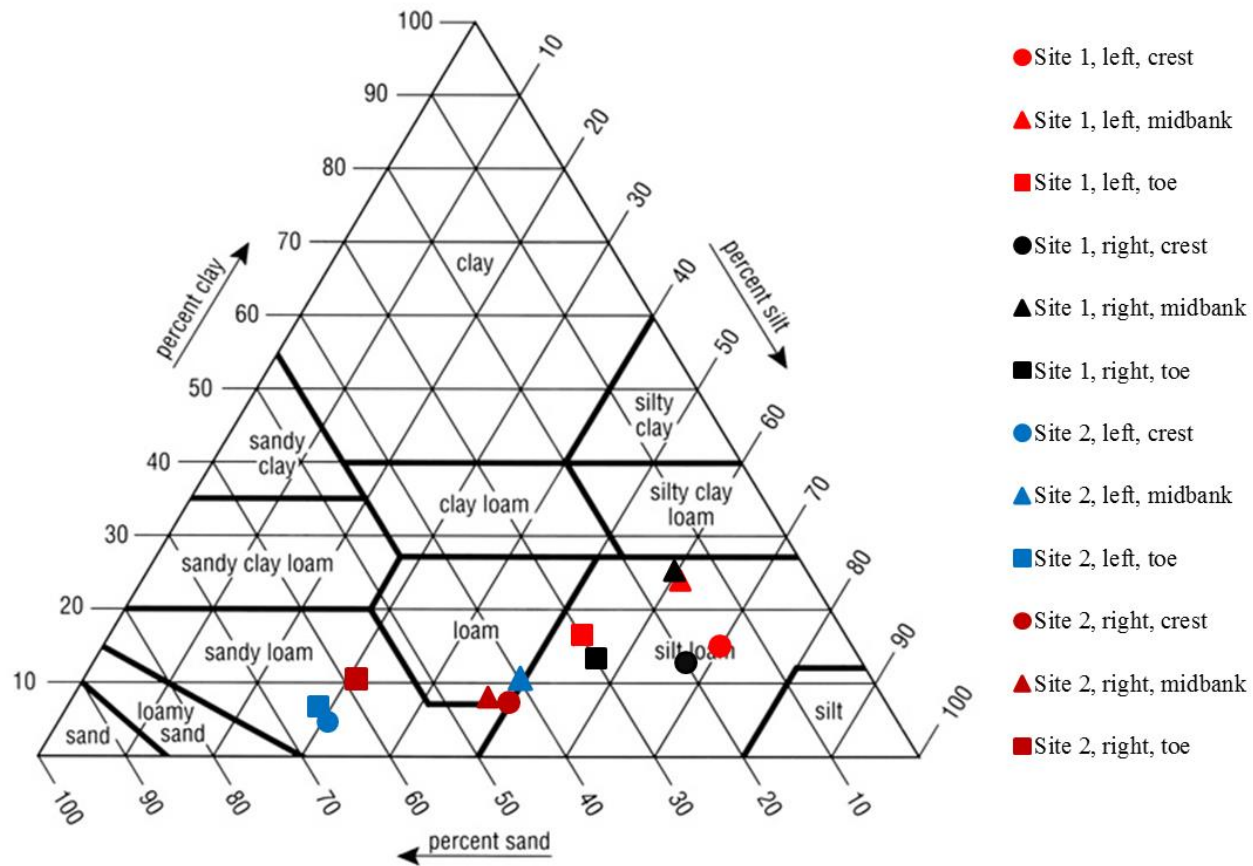


Figure A2. USDA textural classification for twelve (12) bank soil samples extracted from site 1 and 2.

## APPENDIX B DIRECT SHEAR EQUIPMENT AND TEST RESULTS

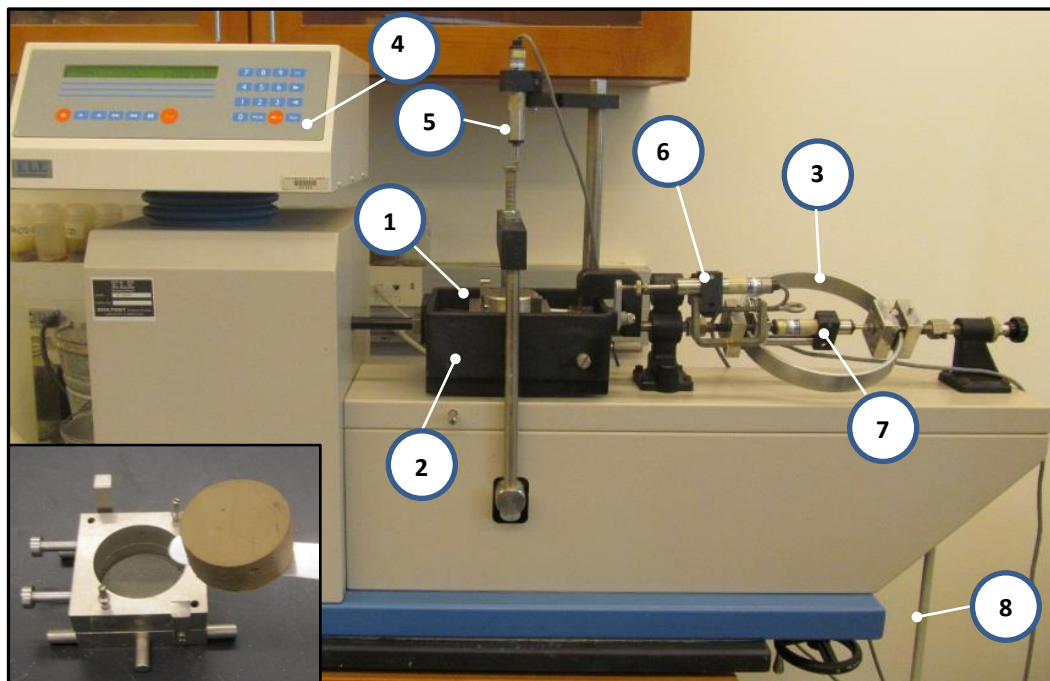


Figure B1. A direct shear test instrument (ELE D-300A series). (1) shear box; (2) container; (3) proving ring; (4) manual control; (5) vertical LVDT transducer (0.4232 v/mm); (6) horizontal LVDT transducer (0.4173 v/mm); (7) LVDT transducer (0.7378 v/mm) for measuring the deflection of proving ring; (8) load hanger. Inset: A soil specimen was carefully placed into the shear box before testing.

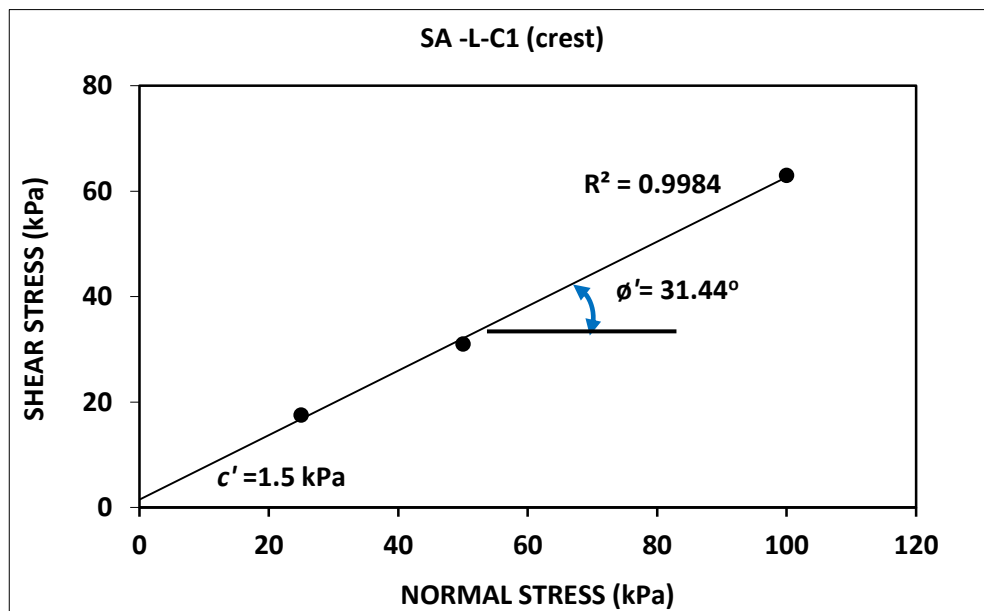


Figure B2. Result of direct shear test for soil sample originated from the crest of the left bank, cross section SA2 at site 1.

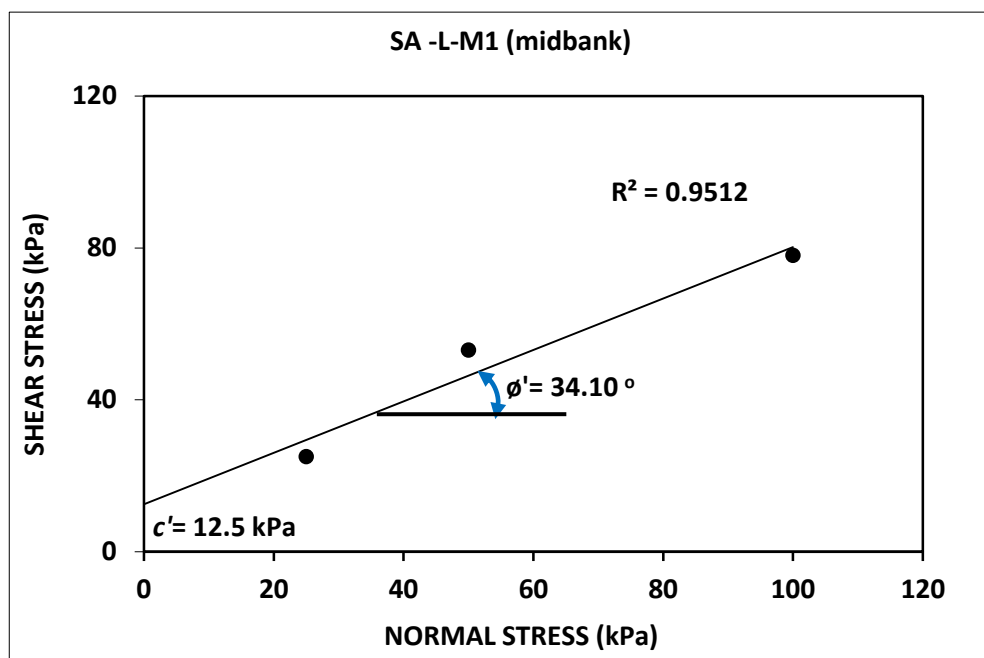


Figure B3. Result of direct shear test for soil sample originated from the midbank of the left bank, cross section SA2 at site 1.

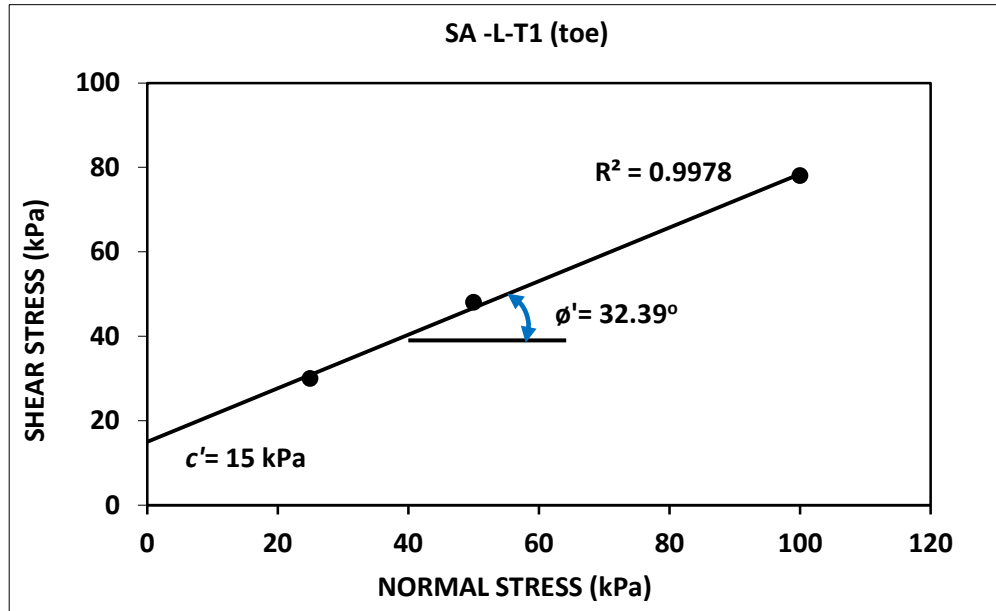


Figure B4. Result of direct shear test for soil sample originated from the toe of the left bank, cross section SA2 at site 1.

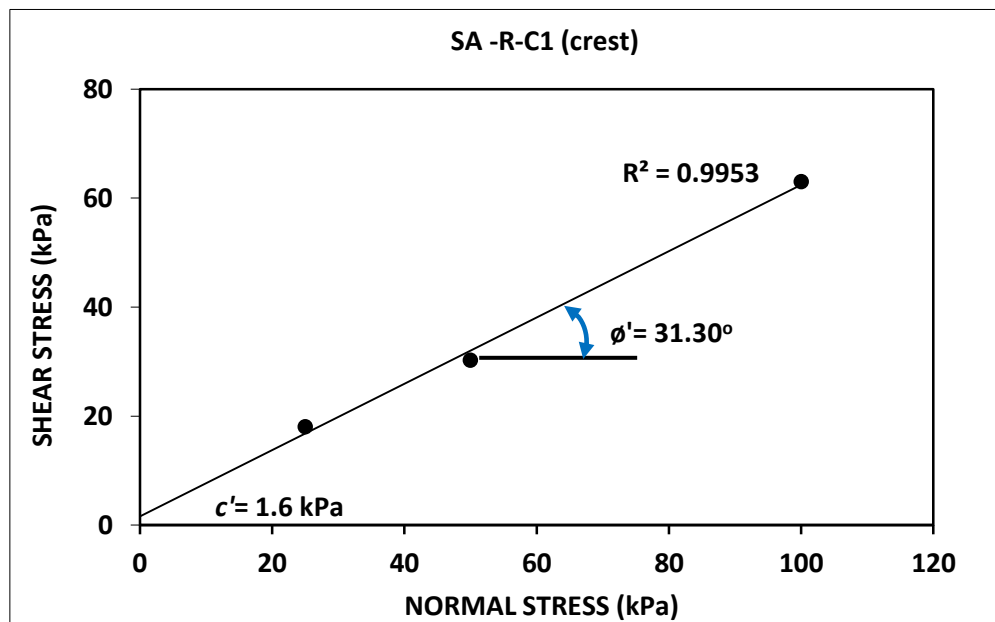


Figure B5. Result of direct shear test for soil sample originated from the crest of the right bank, cross section SA2 at site 1.

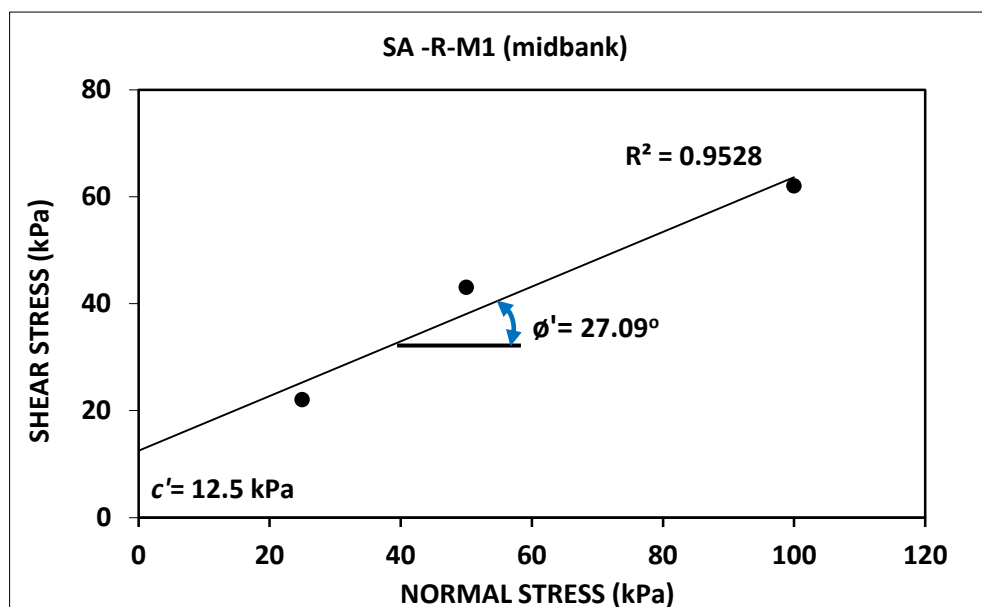


Figure B6. Result of direct shear test for soil sample originated from the midbank of the right bank, cross section SA2 at site 1.

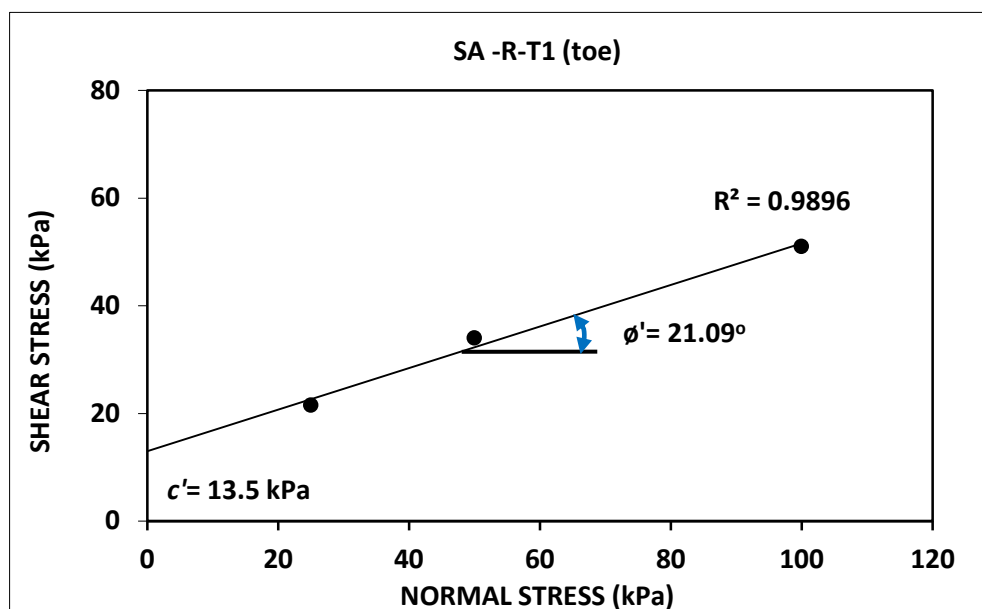


Figure B7. Result of direct shear test for soil sample originated from the toe of the right bank, cross section SA2 at site 1.

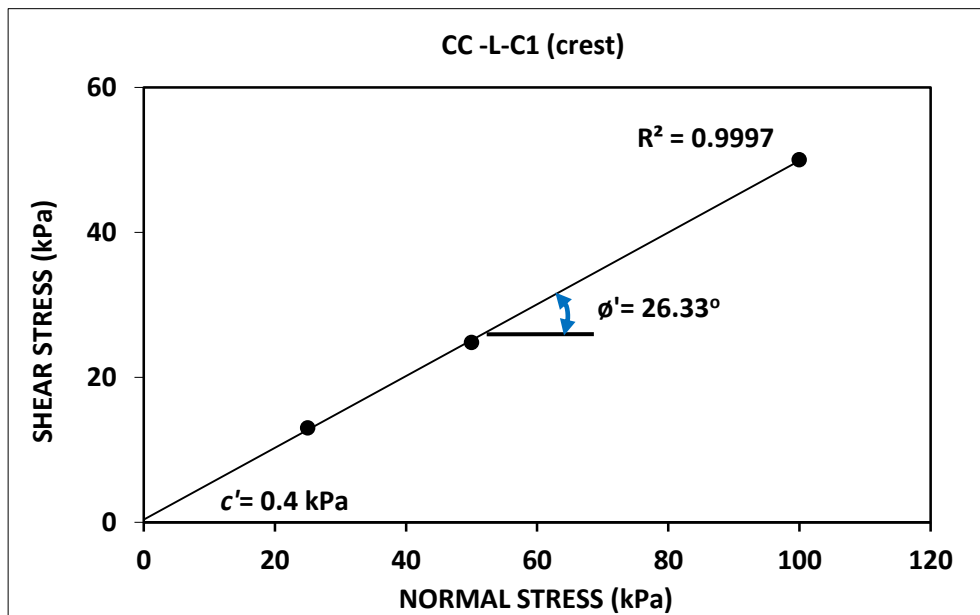


Figure B8. Result of direct shear test for soil sample originated from the crest of the left bank, cross section CC1 at site 2.

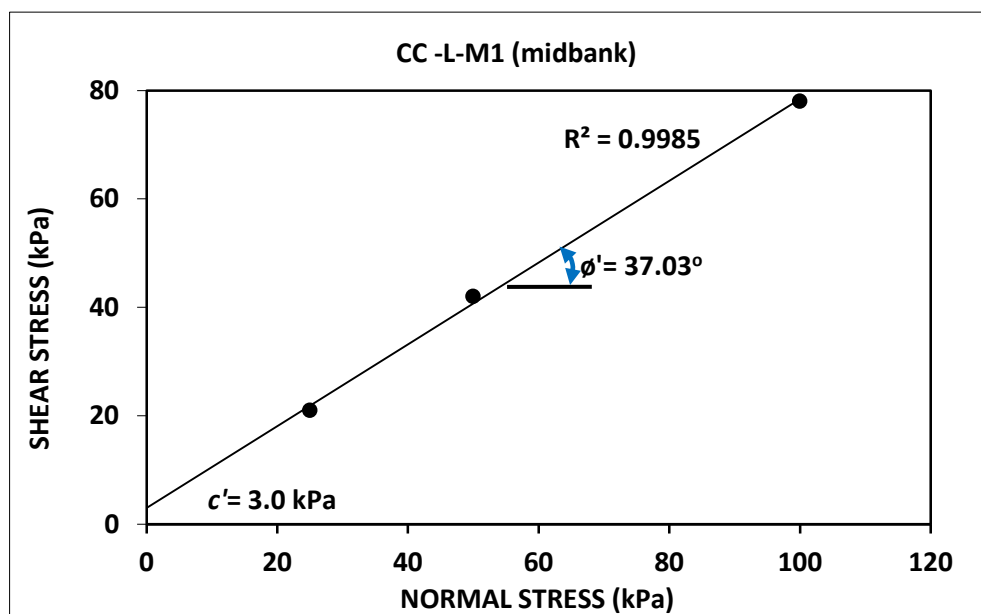


Figure B9. Result of direct shear test for soil sample originated from the midbank of the left bank, cross section CC1 at site 2.

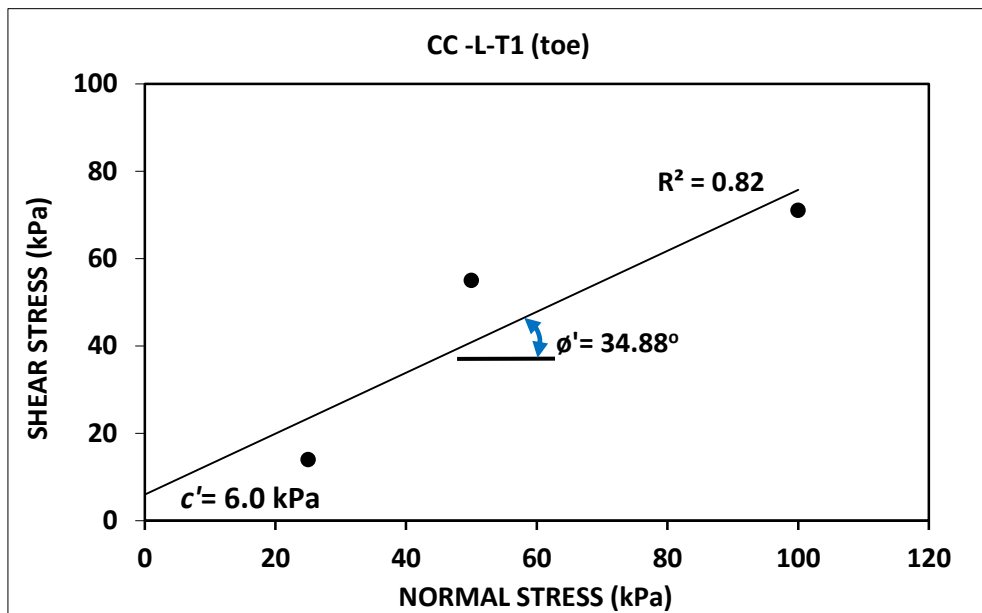


Figure B10. Result of direct shear test for soil sample originated from the toe of the left bank, cross section CC1 at site 2.

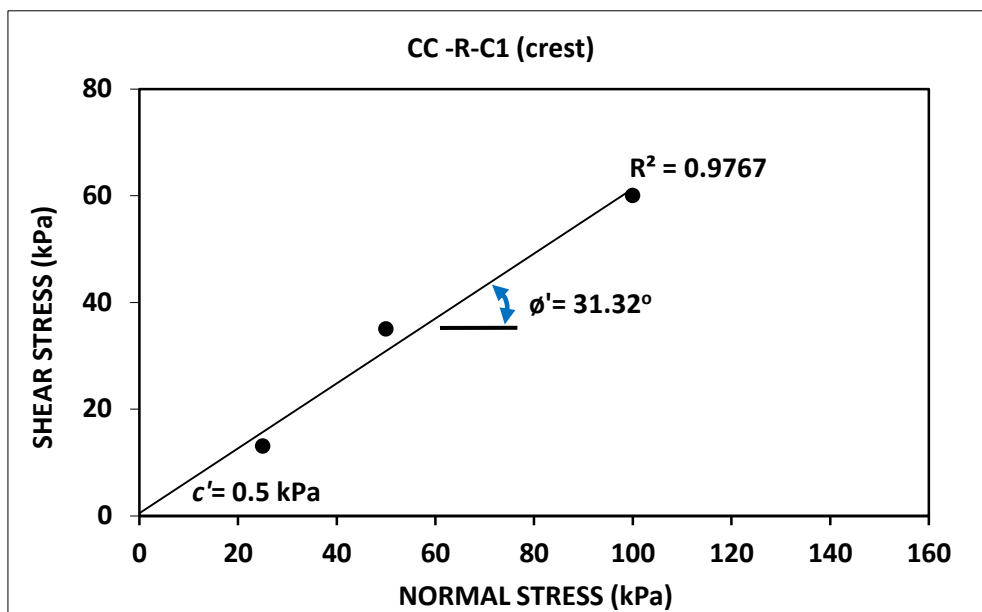


Figure B11. Result of direct shear test for soil sample originated from the crest of the right bank, cross section CC1 at site 2.

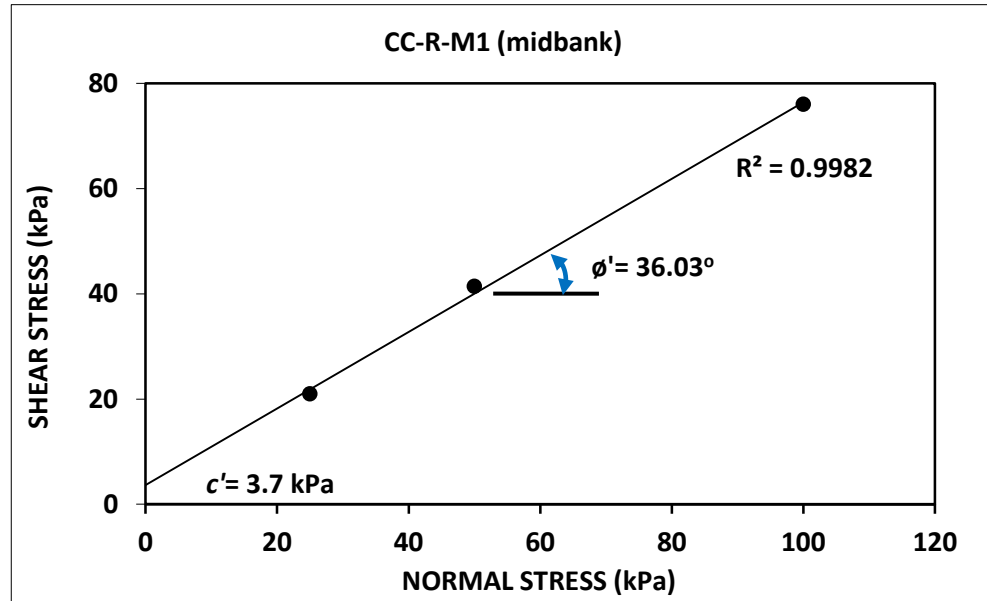


Figure B12. Result of direct shear test for soil sample originated from the midbank of the right bank, cross section CC1 at site 2.



**APPENDIX C**  
**PRELIMINARY CONDUIT FLUME TEST**

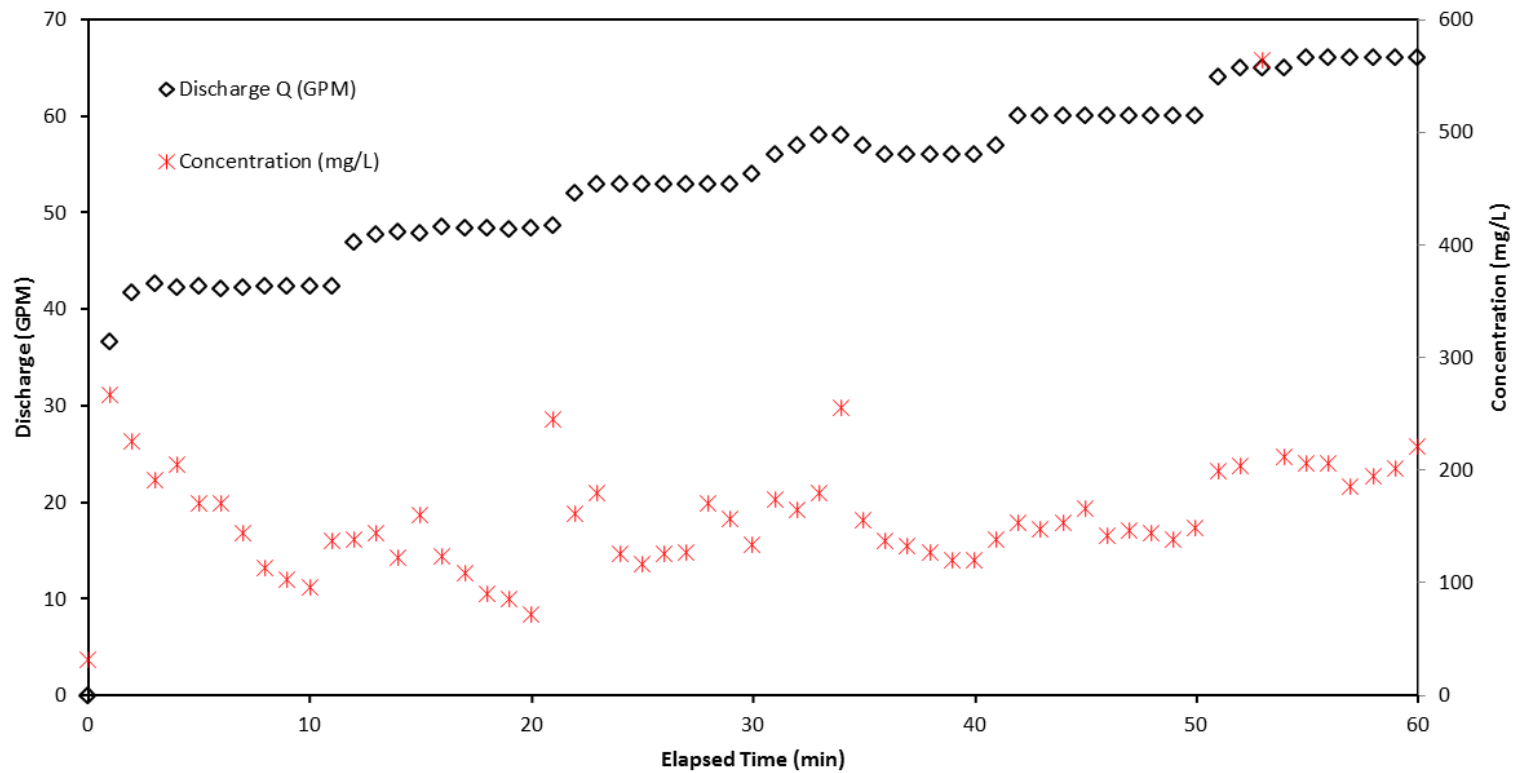


Figure C1. Water-concentration response to the increase of discharge in the conduit flume.

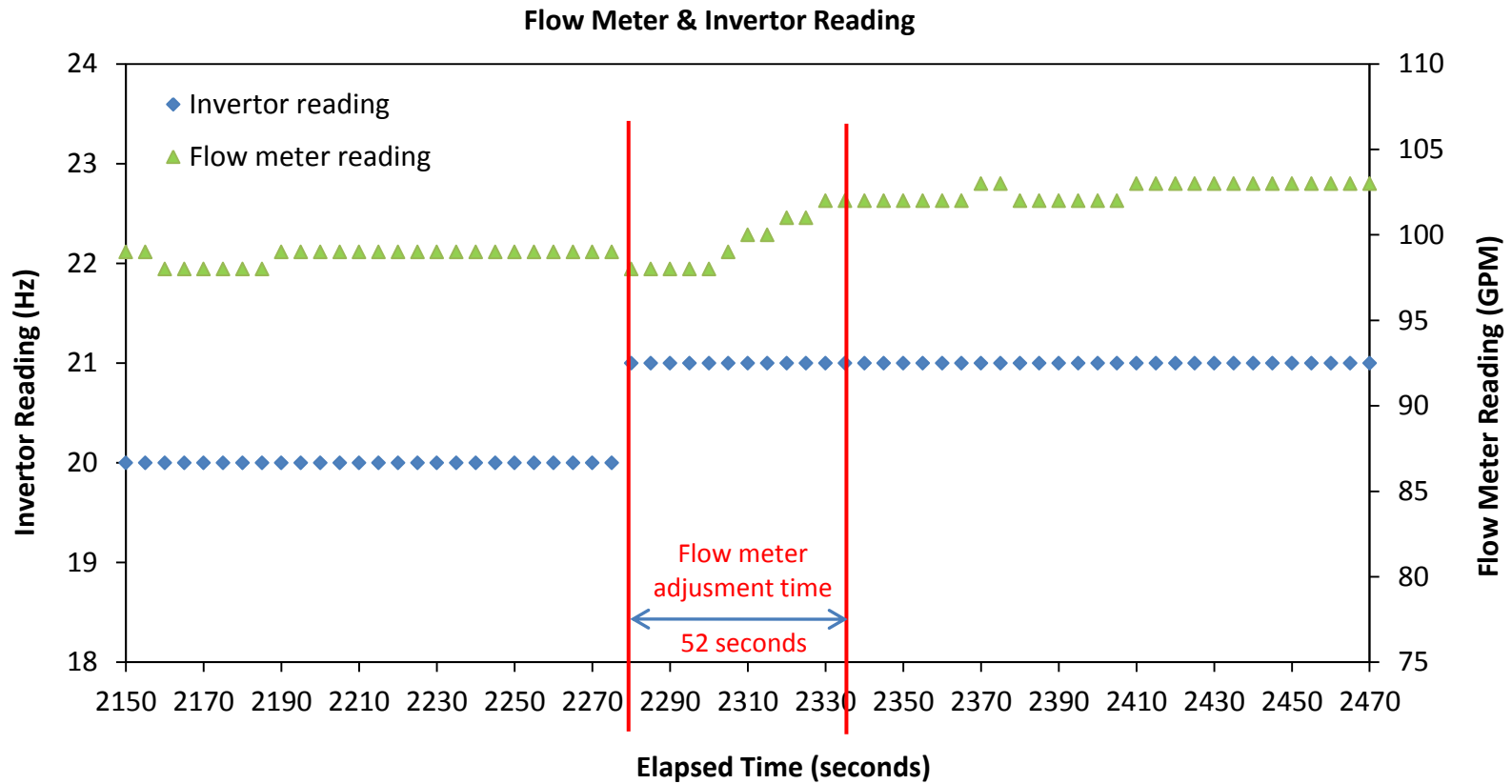


Figure C2. Preliminary conduit flumes run to determine the adjustment time for flow meter due to flow increment.

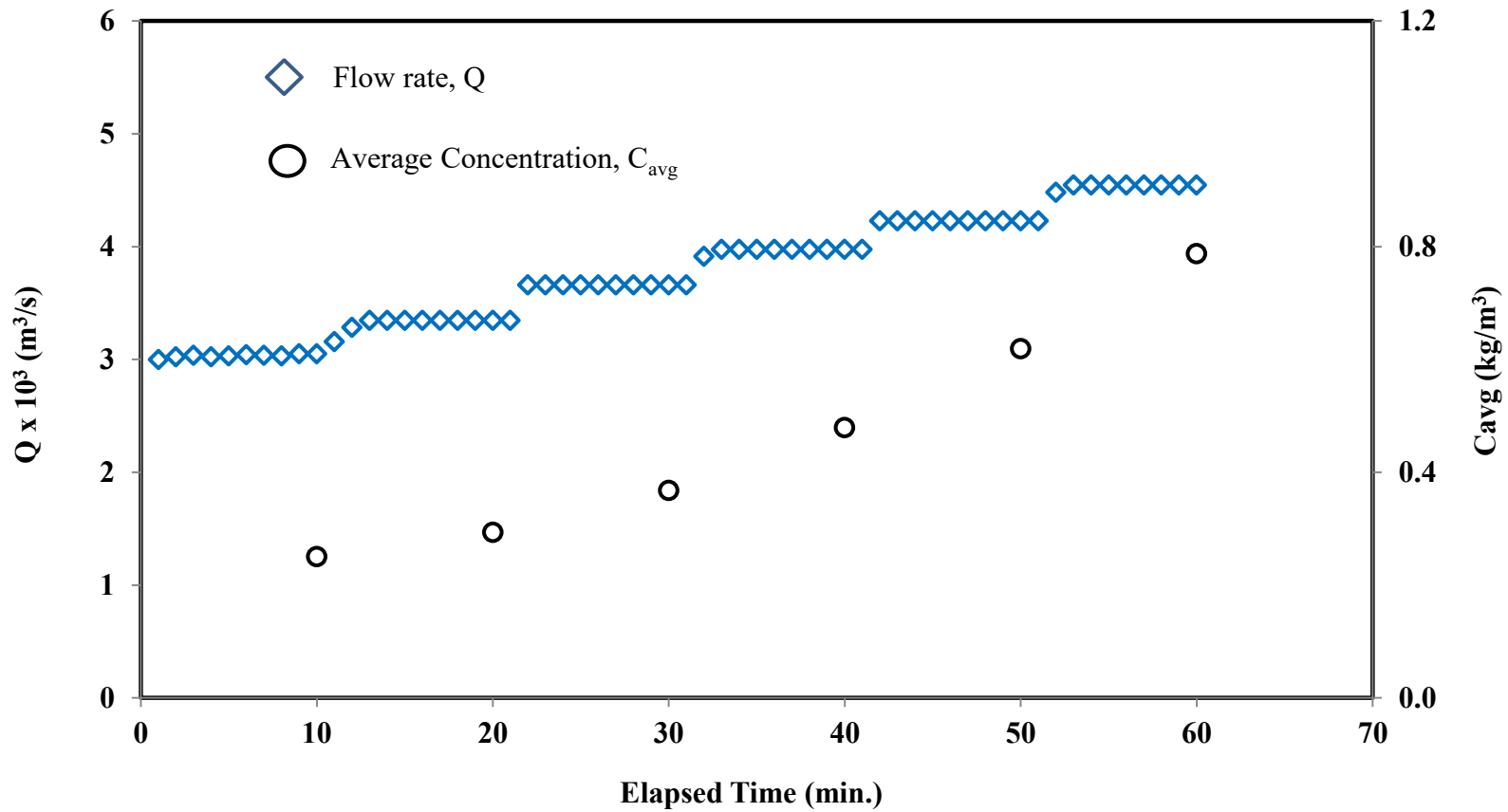


Figure C3. An example of conduit flume run. Flow rate and sediment concentrations were measured during an example 60-minute conduit flume run. Flow rate was increased every 10 minutes resulting in 5 shear stress increments. Sediment concentrations were obtained for each applied flow rate.

## APPENDIX D CONDUIT FLUME TEST CONDITION

In the tables below, the experimental conditions are represented by hydraulic and sediment parameters:

$$Q = \text{flow rate (m}^3/\text{s)}$$

$$U = \text{bulk velocity (m/s)}$$

$$Re_{d_{eff}} = \text{Reynolds number} = Ud_{eff}/\nu$$

where:  $d_{eff}$  = effective diameter (m) =  $(1.029)d_h$

(White, 2008)

$d_h$  = hydraulic diameter of the conduit = 0.0667 m

$\nu$  = water kinematic viscosity =  $1.01 \times 10^{-6}$  m<sup>2</sup>/s

$$\tau_w = \text{wall shear stress (Pa)} = \frac{\rho U^2}{8} f$$

where:  $\rho$  = water density (kg/m<sup>3</sup>)

$f$  = Darcy friction-Weisbach friction factor which is

provided in Haaland (1983):

$$\frac{1}{\sqrt{f}} = -1.8 \log \left[ \frac{6.9}{Re_{d_{eff}}} + \left( \frac{\varepsilon}{3.7d_{eff}} \right)^{1.11} \right]$$

$\varepsilon$  = wall roughness = 0.0002 m

$$u_* = \text{friction velocity (m/s)} = (\tau_w/\rho)^{0.5}$$

$$w_s = \text{average settling velocity (mm/s)}$$

$$= 0.000188 \times (0.5)^{2.34} \times C^{1.37} \text{ (Burt and Stevenson, 1983)}$$

where:  $C$  = water sediment concentration (mg/L).

$$R_o = \text{Rouse number} = w_s/(\kappa u_*), \text{ where } \kappa = 0.41$$

Table D1. Conduit flume test condition.

Sample ID <sup>a</sup>	Elapsed Time (min)	$Q \times 10^3$ (m <sup>3</sup> /s)	$U$ (m/s)	$Re_{D\text{ eff}}$	$\tau_w$ (Pa)	$u_*$ (m/s)	$w_s$ (mm/s)	$R_o \times 10^2$	$C_{avg}$ (kg/m <sup>3</sup> )	$\Delta C_{avg}$ (kg/m <sup>3</sup> )	$E \times 10^3$ (kg/m <sup>2</sup> s)
	(1)	(2)	(3)	(4)	(5)	(6)	(7)	(8)	(9)	(10)	(11)
SA-L-C1	20	3.28	0.66	44570	1.53	0.04	0.003	0.018	0.02	NA	NA
	30	3.91	0.78	53141	2.15	0.05	0.009	0.049	0.06	0.03	4.22
	40	4.48	0.90	60855	2.79	0.05	0.016	0.072	0.08	0.03	3.88
	50	5.11	1.02	69426	3.61	0.06	0.024	0.099	0.11	0.03	5.41
	60	5.74	1.15	77997	4.53	0.07	0.025	0.089	0.11	0.00	0.11
	70	6.37	1.27	86569	5.55	0.07	0.040	0.130	0.16	0.05	10.27
SA-L-C2	10	2.71	0.54	36856	1.10	0.03	0.023	0.170	0.11	NA	NA
	20	3.28	0.66	44570	1.53	0.04	0.034	0.212	0.15	0.04	3.92
	30	3.91	0.78	53141	2.15	0.05	0.035	0.182	0.15	0.00	0.24
	40	4.48	0.90	60855	2.79	0.05	0.030	0.138	0.13	0.00	0.00
	50	5.11	1.02	69426	3.61	0.06	0.030	0.122	0.13	0.00	0.09
	60	5.74	1.15	77997	4.53	0.07	0.068	0.245	0.24	0.11	20.42
SA-L-C3	10	3.15	0.63	42856	1.42	0.04	0.134	0.869	0.40	NA	NA
	20	3.47	0.69	47141	1.71	0.04	0.292	1.720	0.70	0.30	34.89
	30	3.60	0.72	48856	1.83	0.04	0.274	1.560	0.67	0.00	0.00
	40	3.85	0.77	52284	2.08	0.05	0.410	2.191	0.89	0.23	29.24
	50	4.16	0.83	56570	2.43	0.05	0.367	1.813	0.82	0.00	0.00
	60	4.48	0.90	60855	2.79	0.05	0.740	3.414	1.38	0.55	82.33
SA-L-M1	10	2.69	0.54	36513	1.05	0.03	0.003	0.020	0.02	NA	NA
	20	3.12	0.62	42341	1.39	0.04	0.004	0.025	0.03	0.01	0.64
	30	3.72	0.74	50570	1.95	0.04	0.008	0.044	0.05	0.02	2.62
	40	4.29	0.86	58284	2.57	0.05	0.011	0.053	0.06	0.01	1.89
	50	4.86	0.97	65998	3.27	0.06	0.018	0.078	0.09	0.03	4.64
	60	5.43	1.09	73712	4.05	0.06	0.030	0.113	0.13	0.04	7.03
SA-L-M2	10	3.53	0.71	47998	1.77	0.04	0.050	0.289	0.19	NA	NA
	20	4.16	0.83	56570	2.43	0.05	0.037	0.184	0.15	0.00	0.00
	30	4.79	0.96	65141	3.19	0.06	0.045	0.195	0.18	0.02	3.78
	40	5.43	1.09	73712	4.05	0.06	0.121	0.465	0.37	0.19	34.23
	50	6.06	1.21	82283	5.02	0.07	0.129	0.444	0.38	0.02	3.36
	60	6.62	1.32	89997	5.98	0.08	0.162	0.509	0.45	0.07	15.16
SA-L-M3	10	3.41	0.68	46284	1.65	0.04	0.006	0.037	0.04	NA	NA
	20	3.97	0.79	53998	2.22	0.05	0.019	0.098	0.09	0.05	7.02
	30	4.67	0.93	63426	3.03	0.06	0.094	0.415	0.30	0.21	32.60
	40	5.17	1.03	70283	3.70	0.06	0.125	0.499	0.37	0.07	12.12
	50	5.87	1.17	79712	4.72	0.07	0.362	1.282	0.82	0.44	86.24
	60	6.44	1.29	87426	5.66	0.08	0.493	1.597	1.02	0.21	44.37
SA-L-T1	10	2.83	0.57	38484	1.16	0.03	0.019	0.133	0.09	NA	NA
	20	3.47	0.69	47141	1.71	0.04	0.038	0.223	0.16	0.06	7.33
	30	3.97	0.79	53998	2.22	0.05	0.082	0.423	0.28	0.12	15.69
	40	4.48	0.90	60855	2.79	0.05	0.051	0.236	0.20	0.00	0.00
	50	5.05	1.01	68569	3.52	0.06	0.134	0.549	0.39	0.20	33.41
	60	5.80	1.16	78855	4.62	0.07	0.289	1.037	0.69	0.30	57.74

Table D1. Continued.

SA-L-T2	10	3.47	0.69	47141	1.71	0.04	0.028	0.167	0.13	NA	NA
	20	4.10	0.82	55712	2.36	0.05	0.042	0.213	0.17	0.04	5.96
	30	4.67	0.93	63426	3.03	0.06	0.075	0.334	0.26	0.09	13.86
	40	5.30	1.06	71998	3.87	0.06	0.100	0.390	0.32	0.06	10.40
	50	5.99	1.20	81426	4.92	0.07	0.161	0.558	0.45	0.13	26.49
	60	6.62	1.32	89997	5.98	0.08	0.416	1.309	0.90	0.45	99.72
SA-L-T3	10	3.47	0.69	47141	1.71	0.04	0.076	0.449	0.26	NA	NA
	20	3.79	0.76	51427	2.02	0.04	0.057	0.310	0.21	0.00	0.00
	30	4.04	0.81	54855	2.29	0.05	0.068	0.349	0.24	0.03	4.04
	40	4.35	0.87	59141	2.64	0.05	0.075	0.354	0.26	0.02	2.34
	50	4.54	0.91	61712	2.87	0.05	0.114	0.519	0.35	0.09	14.11
	60	4.86	0.97	65998	3.27	0.06	0.119	0.506	0.36	0.01	1.68
SA-R-C1	10	2.61	0.52	35399	1.00	0.03	0.005	0.036	0.03	NA	NA
	20	2.90	0.58	39427	1.21	0.03	0.011	0.076	0.06	0.03	2.78
	30	3.15	0.63	42856	1.42	0.04	0.006	0.039	0.04	0.00	0.00
	40	3.79	0.76	51427	2.02	0.04	0.021	0.113	0.10	0.06	7.57
	50	4.35	0.87	59141	2.64	0.05	0.048	0.227	0.19	0.09	12.38
SA-R-C2	10	2.62	0.52	35570	1.00	0.03	0.005	0.035	0.03	NA	NA
	20	2.91	0.58	39599	1.22	0.03	0.004	0.029	0.03	0.00	0.00
	30	3.53	0.71	47998	1.77	0.04	0.007	0.040	0.05	0.01	1.67
	40	4.04	0.81	54855	2.29	0.05	0.009	0.045	0.05	0.01	1.25
	50	4.61	0.92	62569	2.95	0.05	0.023	0.101	0.11	0.05	8.16
	60	5.11	1.02	69426	3.61	0.06	0.033	0.135	0.14	0.04	6.01
SA-R-C3	10	2.97	0.59	40284	1.26	0.04	0.237	1.625	0.60	NA	NA
	20	3.28	0.66	44570	1.53	0.04	0.175	1.090	0.48	0.00	0.00
	30	3.53	0.71	47998	1.77	0.04	0.319	1.851	0.74	0.26	31.13
	40	3.79	0.76	51427	2.02	0.04	0.311	1.685	0.73	0.00	0.00
	50	4.10	0.82	55712	2.36	0.05	0.407	2.044	0.89	0.16	21.75
	60	4.42	0.88	59998	2.72	0.05	0.343	1.604	0.78	0.00	0.00
SA-R-M1	10	2.66	0.53	36085	1.02	0.03	0.100	0.761	0.32	NA	NA
	20	2.93	0.59	39856	1.24	0.04	0.097	0.671	0.31	0.00	0.00
	30	3.22	0.64	43713	1.48	0.04	0.272	1.727	0.66	0.35	37.67
	40	3.53	0.71	47998	1.77	0.04	0.111	0.643	0.34	0.00	0.00
	50	3.85	0.77	52284	2.08	0.05	0.128	0.681	0.38	0.04	4.76
	60	4.10	0.82	55712	2.36	0.05	0.191	0.959	0.51	0.13	17.84
SA-R-M2	10	2.85	0.57	38656	1.17	0.03	0.060	0.428	0.22	NA	NA
	20	3.41	0.68	46284	1.65	0.04	0.112	0.670	0.35	0.13	14.25
	30	3.91	0.78	53141	2.15	0.05	0.274	1.440	0.67	0.32	41.76
	40	4.48	0.90	60855	2.79	0.05	0.475	2.190	0.99	0.33	49.15
	50	5.05	1.01	68569	3.52	0.06	0.384	1.578	0.85	0.00	0.00
SA-R-M3	10	2.81	0.56	38142	1.14	0.03	0.615	4.439	1.20	NA	NA
	20	3.14	0.63	42684	1.41	0.04	0.898	5.829	1.58	0.38	40.09
	30	3.41	0.68	46284	1.65	0.04	0.211	1.268	0.55	0.00	0.00
	40	3.66	0.73	49713	1.89	0.04	0.332	1.859	0.77	0.22	26.23
	50	3.91	0.78	53141	2.15	0.05	0.220	1.156	0.57	0.00	0.00
	60	4.16	0.83	56570	2.43	0.05	0.184	0.912	0.50	0.00	0.00

Table D1. Continued.

SA-R-T1	10	2.68	0.54	36427	1.04	0.03	0.000	0.000	0.00	NA	NA
	20	2.94	0.59	39942	1.24	0.04	0.004	0.028	0.03	0.03	3.02
	30	3.28	0.66	44570	1.53	0.04	0.012	0.075	0.07	0.04	4.08
	40	3.60	0.72	48856	1.83	0.04	0.026	0.147	0.12	0.05	6.06
	50	3.85	0.77	52284	2.08	0.05	0.017	0.092	0.09	0.00	0.00
	60	4.10	0.82	55712	2.36	0.05	0.015	0.077	0.08	0.00	0.00
	70	4.35	0.87	59141	2.64	0.05	0.024	0.115	0.11	0.03	4.61
	80	4.73	0.95	64284	3.11	0.06	0.041	0.181	0.17	0.05	8.61
SA-R-T2	10	3.15	0.63	42856	1.42	0.04	0.041	0.263	0.17	NA	NA
	20	3.60	0.72	48856	1.83	0.04	0.050	0.284	0.19	0.03	3.15
	30	4.10	0.82	55712	2.36	0.05	0.044	0.220	0.17	0.00	0.00
	40	4.61	0.92	62569	2.95	0.05	0.074	0.332	0.26	0.08	12.45
	50	5.24	1.05	71140	3.78	0.06	0.097	0.386	0.31	0.06	9.92
	60	5.74	1.15	77997	4.53	0.07	0.210	0.762	0.55	0.24	45.22
SA-R-T3	10	2.68	0.54	36427	1.04	0.03	0.010	0.074	0.06	NA	NA
	20	2.95	0.59	40113	1.25	0.04	0.012	0.084	0.07	0.01	1.01
	30	3.22	0.64	43713	1.48	0.04	0.014	0.087	0.07	0.01	0.65
	40	3.47	0.69	47141	1.71	0.04	0.010	0.062	0.06	0.00	0.00
	50	3.79	0.76	51427	2.02	0.04	0.013	0.072	0.07	0.01	1.47
	60	4.10	0.82	55712	2.36	0.05	0.016	0.078	0.08	0.01	1.21
	70	4.35	0.87	59141	2.64	0.05	0.025	0.120	0.12	0.04	5.12
CC-L-C2	10	2.79	0.56	37884	1.12	0.03	0.012	0.089	0.07	NA	NA
	20	3.08	0.62	41827	1.36	0.04	0.009	0.062	0.06	0.00	0.00
	30	3.13	0.63	42513	1.40	0.04	0.008	0.054	0.05	0.00	0.00
	40	3.34	0.67	45427	1.59	0.04	0.011	0.069	0.06	0.01	1.46
	50	3.72	0.74	50570	1.95	0.04	0.013	0.069	0.07	0.01	0.69
	60	3.97	0.79	53998	2.22	0.05	0.017	0.091	0.09	0.02	2.52
	70	4.16	0.83	56570	2.43	0.05	0.021	0.102	0.10	0.01	1.55
CC-L-M1	10	2.97	0.59	40284	1.26	0.04	0.059	0.408	0.22	NA	NA
	20	3.28	0.66	44570	1.53	0.04	0.421	2.623	0.91	0.69	75.81
	30	3.60	0.72	48856	1.83	0.04	0.443	2.525	0.95	0.03	4.10
	40	3.91	0.78	53141	2.15	0.05	0.661	3.476	1.27	0.32	41.87
	50	4.23	0.85	57427	2.50	0.05	1.426	6.954	2.22	0.95	134.27
CC-L-M2	10	3.05	0.61	41399	1.33	0.04	0.072	0.478	0.25	NA	NA
	20	3.34	0.67	45427	1.59	0.04	0.089	0.545	0.29	0.04	4.83
	30	3.66	0.73	49713	1.89	0.04	0.121	0.680	0.37	0.07	9.01
	40	3.97	0.79	53998	2.22	0.05	0.174	0.903	0.48	0.11	14.79
	50	4.23	0.85	57427	2.50	0.05	0.248	1.209	0.62	0.14	19.74
	60	4.54	0.91	61712	2.87	0.05	0.345	1.567	0.79	0.17	25.46
CC-L-T1	10	2.82	0.56	38313	1.15	0.03	0.012	0.088	0.07	NA	NA
	20	3.15	0.63	42856	1.42	0.04	0.010	0.068	0.06	0.00	0.00
	30	3.41	0.68	46284	1.65	0.04	0.031	0.186	0.14	0.07	8.45
	40	3.72	0.74	50570	1.95	0.04	0.048	0.265	0.19	0.05	6.31
	50	3.91	0.78	53141	2.15	0.05	0.037	0.194	0.15	0.00	0.00
	60	4.23	0.85	57427	2.50	0.05	0.054	0.264	0.20	0.05	7.01
	70	4.35	0.87	59141	2.64	0.05	0.081	0.382	0.27	0.07	9.92



Table D1. Continued.

CC-L-T4	10	2.97	0.59	40370	1.27	0.04	0.045	0.306	0.18	NA	NA
	20	3.28	0.66	44570	1.53	0.04	0.010	0.064	0.06	0.00	0.00
	30	3.60	0.72	48856	1.83	0.04	0.012	0.069	0.07	0.01	0.91
	40	3.91	0.78	53141	2.15	0.05	0.015	0.079	0.08	0.01	1.51
	50	4.23	0.85	57427	2.50	0.05	0.015	0.074	0.08	0.00	0.10
	60	4.48	0.90	60855	2.79	0.05	0.035	0.159	0.15	0.07	9.90
	70	4.48	0.90	60855	2.79	0.05	0.053	0.243	0.20	0.05	7.94
	80	4.61	0.92	62569	2.95	0.05	0.039	0.174	0.16	0.00	0.00
CC-R-C3	10	2.57	0.51	34970	0.96	0.03	0.162	1.277	0.45	NA	NA
	20	2.83	0.57	38484	1.16	0.03	0.353	2.532	0.80	0.35	32.78
	30	3.03	0.61	41227	1.26	0.04	0.195	1.338	0.52	0.00	0.00
	40	2.97	0.59	40284	1.43	0.04	0.221	1.424	0.57	0.05	5.01
	50	3.79	0.76	51427	2.02	0.04	0.484	2.625	1.01	0.44	55.34
	60	3.91	0.78	53141	2.15	0.05	0.655	3.444	1.26	0.25	32.60
CC-R-C4	10	2.53	0.51	34370	0.93	0.03	0.103	0.822	0.33	NA	NA
	20	2.70	0.54	36684	1.06	0.03	0.046	0.342	0.18	0.00	0.00
	30	2.88	0.58	39170	1.20	0.03	0.052	0.370	0.20	0.02	1.83
	40	3.04	0.61	41313	1.32	0.04	0.100	0.668	0.32	0.12	12.11
	50	3.34	0.67	45427	1.59	0.04	0.086	0.528	0.29	0.00	0.00
	60	3.85	0.77	52284	2.08	0.05	0.196	1.046	0.52	0.23	30.06
	70	4.42	0.88	59998	2.72	0.05	0.414	1.936	0.90	0.38	55.86
CC-R-C5	20	3.15	0.63	42856	1.61	0.04	0.124	0.755	0.37	NA	NA
	30	3.47	0.69	47141	1.94	0.04	0.045	0.248	0.18	0.00	0.00
	40	3.85	0.77	52284	2.37	0.05	0.083	0.416	0.28	0.10	12.92
	50	4.16	0.83	56570	2.75	0.05	0.059	0.273	0.22	0.00	0.00
	60	4.73	0.95	64284	3.53	0.06	0.112	0.459	0.35	0.13	20.53
	70	5.49	1.10	74569	4.71	0.07	0.147	0.523	0.42	0.08	14.05
	80	5.99	1.20	81426	5.58	0.07	0.201	0.656	0.53	0.11	21.50
CC-R-M1	4	2.86	0.57	38913	1.18	0.03	0.283	2.004	0.68	NA	NA
	8	3.05	0.61	41484	1.34	0.04	0.266	1.772	0.65	0.00	0.00
	12	3.15	0.63	42856	1.42	0.04	0.210	1.357	0.55	0.00	0.00
	16	3.28	0.66	44570	1.53	0.04	0.233	1.451	0.59	0.04	4.74
	20	3.47	0.69	47141	1.71	0.04	0.258	1.523	0.64	0.05	5.31
	28	3.66	0.73	49713	1.89	0.04	1.542	8.641	2.35	1.71	208.80
CC-R-M2	10	2.67	0.53	36256	1.03	0.03	0.020	0.153	0.10	NA	NA
	20	3.05	0.61	41484	1.34	0.04	0.015	0.098	0.08	0.00	0.00
	30	3.41	0.68	46284	1.65	0.04	0.034	0.204	0.15	0.07	7.53
	40	3.53	0.71	47998	1.77	0.04	0.026	0.151	0.12	0.00	0.00
	50	3.79	0.76	51427	2.02	0.04	0.033	0.181	0.14	0.02	3.01
	60	4.16	0.83	56570	2.43	0.05	0.057	0.282	0.21	0.07	9.48
CC-R-M3	10	2.79	0.56	37970	1.14	0.03	0.276	1.991	0.67	NA	NA
	20	2.94	0.59	39942	1.24	0.04	0.259	1.794	0.64	0.00	0.00
	30	3.06	0.61	41570	1.34	0.04	0.331	2.206	0.76	0.13	12.76
	40	3.12	0.62	42427	1.39	0.04	0.534	3.492	1.08	0.32	33.21
	50	3.34	0.67	45427	1.59	0.04	1.839	11.239	2.67	1.59	177.06
	60	3.91	0.78	53141	2.15	0.05	10.136	53.271	9.29	6.62	862.74

Table D1.Continued.

	10	2.01	0.40	27256	0.60	0.02	0.090	0.890	0.29	NA	NA
	20	2.10	0.42	28542	0.66	0.03	0.127	1.202	0.38	0.08	5.94
CC-R-M4	30	2.25	0.45	30513	0.74	0.03	0.288	2.579	0.69	0.31	23.30
	40	2.44	0.49	33170	0.87	0.03	0.378	3.121	0.84	0.15	12.32
	50	2.58	0.52	35056	0.97	0.03	0.672	5.260	1.28	0.44	37.87
	12	3.06	0.61	41570	1.34	0.04	0.131	0.872	0.39	NA	NA
	16	3.15	0.63	42856	1.42	0.04	0.134	0.866	0.39	0.01	0.69
CC-R-T1	20	3.28	0.66	44570	1.53	0.04	0.137	0.854	0.40	0.01	0.76
	24	3.60	0.72	48856	1.83	0.04	0.103	0.588	0.33	0.00	0.00
	28	3.72	0.74	50570	1.95	0.04	0.193	1.064	0.52	0.19	23.49
	32	3.85	0.77	52284	2.08	0.05	0.263	1.403	0.65	0.13	16.69
	10	3.03	0.61	41141	1.31	0.04	2.168	14.573	3.01	NA	NA
	20	3.34	0.67	45427	1.59	0.04	2.222	13.578	3.07	0.05	6.03
CC-R-T5	30	3.60	0.72	48856	1.83	0.04	2.391	13.628	3.24	0.17	20.32
	40	3.91	0.78	53141	2.15	0.05	2.911	15.297	3.74	0.50	65.12
	50	4.10	0.82	55712	2.36	0.05	4.140	20.787	4.83	1.10	149.77

Note: the numbers in parentheses are column numbers.

<sup>a</sup>SA= South Amana; CC= Camp Cardinal; L= left bank; R= right bank; C= crest; M= midbank; T= toe.

## APPENDIX E CONDUIT FLUME TEST RESULTS

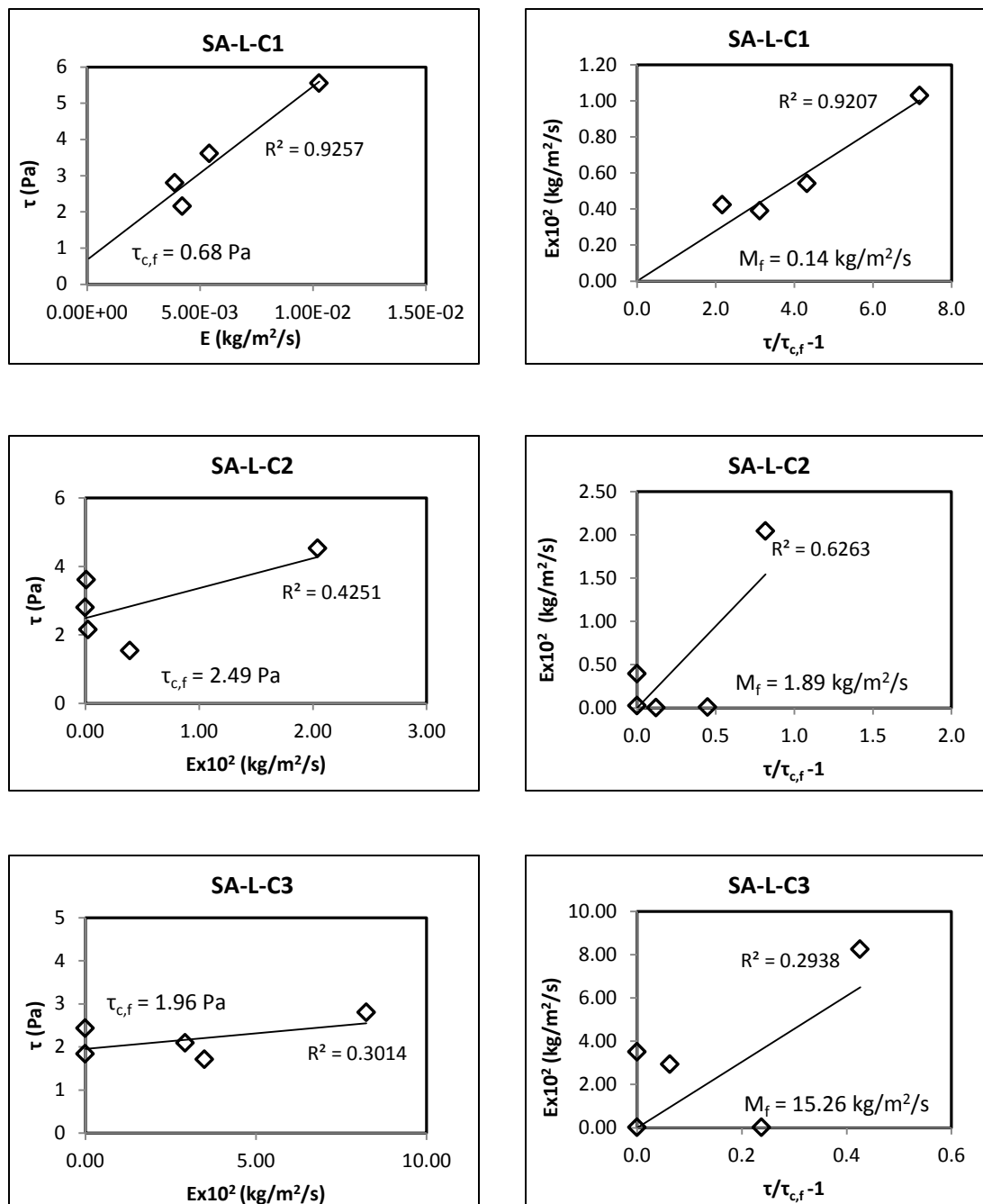


Figure E1. Fluvial erosional strength and erodibility coefficient.

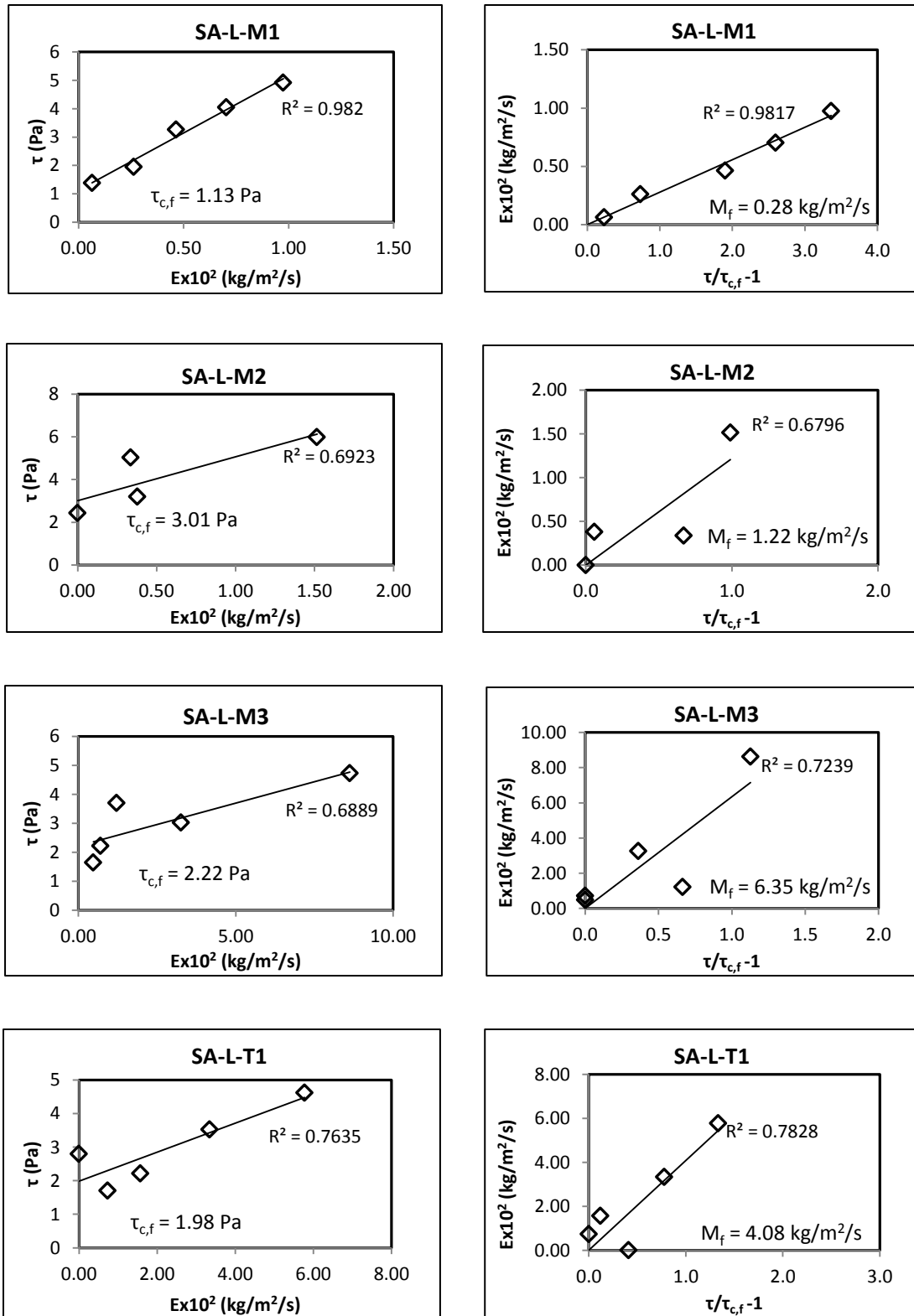


Figure E1. Continued.

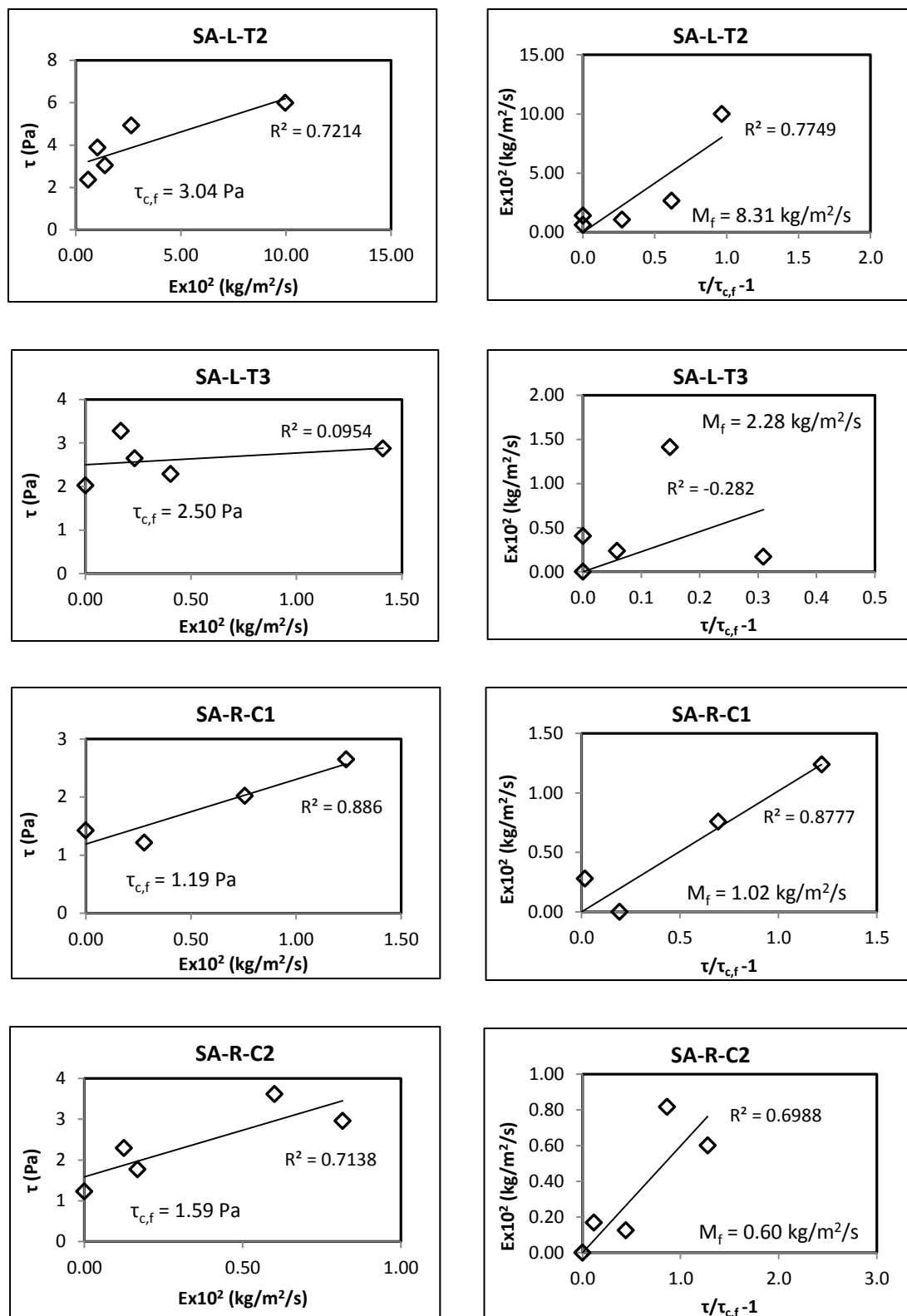


Figure E1. Continued.

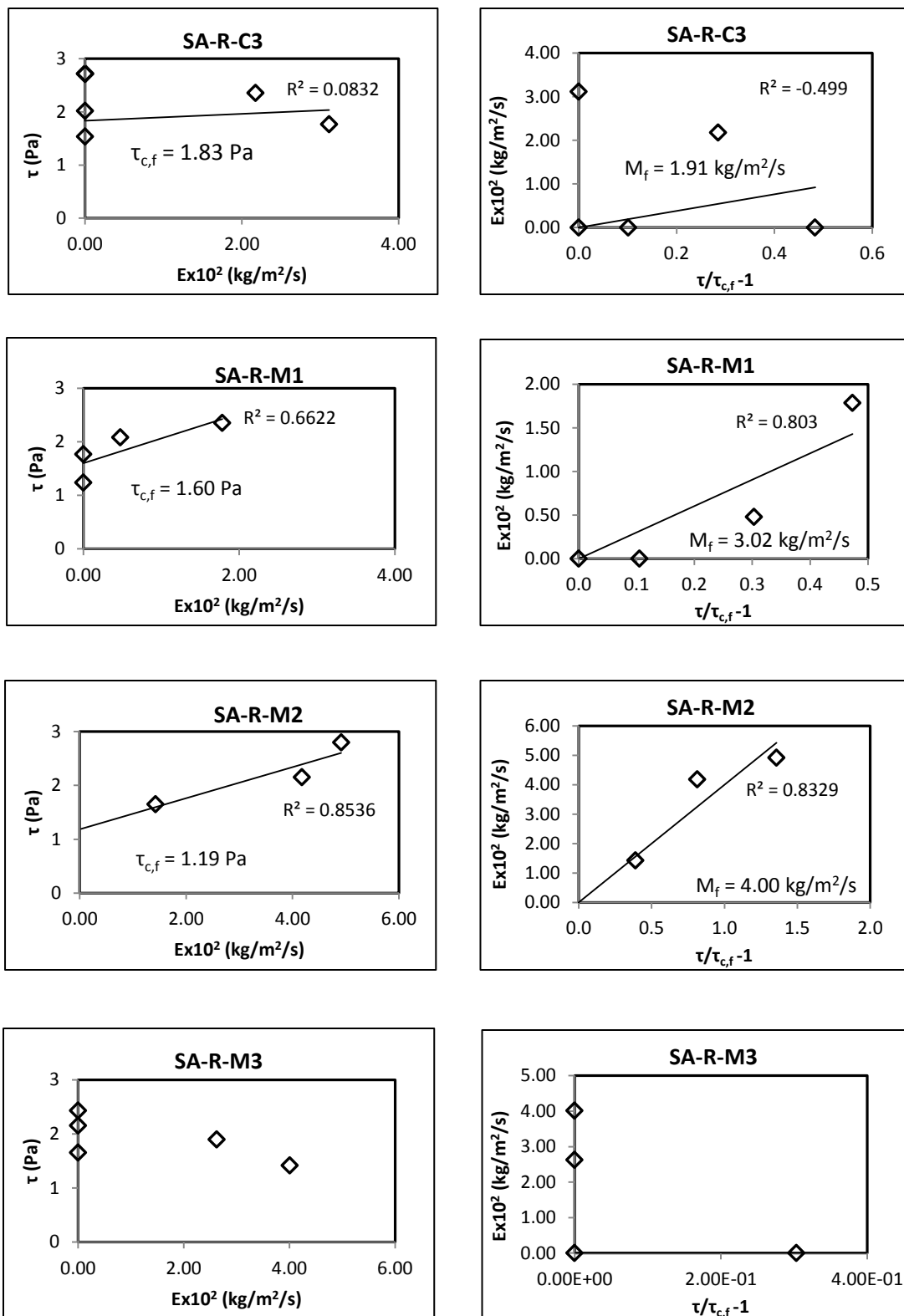


Figure E1. Continued.

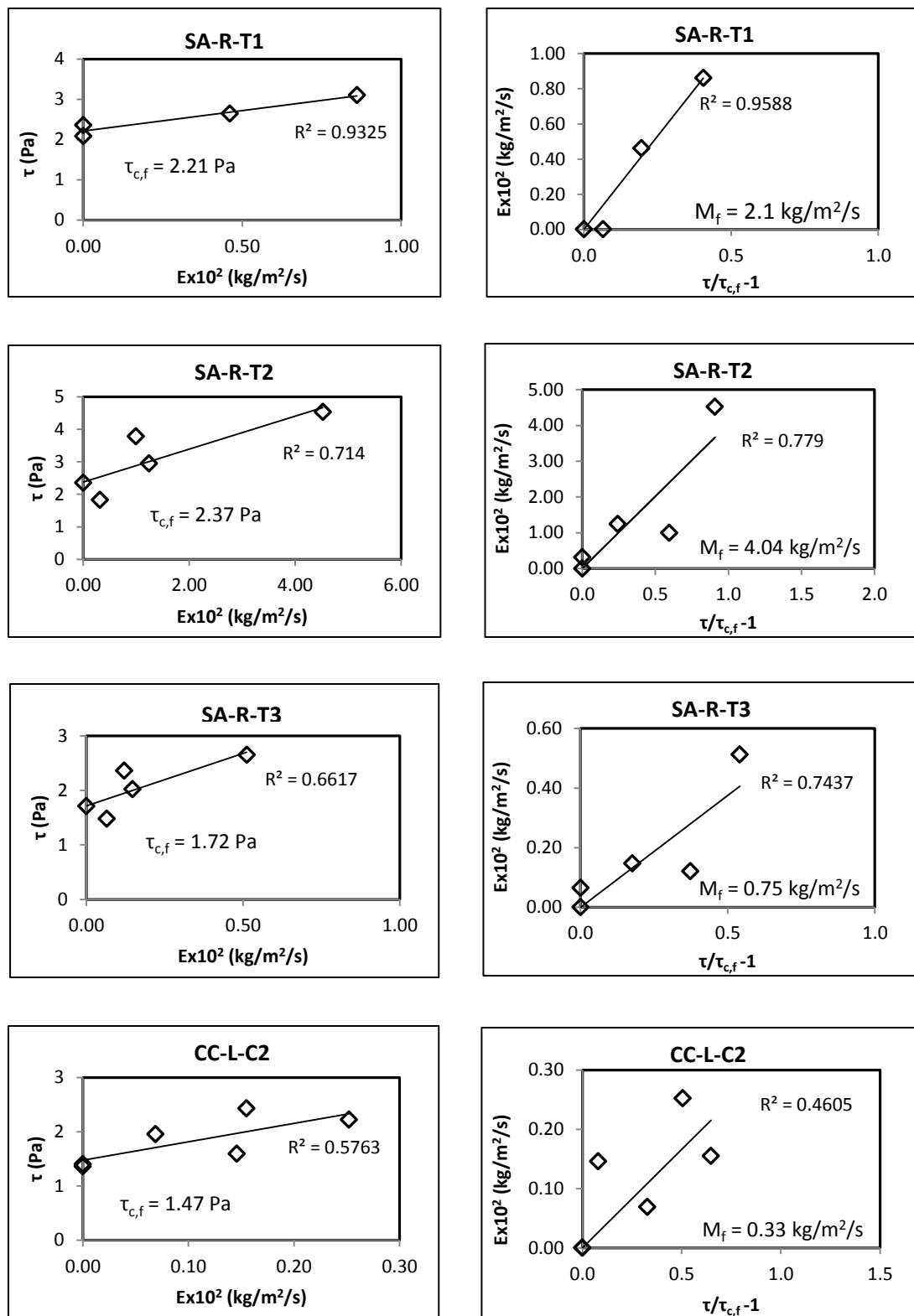


Figure E1. Continued.

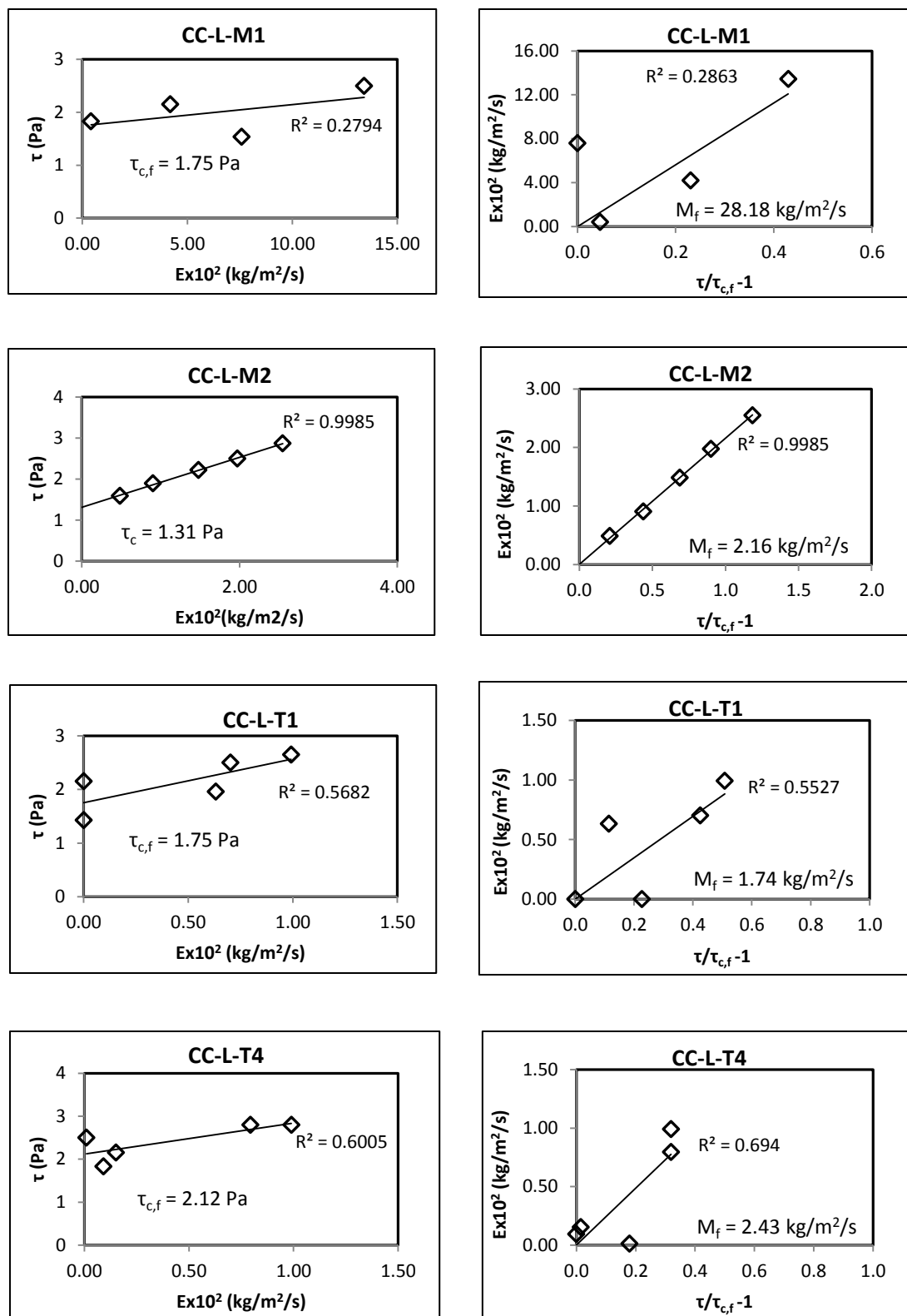


Figure E1. Continued.



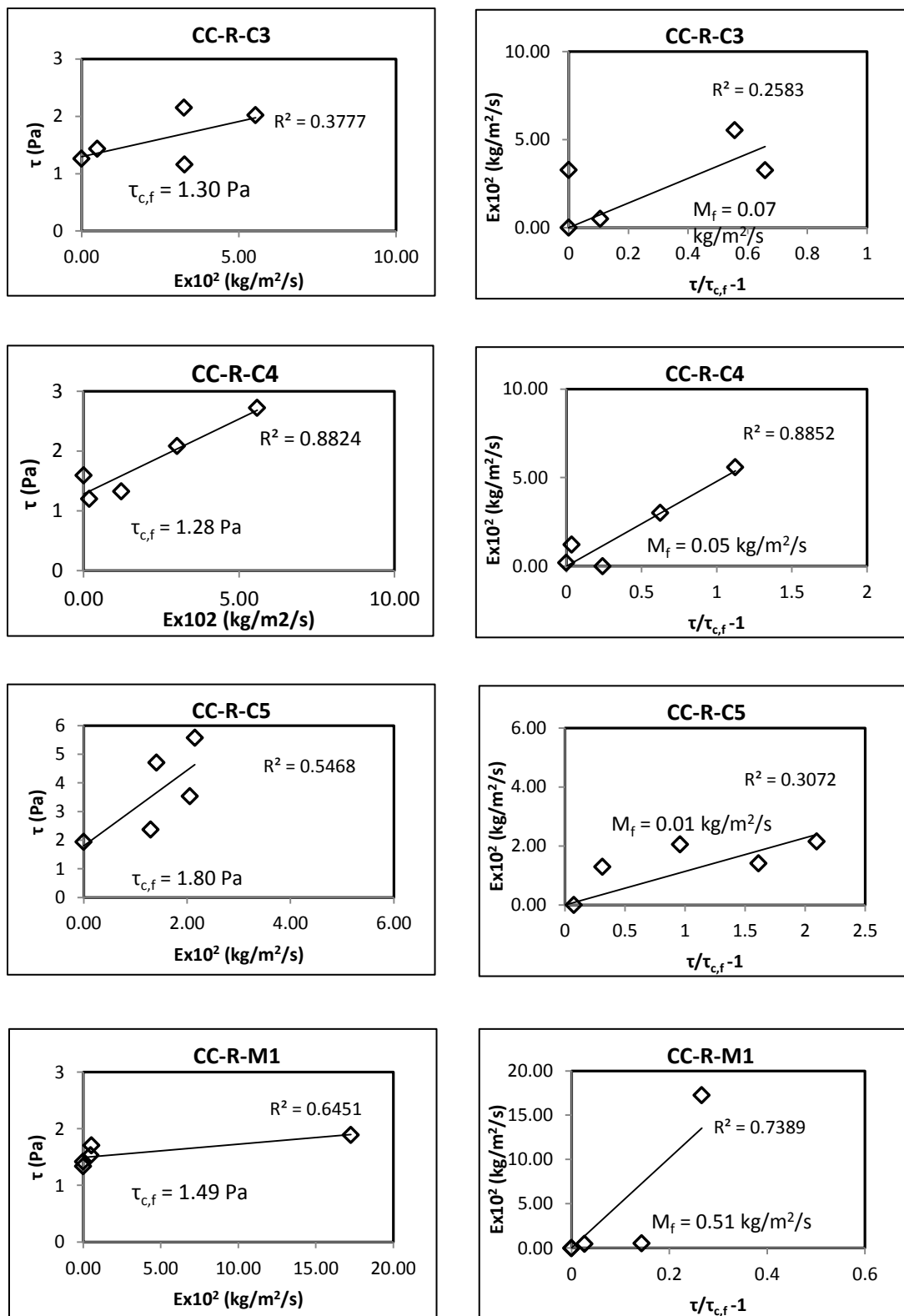


Figure E1. Continued.

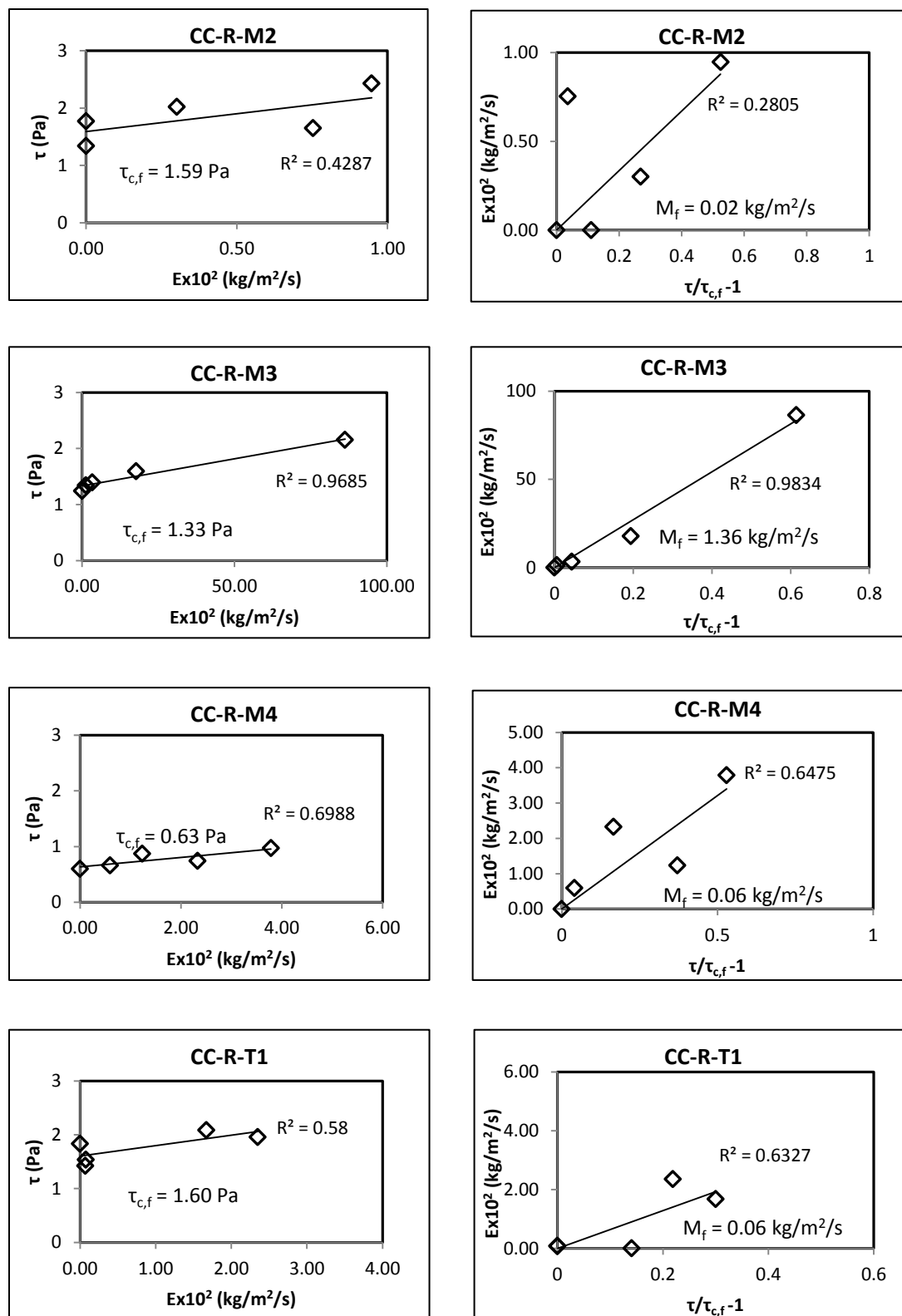


Figure E1. Continued.

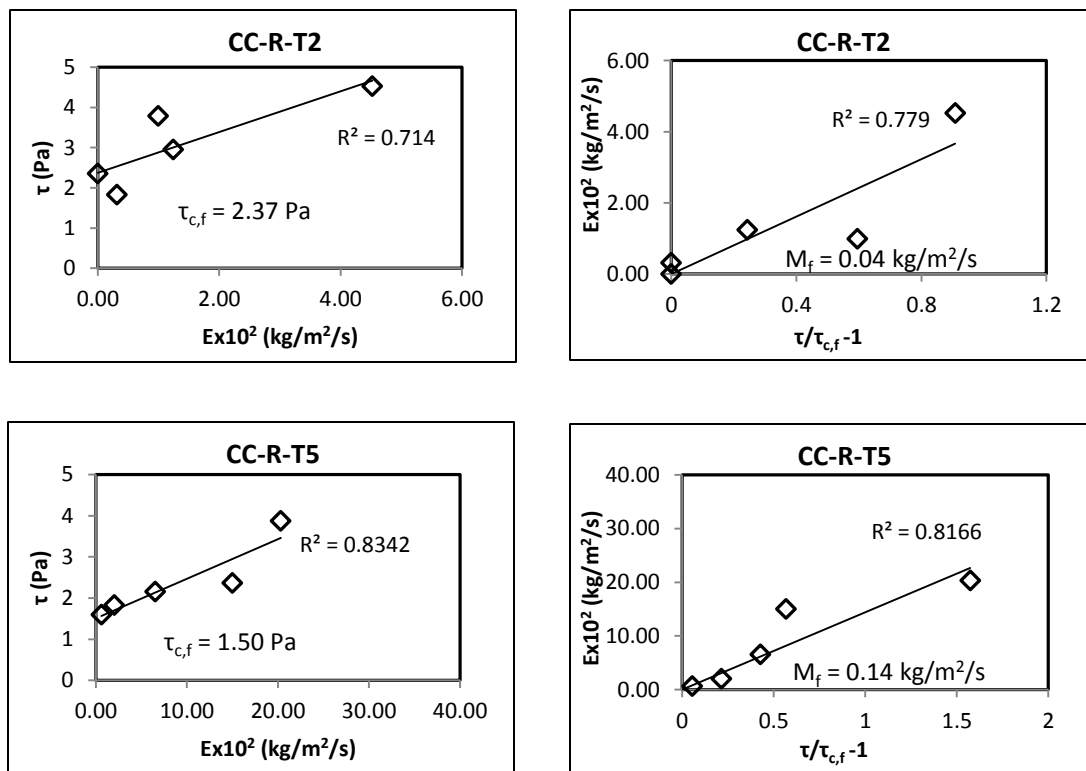


Figure E1. Continued.

## APPENDIX F PHOTO ELECTRONIC EROSION PIN (PEEP)

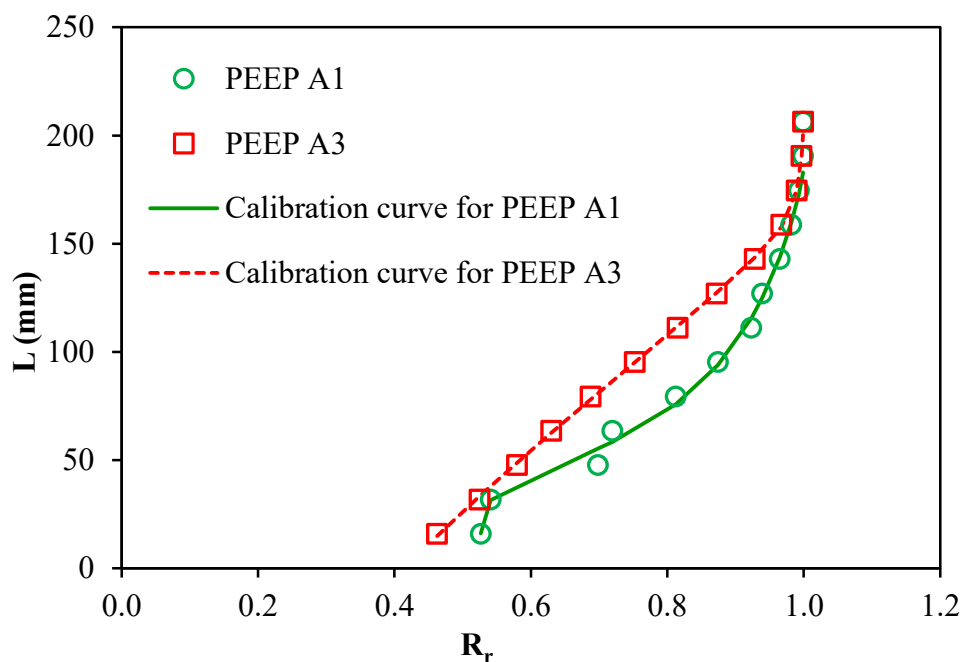


Figure F1. Relation between normalized cell series output,  $R_r$ , and PEEP exposure length,  $L$ , for PEEPs installed at site 1.

Table F1. Calibration coefficients for PEEPs installed at site 1.

Coefficients	PEEP A1	PEEP A3
$c_1$	22.75371726	3.80266E+14
$c_2$	-66.91050207	4.01236E+14
$c_3$	45.30328583	-4.86025E+15
$c_4$	-1.149356173	4.05236E+15
$c_5$	-3.81903143	-2.03543E+13
$c_6$	4.526206083	2.20821E+13
$c_7$	-1.707188487	-1.85576E+12

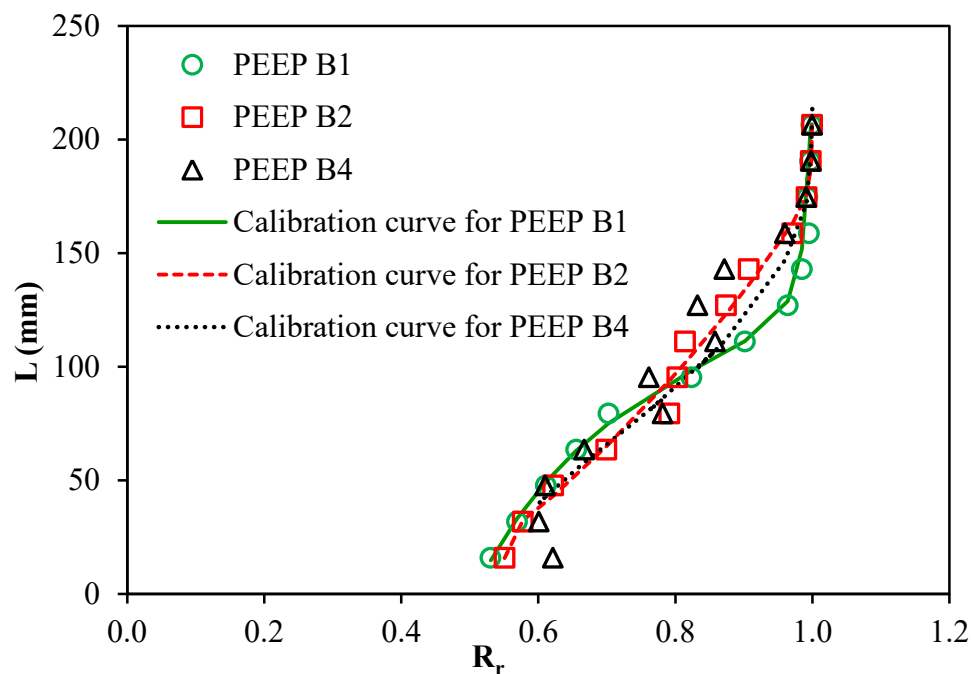


Figure F2. Relation between normalized cell series output,  $R_r$ , and PEEP exposure length,  $L$ , for PEEPs installed at site 2.

Table F2. Calibration coefficients for PEEPs installed at site 2.

Coefficients	PEEP B1	PEEP B2	PEEP B4
$c_1$	433.9940	-81.9883	49.4890
$c_2$	-1723.1469	411.5974	-132.0013
$c_3$	2140.2614	-657.2812	57.7259
$c_4$	-851.1267	327.5335	24.5635
$c_5$	-6.6795	-3.2239	-4.0832
$c_6$	10.3447	2.9865	4.8097
$c_7$	-4.6653	-0.7633	-1.7276

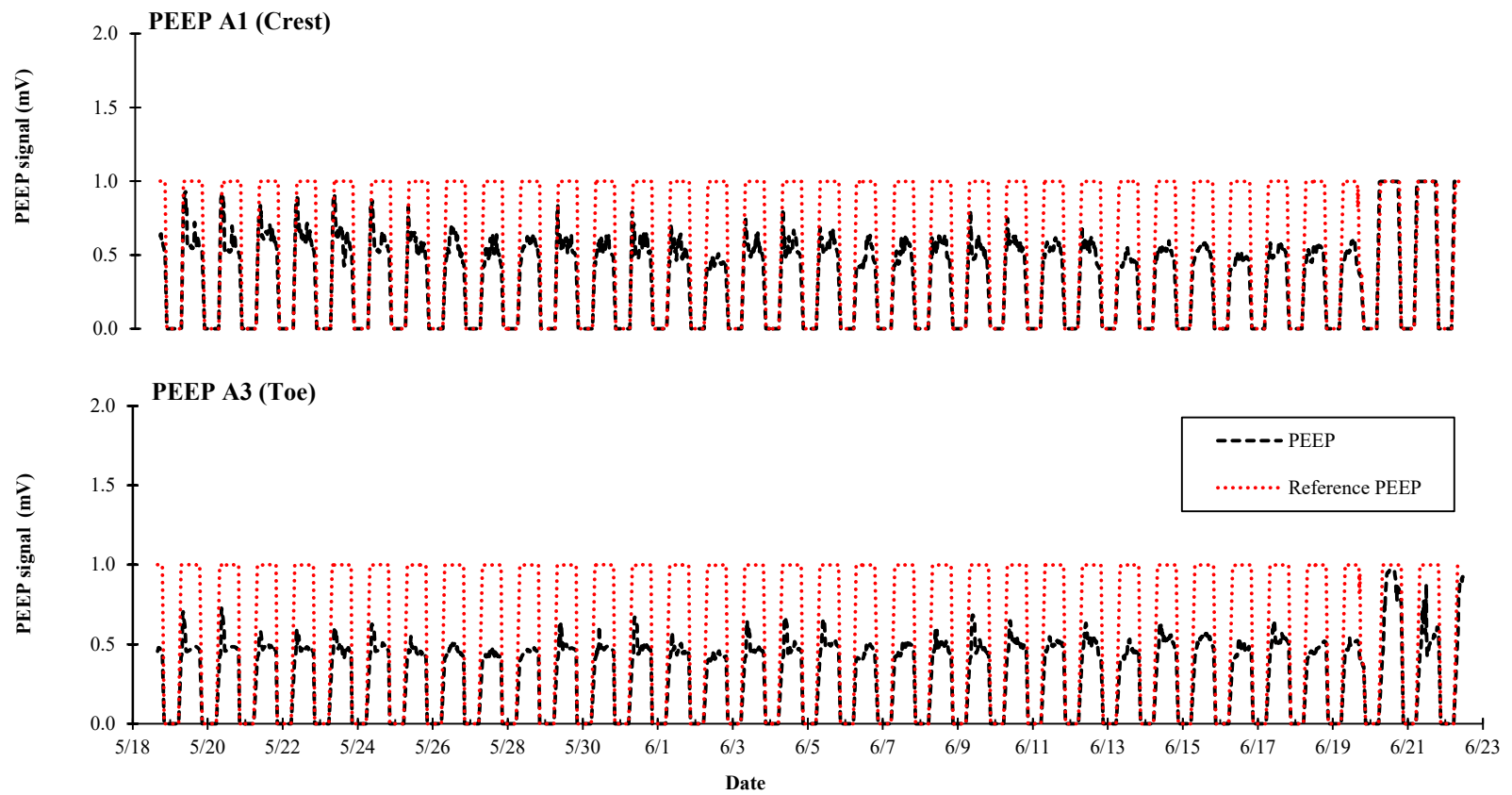


Figure F3. Voltage signal recorded from PEEP A1, A3, and reference PEEP at site 1 during deployment period.

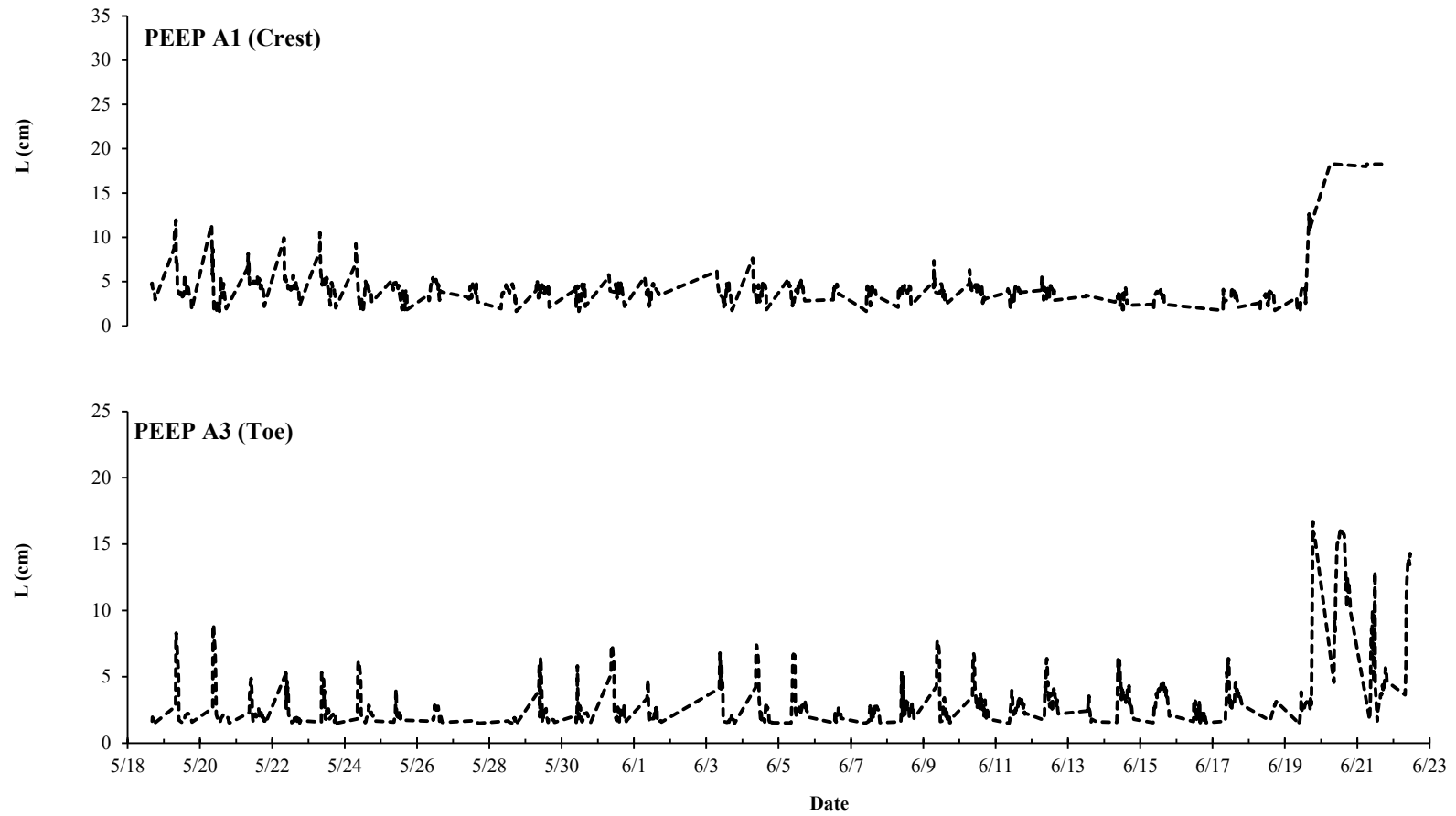


Figure F4. Unprocessed exposure length recorded from PEEPA1 and A3 at site 1 during deployment period.

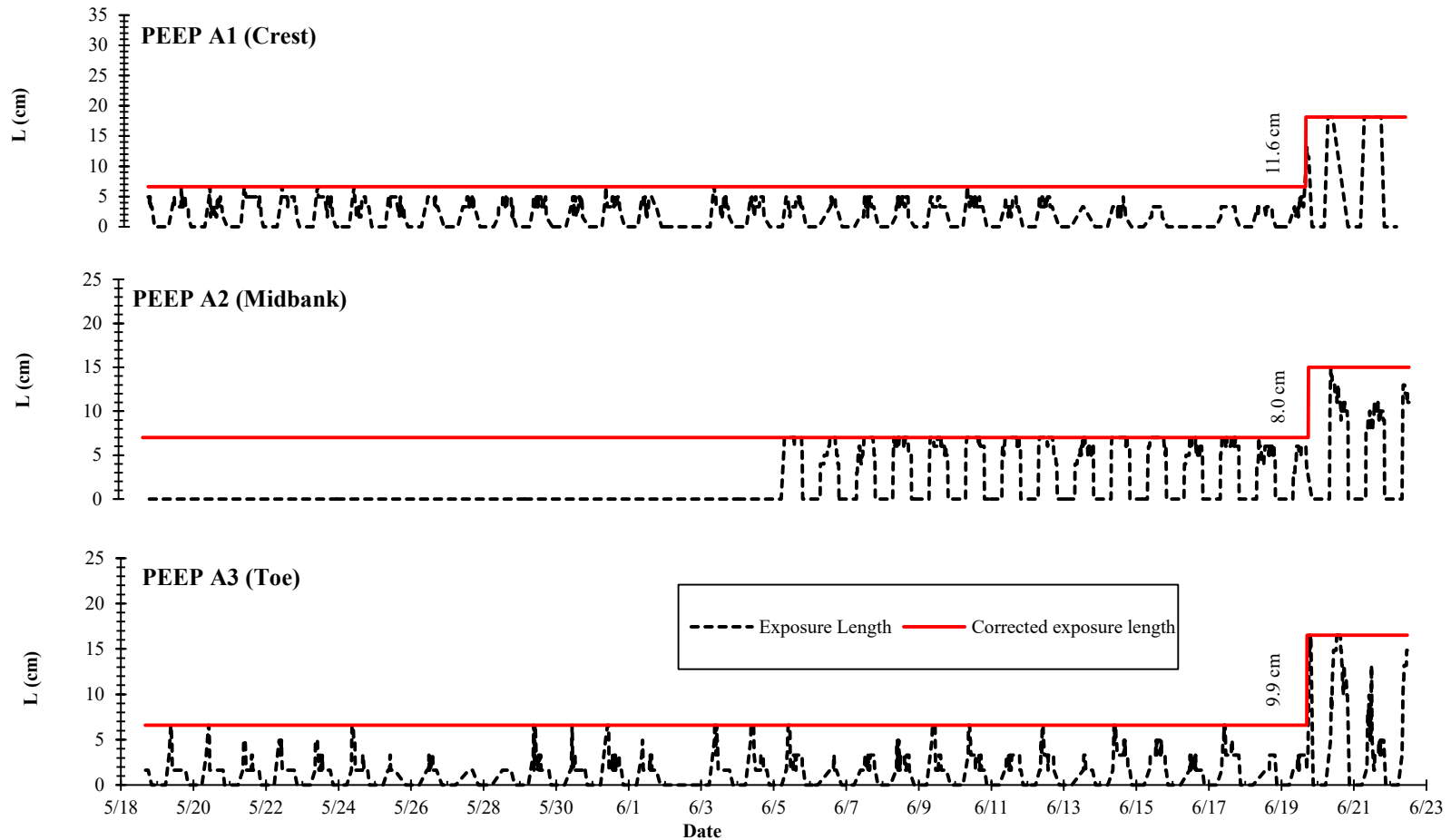


Figure F5. Processed exposure length without moving average analysis for PEEP A1 and A3 at site 1 during deployment period.



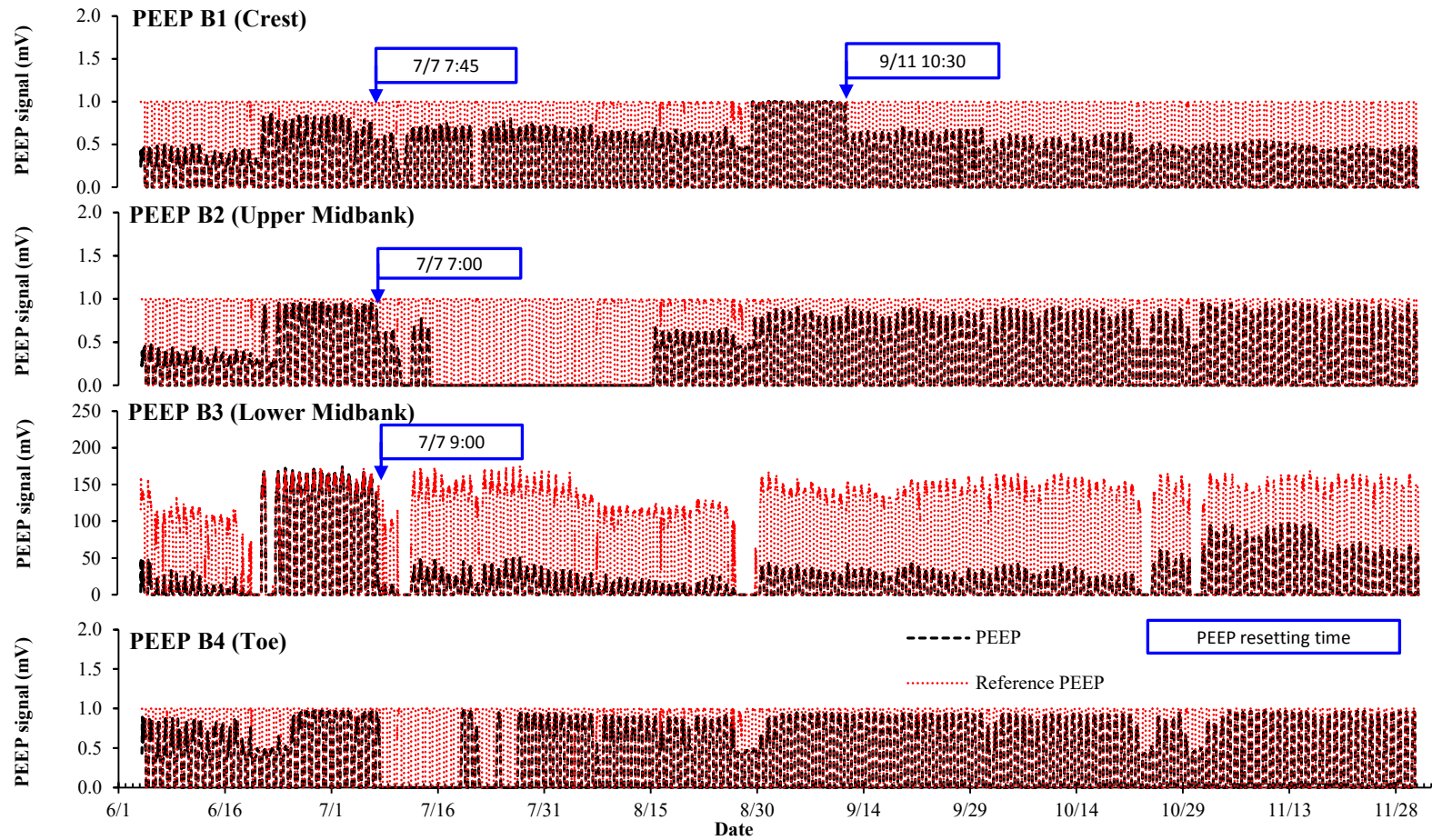


Figure F6. Voltage signal recorded from PEEP B1, B2, B3, and B4 along with their reference cells at site 2 during deployment period.

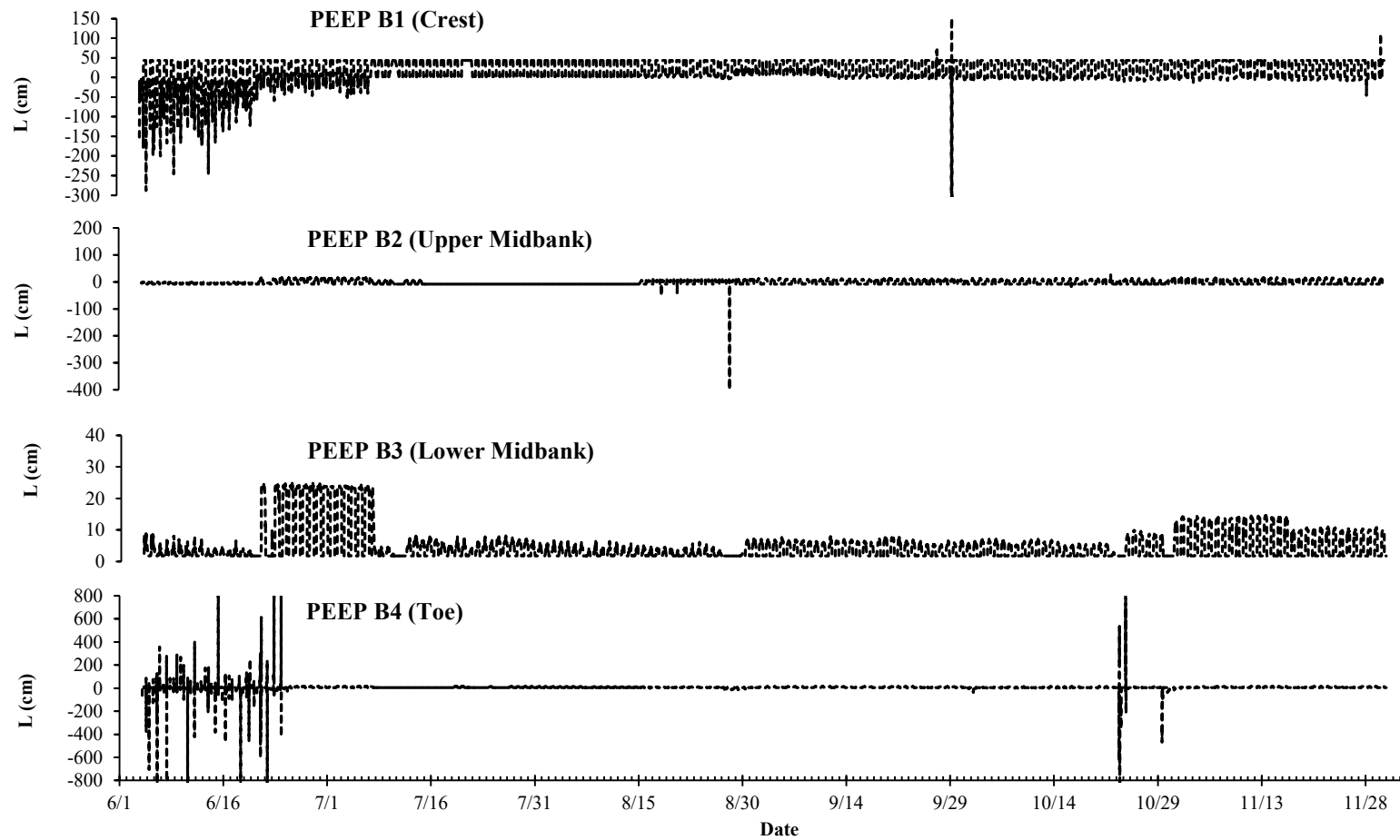


Figure F7. Unprocessed exposure length recorded from PEEP B1, B2, B3, and B4 at site 2 during deployment period.

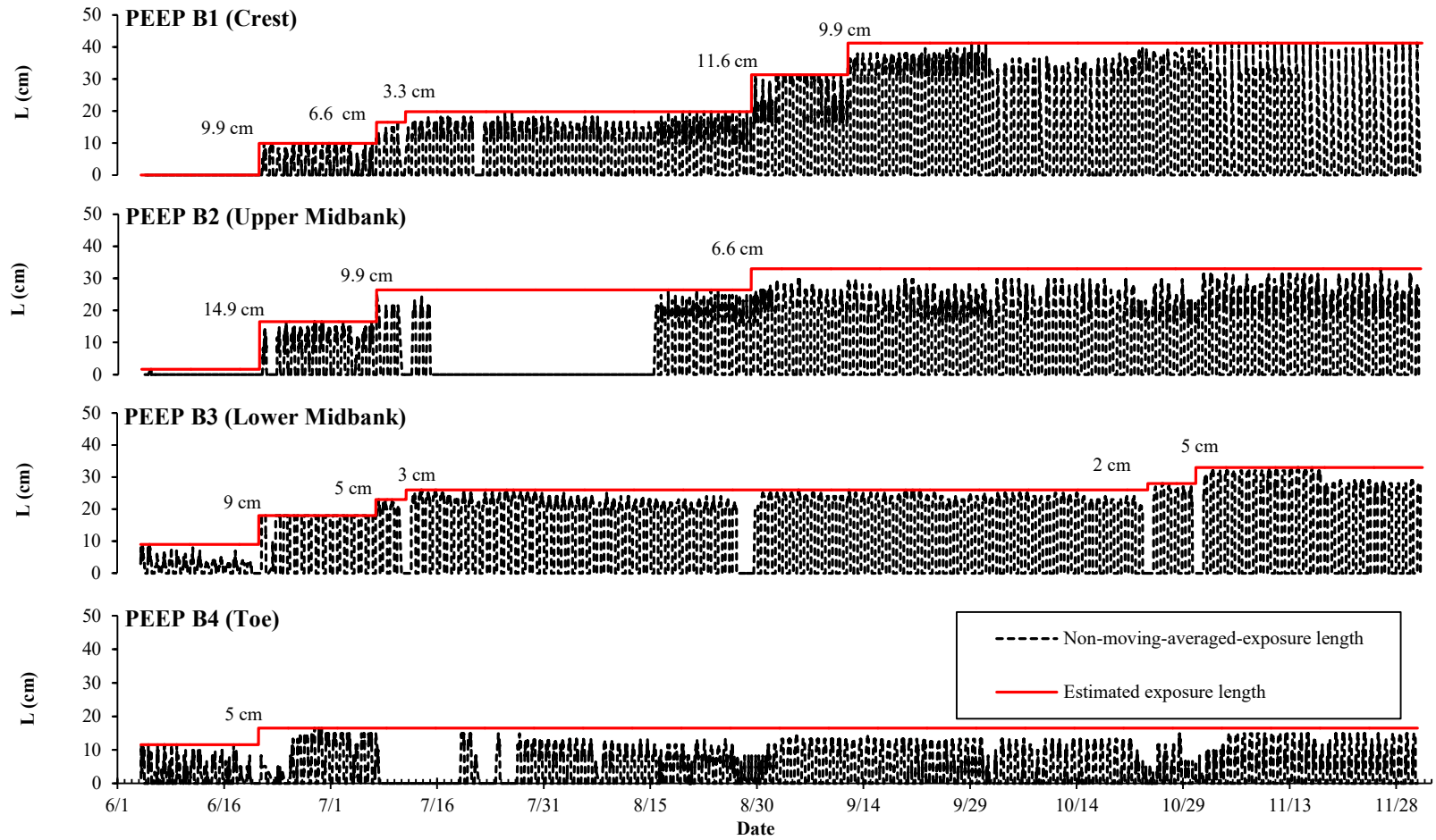


Figure F8. Processed exposure length without moving average analysis for PEEP B1, B2, B3, and B4 at site 2 during deployment period.

**APPENDIX G**  
**INPUTS AND RESULTS OF CONCEPTS SIMULATION**

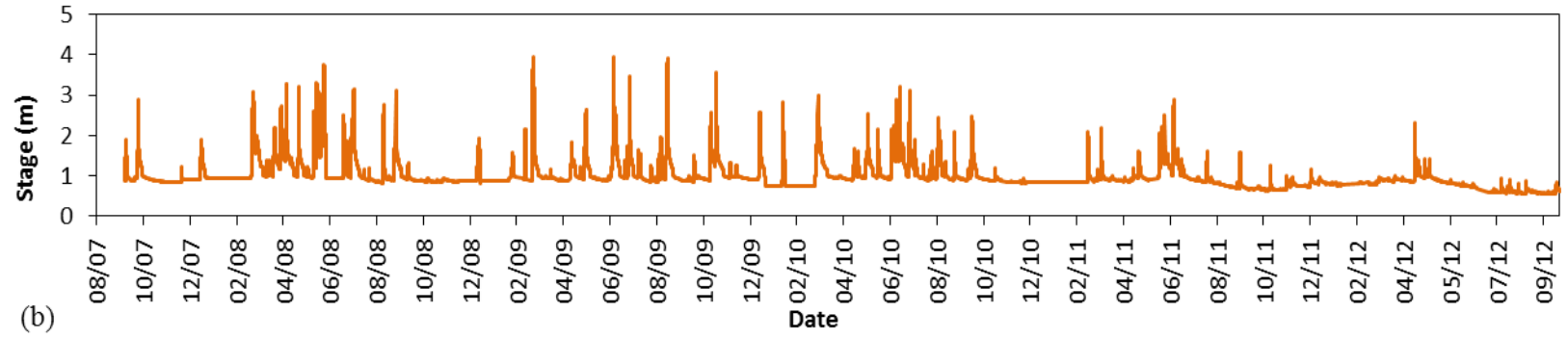
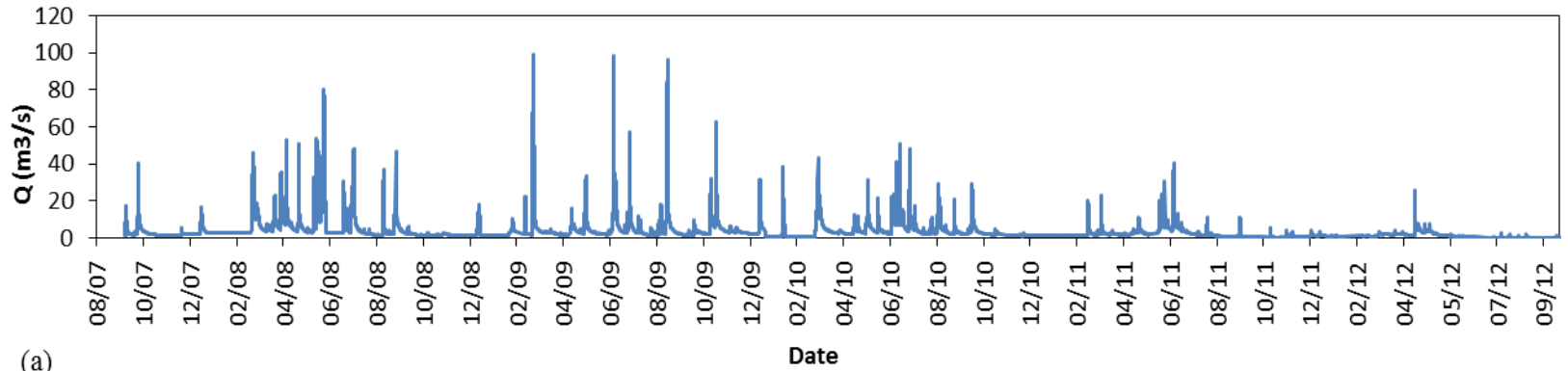


Figure G1. CONCEPTS inputs. (a) Hydrograph. (b) Water level.

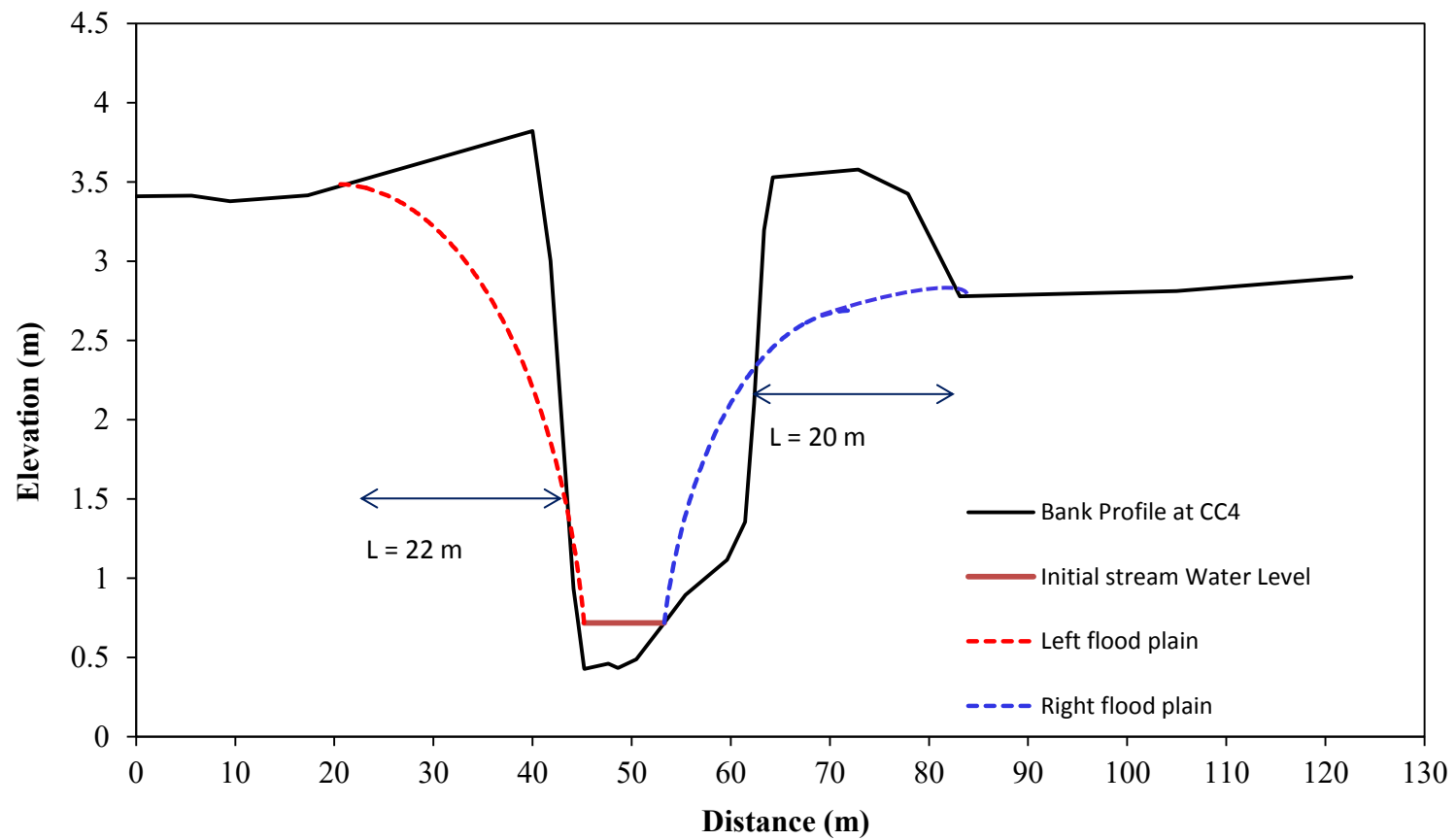


Figure G2. Initial groundwater profile based on Liang and Zang (2012) near the bank at site 2.

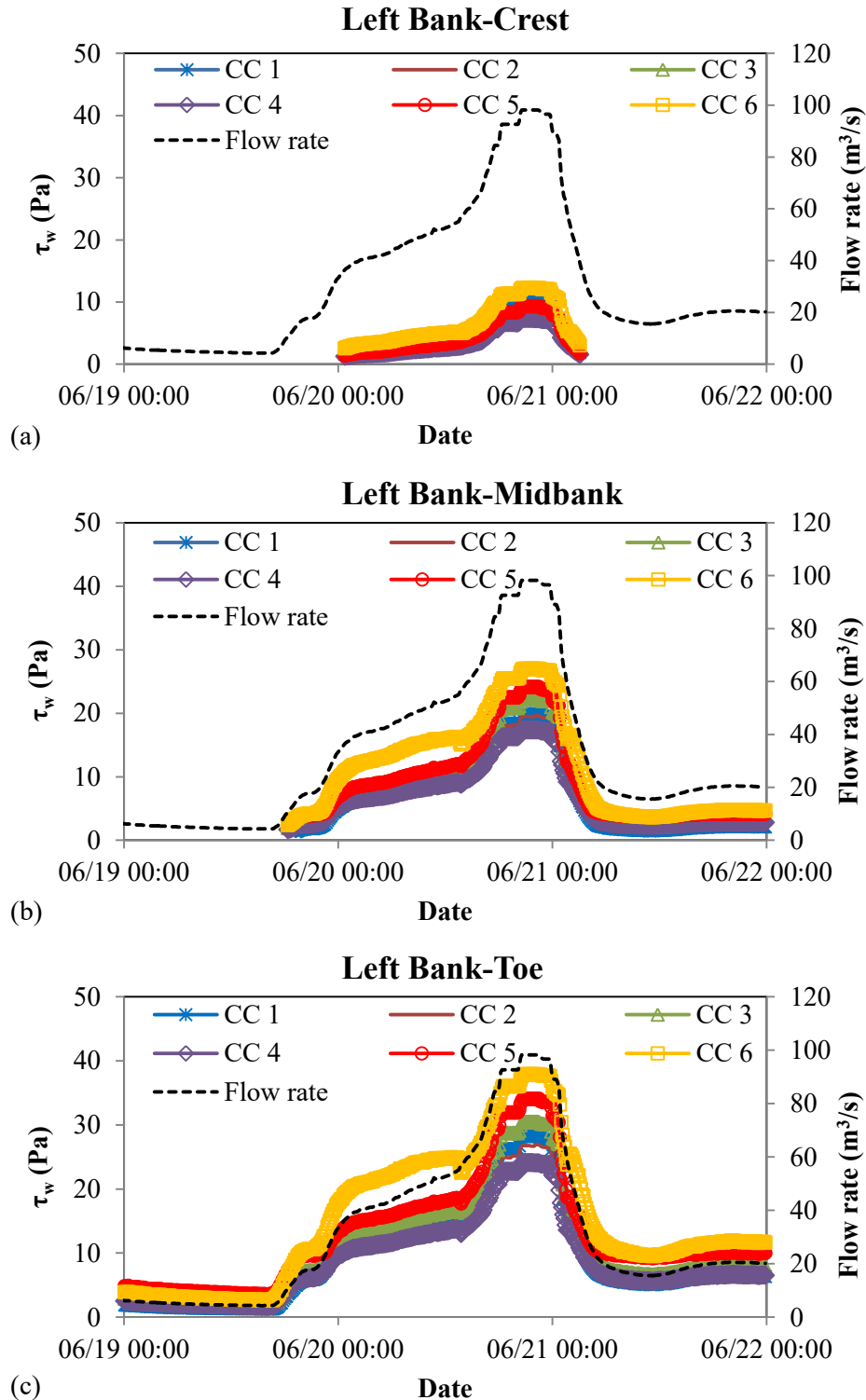


Figure G3. Near bank shear stress,  $\tau_w$ , predicted by CONCEPTS for the left bank of six (6) cross-sections at site 2. The time window was focused on the period prior to, during and right after the June 20, 2009 flood event. (a) Left bank-crest. (b) Left bank-midbank. (c) Left bank-toe.

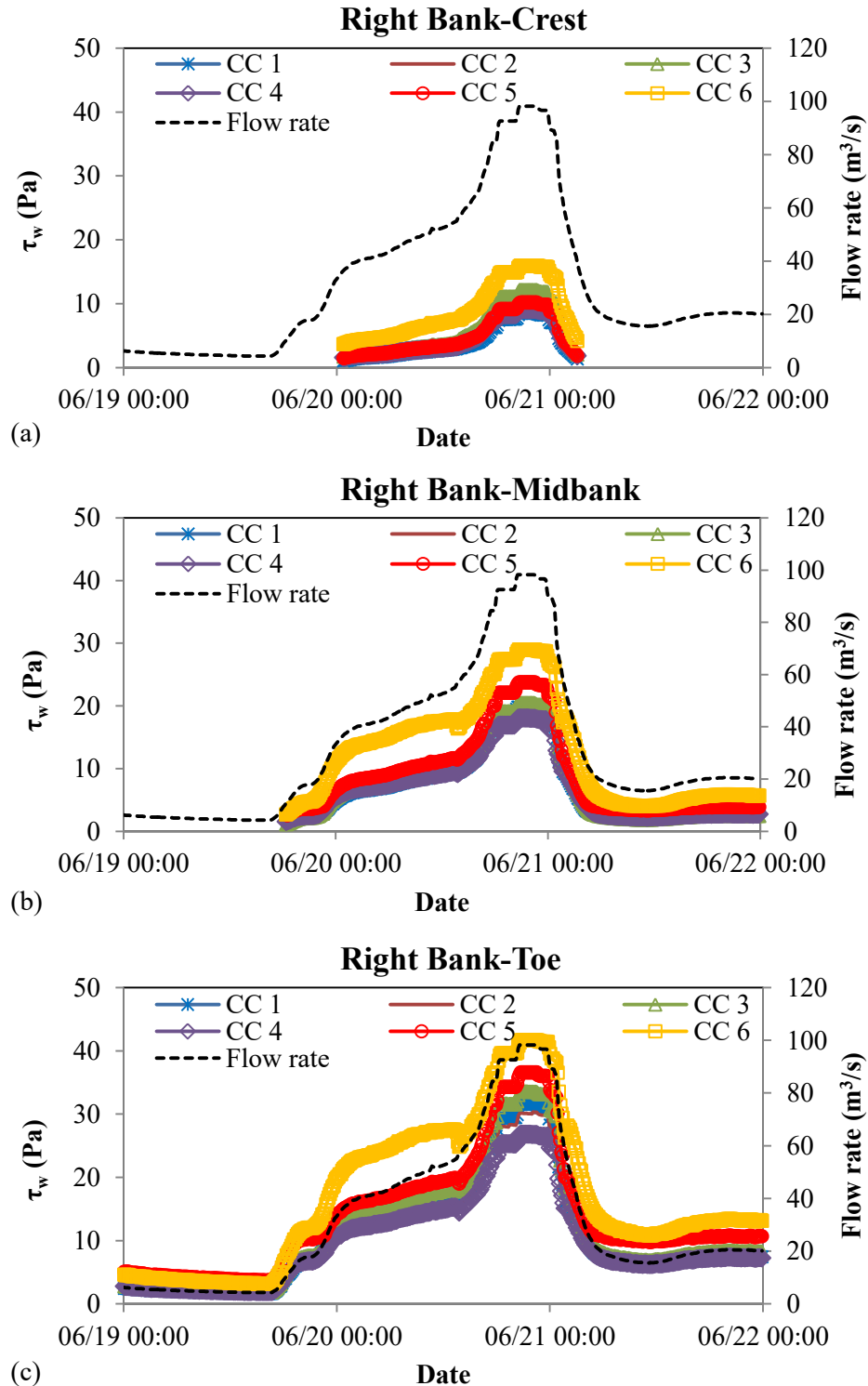


Figure G4. Near bank shear stress,  $\tau_w$ , predicted by CONCEPTS for the right bank of six (6) cross-sections at site 2. The time window was focused on the period prior to, during and right after the June 20, 2009 flood event. (a) Right bank-crest. (b) Right bank-midbank. (c) Right bank-toe.



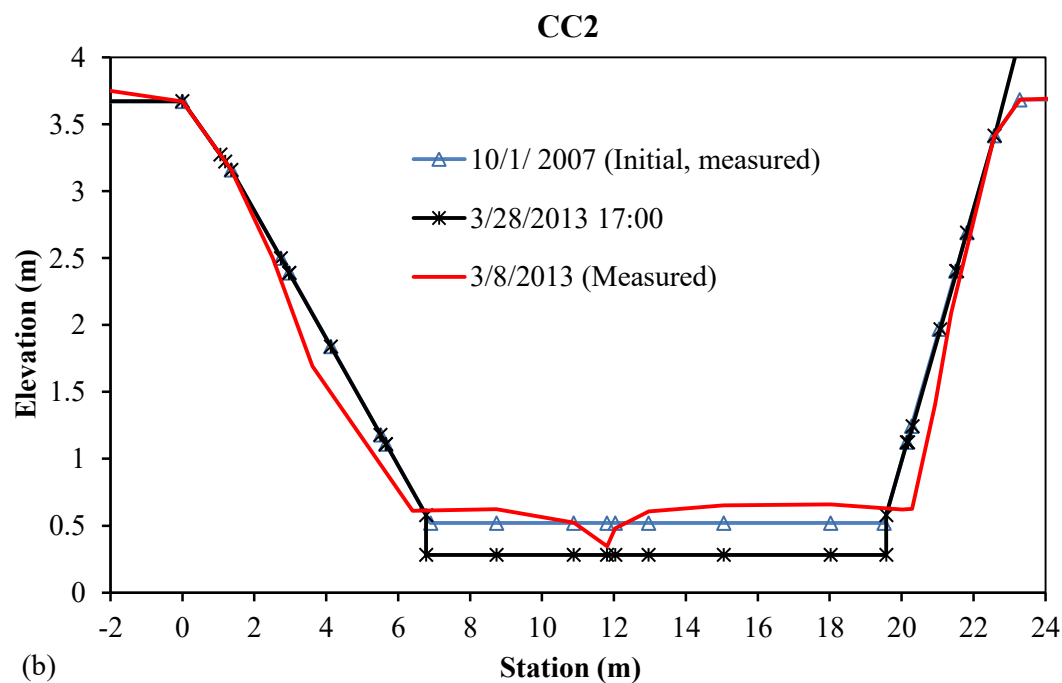
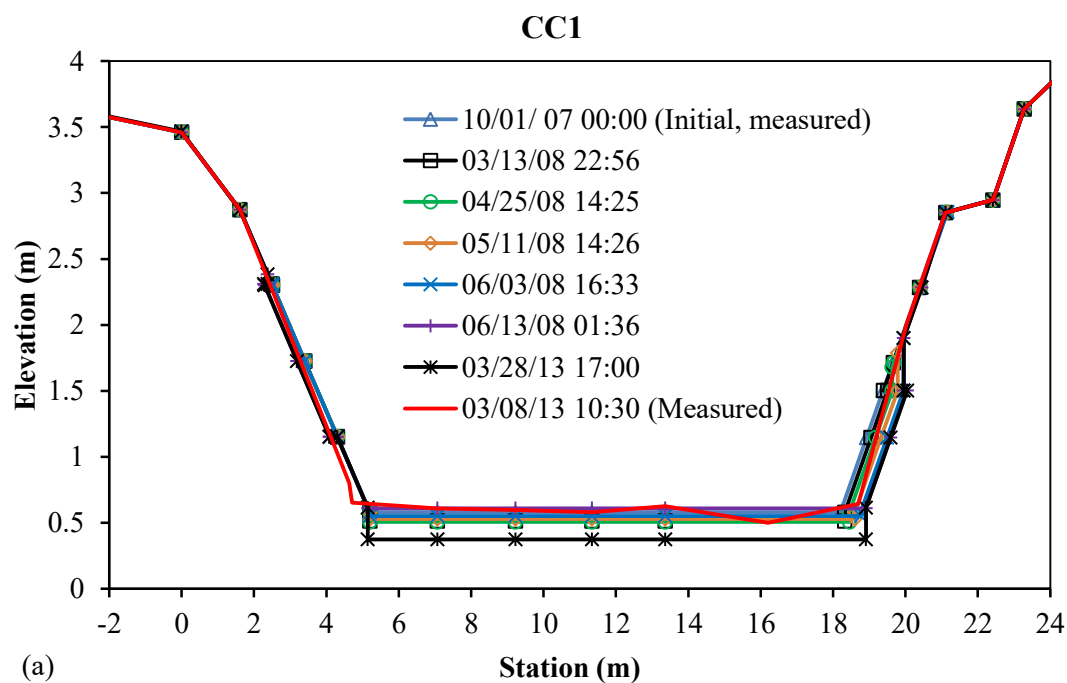


Figure G5. Measured and model-predicted bank cross sections for site 2. (a) Cross section CC1. (b) Cross section CC2. (c) Cross section CC3. (d) Cross section CC4. (e) Cross section CC5. (f) Cross section CC6.

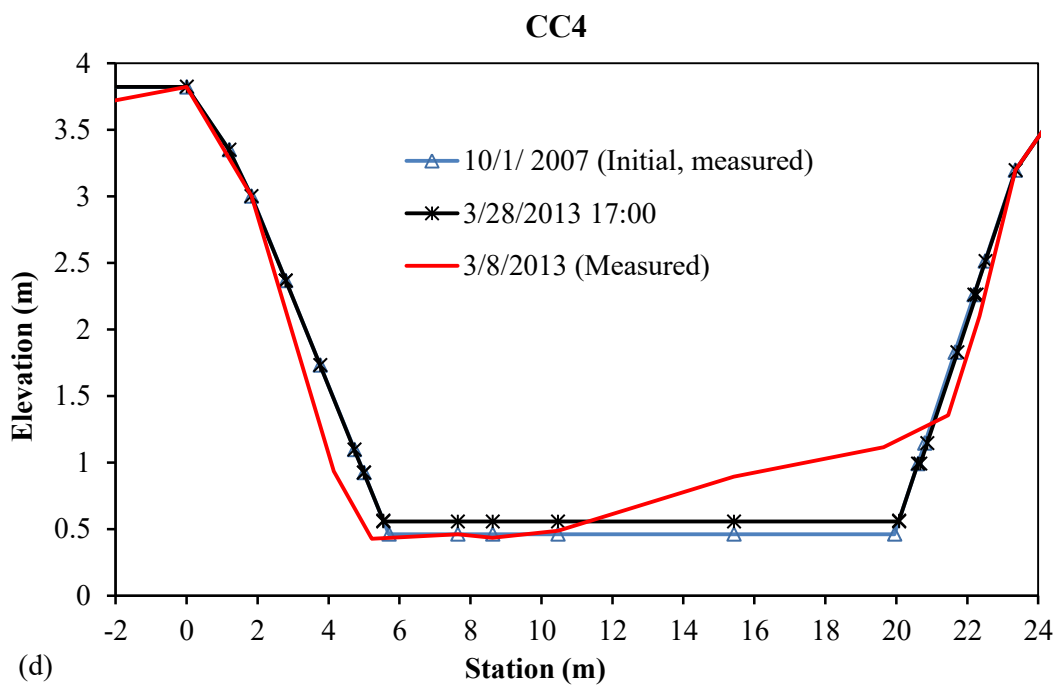
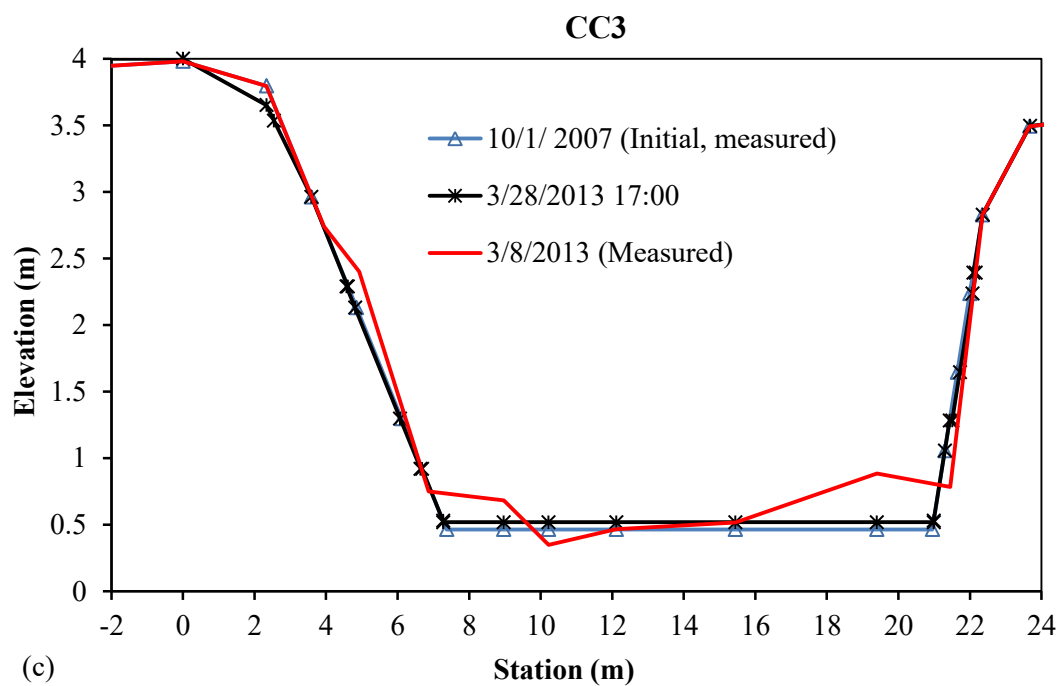


Figure G5. Continued.

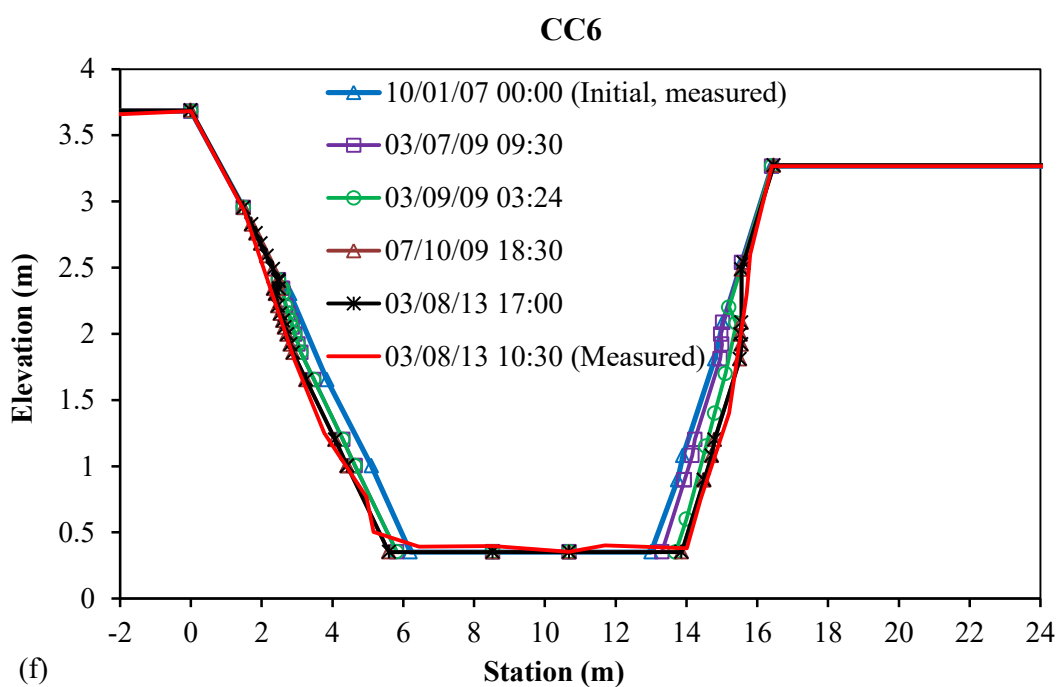
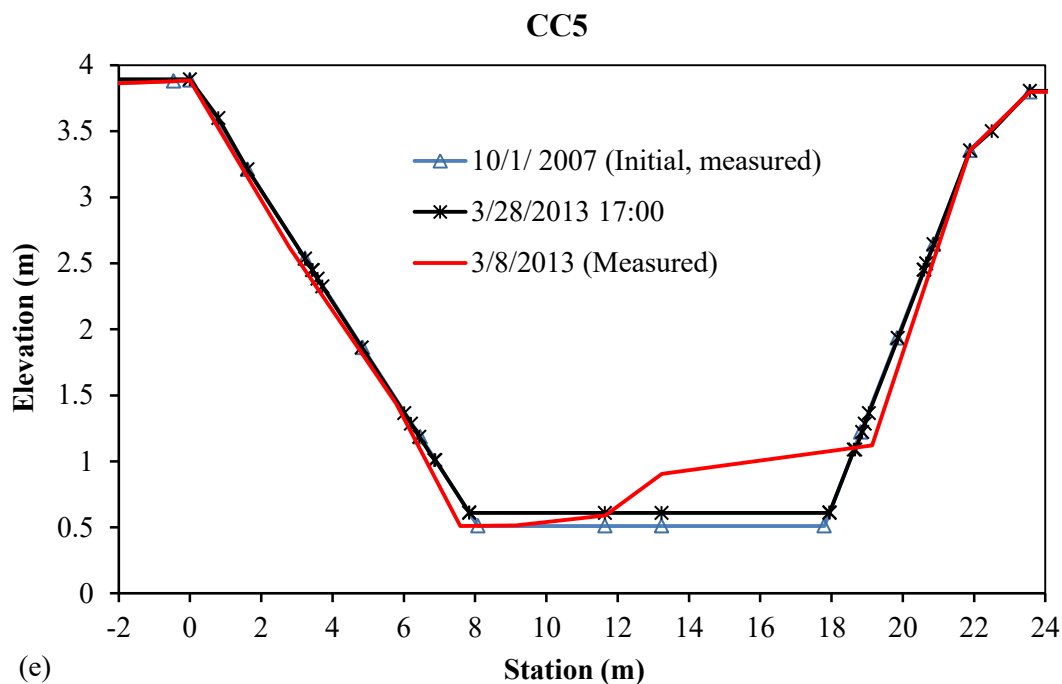


Figure G5. Continued.

**APPENDIX H**  
**RESULTS OF OTHER STUDIES**

Table H1. Results of other studies using undisturbed soils.

Source	Soil origin	Soil condition/treatment		PI	Sand %	Silt %	Clay %	$S_r$ or $c$ or $c'$ (Pa)	$\tau_c$ (Pa)
		Mechanical strength test	Erosional strength test						
Papanicolaou et al. (2007); Hildale (2001)	streambank	rooted and undisturbed	rooted and undisturbed ; laboratory test.	8.9	60	27	13	$S_r = 15,000-25,000^a$ and $S_r = 20,000^b$	4.16 <sup>h</sup>
Darby et al. (2007); Rinaldi et al. (2004)	streambank	undisturbed ; saturated, consolidated, drained	in-situ test	NA	NA	NA	NA	$c' = 2,000^c$	1.8 ± 0.7 <sup>g</sup>
Nam et al. (2010)	streambank	NA	undisturbed ; in-situ test	18.6 ± 3.9	16.6 ± 10.9	50.2 ± 8.1	33.2 ± 7.3	NA	3.8 ± 2.7 <sup>g</sup>
		NA		13.8 ± 7.2	25.8 ± 18.4	47.9 ± 10.9	26.3 ± 9.5	NA	5.2 ± 5.7 <sup>g</sup>
		NA		21.6 ± 2.4	9.2 ± 3.3	44.7 ± 2.9	46.2 ± 2.8	NA	9.6 ± 6.3 <sup>g</sup>
Langendoen & Simon (2008)	streambank	NA	NA	NA	12.6	75.5	11.8	$c = 1,000-6,300^d$	8
Kamphuis et al. (1990)	streambank	undisturbed, saturated	undisturbed, saturated	NA	19	58	23	$c = 160,000$	0.88 <sup>i</sup>
				NA	5	68	27	$c = 100,000$	4.10 <sup>i</sup>
				NA	7	53	40	$c = 75,000$	2.58 <sup>i</sup>
				NA	13	61	26	$c = 137,000$	0.65 <sup>i</sup>
Vermeyen (1995)	Overbank Site No.1	NA	undisturbed	NA	NA	NA	NA	NA	14.36 <sup>h</sup>
	Overbank Site No.2	NA	undisturbed	NA	NA	NA	NA	NA	43.09 <sup>h</sup>
Veeraraghavan (2007)	streambank : 20B Deer	undisturbed	undisturbed	11	32	54	14	$c = 11,300^e$	2.58 <sup>j</sup>
	streambank : 20B Creve			14	9	71	20	$c = 30,300^e$	3.10 <sup>j</sup>
	streambank : 32 Creve			8	22	61	17	$c = 8,630^e$	2.74 <sup>j</sup>
	streambank : 32 Grand			8	54	36	10	$c = 2,760^e$	1.01 <sup>j</sup>
	streambank : 33 Gravois			9	40	46	14	$c = 33,800^e$	2.09 <sup>j</sup>
	streambank : 33 Deer			8	59	32	9	$c = 34,200^e$	1.76 <sup>j</sup>
streambank : 33 Creve	14	11	71	18	$c = 6,940^e$	2.39 <sup>j</sup>			

$S_r$  = undrained shear strength;  $c$  = cohesion;  $c'$  = effective cohesion; **annotation:** a = vane shear test, b = unconfined compression test, c = triaxial test, d = Iowa Borehole Shear Tester (BST),

e = direct shear test, f = fall cone test; g = jet test; h = straight open channel flume; i = flume tunnel; j = conduit flume, value obtained by analyzing experimental data from the author.

## REFERENCES

- Abaci, O., and Papanicolaou, A.N. 2009. "Long-term effects of management practices on water-driven soil erosion in an intense agricultural sub-watershed: Monitoring and modeling." *Hydrological Processes* 23(19):2818-2837.
- Abderrezzak, K.E.K., Die Moran, A., Mosselman, E., Bouchard, J.P., Habersack H., Aelbrecht, D. 2013. "A physical, movable-bed model for non-uniform sediment transport, fluvial erosion and bank failure in rivers." *Journal of Hydro-environment Research* xx:1-20.
- Aberle, J., Nikora, V., McLean, S., Doscher C., McEwan, I., Green, M., Goring, D., and Walsh, J. 2003. "Straight benthic flow-through flume for in situ measurement of cohesive sediment dynamics." *Journal of Hydraulic Engineering* 129(1):63-67.
- Alkhalidi, M., and Mehta, A.J. 2005. "Discussion of Measurements of Sediment Erosion and Transport with the Adjustable Shear Stress Erosion and Transport Flume by Jesse D. Roberts, Richard A. Jepsen, and Scott C. James." *Journal of Hydraulic Engineering* 131(7):624-625.
- Arcement, G.J., and Schneider, V.R. 1989. "Guide for selecting Manning's roughness coefficients for natural channels and flood plains." *Report water supply paper 2339*, U.S. Geological Survey (USGS), Denver, USA.
- Arulanandan, K. 1975. Fundamental aspects of erosion of cohesive soils. *Journal of the Hydraulics Division-ASCE* 101(NHY5):635-639.
- Arulanandan, K., Gillogley, E., and Tully, R. 1980. "Development of a quantitative method to predict critical shear stress and rate of erosion of natural undisturbed cohesive soils." U.S. Army Corps of Engineers Report GL-80-5. USACE Waterways Experiment Station. Vicksburg, USA.
- ASCE Task Committee on Hydraulics, Bank Mechanics and Modeling of River Width Adjustment. 1998. "River width adjustment II: Modeling." *Journal of Hydraulic Engineering* 124(9):903-917.
- Ayers, P.D. 1987. "Moisture and Density Effects on Soil Shear Strength Parameters for Coarse Grained Soils." *Transactions of ASAE* 30(5):1282-1287.
- Bailly, J.S., Lagacherie, P., Millier, C., Puech, C., and Kosuth, P. 2008. "Agrarian landscapes linear features detection from LiDAR: application to artificial drainage networks." *International Journal of Remote Sensing* 29(12):3489-3508.
- Bankhead, N.P., and Simon, A. 2010. "Hydrologic and hydraulic effects of riparian root networks on streambank stability: Is mechanical root-reinforcement the whole story?" *Geomorphology* 116:353-362.

- Bardet J.P., Jesmani, M., and Jabbari, N. 2011. "Effect of Compaction on Shear Strength of Wax-Coated Sandy Soils." *Electronic Journal of Geotechnical Engineering* 16:451-461.
- Bertrand, F. 2010. "Fluvial Erosion Measurements of Stream bank Using Photo-Electronic Erosion Pins (PEEP)." Master thesis, University of Iowa, Iowa City, USA.
- Bettis, E.A. 1995. "The Holocene stratigraphic record of entrenched stream systems in thick loess regions of the Mississippi river basin." Ph.D. thesis, University of Iowa, Iowa City, USA.
- Biedenharn, D.S., Elliott, C.M., and Watson, C.C. 1997. "The WES Stream Investigation and Stream bank Stabilization Handbook." U.S. Army Corps of Engineers, Waterways Experiment Station (WES), Vicksburg, USA.
- Boulton, A.J., and Suter, P.J. 1986. "Ecology of temporary streams: An Australian perspective." *Limnology in Australia*, DeDecker, P. and Williams, W.D., eds., Commonwealth Scientific & Industrial Research Org./ Dr. W. Junk, Melbourne, Victoria, Australia, 313-327.
- Brownlie, W. R. 1981. "Prediction of flow depth and sediment discharge in open channels." *Report No. KH-R-43A*, W. M. Keck Laboratory of Hydraulics and Water Resources, California Institute of Technology, Pasadena, California, USA.
- Budhu, M. 2011. "Physical soil state and soil classification." *Soil mechanics and foundations*, 6th Ed., John Wiley and Sons, Hoboken, NJ, 65-66.
- Bullock, M.S., Kemper, W.D., and Nelson, S.D. 1988. "Soil cohesion as affected by freezing, water content, time and tillage." *Soil Science Society of America Journal* 52:770-776.
- Burt, T. N., and Stevenson, J. R. 1983. "Field settling velocity of Thames mud." *Technical Report IT-215*, Hydraulic Research Station, Wallingford, U. K.
- Chapuis. R.P. 1986a. Quantitative measurement of the scour resistance of natural solid clays. *Canadian Geotechnical Journal* 23(2):132-141.
- Chapuis. R.P. 1986b. Use of rotational erosion device on cohesive soils. Transportation Research Record N1089, Geotechnical Engineering. Transportation Research Board, Washington DC, pp. 23-28.
- Chapuis, R.P., and Gatién, T. 1986. An improved rotating cylinder technique for quantitative measurements of the scour resistance of clays. *Canadian Geotechnical Journal* 23:83-87.

- Chu-Agor, M.L., Fox, G.A., and Wilson, G.V. 2009. Empirical sediment transport function predicting seepage erosion undercutting for cohesive bank failure prediction. *Journal of Hydrology* 377:155-164.
- Clark, L.A., and Wynn, T.A. 2007. "Methods for determining streambank critical shear stress and soil erodibility: Implications for erosion rate predictions." *Transaction of the American Society of Agricultural and Biological Engineering* 50(1):95-106.
- Commission of the European Community. 1993. Coastal morpho- dynamics: On the methodology and accuracy of measuring physic-chemical properties to characterize cohesive sediments. EC MAST-I Report, the Netherlands.
- Couperthwaite, J.S., Mitchell, S.B., West, J.R. and Lawler, D.M. 1998. Cohesive sediment dynamics on an inter-tidal bank on the Tidal Trent, UK. *Marine Pollution Bulletin* 37(3-7):144-154.
- Dapporto, S., Rinaldi, M., Casagli, N., and Vannocci, P. 2003. "Mechanisms of riverbank failure along the Arno River, Central Italy." *Earth Surface Processes and Landforms* 28:1303-1323.
- Darby, S.E., Rinaldi, M., and Dapporto, S. 2007. "Coupled simulations of fluvial erosion and mass wasting for cohesive river banks." *Journal of Geophysical Research: Earth Surface* 112, F03022.
- Darby, S.E., Trieu, H.Q., Carling, P.A., Sarkkula, J., Koponen, J., Kummu, M., Conlan, I., Leyland, J. 2010. "A physically based model to predict hydraulic erosion of fine-grained riverbanks: The role of form roughness in limiting erosion." *Journal of Geophysical Research: Earth Surface* 115, F04003.
- Denn, K.D. 2010. "Sedimentbudget closure during runoff-generated high flow events in the South Amana sb-watershed, IA." Master thesis, University of Iowa, Iowa City, USA.
- Dennett, K.E., Sturm, T.W., Amirtharajah, A., and Mahmood, T. 1998. "Effects of adsorbed natural organic matter on the erosion of kaolinite sediments." *Water Environmental Research* 70(3):268-275.
- Duan, J.G. 2005. "Analytical approach to calculate rate of bank erosion." *Journal of Hydraulic Engineering* 131(11):980-990.
- Dunn, I.S. 1959. Tractive resistance of cohesive channels. *Journal of the Soil Mechanics and Foundations Division, Proceedings of the American Society of Civil Engineering* 85 (SM 3):1-24.
- Dunn, I.S., Anderson, L.R., and Kiefer, F.W. 1980. *Fundamentals of Geotechnical Analysis*. Wiley, New York.



- Flosi, G., Downie, S., Hopelain, J., Bird, M., Coey, R., and Collins, B. 2010. "California Salmonid Stream Habitat Restoration Manual." 4th Ed. State of California, The Resources Agency, California Department of Fish and Game, Wildlife and Fisheries Division, Sacramento, USA.
- Fox, G.A., and Felice, R.G. 2013. "Bank undercutting and tension failure by groundwater seepage: predicting failure mechanisms." *Earth Surface and Landforms*. doi:10.1002/esp.3481.
- Fredlund, D.G., and Rahardjo, H. 1993. *Soil mechanics for unsaturated soils*, John Wiley and Sons, Hoboken, NJ, 517.
- Gaskin, S.J., Pieterse, J., Al Shafie, A., Lepage, S. 2003. Erosion of undisturbed clay samples from the banks of the St. Lawrence River. *Canadian Journal of Civil Engineering* 30:585-595.
- Gauge, M., Spivak, A., Paradise, C. 2004. "Effect of land use and disturbance on benthic insects in headwater streams draining small watersheds north of Charlotte, NC." *Southeastern Naturalist* 3:345-358.
- Gharabaghi, B., Inkratas, C., Krishnappan, B.G., and Rudra, R.P. 2007. "Flow characteristics in a rotating circular flume." *The Open Civil Engineering Journal* 1:30-36.
- Ghebreiyessus, Y.T., Gantzer, C.J., Alberts, E.E., and Lentz, R.W. 1994. "Soil erosion by concentrated flow: Shear stress and bulk density." *Transactions of the ASAE* 37(6):1791-1797.
- Global Water Instrumentation. 2009. WL-16 Water Level Logger, Gold River, CA.
- Grabowski, R.C., Droppo, I.G., and Wharton, G. 2011. "Erodibility of cohesive sediment: The importance of sediment properties." *Earth-Science Reviews* 105: 101-120.
- Gray D.H., and Barker, D. 2004. "Root-soil mechanics and interactions." *Riparian Vegetation and Fluvial Geomorphology. Water Science and Application* (8), Bennett, S.J., and Simon, A., eds., American Geophysical Union, Washington, DC, pp. 113-123.
- Haaland, S.E. 1983. "Simple and explicit formulas for the friction factor in turbulent pipe flow." *Journal of Fluids Engineering* 105:89-90.
- Hadish, G.A. 1994. "Stream Stabilization in Western Iowa." Report No. HR-352, Iowa Department of Transportation, Golden Hills Resource Conservation and Development, Oakland, USA.
- Hanson, G.J., and Simon, A. 2001. "Erodibility of cohesive streambeds in the loess area of the Midwestern USA." *Hydrological Processes* 15(1):23-38.

- Hanson, G.J., and Cook, K.R. 2004. "Apparatus, test procedures, and analytical methods to measure soil erodibility in situ." *Applied Engineering in Agriculture* 20(4):455-462.
- Hilldale, R.C. 2001. "Fluvial erosion of cohesive banks considering turbulence and secondary flow." M.S. thesis, Washington State University, Pullman, USA.
- Hilldale, R.C., and Raff, D. 2008. "Assessing the ability of airborne LiDAR to map river bathymetry." *Earth Surface Processes and Landforms* 33:773-783.
- Horn, D.P., and Lane, S.P.H. 2006. Measurement of high-frequency bed level changes in the swash zone using Photo-Electronic Erosion Pins (PEEPs). In: Proceedings of the 30<sup>th</sup> International Conference on Coastal Engineering, San Diego, California, pp. 2591-2603.
- Huang, J., Hilldale, R. C., and Greimann, B.P. 2006. "Cohesive sediment transport." *Erosion and sedimentation manual*, C.T. Yang, ed., The United States Department of Interior, Bureau of Reclamation, Technical Service Center, Denver, CO. 4.1-4.54.
- Hydro Scientific Ltd. 2004. The Photo-Electronic Erosion Pin (PEEP) System: User Guide. Stratford-upon-Avon, United Kingdom: Hydro Scientific Ltd.
- Julian, J. P., and Torres. R. 2006. "Hydraulic erosion of cohesive riverbanks." *Geomorphology* 76(1-2):193-206.
- Kamphuis, J.W., and Hall, K.R. 1983. "Cohesive material erosion by unidirectional current." *Journal of Hydraulic Engineering* 109(1):49-61.
- Kamphuis, J.W., Gaskin, P.N., and Hoogendoorn, E. 1990. "Erosion test on four intact Ontario clays." *Canadian Geotechnical Journal* 27:692-696.
- Kandiah, A. 1974. "Fundamental aspects of surface erosion of cohesive soils." Ph.D. dissertation, University of California, Davis, USA.
- Kennedy, E.J. 1984. "Discharge ratings at gauging stations." *U.S. Geological Survey Techniques of Water Resources Investigations*, Book 3, Chapter A10. Reston, VA. 59pp.
- Knoll, G.F. 1979. *Radiation Detection and Measurement*. John Wiley and Sons, New York.
- Kothyari, U.C., and Jain, R. K. 2008. "Influence of cohesive on the incipient motion condition of sediment mixtures." *Water Resources Research* 44(4), W04410.
- Krishnappan, B.G.1993. "Rotating circular flume." *Journal of Hydraulic Engineering* 119(6):758-767.

- Krone, R. B. 1999. "Effects of bed structure on erosion of cohesive sediments." *Journal of Hydraulic Engineering* 125 (12):1297-1301.
- Kuijper, C., Cornelisse, J.M., and Winterwerp, J.C. 1989. "Research on erosive properties of cohesive sediments." *Journal of Geophysical Research* 94(C10):14341-14350.
- Landwehr, K., and Rhoads, B.L. 2003. "Depositional response of a headwater stream to channelization, East Central Illinois, USA." *River Research and Application* 19:77-100.
- Langel, R.J. 1996. "An Evaluation of Stream bank Stabilization Utilizing Deep-Planted Cuttings, Clear Creek, Johnson County, Iowa." M.S. thesis, University of Iowa, Iowa City, USA.
- Langendoen, E.J. 2000. "CONCEPTS – Conservational Channel Evolution and Pollutant Transport System." *Research Report No. 16*, National Sedimentation Laboratory, U.S. Department of Agriculture (USDA) – Agricultural Research Service (ARS), Oxford, USA.
- Langendoen, E.J. 2010. Assessing post-dam removal sediment dynamics using the CONCEPTS computer model. 2nd Joint Federal Interagency Conference, June 27-July 1, Las Vegas, USA.
- Langendoen, E.J., and Alonso, C.V. 2008. "Modeling the evolution of incised streams: I. Model formulation and validation of flow and streambed evolution components." *Journal of Hydraulic Engineering* 134(6):749-762.
- Langendoen, E.J., and Simon, A. 2008. "Modeling the evolution of incised streams. II: Stream bank erosion." *Journal of Hydraulic Engineering* 134(7):905-915.
- Langendoen, E.J., Wells, R.R., Thomas, R.E., Simon, A., and Bingner, R.L. 2009. "Modeling the evolution of incised streams. III: model application." *Journal of Hydraulic Engineering* 135(6):476- 486.
- Layzell, A.L., and Mandel, R.D. 2014. "An assessment of the erodibility of Holocene lithounits comprising stream-banks in northeastern Kansas, USA." *Geomorphology*. doi: 10.1016/j.geomorph.2014.01.003.
- Lawler, D.M, 1991. "A New Technique for the Automatic Monitoring of Erosion and Deposition Rates." *Water Resources Research* 27(8):2125-2128.
- Lawler, D.M., 1992. "Design and installation of a novel automatic erosion monitoring system." *Earth Surface Processes and Landforms* 17, 455-463.
- Lawler, D.M. 1993. "The measurement of river bank erosion and lateral channel change: A review." *Earth Surface Processes and Landforms* 18:777–821.

- Lawler, D.M. 1995. "The impact of scale on the process of channel-side sediment supply: A conceptual model" *Effects of scale on interpretation and management of sediment and water quality*, International Association of Hydrological Sciences (IAHS), 226:175-184.
- Lawler, D.M. 2003. "Application of an improved PEEP system to bank erosion investigations on the River Wharfe, UK." *Erosion and Sediment Transport Measurement in Rivers: Technological and Methodological Advances*, Bogen, J., Fergus, T., and Walling, D.E. eds., Proceedings of the Oslo Workshop, June 2002. International Association of Hydrological Sciences. Publ. 283. pp. 88-95.
- Lawler, D.M. 2005. The importance of high-resolution monitoring in erosion and deposition dynamics studies: Examples from estuarine and fluvial systems. *Geomorphology* 64:1-23.
- Lawler, D.M. 2008. Advances in the continuous monitoring of erosion and deposition dynamics: Developments and applications of the new PEEP-3T system. *Geomorphology*. 93:17-39.
- Lawler, D.M., Couperthwaite, J., Bull, L.J., and Harris, N.M. 1997. "Bank erosion events and processes in the upper Severn basin." *Hydrology and Earth System Sciences* 1(3):523-534.
- Lawler, D.M., West, J.R., Couperthwaite, J.S., Mitchell, S.B. 2001. "Application of a novel automatic erosion and deposition monitoring system at a channel bank site on the tidal River Trent, U.K. Estuarine." *Coastal and Shelf Science* 53:237-247.
- Liang, X., and Zhang, Y.K. 2012. "Analytical solution for drainage and recession from an unconfined aquifer." *Ground Water* 50(5):793-798.
- Lim S.S., and Khalili, N. 2009. "An improved rotating cylinder test design for laboratory measurement of erosion in clayey soils." *Geotechnical Testing Journal* 32(3):1-7.
- Lohnes, R.A., and Handy, R.L. 1968. "Slope angles in friable loess." *Journal of Geology* 76(3):247-258.
- Lohnes, R.A., Kjartanson, B.H. and Barnes A. 2001. "Regional Approach to Landslide Interpretation and Repair." *Final Report TR 43*, Iowa Department of Transportation (DOT), Iowa, USA.
- Loperfido, J.V., Just, C.L., and Schnoor, J.L. 2009. "High-frequency diel dissolved oxygen stream data modeled for variable temperature and scale." *Journal of Environmental Engineering* 135(12):1250-1256.
- Loperfido, J.V. 2009. "High-frequency sensing of Clear Creek water quality: mechanisms of dissolved oxygen and turbidity dynamics, and nutrient transport." Ph.D. dissertation, University of Iowa, Iowa City, USA.

- Luppi, L., Rinaldi, M., Teruggi, L.B., Darby, S.E., and Nardi, L. 2009. "Monitoring and numerical modeling of riverbank erosion processes: a case study along the Cecina River (central Italy)." *Earth Surface Processes and Landforms* 34(4):530-546.
- Mazurek, K.A., Rajaratnam, N., Segoo, D.C. 1999. The characteristics of erosion of a consolidated clay. Annual Conference of the Canadian Society for Civil Engineering, June 2-5, Regina, Saskatchewan, Canada.
- McCave, I. N. 1971. "Sand waves in the North Sea off the coast of Holland." *Marine Geology* 10:199-225.
- McDermott, J.P, and Sherman, D.J. 2009. "Using photo-electronic erosion pins for measuring bed elevation changes in the swash zone." *Journal of Coastal Research* 25(3):788-792.
- McNeil, J., Taylor, C., and Lick, W. 1996. "Measurement of erosion of undisturbed bottom sediments with depth." *Journal of Hydraulic Engineering* 112(6):316-324.
- Midgley, T.L., Fox, G.A., and Heeren, D.M. 2012. "Evaluation of the bank stability and toe erosion model (BSTEM) for predicting lateral retreat on composite streambanks." *Geomorphology* 145-146:107-114.
- Midgley, T.L., Fox, G.A., Wilson, G.V., Heeren, D.M., Langendoen, E.J., Simon, A. 2013. "Seepage-induced stream bank erosion and instability: In situ constant-head experiments." *Journal of Hydrologic Engineering* 18(10):1200-1210.
- Millar, R.G., and Quick, M.C. 1998. "Stable width and depth of gravel-bed rivers with cohesive banks." *Journal of Hydraulic Engineering* 124(10):1005-1013.
- Mitchell, S.B., Couperthwaite, J.S., West, J.R., Lawler, D.M. 1999. "Dynamics of erosion and deposition events on an intertidal mudbank at Burringham, River Trent, UK." *Hydrological Processes* 13(7): 1155-1166.
- Mitchell, S.B., Couperthwaite, J.S., West, J.R., Lawler, D.M. 2003. Measuring sediment exchange rates on an intertidal bank at Blacktoft, Humber Estuary, UK. *The Science of the Total Environment* 314-316:535-549.
- Muste, M., Kim, D., Merwade, V. 2012. "Modern digital instruments and techniques for hydrodynamic and morphologic characterization of streams." *Gravel-bed rivers VII: processes, tools, environments*, Church, M., Biron, P.M., and Roy, A.G., eds., John Wiley & Sons, Chichester, UK, 315-342.
- Nam, S., M.S. Gutierrez, P. Diplas, and J. Petrie. 2011. "Determination of the shear strength of unsaturated soils using the multistage direct shear test." *Engineering Geology* 122:272-280.

- Notebaert, B., Verstraeten, G., Govers, G., and Poesen, J. 2009. "Qualitative and quantitative applications of LiDAR imagery in fluvial geomorphology." *Earth Surface Processes and Landforms* 34:217-231.
- Oneal, B. R. 2009. "Quaternary stratigraphy and pedology of Clear Creek watershed in Iowa County, Iowa." M.S. thesis, Iowa State University, Ames, USA.
- Panagiotopoulos, I., Voulgaris, G., and Collins, M.B. 1997. "The influence of clay on the threshold of movement of fine sandy beds." *Coastal Engineering* 32(1):19-43.
- Papanicolaou, A.N. 2012. "Aspect of secondary flow in open channels: A critical literature review." *Gravel-bed rivers VII: processes, tools, environments*, Church, M., Biron, P.M., and Roy, A., eds., John Wiley & Sons, Chichester, UK, 31-35.
- Papanicolaou, A.N., and Maxwell, A.R. 2006. "Methodological considerations for studying self-weight fluidization in a sedimentation column." *International Journal of Mineral Processing* 78(3):140-152.
- Papanicolaou, A.N., and Abaci, O. 2008. "Upland erosion modeling in a semi-humid environment via the water erosion prediction project model." *Journal of Irrigation and Drainage Engineering* 134(6):796-806.
- Papanicolaou, A.N., Elhakeem, M., and Hilldale, R. 2007. "Secondary current effects on cohesive river bank erosion." *Water Resources Research* 43(12), W12418.
- Papanicolaou, A.N., Dey, S., Rinaldi, M., Mazumdar, A. 2006. "Research issues for riverine bank stability analysis in the 21st century." *Report*, Obermann Center, University of Iowa, Iowa City, USA.
- Papanicolaou, A.N., Elhakeem, M., Wilson, C.G., Burras, C.L., and Oneal, B. 2008. "Observations of soils at the hillslope scale in the Clear Creek watershed in Iowa, USA." *Soil Survey Horizons* 49:83-86.
- Papanicolaou, A.N., Sanford, J.T., Dermisis, D.C., Mancilla, G.A. 2010. "A 1-D morphodynamic model for rill erosion." *Water Resources Research*, 46(9), W09541.
- Parker, D.B., Michel, T.G., and Smith, J.L. 1995. "Compaction and water velocity effects on soil erosion in shallow flow." *Journal of Irrigation and Drainage Engineering* 121(2):170-178.
- Partheniades, E. 1965. "Erosion and deposition of cohesive soils." *Journal of Hydraulics Division-ASCE* 91(HY1), 105-138.
- Partheniades, E. 2009. "Erosion of cohesive soil." *Cohesive sediments in open channels: properties, transport, and applications*, Elsevier, Amsterdam, the Netherlands. 173-121.



- Parchure, T.M., and Mehta, A.J. 1985. "Erosion of soft cohesive sediment deposits." *Journal of Hydraulic Engineering* 111(10):1309-1326.
- Paterson, D.M. 1989. "Short-term changes in the erodibility of intertidal cohesive sediments related to the migratory behavior of epipelagic diatoms." *Limnology and Oceanography*. 34(1):223-234.
- Pizzuto, J.E. 1984. "Equilibrium bank geometry and the width of shallow sandbed streams." *Earth Surface Processes and Landforms* 9:199-207.
- Pizzuto, J. 2009. "An empirical model of event scale cohesive bank profile evolution." *Earth Surface Processes Landforms* 34(9):1234-1244.
- Pizzuto, J., O'neal, M., Stotts, S. 2010. "On the retreat of forested, cohesive riverbanks." *Geomorphology* 116:341-352.
- Pollen, N., and Simon, A. 2005. "Estimating the mechanical effects of riparian vegetation on streambank stability using a fiber bundle model." *Water Resources Research* 41(7), W07025.
- Prosser, I.P., Hughes, A.O., Rutherford, I.D. 2000. "Bank erosion of an incised upland channel by subaerial processes: Tasmania, Australia." *Earth Surface and Landforms* 25:1085-1101.
- Prior, J.C. 1976. "A regional guide to Iowa landforms." *Iowa geological survey educational series* 3. Iowa Department of Natural Resources, Geological Survey Division, Iowa City, USA.
- Raudkivi, A.J. 1998. *Loose boundary hydraulics*, A. A. Balkema, Rotterdam, the Netherlands, 271-311.
- Ravisangar, V., Sturm, T.W., and Amirtharaja, A. 2005. "Influence of sediment structure on erosional strength and density of kaolinite sediment beds." *Journal of Hydraulic Engineering* 131(5):356-365.
- Rayburn, A.R., and Schulte, L.A. 2009. "Landscape change in an agricultural watershed in the US Midwest." *Landscape and Urban Planning* 93(2):132-141.
- Rinaldi, M., and Darby, S.E. 2008. "Modeling river-bank-erosion processes and mass failure mechanisms: Progress towards fully coupled simulations." *Gravel-bed rivers VI: From process understanding to river restoration*, H. Habersack, H. Piegay, and M. Rinaldi, eds., Elsevier, Amsterdam, the Netherlands. 213-239.
- Rinaldi, M., Casagli, N., Dapporto, S., and Gargini, A. 2004. "Monitoring and Modelling of Pore Water Pressure Changes and Riverbank Stability during Flow Events." *Earth Surface Processes and Landforms* 29:237-254.

- Rinaldi, M., Mengoni, B., Luppi, L., Darby, S.E., and Mosselman, E. 2008. "Numerical simulation of hydrodynamics and bank erosion in a river bend." *Water Resources Research* 44, W09428. doi:10.1029/2008WR007008.
- Roberts, J., and Jepsen, R. 2001. "Development for optional use of circular core tubes with the high shear stress flume." *SANDIA report: SAND2001-0424*, Sandia National Laboratories, Albuquerque, USA.
- Roberts, J.D., Jepsen, R.A., and James, S.C. 2003. "Measurements of Sediment Erosion and Transport with the Adjustable Shear Stress Erosion and Transport Flume." *Journal of Hydraulic Engineering* 129 (11):862-871.
- Schofield, A.N. 1998. "Mohr Coulomb Error Correction." *Ground Engineering*, August, 30-32.
- Simon, A., and Rinaldi, M. 2000. "Channel instability in the loess area of the Midwestern United States." *Journal of the American Water Resources Association* 36(1):113-150.
- Simon, A., and Collison, A.J.C. 2002. "Quantifying the mechanical and hydrologic effects of riparian vegetation on streambank stability." *Earth Surface Processes and Landforms* 27(5):527-546.
- Simon, A., and Pollen, N. 2006. "A model of streambank stability incorporating hydraulic erosion and the effects of riparian vegetation." *Proc., 8th Federal Interagency Sedimentation Conference (FISC)*, Reno, NV, 870-877.
- Simon, A., and Klimetz, L. 2008. "Relative magnitudes and sources of sediment in benchmark watersheds of the Conservation Effects Assessment Project." *Journal of Soil and Water Conservation* 63(6):504-522.
- Simon, A., Curini, A., Darby, S.E., Langendoen, E.J. 2000. "Bank and near-bank processes in an incised channel." *Geomorphology* 35:193-217.
- Simon, A., Langendoen, E.J., Collison, A. & Layzell, A. 2003. Incorporating bank-toe erosion by hydraulic shear into a bank-stability model: Missouri River, Eastern Montana. In: *Proceedings of World Water & Environmental Resources Congress*, Philadelphia, Pennsylvania[CD ROM].
- Sutarto, T.E., Papanicolaou, A.N., Wilson, C.G., Langendoen, E.J. 2014. "A stability analysis of semi-cohesive streambanks with CONCEPTS: Coupling field and laboratory investigations to quantify the onset of fluvial erosion and mass failure." *Journal of Hydraulic Engineering* (in press).
- Theregowda, R., Abaci, O., Papanicolaou, A. N. 2006. "The Use of Sediment Tracers in Watershed Processes." *World Environmental & Water Resources Congress*, Omaha, Nebraska.



- Thoma, D.P., Gupta, S.C., Bauer, M.E., and Kirchoff, C.E. 2005. Airborne laser scanning for riverbank erosion assessment. *Remote Sensing of Environment* 95, 493-501.
- Thorne, C.R. 1982. "Processes and mechanisms of river bank erosion." *Gravel-bed rivers*, R.D. Hey, J.C. Bathurst, and C.R. Thorne, eds., John Wiley & Sons, Chichester, UK, 227-271.
- Thorne, C.R., and Tovey, N.K. 1981. "Stability of composite river bank." *Earth Surface Processes and Landforms* 6:469-484.
- Van De Wiel, M.J., and Darby, S.E. 2004. "Numerical modeling of bed topography and bank erosion along three-lined meandering rivers." *Riparian Vegetation and Fluvial Geomorphology. Water Science and Application (8)*, Bennett, S.J., and Simon, A., eds., American Geophysical Union, Washington, DC, pp. 267-282.
- Van Klaveren, R.W., and McCool, D.K. 1998. "Erodibility and critical shear of a previously frozen soil." *Transactions of the American Society of Agricultural Engineers* 41(5):1315-1321.
- Veeraraghavan, P. 2007. "Analysis of soil erosion based on soil properties." M.S. thesis, University of Missouri, Rolla, USA.
- Vermeyen, T. 1995. "Erosional and depositional characteristics of cohesive sediments found in Elephant Butte Reservoir, New Mexico." *Technical report R-95-15*, Water Resources Services, Technical Service Center, Bureau of Reclamation, Denver, USA.
- Walling, D.E., Blake, W., and He, Q. 1999. "Use  $^7\text{Be}$  and  $^{137}\text{Cs}$  measurements to document short-and medium-term rates of water-induced soil erosion on agricultural land." *Water Resources Research* 35(12):3865-3874.
- White, F.M. 2008. *Fluid mechanics*, 6th Ed., McGraw-Hill, New York, USA.
- Widdow, J., Brinsley, M.D., Bowley, N., and Barrett, C. 1998. "A benthic annular flume for in situ measurement of suspension feeding/biodeposition rates and erosion potential of intertidal cohesive sediments." *Estuarine, Coastal and Shelf Science* 46(1):27-38.
- Wilson, C.G., Kuhnle, R.A., Bosch, D.D., Steiner, J.L., Starks, P.J., Tomer, M.D., Wilson, G.V. 2008. "Quantifying relative contributions from sediment sources in Conservation Effects Assessment Project watersheds." *Journal of Soil and Water Conservation* 63:523-532.
- Wilson, C.G., Papanicolaou, A.N., and Denn, K.D. 2012. "Quantifying and partitioning fine sediment loads in an intensively agricultural headwater system." *Journal of Soils and Sediments* 12(6):966-981.

- Winterwerp, J.C., and Van Kesteren, W.G.M. 2004. Introduction to the Physics of Cohesive Sediment in the Marine Environment (1<sup>st</sup> ed.). Elsevier, New York, pp. 343-379.
- Winterwerp, J.C., Van Kesteren, W.G.M., Van Prooijen, B., and Jacobs, W., 2012. A conceptual framework for shear flow-induced erosion of soft cohesive sediment beds. *Journal of Geophysical Research* 117, C10020. doi:10.1029/2012JC008072.
- Whittaker, E.T., and Robinson, G. 1967. *The calculus of observations: An introduction to numerical analysis*, 4th Ed., Dover Publications, New York.”
- Wynn, T., and Mostaghimi, S. 2006. “The effect of vegetation and soil type on streambank erosion, Southwestern Virginia, USA.” *Journal of the American Water Resources Association* 42(1):69-82.
- Yang, H., White, D.J., and Schaefer, V.R. 2005. “Innovative Solutions for Slope Stability Reinforcement and Characterization: Vol.II.” Report No. TR-489, Iowa Highway Research Board (IHRB), Iowa, USA.
- YongHui, Z., JinYou, L., HongZhi, L., JiaSheng, W., Beilin, F., Shiming, Y. 2008. Research on cohesive sediment erosion by flow: An overview. *Science in China Series E- Technological Sciences* 51(11):2001-2012.
- Zreik, D.A., Krishnappan, B.G., Germaine, J.T., Madsen, O.S., and Ladd, C.C. 1998. “Erosional and mechanical strengths of deposited cohesive sediments.” *Journal of Hydraulic Engineering* 124(11):1076-1085.